JSCSEN 87(6)669–784(2022)

ISSN 1820-7421(Online)

Journal of the Serbian Chemical Society

Electronic version

Serbian Chemical Society 125 ANNIVERSARY

Available on line at

CXII 1897

www.shd.org.rs/JSCS/

VOLUME 87

No 6

BELGRADE 2022

The **Journal of the Serbian Chemical Society** (formerly Glasnik Hemijskog društva Beograd), one volume (12 issues) per year, publishes articles from the fields of chemistry. The **Journal** is financially supported by the **Ministry of Education, Science and Technological Development of the Republic of Serbia.**

Articles published in the **Journal** are indexed in **Clarivate Analytics products: Science Citation Index-Expanded™** – accessed *via* **Web of Science®** and **Journal Citation Reports®**.

Impact Factor announced 2021: **1.240; 5-year Impact Factor**: **1.144**.

Articles appearing in the **Journal** are also abstracted by: **Scopus, Chemical Abstracts Plus (CAplus℠), Directory of Open Access Journals, Referativnii Zhurnal (VINITI), RSC Analytical Abstracts, EuroPub, Pro Quest** and **Asian Digital Library.**

Publisher: **Serbian Chemical Society**, Karnegijeva 4/III, P. O. Box 36, 1120 Belgrade 35, Serbia
tel./fax: +381–11–3370–467, E-mails: **Society** – shd@shd.org.rs; **Journal** – jscs@shd.org.rs
Home Pages: **Society** – http://www.shd.org.rs/, **Journal** – http://www.shd.org.rs/JSCS/

Internet Service: Contents, Abstracts and full papers (from Vol 64, No. 1, 1999) are available in the electronic form at the Web Site of the **Journal** (http://www.shd.org.rs/JSCS/).

Subscription: The annual subscription rate is **150.00 €** including postage (surface mail) and handling. For Society members from abroad rate is **50.00 €**. For the proforma invoice with the instruction for bank payment contact the Society Office (E-mail: shd@shd.org.rs) or see JSCS Web Site: http://www.shd.org.rs/JSCS/, option Subscription.

Godišnja pretplata: Za članove SHD: **2.500,00 RSD**, za penzionere i studente: **1000,00 RSD**, a za ostale: **3.500,00 RSD**:za organizacije i ustanove: **16.000,00 RSD**. Uplate se vrše na tekući račun Društva: **205-13815-62**, poziv na broj **320**, sa naznakom "pretplata za JSCS".

Nota: Radovi čiji su svi autori članovi SHD prioritetno se publikuju.

Odlukom Odbora za hemiju Republičkog fonda za nauku Srbije, br. 66788/1 od 22.11.1990. godine, koja je kasnije potvrđena odlukom Saveta Fonda, časopis je uvršten u kategoriju međunarodnih časopisa (**M-23**). Takođe, aktom Ministarstva za nauku i tehnologiju Republike Srbije, 413-00-247/2000-01 od 15.06.2000. godine, ovaj časopis je proglašen za publikaciju od posebnog interesa za nauku. **Impact Factor** časopisa objavljen 2021. godine iznosi **1,240**, a petogodišnji **Impact Factor 1,144**.

INSTRUCTIONS FOR AUTHORS (2021)

GENERAL

The *Journal of the Serbian Chemical Society* (the *Journal* in further text) is an international journal publishing papers from all fields of chemistry and related disciplines. Twelve issues are published annually. The Editorial Board expects the editors, reviewers, and authors to respect the well-known standard of professional ethics.

Types of Contributions

Original scientific papers	(up to 15 typewritten pages, including Figures, Tables and References) report original research which must not have been previously published.
Short communications	(up to 8 pages) report unpublished preliminary results of sufficient importance to merit rapid publication.
Notes	(up to 5 pages) report unpublished results of short, but complete, original research
Authors' reviews	(up to 40 pages) present an overview of the author's current research with comparison to data of other scientists working in the field
Reviews[a]	(up to 40 pages) present a concise and critical survey of a specific research area. Generally, these are prepared at the invitation of the Editor
Surveys	(about 25 pages) communicate a short review of a specific research area.
Book and Web site reviews	(1 - 2 pages)
Extended abstracts	(about 4 pages) of Lectures given at meetings of the Serbian Chemical Society Divisions
Letters to the Editor	report miscellaneous topics directed directly to the Editor

[a]Generally, Authors' reviews, Reviews and Surveys are prepared at the invitation of the Editor.

Submission of manuscripts

Manuscripts should be submitted using the **OnLine Submission Form**, available on the JSCS Web Site (**http://www.shd-pub.org.rs/index.php/JSCS**). The manuscript must be uploaded as a Word.doc or .rtf file, with tables and figures (including the corresponding captions – above Tables and below Figures), placed within the text to follow the paragraph in which they were mentioned for the first time.

Please note that **Full Names (**First Name, Last Name), **Full Affiliation** and **Country** (from drop down menu) of **ALL OF AUTHORS** (written in accordance with English spelling rules - the first letter capitalized) must be entered in the manuscript Submission Form (Step 3). Manuscript Title, authors' names and affiliations, as well as the Abstract, **WILL APPEAR** in the article listing, as well as in **BIBLIOGRAPHIC DATABASES (WoS, SCOPUS...)**, in the form and in the order entered in the author details

Graphical abstract

Graphical abstract is a one-image file containing the main depiction of the authors work and/or conclusion and must be supplied along with the manuscript. It must enable readers to quickly gain the main message of the paper and to encourage browsing, help readers identify which papers are most relevant to their research interests. Authors must provide an image that clearly represents the research described in the paper. The most relevant figure from the work, which summarizes the content, can also be submitted. The image should be submitted as a separate file in **Online Submission Form - Step 2**.

Specifications: The graphical abstract should have a clear start and end, reading from top to bottom or left to right. Please omit unnecessary distractions as much as possible.

- **Image size:** minimum of 500×800 pixels (W×H) and a minimum resolution of 300 dpi. If a larger image is sent, then please use the same ratio: 16 wide × 9 high. Please note that your image will be scaled proportionally to fit in the available window in TOC; a 150x240 pixel rectangle. Please be sure that the quality of an image cannot be increased by changing the resolution from lower to higher, but only by rescanning or exporting the image with a higher resolution, which can be set in usual "settings" option.
- **Font:** Please use Calibri and Symbol font with a large enough font size, so it is readable even from the image of a smaller size (150 × 240 px) in TOC.
- **File type:** JPG and PNG only.

No additional text, outline or synopsis should be included. Please do not use white space or any heading within the image.

Cover Letter

Manuscripts must be accompanied by a cover letter (strictly uploaded in **Online Submission Step 2**) in which the type of the submitted manuscript and a warranty as given below are given. The Author(s) has(have) to warranty that the manuscript submitted to the *Journal* for review is original, has been written by the stated author(s) and has not been published elsewhere; is currently not being considered for publication by any other journal and will not be submitted for such a review while under review by the *Journal*; the manuscript contains no libellous or other unlawful statements and does not contain any materials that violate any personal or proprietary rights of any other person or entity. All manuscripts will be acknowledged on receipt (by e-mail).

Illustrations

Illustrations (Figs, schemes, photos…) in TIF or EPS format (JPG format is acceptable for colour and greyscale photos, only), must be additionally uploaded (Online Submission Step 2) as a separate file or one archived (.zip, .rar or .arj) file. Figures and/or Schemes should be prepared according to the **Artwork Instructions -** http://www.shd.org.rs/JSCS/jscs-pdf/Artwork_Instructions.pdf!

For any difficulties and questions related to **OnLine Submission Form -** https://www.shd-pub.org.rs/index.php/JSCS/submission/wizard, please refer to **User Guide -** https://openjournal-systems.com/ojs-3-user-guide/ , Chapter **Submitting an Article -** https://openjournalsystems.com/ojs-3-user-guide/submitting-an-article/. If difficulties still persist, please contact JSCS Editorial Office at **JSCS@shd.org.rs**

A manuscript not prepared according to these instructions will be returned for resubmission without being assigned a reference number.

Conflict-of-Interest Statement*: Public trust in the peer review process and the credibility of published articles depend in part on how well a conflict of interest is handled during writing, peer review, and editorial decision making. A conflict of interest exists when an author (or the author's institution), reviewer, or editor has financial or personal relationships that inappropriately influence (bias) his or her actions (such relationships are also known as dual commitments, competing interests, or competing loyalties). These relationships vary from those with negligible potential to those with great potential to influence judgment, and not all relationships represent true conflict of interest. The potential for a conflict of interest can exist whether or not an individual believes that the relationship affects his or her scientific judgment. Financial relationships (such as employment, consultancies, stock ownership, honoraria, paid expert testimony) are the most easily identifiable conflicts of interest and the most likely to undermine the credibility of the journal, the authors, and of science itself. However, conflicts can occur for other reasons, such as personal relationships, academic competition, and intellectual passion.

Informed Consent Statement*: Patients have a right to privacy that should not be infringed without informed consent. Identifying information, including patients' names, initials, or hospital numbers, should not be published in written descriptions, photographs, and pedigrees unless the information is essential for scientific purposes and the patient (or parent or guardian) gives written informed consent for publication. Informed consent for this purpose requires that a patient who is identifiable be shown the manuscript to be published. Authors should identify Individuals who provide writing assistance and disclose the funding source for this assistance. Identifying details should be omitted if they are not essential. Complete anonymity is difficult to achieve, however, and informed consent should be obtained if there is any doubt. For example, masking the eye region in photographs of patients is inadequate protection of anonymity. If identifying characteristics are altered to protect anonymity, such as in genetic pedigrees, authors should provide assurance that alterations do not distort scientific meaning and editors should so note. The requirement for informed consent should be included in the journal's instructions for authors. When informed consent has been obtained it should be indicated in the published article.

Human and Animal Rights Statement* When reporting experiments on human subjects, authors should indicate whether the procedures followed were in accordance with the ethical standards of the responsible committee on human experimentation (institutional and national) and with the Helsinki Declaration of 1975, as revised in 2000 (5). If doubt exists whether the research was conducted in accordance with the Helsinki Declaration, the authors must explain the rationale for their approach, and demonstrate that the institutional review body explicitly approved the doubtful aspects of the study. When reporting experiments on animals, authors should be asked to indicate whether the institutional and national guide for the care and use of laboratory animals was followed.

---

*International Committee of Medical Journal Editors ("Uniform Requirements for Manuscripts Submitted to Biomedical Journals"), February 2006

PROCEDURE

All contributions will be peer reviewed and only those deemed worthy and suitable will be accepted for publication. The Editor has the final decision. To facilitate the reviewing process, authors are encouraged to suggest up to three persons competent to review their manuscript. Such suggestions will be taken into consideration but not always accepted. If authors would prefer a specific person not be a reviewer, this should be announced. The Cover Letter must be accompanied by these suggestions. Manuscripts requiring revision should be returned according to the requirement of the Editor, within 60 days upon reception of the reviewing comments by e-mail.

The *Journal* maintains its policy and takes the liberty of correcting the English as well as false content of manuscripts **provisionally accepted** for publication in the first stage of reviewing process. In this second stage of manuscript preparation by JSCS Editorial Office, the author(s) may be required to supply some **additional clarifications and corrections**. This procedure will be executed during copyediting actions, with a demand to author(s) to perform corrections of unclear parts before the manuscript would be published OnLine as **finally accepted manuscript (OLF Section of the JSCS website)**. Please note that the manuscript can receive the status of **final rejection** if the author's corrections would not be satisfactory.

When finally accepted manuscript is ready for printing, the corresponding author will receive a request for proof reading, which should be performed within 2 days. Failure to do so will be taken as the authors agree with any alteration which may have occurred during the preparation of the manuscript for printing.

Accepted manuscripts of active members of the Serbian Chemical Society (all authors) have publishing priority.

MANUSCRIPT PRESENTATION

Manuscripts should be typed in English (either standard British or American English, but consistent throughout) with 1.5 spacing (12 points Times New Roman; Greek letters in the character font Symbol) in A4 format leaving 2.5 cm for margins. For Regional specific, non-standard characters that may appear in the text, save documents with Embed fonts Word option: *Save as -> (Tools) -> Save Options… -> Embed fonts in the text.*

The authors are requested to seek the assistance of competent English language expert, if necessary, to ensure their English is of a reasonable standard. The Serbian Chemical Society can provide this service in advance of submission of the manuscript. If this service is required, please contact the office of the Society by e-mail (jscs-info@shd.org.rs).

Tables, figures and/or schemes must be embedded in the main text of the manuscript and should follow the paragraph in which they are mentioned for the first time. **Tables** must be prepared with the aid of the **WORD table function**, without vertical lines. The minimum size of the font in the tables should be **10 pt**. Table columns must not be formatted using multiple spaces. Table rows must not be formatted using any returns (enter key; ↵ key) and are **limited to 12 cm width**. Tables should not be incorporated as graphical objects. **Footnotes to Tables** should follow them and are to be indicated consequently (in a single line) in superscript letters and separated by semi-column.

Table caption must be placed above corresponding Table, while **Captions of the Illustrations** (Figs. Schemes...) must follow the corresponding item. **The captions, either for Tables or Illustrations**, should make the items comprehensible without reading of the main text (but clearly referenced in), must follow numerical order (Roman for Tables, Arabic for Illustrations), and should not be provided on separate sheets or as separate files.

High resolution Illustrations (named as Fig. 1, Fig. 2… and/or Scheme 1, Scheme 2…) in **TIF or EPS format** (JPG format is acceptable for photos, only) **must be additionally uploaded as a separate files or one archived (.zip, .rar) file.**

Illustrations should be prepared according to the ARTWORK INSTRUCTIONS - http://www.shd.org.rs/JSCS/jscs-pdf/Artwork_Instructions.pdf. **!**

All pages of the manuscript must be numbered continuously.

DESIGNATION OF PHYSICAL QUANTITIES AND UNITS

IUPAC recommendations for the naming of compounds should be followed. SI units, or other permissible units, should be employed. The designation of physical quantities must be in italic throughout the text (including figures, tables and equations), whereas the units and indexes (except for indexes having the meaning of physical quantities) are in upright letters. They should be in Times New Roman font. In graphs and tables, a slash should be used to separate the designation of a physical quantity from the unit

(example: p / kPa, j / mA cm^{-2}, t / °C, T_0 / K, τ / h, ln (j / mA cm^{-2})…). Designations such as: p (kPa), t [min]…, are not acceptable. However, if the full name of a physical quantity is unavoidable, it should be given in upright letters and separated from the unit by a comma (example: Pressure, kPa; Temperature, K; Current density, mA cm^{-2}…). Please do not use the axes of graphs for additional explanations; these should be mentioned in the figure captions and/or the manuscript (example: "pressure at the inlet of the system, kPa" should be avoided). The axis name should follow the direction of the axis (the name of y-axis should be rotated by 90°). Top and right axes should be avoided in diagrams, unless they are absolutely necessary.

Latin words, as well as the names of species, should be in *italic*, as for example: *i.e.*, *e.g.*, *in vivo*, *ibid*, *Calendula officinalis* L., *etc*. The branching of organic compound should also be indicated in *italic*, for example, *n*-butanol, *tert*-butanol, *etc*.

Decimal numbers must have decimal points and not commas in the text (except in the Serbian abstract), tables and axis labels in graphical presentations of results. Thousands are separated, if at all, by a comma and not a point.

Mathematical and chemical equations should be given in separate lines and must be numbered, Arabic numbers, consecutively in parenthesis at the end of the line. All equations should be embedded in the text Complex equations (fractions, integrals, matrix…) should be prepared with the aid of the **Microsoft Equation 3.0** (or higher) or **MathType** (Do not use them to create simple equations and labels). **Using the Insert -> Equation option, integrated in MS Office 2010 and MS Office 2013, as well as insertion of equation objects within paragraph text IS NOT ALLOWED.**

ARTICLE STRUCTURE

- TITLE PAGE;
- MAIN TEXT – including Tables and Illustrations with corresponding captions;
- SUPPLEMENTARY MATERIAL (optional**)**

Title page

- **Title** in bold letters, should be clear and concise, preferably 12 words or less. The use of non-standard abbreviations, symbols and formulae is discouraged.
- AUTHORS' NAMES in capital letters with the full first name, initials of further names separated by a space and surname. Commas should separate the author's names except for the last two names when 'and' is to be used. In multi-affiliation manuscripts, the author's affiliation should be indicated by an Arabic number placed in superscript after the name and before the affiliation. Use * to denote the corresponding author(s).
- *Affiliations* should be written in italic. The e-mail address of the corresponding author should be given after the affiliation(s).
- *Abstract:* A one-paragraph abstract written of 150 – 200 words in an impersonal form indicating the aims of the work, the main results and conclusions should be given and clearly set off from the text. Domestic authors should also submit, on a separate page, an Abstract - Izvod, the author's name(s) and affiliation(s) in Serbian (Cyrillic letters). (Домаћи аутори морају доставити Извод (укључујући имена аутора и афилијацију) на српском језику, исписане ћирилицом, иза Захвалнице, а пре списка референци.) For authors outside Serbia, the Editorial Board will provide a Serbian translation of their English abstract.
- *Keywords:* Up to 6 keywords should be given. Do not use words appearing in the manuscript title
- RUNNING TITLE: A one line (maximum five words) short title in capital letters should be provided.

Main text – should have the form:

- **INTRODUCTION,**
- **EXPERIMENTAL (RESULTS AND DISCUSSION),**
- **RESULTS AND DISCUSSION (EXPERIMENTAL),**
- **CONCLUSIONS,**
- **NOMENCLATURE (optional) and**
- ***Acknowledgements*: If any.**
- REFERENCES (Citation of recent papers published in chemistry journals that highlight the significance of work to the general readership is encouraged.)

The sections should be arranged in a sequence generally accepted for publication in the respective fields. They subtitles should be in capital letters, centred and NOT numbered.

- The INTRODUCTION should include the aim of the research and a concise description of background information and related studies directly connected to the paper.
- The EXPERIMENTAL section should give the purity and source of all employed materials, as well as details of the instruments used. The employed methods should be described in sufficient detail to enable experienced persons to repeat them. Standard procedures should be referenced and only modifications described in detail. On no account should results be included in the experimental section.

Chemistry

Detailed information about instruments and general experimental techniques should be given in all necessary details. If special treatment for solvents or chemical purification were applied that must be emphasized.

Example: Melting points were determined on a Boetius PMHK or a Mel-Temp apparatus and were not corrected. Optical rotations were measured on a Rudolph Research Analytical automatic polarimeter, Autopol IV in dichloromethane (DCM) or methanol (MeOH) as solvent. IR spectra were recorded on a Perkin-Elmer spectrophotometer FT-IR 1725X. ^{1}H and ^{13}C NMR spectra were recorded on a Varian Gemini-200 spectrometer (at 200 and 50 MHz, respectively), and on a Bruker Ultrashield Advance III spectrometer (at 500 and 125 MHz, respectively) employing indicated solvents (*vide infra*) using TMS as the internal standard. Chemical shifts are expressed in ppm (δ / ppm) values and coupling constants in Hz (J / Hz). ESI-MS spectra were recorded on Agilent Technologies 6210 Time-Of-Flight LC-MS instrument in positive ion mode with CH_3CN/H_2O 1/1 with 0.2 % HCOOH as the carrying solvent solution. Samples were dissolved in CH_3CN or MeOH (HPLC grade purity). The selected values were as follows: capillary voltage = 4 kV, gas temperature = 350 °C, drying gas flow 12 L min^{-1}, nebulizer pressure = 310 kPa, fragmentator voltage = 70 V.The elemental analysis was performed on the Vario EL III- C,H,N,S/O Elemental Analyzer (Elementar Analysensysteme GmbH, Hanau-Germany). Thin-layer chromatography (TLC) was performed on precoated Merck silica gel 60 F254 and RP-18 F254 plates. Column chromatography was performed on Lobar LichroPrep Si 60 (40-63 μm), RP-18 (40-63 µm) columns coupled to a Waters RI 401 detector, and on Biotage SP1 system with UV detector and FLASH 12+, FLASH 25+ or FLASH 40+ columns pre packed with KP-SIL [40-63 µm, pore diameter 6 nm (60 Å)], KP-C18-HS (40-63 µm, pore diameter 9 nm (90 Å) or KP-NH [40-63 µm, pore diameter 10 nm (100 Å)] as adsorbent. Compounds were analyzed for purity (HPLC) using a Waters 1525 HPLC dual pump system equipped with an Alltech, Select degasser system, and dual λ 2487 UV-VIS detector. For data processing, Empower software was used (methods A and B). Methods C and D: Agylent Technologies 1260 Liquid Chromatograph equipped with Quat Pump (G1311B), Injector (G1329B) 1260 ALS, TCC 1260 (G1316A) and Detector 1260 DAD VL+ (G1315C). For data processing, LC OpenLab CDS ChemStation software was used. For details, see Supporting Information.

1. Synthesis experiments

Each paragraph describing a synthesis experiment should begin with the name of the product and any structure number assigned to the compound in the Results and Discussions section. Thereafter, the compound should be identified by its structure number. Use of standard abbreviations or unambiguous molecular formulas for reagents and solvents, and of structure numbers rather than chemical names to identify starting materials and intermediates, is encouraged.

When a new or improved synthetic method is described, the yields reported in key experimental examples, and yields used for comparison with existing methods, should represent amounts of isolated and purified products, rather than chromategraphically or spectroscopically determined yields. Reactant quantities should be reported in weight and molar units and for product yields should be reported in weight units; percentage yields should only be reported for materials of demonstrated purity. When chromatography is used for product purification, both the support and solvent should be identified.

2. Microwave experiments

Reports of syntheses conducted in microwave reactors must clearly indicate whether sealed or open reaction vessels were used and must document the manufacturer and model of the reactor, the method of monitoring the reaction mixture temperature, and the temperature-time profile. Reporting a wattage rating or power setting is not an acceptable alternative to providing temperature data. Manuscripts describing work done with domestic (kitchen) microwave ovens will not be accepted except for studies where the unit is used for heating reaction mixtures at atmospheric pressure.

3. Compound characterization

The Journal upholds a high standard for compound characterization to ensure that substances being added to the chemical literature have been correctly identified and can be synthesized in known yield and purity by the reported preparation and isolation methods. For **all new** compounds, evidence adequate to establish both **identity** and **degree of purity** (homogeneity) must be provided.

Identity - *Melting point.* All homogeneous solid products (*e.g.* not mixtures of isomers) should be characterized by melting or decomposition points. The colors and morphologies of the products should also be noted.

Specific rotations. Specific rotations based on the equation $[\alpha]^t;D = (100\ \alpha) / (l\ c)$ should be reported as unitless numbers as in the following example: $[\alpha]^{20}$; D = -25.4 (c 1.93, $CHCl_3$), where c / g mL^{-1} is concentration and l / dm is path length. The units of the specific rotation, (deg mL) / (g dm), are implicit and are not included with the reported value.

Spectra/Spectral Data. Important IR adsorptions should be given.

For all new diamagnetic substances, NMR data should be reported (^1H, ^{13}C, and relevant heteronuclei). ^1H NMR chemical shifts should be given with two digits after the decimal point. Include the number of protons represented by the signal, signal multiplicity, and coupling constants as needed (J italicized, reported with up to one digit after the decimal). The number of bonds through which the coupling is operative, ^xJ, may be specified by the author if known with a high degree of certainty. ^{13}C NMR signal shifts should be rounded to the nearest 0.01 ppm unless greater precision is needed to distinguish closely spaced signals. Field strength should be noted for each spectrum, not as a comment in the general experimental section. Hydrogen multiplicity (C, CH, CH_2, CH_3) information obtained from routine DEPT spectra should be included. If detailed signal assignments are made, the type of NOESY or COSY methods used to establish atom connectivity and spatial relationships should be identified in the Supporting Information. Copies of spectra should also be included where structure assignments of complex molecules depend heavily on NMR interpretation. Numbering system used for assignments of signals should be given in the Supporting Information with corresponding general structural formula of named derivative.

HPLC/LCMS can be substituted for biochemistry papers where the main focus is not on compound synthesis.

HRMS/elemental analysis. To support the molecular formula assignment, HRMS data accurate within 5 ppm, or combustion elemental analysis [carbon and hydrogen (and nitrogen, if present)] data accurate within 0.5 %, should be reported for new compounds. HRMS data should be given in format as is usually given for combustion analysis: calculated mass for given formula following with observed mass: (+)ESI-HRMS *m/z*: [molecular formula + H]$^+$ calculated mass, observed mass. Example: (+)ESI-HRMS *m/z*: calculated for [$C_{13}H_8BrCl_2N$ + H^+] 327.92899, observed 327.92792.

NOTE: in certain cases, a crystal structure may be an acceptable substitute for HRMS/elemental analysis.

Biomacromolecules. The structures of biomacromolecules may be established by providing evidence about sequence and mass. Sequences may be inferred from the experimental order of amino acid, saccharide, or nucleotide coupling, from known sequences of templates in enzyme-mediated syntheses, or through standard sequencing techniques. Typically, a sequence will be accompanied by MS data that establish the molecular weight.

Example: Product was isolated upon column chromatography [dry flash (SiO_2, eluent EA, EA/MeOH gradient 95/5 → 9/1, EA/MeOH/NH_3 gradient 18/0.5/0.5 → 9/1/1, and flash chromatography (Biotage SP1, RP column, eluent MeOH/H_2O gradient 75/25 → 95/5, N-H column, eluent EA/Hex gradient 6/3 → EA). was obtained after flash column chromatography (Biotage SP NH column, eluent hexane/EA 4:6 → 2:6). Yield 968.4 mg (95 %). Colorless foam softens at 96-101 °C. $[\alpha]^{20}$; D = +0,163 (c =2.0×10^{-3} g/mL, CH_2Cl_2). IR (ATR): 3376w, 2949m, 2868w, 2802w, 1731s, 1611w, 1581s, 1528m, 1452m, 1374s, 1331w, 1246s, 1171m, 1063w, 1023m, 965w, 940w, 881w, 850w, 807w, cm^{-1}. ^1H NMR (500 MHz, $CDCl_3$, δ): 8.46 (*d*, 1H, J = 5.4, H-2'), 7.89 (*s*, 1H, J = 2.0, H-8'), 7.71 (*d*, 1H, J = 8.9, H-5'), 7.30 (*dd*, 1H, J_1 = 8.8, J_2 = 2.1, H-6'), 6.33 (*d*, 1H, J = 5.4, H-3'), 6.07 (*s*, HN-Boc, exchangeable with D_2O), 5.06 (*s*, 1H, H-12), 4.92-4.88 (*m*, 1H, H-7), 4.42 (*bs*, H-3), 3.45 (*s*,CH_3-N), 3.33 (*bs*, H-9'), 3.05-2.95 (*m*, 2H, H-11'), 2.70-2.43 (*m*, 2H, H-24) and HN, exchangeable with D_2O), 2.07 (*s*, CH_3COO), 2.04 (*s*, CH_3COO), 1.42 (*s*, 9H, $(CH_3)_3C$-N(Boc)), 0.88 (*s*, 3H, CH_3-10), 0.79 (*d*, 3H,J = 6.6, CH_3-20), 0.68 (*s*, 3H, CH_3-13). ^{13}C NMR (125 MHz, $CDCl_3$, δ): 170.34, 170.27, 151.80, 149.92, 148.87, 134.77, 128.36, 125.11, 121.43, 117.29, 99.98, 75.41, 70.82, 50.43, 49.66, 47.60, 47.33, 44.97, 43.30, 41.83, 41.48, 37.65, 36.35, 35.44, 34.89,

34.19, 33.23, 31.24, 28.79, 28.35, 27.25, 26.45, 25.45, 22.74, 22.63, 21.57, 21.31, 17.85, 12.15. (+)ESI-HRMS (*m/z*): calculated for $[C_{45}H_{67}ClN_4O_6 + H]^+$ 795.48219, observed 795.48185. Combustion analysis for $C_{45}H_{67}ClN_4O_6$: Calculated. C 67.94, H 8.49, N 7.04; found C 67.72, H 8.63, N 6.75. HPLC purity: method A: RT 1.994, area 99.12 %; method C: RT 9.936, area 98.20 %.

Purity **-** Evidence for documenting compound purity should include one or more of the following:

a) Well-resolved high field 1D ^{1}H NMR spectrum showing at most only trace peaks not attributable to the assigned structure and a standard 1D proton-decoupled ^{13}C NMR spectrum. Copies of the spectra should be included as figures in the Supporting Information.
b) Quantitative gas chromatographic analytical data for distilled or vacuum-transferred samples, or quantitative HPLC analytical data for materials isolated by column chromatography or separation from a solid support. HPLC analyses should be performed in two diverse systems. The stationary phase, solvents (HPLC), detector type, and percentage of total chromatogram integration should be reported; a copy of the chromatograms may be included as a figure in the Supporting Information.
c) Electrophoretic analytical data obtained under conditions that permit observing impurities present at the 5 % level.

HRMS data may be used to support a molecular formula assignment **but cannot be used as a criterion of purity**.

4. Biological Data

Quantitative biological data are required for all tested compounds. Biological test methods must be referenced or described in sufficient detail to permit the experiments to be repeated by others. Detailed descriptions of biological methods should be placed in the experimental section. Standard compounds or established drugs should be tested in the same system for comparison. Data may be presented as numerical expressions or in graphical form; biological data for extensive series of compounds should be presented in tabular form. Tables consisting primarily of negative data will not usually be accepted; however, for purposes of documentation they may be submitted as supporting information. Active compounds obtained from combinatorial syntheses should be resynthesized and retested to verify that the biology conforms to the initial observation.

Statistical limits (statistical significance) for the biological data are usually required. If statistical limits cannot be provided, the number of determinations and some indication of the variability and reliability of the results should be given. References to statistical methods of calculation should be included. Doses and concentrations should be expressed as molar quantities (*e.g.*, mol/kg, μmol/kg, M, mM). The routes of administration of test compounds and vehicles used should be indicated, and any salt forms used (hydrochlorides, sulfates, *etc.*) should be noted. The physical state of the compound dosed (crystalline, amorphous; solution, suspension) and the formulation for dosing (micronized, jet-milled, nanoparticles) should be indicated. For those compounds found to be inactive, the highest concentration (*in vitro*) or dose level (*in vivo*) tested should be indicated.

- The RESULTS AND DISCUSSION should include concisely presented results and there significance discussed and compared to relevant literature data. The results and discussion may be combined or kept separate.
- The inclusion of a CONCLUSION section, which briefly summarizes the principal conclusions, is recommended.
- NOMENCLATURE is optional but, if the authors wish, a list of employed symbols may be included.
- REFERENCES should be numbered sequentially as they appear in the text. Please note that any reference numbers appearing in the Illustrations and/or Tables and corresponding captions must follow the numbering sequence of the paragraph in which they appear for the first time. When cited, the reference number should be superscripted in Font 12, following any punctuation mark. In the reference list, they should be in normal position followed by a full stop. Reference entry must not be formatted using Carriage returns (enter key; ↵ key) or multiple space key. The formatting of references to published work should follow the *Journal'*s style as follows:

Journals[a]:	A. B. Surname1, C. D. Surname2, *J. Serb. Chem. Soc.* **Vol** (Year) first page Number (https://doi.org/doi)[b]
Books:	A. B. Surname1, C. D. Surname2, *Name of Book*, Publisher, City, Year, pp. 100-101 (https://doi.org/doi)[b]
Compilations:	A. B. Surname1, C. D. Surname2, in *Name of Compilation*, A. Editor1, C. Editor2, Ed(s)., Publisher, City, Year, p. 100 (https://doi.org/doi)[b]
Proceedings:	A. B. Surname1, C. D. Surname2, in *Proceedings of Name of the Conference or Symposium*, (Year), Place of the Conference, Country, *Title of the Proceeding*, Publisher, City, Year, p. or Abstract No. 100
Patents:	A. B. Inventor1, C. D. Inventor2, (Holder), Country Code and patent number (registration year)
Chemical Abstracts:	A. B. Surname1, C. D. Surname2, *Chem. Abstr*. CA 234 567a; For non-readily available literature, the Chemical Abstracts reference should be given in square brackets: [C.A. 139/2003 357348t] after the reference
Standards:	EN ISO 250: *Name of the Standard* (Year)
Websites:	Title of the website, URL in full (date accessed)

[a] When citing Journals, the International Library Journal abbreviation is required. Please consult, *e.g.*, https://images.webofknowledge.com/WOK46/help/WOS/A_abrvjt.html

[b] doi should be replaced by doi number of the Article, for example: http://dx.doi.org/10.2298/JSC161212085B (as active link). If doi do not exist, provide the link to the online version of the publication.

Only the last entry in the reference list should end with a full stop.

The names of all authors should be given in the list of references; the abbreviation *et al.* may only be used in the text. The original journal title is to be retained in the case of publications published in any language other than English (please denote the language in parenthesis after the reference). Titles of publications in non-Latin alphabets should be transliterated. Russian references are to be transliterated using the following transcriptions:

ж→zh, х→kh, ц→ts, ч→ch, ш→sh, щ→shch, ы→y, ю→yu, я→ya, э→e, й→i, ь→’.

Supplementary material

Authors are encouraged to presentthe information and results non-essential to the understanding of their paper as SUPPLEMENTARY MATERIAL (can be uploaded inStep 4 of Online Submission). This material may include as a rule, but is not limited to, the presentation of analytical and spectral data demonstrating the identity and purity of synthesized compounds, tables containing raw data on which calculations were based, series of figures where one example would remain in the main text, etc. The Editorial Board retain the right to assign such information and results to the Supplementary material when deemed fit. Supplementary material does not appear in printed form but can be downloaded from the web site of the JSCS.

Mathematical and chemical equations should be given in separate lines and must be numbered, Arabic numbers, consecutively in parenthesis at the end of the line. All equations should be embedded in the text Complex equations (fractions, integrals, matrix…) should be prepared with the aid of the Microsoft Equation 3.0 (or higher) or MathType (Do not use them to create simple equations and labels). Using the Insert -> Equation option, integrated in MS Office 2010 and MS Office 2013, as well as insertion of equation objects within paragraph text IS NOT ALLOWED.

Deposition of crystallographic data

Prior to submission, the crystallographic data included in a manuscript presenting such data should be deposited at the appropriate database. Crystallographic data associated with organic and metal-organic structures should be deposited at the Cambridge Crystallographic Data Centre (CCDC) by e-mail to **deposit@ccdc.cam.ac.uk**

Crystallographic data associated with inorganic structures should be deposited with the Fachinformationszentrum Karlsruhe (FIZ) by e-mail to **crysdata@fiz-karlsruhe.de**. A deposition number will then be provided, which should be added to the reference section of the manuscript.

For detailed instructions please visit the JSCS website:
https://www.shd-pub.org.rs/index.php/JSCS/Instructions

ARTWORK INSTRUCTIONS

JSCS accepts only **TIFF** or **EPS** formats, as well as **JPEG** format (only for colour and greyscale photographs) for electronic artwork and graphic files. **MS files** (Word, PowerPoint, Excel, Visio) **NOT acceptable**. Generally, scanned instrument data sheets should be avoided. Authors are responsible for the quality of their submitted artwork. Every single Figure or Scheme, as well as any part of the Figure (A, B, C…) should be prepared according to following instructions (every part of the figure, A, B, C…, must be submitted as an independent single graphic file):

TIFF

Virtually all common artwork and graphic creation software is capable of saving files in TIFF format. This 'option' can normally be found under 'the 'Save As...' or 'Export...' commands in the 'File' menu.

TIFF (Tagged Image File Format) is the recommended file format for bitmap, greyscale and colour images.

- Colour images should be in the RGB mode
- When supplying TIFF files, please ensure that the files are supplied at the correct resolution:
    1. Line artwork: minimum of 1000 dpi
    2. RGB image: minimum of 300 dpi
    3. Greyscale image: minimum of 300 dpi
    4. Combination artwork (line/greyscale/RGB): minimum of 500 dpi
- Images should be tightly cropped, without frame and any caption.
- If applicable please re-label artwork with a font supported by JSCS (Arial, Helvetica, Times, Symbol) and ensure it is of an appropriate font size.
- Save an image in TIFF format with LZW compression applied.
- It is recommended to remove Alpha channels before submitting TIFF files.
- It is recommended to flatten layers before submitting TIFF files.

Please be sure that quality of an image cannot be increased by changing the resolution from lower to higher, but only by rescanning or exporting the image with higher resolution, which can be set in usual "settings" facilities.

EPS

Virtually all common artwork creation software, such as Canvas, ChemDraw, CorelDraw, SigmaPlot, Origin Lab…, are capable of saving files in EPS format. This 'option' can normally be found under the 'Save As...' or 'Export...' commands in the 'File' menu.

For vector graphics, EPS (Encapsulated PostScript) files are the preferred format as long as they are provided in accordance with the following conditions:

- when they contain bitmap images, the bitmaps should be of good resolution (see instructions for TIFF files)
- when colour is involved, it should be encoded as RGB
- an 8-bit preview/header at a resolution of 72 dpi should always be included
- embed fonts should always included and only the following fonts should be used in artwork: Arial, Helvetica, Times, Symbol
- the vertical space between the parts of an illustration should be limited to the bare necessity for visual clarity
- no data should be present outside the actual illustration area
- line weights should range from 0.35 pt to 1.5 pt
- when using layers, they should be reduced to one layer before saving the image (Flatten Artwork)

JPEG

Virtually all common artwork and graphic creation software is capable of saving files in JPEG format. This 'option' can normally be found under 'the 'Save As...' or 'Export...' commands in the 'File' menu.

JPEG (Joint Photographic Experts Group) is the acceptable file format **only for colour and greyscale photographs**. JPEG can be created with respect to photo quality (low, medium, high; from 1 to 10), ensuring file sizes are kept to a minimum to aid easy file transfer. Images should have a minimum resolution of 300 dpi. Image width: minimum 3.0 cm; maximum 12.0 cm.

Please be sure that quality of an image cannot be increased by changing the resolution from lower to higher, but only by rescanning or exporting the image with higher resolution, which can be set in usual "settings" facilities.

SIZING OF ARTWORK

- JSCS aspires to have a uniform look for all artwork contained in a single article. Hence, it is important to be aware of the style of the journal.
- Figures should be submitted in black and white or, if required, colour (charged). If coloured figures or photographs are required, this must be stated in the cover letter and arrangements made for payment through the office of the Serbian Chemical Society.
- As a general rule, the lettering on an artwork should have a finished, printed size of 11 pt for normal text and no smaller than 7 pt for subscript and superscript characters. Smaller lettering will yield a text that is barely legible. This is a rule-of-thumb rather than a strict rule. There are instances where other factors in the artwork, (for example, tints and shadings) dictate a finished size of perhaps 10 pt. Lines should be of at least 1 pt thickness.
- When deciding on the size of a line art graphic, in addition to the lettering, there are several other factors to address. These all have a bearing on the reproducibility/readability of the final artwork. Tints and shadings have to be printable at the finished size. All relevant detail in the illustration, the graph symbols (squares, triangles, circles, *etc*.) and a key to the diagram (to explain the explanation of the graph symbols used) must be discernible.
- The sizing of halftones (photographs, micrographs,...) normally causes more problems than line art. It is sometimes difficult to know what an author is trying to emphasize on a photograph, so you can help us by identifying the important parts of the image, perhaps by highlighting the relevant areas on a photocopy. The best advice that can be given to graphics suppliers is not to over-reduce halftones. Attention should also be paid to magnification factors or scale bars on the artwork and they should be compared with the details inside. If a set of artwork contains more than one halftone, again please ensure that there is consistency in size between similar diagrams.

General sizing of illustrations which can be used for the Journal of the Serbian Chemical Society:

- Minimum fig. size: 30 mm width
- Small fig. size - 60 mm width
- Large fig. size - 90 mm width
- Maximum fig. size - 120 mm width

Pixel requirements (width) per print size and resolution for bitmap images:

	Image width	A	B	C
Minimal size	30 mm	**354**	**591**	**1181**
Small size	60 mm	**709**	**1181**	**2362**
Large size	90 mm	**1063**	**1772**	**3543**
Maximal size	120 mm	**1417**	**2362**	**4724**

A: 300 dpi > RGB or Greyscale image
B: 500 dpi > Combination artwork (line/greyscale/RGB)
C: 1000 dpi> Line artwork

The designation of physical quantities and graphs formatting

The designation of physical quantities on figures must be in italic, whereas the units are in upright letters. They should be in Times New Roman font. In graphs a slash should be used to separate the designation of a physical quantity from the unit (example: p / kPa, t °C, T_0 / K, τ / h, ln (j / mA cm^{-2})…). Designations such as: p (kPa), t [min]…, are not acceptable. However, if the full name of a physical quantity is unavoiable, it should be given in upright letters and separated from the unit by a comma (example: Pressure, kPa, Temperature, K…). Please do not use the axes of graphs for additional explanations; these should be mentioned in the figure captions and/or the manuscript (example: "pressure at the inlet of the system, kPa" should be avoided). The axis name should follow the direction of the axis (the name of y-axis should be rotated by 90°). Top and right axes should be avoided in diagrams, unless they are absolutely necessary. Decimal numbers must have decimal points and not commas in the axis labels in graphical presentations of results. Thousands are separated, if at all, by a comma and not a point.

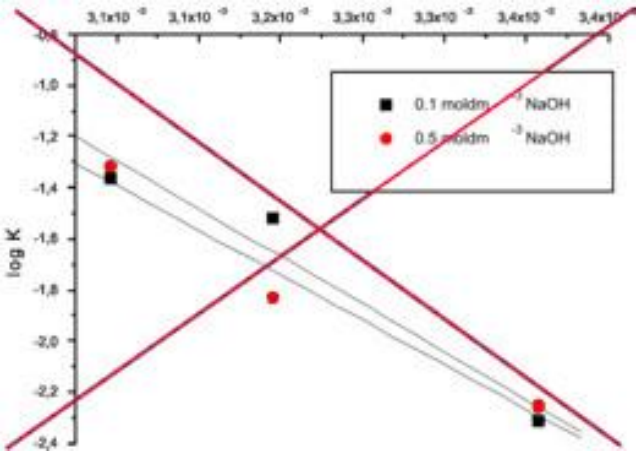

INCORRECT

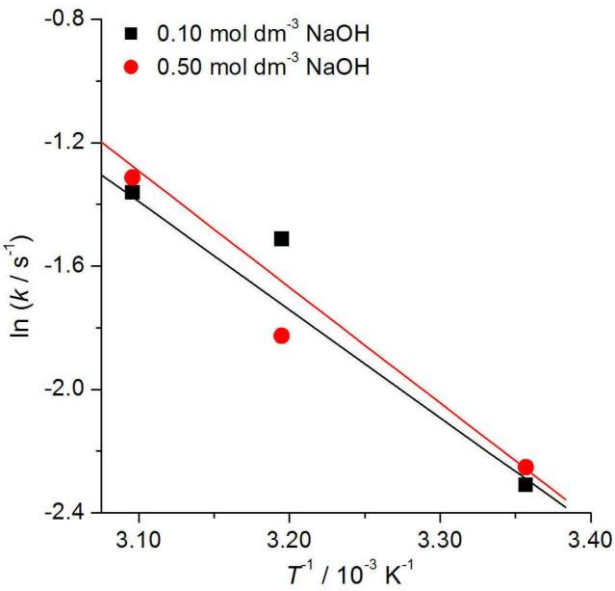

CORRECT

Journal of the Serbian Chemical Society
JSCS-info@shd.org.rs • www.shd.org.rs/JSCS

J. Serb. Chem. Soc. Vol. 87, No. 6 (2022)

CONTENTS*

Published by the Serbian Chemical Society
Karnegijeva 4/III, P.O. Box 36, 11120 Belgrade, Serbia
Printed by the Faculty of Technology and Metallurgy
Karnegijeva 4, P.O. Box 35-03, 11120 Belgrade, Serbia

* For colored figures in this issue please see electronic version at the Journal Home Page: http://www.shd.org.rs/JSCS/

Journal of the Serbian Chemical Society
JSCS@tmf.bg.ac.rs • www.shd.org.rs/JSCS

J. Serb. Chem. Soc. *87* (6) 669–675 (2022)
JSCS–5549

Original scientific paper
Published 28 April 2022

Palladium on carbon in PEG-400/cyclohexane: Recoverable and recyclable catalytic system for efficient decarbonylation of aldehydes

NATAŠA TERZIĆ-JOVANOVIĆ[1] and VLADIMIR AJDAČIĆ[2*#]

[1]*University of Belgrade – Institute of Chemistry, Technology and Metallurgy, National Institute of the Republic of Serbia, Njegoševa 12, 11000 Belgrade, Serbia and* [2]*Innovative Centre Ltd., Faculty of Chemistry, Studentski Trg 12–16, 11158 Belgrade, Serbia*

(Received 28 January, revised 28 February, accepted 7 March 2022)

Abstract: A simple methodology for the decarbonylation of aldehydes catalysed by commercially available palladium on carbon in a green two-solvent system is reported. Various aromatic, aliphatic and heteroaromatic aldehydes were transformed to the corresponding decarbonylated products in good yields. Product isolation from the reaction mixture is simple in practice, and the catalyst can be reused three times.

Keywords: green chemistry; defunctionalization; heterogeneous catalysis.

INTRODUCTION

The transformation of aldehydes into hydrocarbons (deformylation/decarbonylation) promoted by enzymes,[1] transition-metals[2] or metal-free reagents[3] is an important reaction in academic research[4] and industry.[5] The aldehyde group is an useful promoter of certain transformations, such as the Diels–Alder reaction, C–H activation, and domino oxa-Michael-aldol reaction, and its simple removal *via* decarbonylation after it has served its purpose has been extensively applied in numerous methodologies[6] and in the synthesis of complex molecules and natural products.[7] Some metals of the first, second and third transition series, including Ni,[8] Ru,[9] Rh,[10] Pd[11] and Ir[12] as well as complexes thereof, efficiently perform the mentioned transformation (Fig. 1). However, the toxicity and high cost of these metals is a major drawback from an economic and environmental point of view. Therefore, the use of recyclable heterogeneous catalysts for decarbonylation is both a greener and more economical alternative to homogeneous catalysis.[13]

* Corresponding author. E-mail: ajdacic@chem.bg.ac.rs
# Serbian Chemical Society member.
https://doi.org/10.2298/JSC220128024T

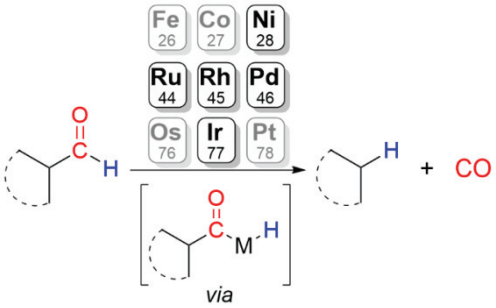

Fig. 1. Decarbonylation of aldehydes promoted by transition-metals.

EXPERIMENTAL

The general information

Pd/C (10 wt.% loading) was purchased from Sigma Aldrich. Aldehydes were mostly obtained from commercial sources and used without further purification, except for the 1-adamantanecarboxaldehyde,[14] 1-adamantaneacetaldehyde,[14] 1-prop-2-yn-1-yl-1*H*-indole-3-carbaldehyde[15] and 1-benzyl-1*H*-indole-3-carbaldehyde,[15] which were synthesized according to known procedures. Unless stated otherwise, solvents and other reagents were obtained from commercial sources and used without further purification. Dry-flash chromatography was performed on SiO_2 (0.018–0.032 mm). ^{1}H- and ^{13}C-NMR spectra were recorded on a Bruker Ultrashield Avance III spectrometer (at 500 and 125 MHz, respectively) and Varian 400/54 Premium Shielded spectrometer (at 400 and 101 MHz, respectively) using $CDCl_3$ (unless stated otherwise) as the solvent and tetramethylsilane (TMS) as an internal standard. The chemical shifts are expressed in ppm on the δ scale and they were calibrated relative to those of the solvent. GC–MS spectra of the synthesized compounds were acquired on an Agilent Technologies 7890A apparatus equipped with a DB-5 MS column (30 m×0.25 mm×0.25 µm), a 5975C MSD and FID detector. The selected values are as follows: carrier gas was He (1.0 mL/min), temperature linearly increased from 40–315 °C (10 °C/min), injection volume: 1 µL, temperature: 250 °C, temperature (FID detector): 300 °C, and EI mass spectra range: *m*/*z* 40–550. For determination of GC–MS yield, the internal standard (naphthalene) was added to the reaction mixture after the workup.

*General procedure for decarbonylation of aldehydes **2a**–**n***

*Decarbonylation of biphenyl-4-carbaldehyde to biphenyl (**2a**) (CAS Reg. No. 92-52-4).* Dry glass reaction tube purged with argon and equipped with a magnetic stir bar was charged with aldehyde (90 mg, 0.5 mmol), Pd/C (26 mg, 5 mol.% Pd), cyclohexane (750 µL) and PEG-400 (750 µL). The sealed tube was heated at 140 °C for 24 h. The reaction medium was then cooled to room temperature. The mixture of water and cyclohexane was then added to the reaction mixture. The layers were afterwards separated and the aqueous layer was washed with cyclohexane (5×5 mL). The organic layer was dried over Na_2SO_4, and the solvent was evaporated under reduced pressure. Compound **2a** was obtained after dry-flash column chromatography (SiO_2:cyclohexane) as a white solid (69.0 mg, 90 %).

*Decarbonylation of 2-naphthaldehyde to naphthalene (**2b**) (CAS Reg. No. 91-20-3).* Following the general procedure for decarbonylation, compound **2b** was prepared from aldehyde (78.0 mg, 0.5 mmol) using Pd/C (26.0 mg, 5 mol.% Pd) in a mixture of cyclohexane (750 µL) and PEG-400 (750 µL) and was obtained after dry-flash column chromatography (SiO_2:cyclohexane) as a white solid (45.1 mg, 70 %).

*Decarbonylation of anthracene-9-carbaldehyde to anthracene (**2c**) (CAS Reg. No. 120--12-7).* Following the general procedure for decarbonylation, compound **2c** was prepared from aldehyde (103.2 mg, 0.5 mmol) using Pd/C (26.0 mg, 5 mol % Pd) in a mixture of cyclohexane (750 μL) and PEG-400 (750 μL) and was obtained after dry-flash column chromatography (SiO_2:cyclohexane) as a white crystalline solid (73.2 mg, 82 %).

*Decarbonylation of 4-nitrobenzaldehyde to nitrobenzene (**2d**) (CAS Reg. No. 98-95-3).* Following the general procedure for decarbonylation, compound **2d** was prepared from aldehyde (75.6 mg, 0.5 mmol) using Pd/C (26.0 mg, 5 mol % Pd) in a mixture of cyclohexane (750 μL) and PEG-400 (750 μL) and was obtained as a yellow oil (GC–MS yield 90 % based on naphthalene).

*Decarbonylation of 5-fluoro-2-methoxybenzaldehyde to 4-fluoroanisol (**2e**) (CAS Reg. No. 459-60-9).* Following the general procedure for decarbonylation, compound **2e** was prepared from aldehyde (77 mg, 0.5 mmol) using Pd/C (26 mg, 5 mol % Pd) in a mixture of cyclohexane (750 μL) and PEG-400 (750 μL) (GC–MS yield 60 % based on methyl benzoate as standard).

*Decarbonylation of diphenylacetaldehyde to diphenylmethyl (**2h**) (CAS Reg. No. 101-81--5).* Following the general procedure for decarbonylation, compound **2h** was prepared from aldehyde (89 μL, 0.5 mmol) using Pd/C (26.0 mg, 5 mol % Pd) in a mixture of cyclohexane (750 μL) and PEG-400 (750 μL) and was obtained after dry-flash column chromatography (SiO_2:cyclohexane) as a colorless oil (78.1 mg, 93 %).

*Decarbonylation of 3-(1,3-benzodioxol-5-yl)-2-methylpropanal to dihydrosafrole (**2i**) (CAS Reg. No. 94-58-6).* Following the general procedure for decarbonylation, compound **2i** was prepared from aldehyde (83 μL, 0.5 mmol) using Pd/C (26 mg, 5 mol % Pd) in a mixture of cyclohexane (750 μL) and PEG-400 (750 μL) and was obtained after dry-flash column chromatography (SiO_2:cyclohexane) as a colorless oil (59.3 mg, 72 %).

*Decarbonylation of 1-adamantanecarboxaldehyde to adamantane (**2j**) (CAS Reg. No. 281-23-2).* Following the general procedure for decarbonylation, compound **2j** was prepared from aldehyde (82.3 mg, 0.5 mmol) using Pd/C (26.0 mg, 5 mol % Pd) in a mixure of cyclohexane (750 μL) and PEG-400 (750 μL) and was obtained after dry-flash column chromatography (SiO_2:cyclohexane) as a colorless solid (67.3 mg, 84 %).

*Decarbonylation of 1-adamantaneacetaldehyde to 1-methyl adamantane (**2k**) (CAS Reg. No. 768-91-2).* Following the general procedure for decarbonylation, compound **2k** was prepared from aldehyde (89.1 mg, 0.5 mmol) using Pd/C (26.0 mg, 5 mol % Pd) in a mixure of cyclohexane (750 μL) and PEG-400 (750 μL) and was obtained after dry-flash column chromatography (SiO_2:cyclohexane) as a colorless solid (74.0 mg, 73 %).

*Decarbonylation of benzo[*b*]thiophene-3-carboxaldehyde to benzo[*b*]thiophene (**2l**) (CAS Reg. No. 95-15-8).* Following the general procedure for decarbonylation, compound **2l** was prepared from aldehyde (81.1 mg, 0.5 mmol) using Pd/C (26.0 mg, 5 mol % Pd) in a mixture of cyclohexane (750 μL) and PEG-400 (750 μL) and was obtained after dry-flash column chromatography (SiO_2:cyclohexane) as a colorless solid (47.1 mg, 70 %).

*Decarbonylation of 1-prop-2-yn-1-yl-1*H*-indole-3-carbaldehyde to 1-prop-2-yn-1-yl--1*H*-indole (**2m**) (CAS Reg. No. 19017-00-6).* Following the general procedure for decarbonylation, compound **2m** was prepared from aldehyde (92.3 mg, 0.5 mmol) using Pd/C (26.1 mg, 5 mol % Pd) in a mixure of cyclohexane (750 μL) and PEG-400 (750 μL) and was obtained after dry-flash column chromatography (SiO_2:cyclohexane) as a colorless solid (53.3 mg, 68 %).

*Decarbonylation of 1-benzyl-1*H*-indole-3-carbaldehyde to 1-benzyl-1*H*-indole (**2n**) (CAS Reg. No. 3377-71-7).* Following the general procedure for decarbonylation, compound

2n was prepared from aldehyde (89.2 mg, 0.5 mmol) using Pd/C (118.0 mg, 5 mol % Pd) in a mixture of cyclohexane (750 µL) and PEG-400 (750 µL) and was obtained after dry-flash column chromatography (SiO_2:cyclohexane) as a colorless solid (68.0 mg, 66 %).

Spectral data of the compounds are given in Supplementary material to this paper

*Recycling of Pd/C and PEG-400 catalytic system for decarbonylation of aldehyde (**1a**)*

Dry glass reaction tube purged with argon and equipped with a magnetic stir bar was charged with aldehyde (**1a**, 90 mg, 0.5 mmol), Pd/C (26 mg, 5 mol % Pd), cyclohexane (750 µL) and PEG-400 (750 µL). The sealed tube was heated at 140 °C for 24 h. After the completion of the reaction, the cyclohexane layer was decanted with a pipette and PEG-400 layer was washed with cyclohexane (5×2 mL). The formed residue (Pd/C in PEG-400) was used for next reaction cycles following the general reaction procedure.

RESULTS AND DISCUSSION

Herein we report the efficient decarbonylation of aromatic, heteroaromatic and aliphatic aldehydes mediated by palladium on carbon in ecologically acceptable solvents, cyclohexane and PEG-400. To determine the optimal reaction conditions, biphenyl-4-carboxaldehyde (**1a**) was used as the model substrate (TABLE I).

TABLE I. Optimization of reaction conditions

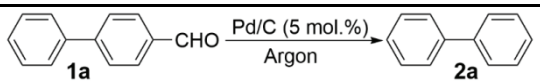

Entry	Solvent	*t* / °C	Time, h	Yield[a], %
1	H_2O	160	24	trace
2	PEG-400	140	24	42
3	PEG-400	140	44	26
4	PEG-400/ cyclohexane (1:1, v,v)	140	24	90

[a]Isolated yield

The initial conditions of 5 mol % palladium on carbon in H_2O at 160 °C provided only trace amounts of the corresponding decarbonylated product (entry 1). When PEG-400 was used instead of H_2O, the yield increased to 42 % (entry 2). Increasing the reaction time from 24 to 44 h led to a significant reduction in the yield (26 %, entry 3). After a detailed analysis of the reaction mixture, it was found that the reduced yield resulted from product evaporation. Finally, the addition of cyclohexane as a co-solvent increased the yield to 90 %.

To our surprise, after the reaction mixture had cooled, the catalyst particles were located exclusively in the PEG-400 layer (Fig. 2).

The product was isolated by careful decantation of cyclohexane and additional extraction of the PEG-400 layer with cyclohexane. The residual catalyst in PEG-400 was used successively three more times under the same reaction conditions, without a significant loss of activity (Fig. 3).

Fig. 2. Reaction mixture after completion of the reaction.

Employing the optimized decarbonylation conditions, the aldehyde substrate scope was investigated (Scheme 1). The non-functional polycyclic aromatic aldehydes (**1a**–**c**) were efficiently decarbonylated and the corresponding products (**2a**–**c**) were obtained in good yields. Benzaldehyde bearing an electron-withdrawing substituent (NO_2) **1d** generated the desired product **2d** in high yield. 2-Fluoro-4-methoxybenzaldehyde afforded the decarbonylated product **2e** in moderate yield. In the case of 4-bromobenzaldehyde (**1f**) and 4-formylbenzoic acid (**1g**) there was no reaction.

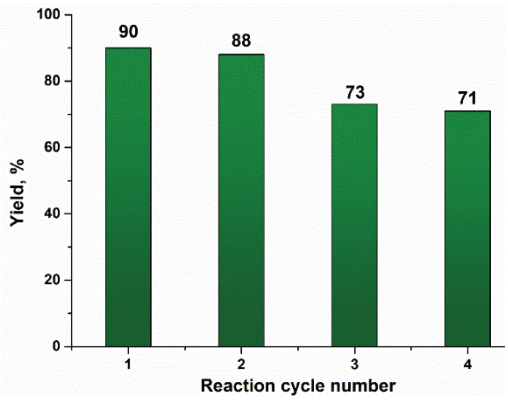

Fig. 3. Reusability of the Pd/C/PEG-400 catalytic system.

The substrate scope was then extended to aliphatic aldehydes. The aliphatic aldehydes with an aromatic core successfully produced the desired products (**2h**, and **i**) in good to excellent yields. Furthermore, the methodology was applied to the sterically demanding aldehydes, adamantane-1-carbaldehyde (**1j**) and 1-adamantylacetaldehyde (**1k**). The decarbonylated products, adamantane (**2j**) and methyladamantane (**2k**) were isolated in good yields. The decarbonylation of several heterocyclic aldehydes was also explored under the optimal reaction conditions. The decarbonylation of benzo[*b*]thiophene-3-carboxaldehyde (**1l**) afforded the desired product benzo[*b*]thiophene (**2l**) in good yield. In addition, the *N*-substituted indole derivates (**1m** and **n**) gave the corresponding decarbonylated products (**2m** and **n**) in good yields.

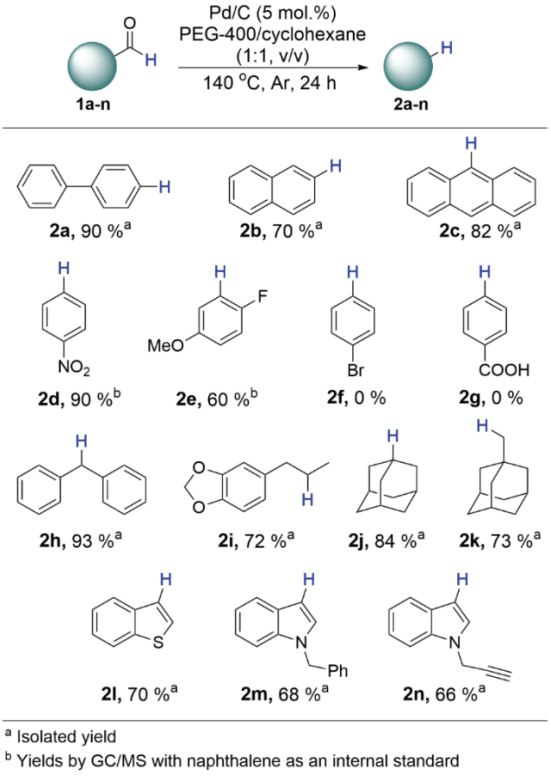

Scheme 1. Substrate scope.

CONCLUSION

To conclude, the ligand-free palladium-on-carbon-catalysed decarbonylation of aldehydes in ecologically acceptable solvents as an alternative to homogeneous catalysis was reported in this study. Various aldehydes were successfully decarbonylated in moderate to excellent yields. The formation of byproducts during the reaction and chromatography was not observed. Also, Pd/C and PEG-400 system could be recycled and reused in at least four consecutive reaction cycles, without significant loss of catalytic activity.

SUPPLEMENTARY MATERIAL

Additional data and information are available electronically at the pages of journal website: https://www.shd-pub.org.rs/index.php/JSCS/article/view/11599, or from the corresponding author on request.

Acknowledgments. This research was financially supported by the Ministry of Education, Science and Technological Development of Republic of Serbia (contract numbers: 451-03-9/2021-14/200168, 451-03-9/2021-14/200288 and 451-03-9/2021-14/200026) and Serbian Academy of Sciences and Arts under strategic projects programme-grant agreement No. 01-2019-F65.

ИЗВОД

ПАЛАДИЈУМ НА УГЉЕНИКУ У PEG-400/ЦИКЛОХЕКСАНУ: КАТАЛИТИЧКИ СИСТЕМ КОЈИ СЕ МОЖЕ РЕЦИКЛИРАТИ И ПОНОВО УПОТРЕБИТИ ЗА ЕФИКАСНО ДЕКАРБОНИЛОВАЊЕ АЛДЕХИДА

НАТАША ТЕРЗИЋ-ЈОВАНОВИЋ[1] и ВЛАДИМИР АЈДАЧИЋ[2]

[1]*Универзитету Београду, Институт за хемију, технологију и металургију (ИХТМ), Његошева 12, 11000 Београд и* [2]*Иновациони центар Хемијског факултета, Студентски трг 12–16, 11000 Београд*

Развијена је једноставна метода за декарбониловање алдехида користећи комерцијално доступни паладијум на угљенику уз употребу зелених растварача. Различити ароматични, алифатични и хетероароматични алдехиди могу се трансформисати у декарбониловане производе у добром приносу и без настајања споредних производа. Производи се једноставно изолују из реакционе смеше, а исти катализатор се може употребити још три пута без значајног смањења приноса.

(Примљено 28. јануара, ревидирано 28. фебруара, прихваћено 7. марта 2022)

REFERENCES

1. N. Li, H. Nørgaard, D. M. Warui, S. J. Booker, C. Krebs, J. M. B., Jr., *J. Am. Chem. Soc.* **133** (2011) 6158 (https://doi.org/10.1021/ja2013517)
2. A. Modak, D. Maiti, *Org. Biomol. Chem.* **14** (2016) 21 (https://doi.org/10.1039/C5OB01949D)
3. V. Ajdačić, S. Stepanović, M. Zlatovića, M. Grudena, I. M. Opsenica, *Synthesis* **48** (2016) 4423 (https://doi.org/10.1055/s-0035-1562615)
4. A G. J. S. Dawes, E. L. Scott, J. Le Nôtre, J. P. M. Sanders, J. H. Bitter, *Green Chem.* **17** (2015) 3231(https://doi.org/10.1039/C5GC00023H)
5. U. K. Bagha, J. K. Satpathy, G. Mukherjee, C. V. Sastri, S. P. de Visser, *Org. Biomol. Chem.* **19** (2021) 1879 (https://doi.org/10.1039/D0OB02204G)
6. H. Lu, T.-Y. Yu, P.-F. Xu, H. Wei, *Chem. Rev.* **121** (2021) 365 (https://doi.org/10.1021/acs.chemrev.0c00153)
7. Ž. Selaković, A. M. Nikolić, V. Ajdačić, I. M. Opsenica, *Eur. J. Org. Chem.* (**2022**) (https://doi.org/10.1002/ejoc.202101265)
8. K. Ding, S. Xu, R. Alotaibi, K. Paudel, E. W. Reinheimer, J. Weatherly, *J. Org. Chem.* **82** (2017) 4924 (https://doi.org/10.1021/acs.joc.7b00284)
9. G. Domazetis, B. Tarpey, D. Dolphin, B. R. James, J. *Chem. Soc. Chem. Commun.* (1980) 939 (https://doi.org/10.1039/C39800000939)
10. M. Kreis, A. Palmelund, L. Bunch, R. Madsen, *Adv. Synth. Catal.* **348** (2006) 2148 (https://doi.org/10.1002/adsc.200600228)
11. V. Ajdačić, A. Nikolić, M. Kerner, P. Wipf, I. M. Opsenica, *Synlett* **29** (2018) 1781(https://doi.org/10.1055/s-0037-1610433)
12. T. Iwai, T. Fujihara, Y. Tsuji, *Chem. Commun.* **46** (2008) 6215 (https://doi.org/10.1039/B813171F)
13. V. Ajdačić, A. Nikolić, S. Simić, D. Manojlović, Z. Stojanović, J. Nikodinović-Runić, I. M. Opsenica, *Synthesis* **50** (2018) 119 (https://doi.org/10.1055/s-0036-1590892).
14. N. Terzic, J. Konstantinovic, M. Tot, J. Burojevic, O. Djurkovic-Djakovic, J. Srbljanovic, T. Stajner, T. Verbic, M. Zlatovic, M. Machado, I.S. Albuquerque, M. Prudencio, R. J. Sciotti, S. Pecic, S. D'Alessandro, D. Taramelli, B. Solaja, *J. Med. Chem*. **59** (2016) 264 (https://doi.org/10.1021/acs.jmedchem.5b01374)
15. Y. Sawama, Y. Miki, H. Sajiki, *Synlett* **31** (2020) 699 (https://doi.org/10.1055/s-0040-1707993).

Journal of the Serbian Chemical Society
JSCS@tmf.bg.ac.rs • www.shd.org.rs/JSCS
J. Serb. Chem. Soc. 87 (6) S135–S147 (2022)
Supplementary material

SUPPLEMENTARY MATERIAL TO

Palladium on carbon in PEG-400/cyclohexane: Recoverable and recyclable catalytic system for efficient decarbonylation of aldehydes

NATAŠA TERZIĆ-JOVANOVIĆ[1] and VLADIMIR AJDAČIĆ[2]*

[1]*University of Belgrade – Institute of Chemistry, Technology and Metallurgy, National Institute of the Republic of Serbia, Njegoševa 12, 11000 Belgrade, Serbia and* [2]*Innovative Centre Ltd., Faculty of Chemistry, Studentski Trg 12–16, 11158 Belgrade, Serbia*

J. Serb. Chem. Soc. 87 (6) (2022) 669–675

SPECTRAL DATA OF THE SYNTHESIZED COMPOUNDS

*Biphenyl-4-carbaldehyde to biphenyl (**2a**).* ^{1}H-NMR (500 MHz, $CDCl_3$, δ / ppm): 7.60–7.55 (*m*, 4H), 7.45–7.40 (*m*, 4H), 7.36–7.31 (*m*, 2H). ^{13}C-NMR (125 MHz, $CDCl_3$, δ / ppm): 141.2, 128.7, 127.2, 127.2. EI-MS (*m*/*z* (%)): 154.1 $[M]^+$ (100), 153.1 (38), 152.1 (26), 76.1 (7).

*2-Naphthaldehyde to naphthalene (**2b**).* ^{1}H-NMR (500 MHz, $CDCl_3$, δ / ppm): 7.89 (*dd*, J_1 = 8.0 Hz, J_2 = 4.0 Hz, 4H), 7.53 (*dd*, J_1 = 8.0 Hz, J_2 = 4.0 Hz,4H). ^{13}C-NMR (125 MHz, $CDCl_3$, δ / ppm): 133.6, 128.0, 126.0. EI-MS (*m*/*z* (%)): 128.2 $[M]^+$ (100), 127.1 (16), 83.7 (11), 48.9 (16).

*Anthracene-9-carbaldehyde to anthracene (**2c**).* ^{1}H-NMR (500 MHz, $CDCl_3$, δ / ppm): 8.42 (*s*, 2 H), 8.05–7.95 (*m*, 4 H), 7.50–7.45 (*m*, 4 H). ^{13}C-NMR (125 MHz, $CDCl_3$, δ / ppm): 131.7, 128.1, 126.2, 125.3. EI-MS (*m*/*z* (%)): 178.1 $[M]^+$ (100), 176.0 (18), 152.0 (7), 89.2 (8).

*4-Nitrobenzaldehyde to nitrobenzene (**2d**).* EI-MS (*m*/*z* (%)): 123.0 $[M]^+$ (66), 93.1 (13), 77.0 (100), 51.1 (39).

*5-Fluoro-2-methoxybenzaldehyde to 4-fluoroanisol (**2e**).* EI-MS(*m*/*z* (%)): 126.0 $[M]^+$ (100), 96.0 (71), 83.1 (40), 57.1 (14).

*Diphenylacetaldehyde to diphenylmethyl (**2h**).* ^{1}H-NMR (400 MHz, $CDCl_3$, δ / ppm): 7.33-7.23 (*m*, 4H), 7.30–7.20 (*m*, 6H), 3.97 (*s*, 2H). ^{13}C-NMR (101 MHz, $CDCl_3$, δ / ppm): 140.9, 128.8, 128.3, 125.9, 41.8. EI-MS (*m*/*z* (%)): 168.1 $[M]^+$ (100). 152,1 (30), 91.1 (20).

*3-(1,3-Benzodioxol-5-yl)-2-methylpropanal to dihydrosafrole (**2i**).* ^{1}H-NMR (400 MHz, $CDCl_3$, δ / ppm): 6.79–6.56 (*m*, 3H), 5.90 (*s*, 2H), 2.50 (*dd*, J_1 = 8.5 Hz, J_2 = 6.7 Hz, 2H), 1.59 (*d*, J = 7.5 Hz, 2H), 1.26 (*s*, 2H), 0.92 (*t*, J = 7.3 Hz, 3H). ^{13}C-NMR (101 MHz, $CDCl_3$, δ / ppm): 147.3, 145.2, 136.4, 120.9, 108.7, 107.8, 100.5, 37.6, 29.5, 24.6, 13.5. EI-MS (*m*/*z* (%)): 164.1 $[M]^+$ (40), 135,1 (100), 105,1 (10), 77,1 (20).

* Corresponding author. E-mail: ajdacic@chem.bg.ac.rs

*1-Adamantanecarboxaldehyde to adamantane (**2j**).* ^{1}H-NMR (400 MHz, $CDCl_3$, δ / ppm): 1.86 (*bs*, 4H), 1.74 (*bs*, 12H). ^{13}C-NMR (101 MHz, $CDCl_3$, δ / ppm): 38.2, 28.8. EI--MS (*m/z* (%)): 136.1 $[M]^+$ (100), 121.1 (10), 107,1 (10), 93,1 (40), 79,1 (40).

*1-Adamantaneacetaldehyde to 1-methyl adamantane (**2k**).* ^{1}H-NMR (400 MHz, $CDCl_3$, δ / ppm): 1.92 (*bs*, 3H), 1.56–1.72 (*m*, 6H), 1.45 (*d*, *J* = 2.8 Hz, 6H), 0.76 (*s*, 3H). ^{13}C--NMR (125 MHz, $CDCl_3$, δ / ppm): 44.8, 37.1, 31,6, 29,0, 27.1. EI-MS (*m/z* (%)): 150.1 $[M]^+$ (20), 135,1 (100), 107,1 (10), 93,1 (30), 79,1 (20).

*Benzo[*b*]thiophene-3-carboxaldehyde to benzo[*b*]thiophene (**2l**).* ^{1}H-NMR (500 MHz, $CDCl_3$, δ / ppm): 7.88 (*d*, *J* = 8.0 Hz, 1H), 7.80–7.84 (*m*, 1H), 7.43 (*d*, *J* = 5.5 Hz, H), 7.30–7.37 (*m*, 3H). ^{13}C-NMR (125 MHz, $CDCl_3$, δ / ppm): 139.7, 139.6, 126.3, 124.2, 124.1, 123.8, 123.6, 122.5. EI-MS (*m/z* (%)): 134.0 $[M]^+$ (100), 128.1 (14), 89.1 (10).

*1-Prop-2-yn-1-yl-1*H*-indole-3-carbaldehyde to 1-prop-2-yn-1-yl-1*H*-indole (**2m**).* ^{1}H-NMR (400 MHz, $CDCl_3$, δ / ppm): 7.68-7.60 (*m*, 1H), 7.29–7.06 (*m*, 9H), 6.54 (*dd*, J_1 = 3.2, Hz, J_2 = 0.8 Hz, 1H), 5.27 (*s*, 2H). ^{13}C-NMR (101 MHz, $CDCl_3$, δ / ppm): 137.7, 136.4, 128.9, 128.8, 128.0, 127.7, 121.8, 121.1, 119.6, 109.8, 101.8, 50.2. EI-MS (*m/z* (%)): 207.1 $[M]^+$ (70), 91,1 (100), 65,1 (20).

*1-Benzyl-1*H*-indole-3-carbaldehyde to 1-benzyl-1*H*-indole (**2n**).* ^{1}H-NMR (400 MHz, $CDCl_3$, δ / ppm): 7.62 (*dt*, J_1 = 7.9 Hz, J_2 = 1.0 Hz, 1H), 7.36 (*dd*, J_1 = 8.2 Hz, J_2 = 0.9 Hz, 1H), 7.23 (*d*, *J* = 1.2 Hz, 1H), 7.18-7.08 (*m*, 2H), 6.51 (*dd*, J_1 = 3.2 Hz, J_2 = 0.9 Hz, 2H), 4.79 (*d*, *J* = 2.5 Hz, 2H), 2.37 (*t*, *J* = 2.6 Hz, 1H). ^{13}C-NMR (125 MHz, $CDCl_3$, δ / ppm): 135.6, 128.7, 127.0, 121.7, 121.0, 120.9; 119.7, 109.1, 101.9, 73.3, 35.5. EI-MS (*m/z* (%)): 154.1 $[M]^+$ (100), 127,1 (10), 116,1 (30), 89,1 (20).

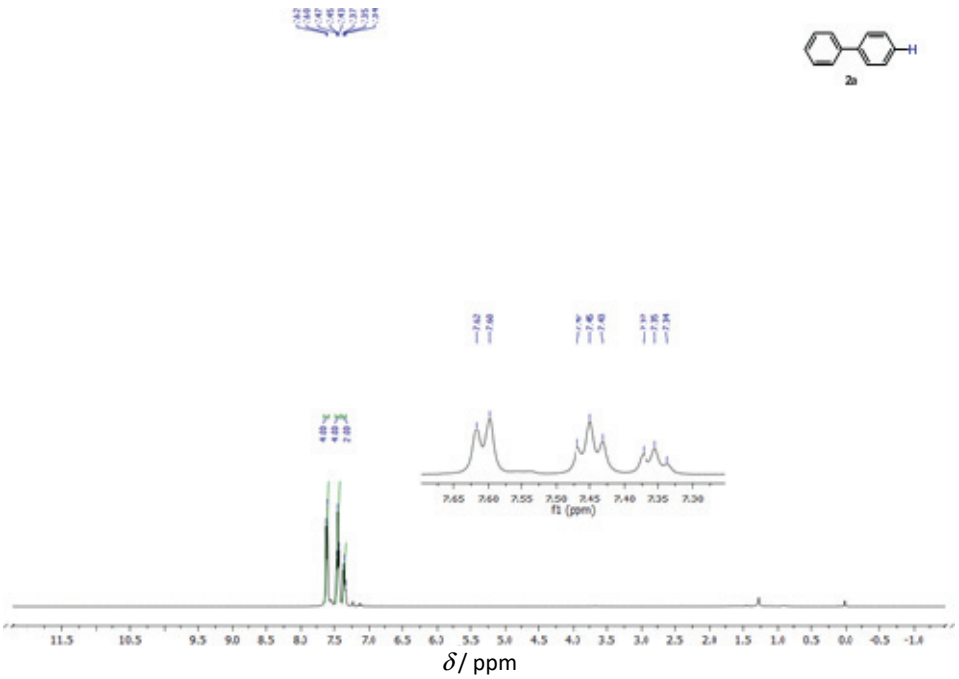

Fig. S-1. ^{1}H-NMR spectra of compound **2a**.

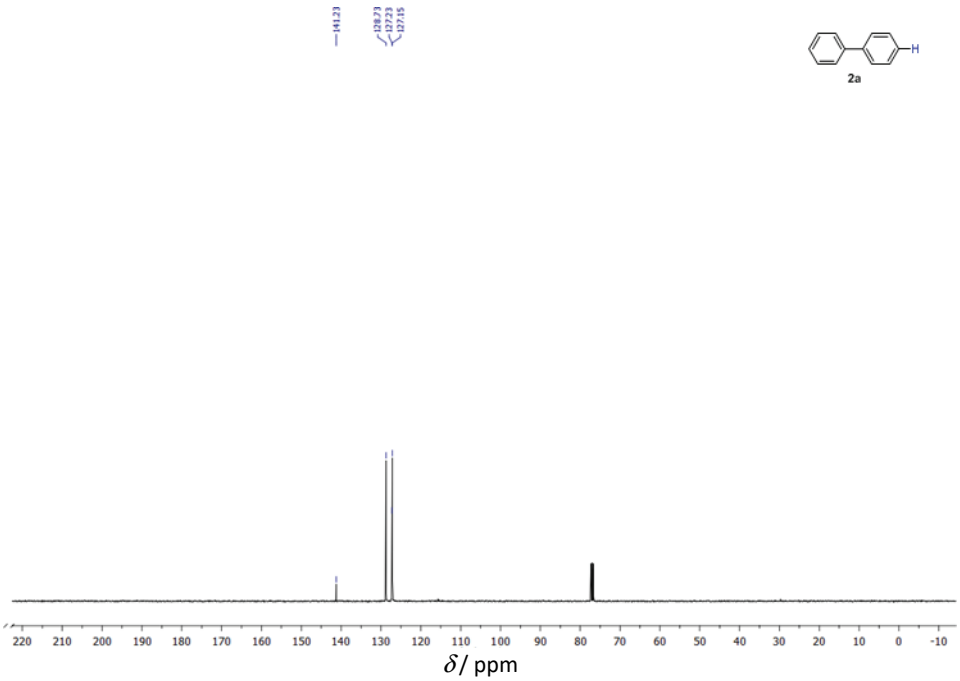

Fig. S-2. ^{13}C-NMR spectra of compound **2a**.

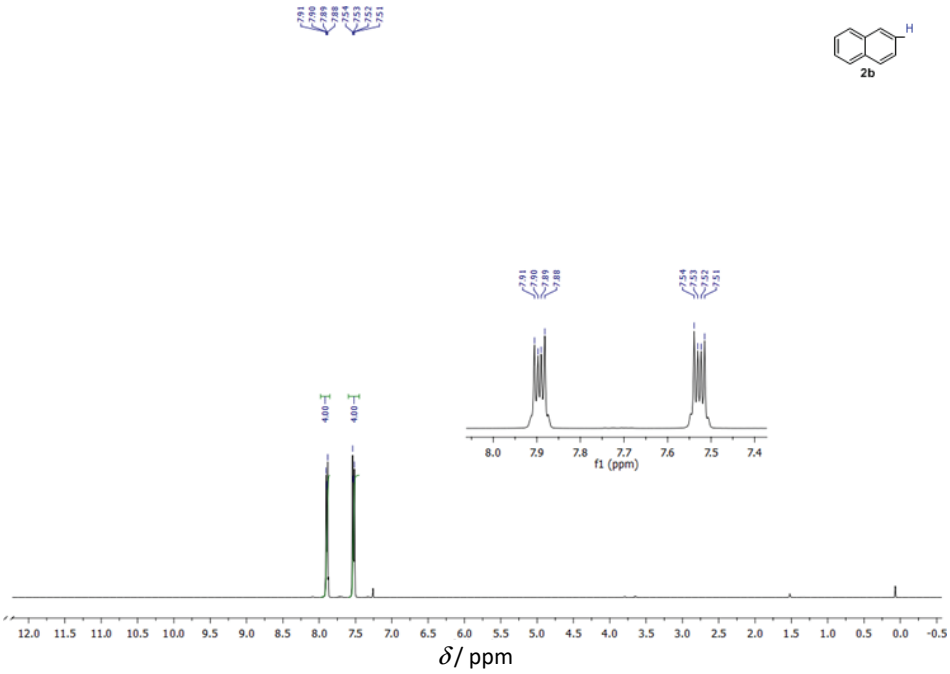

Fig. S-3. ^{1}H-NMR spectra of compound **2b**.

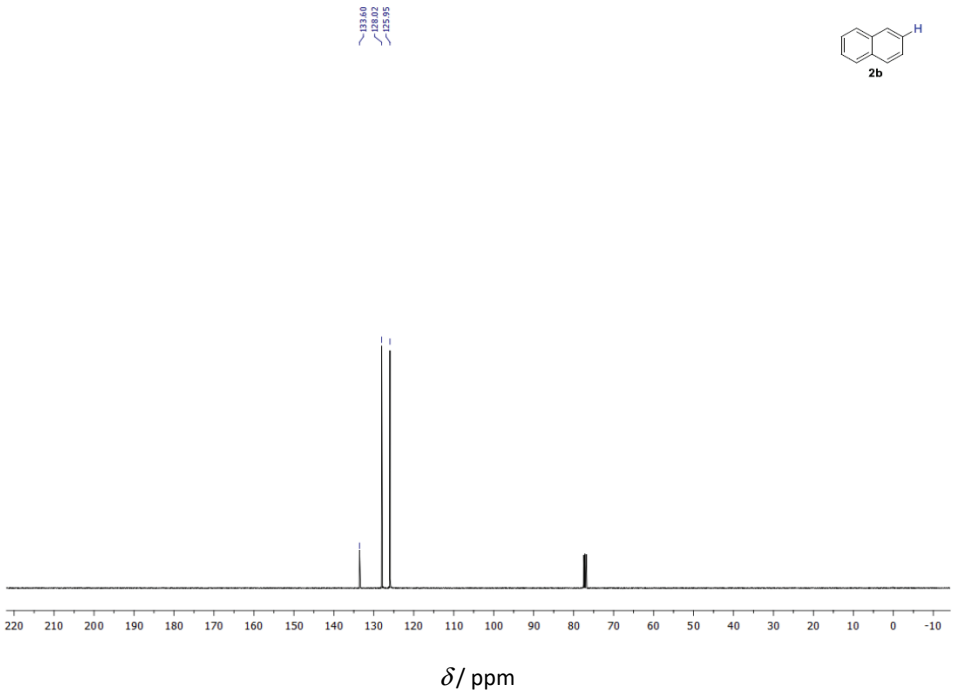

Fig. S-4. ^{13}C-NMR spectra of compound **2b**.

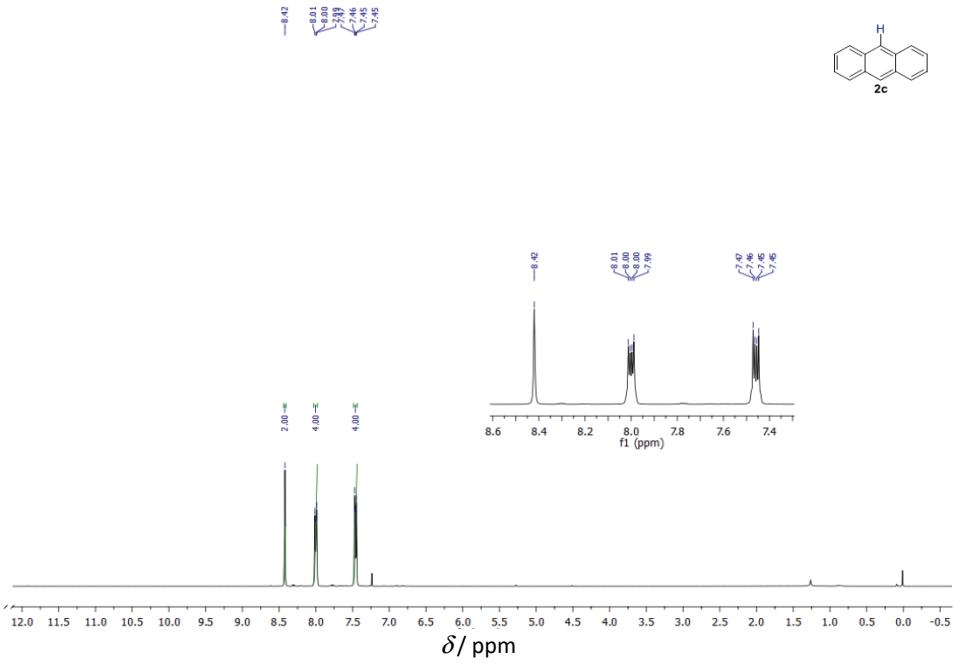

Fig. S-5. ^{1}H-NMR spectra of compound **2c**.

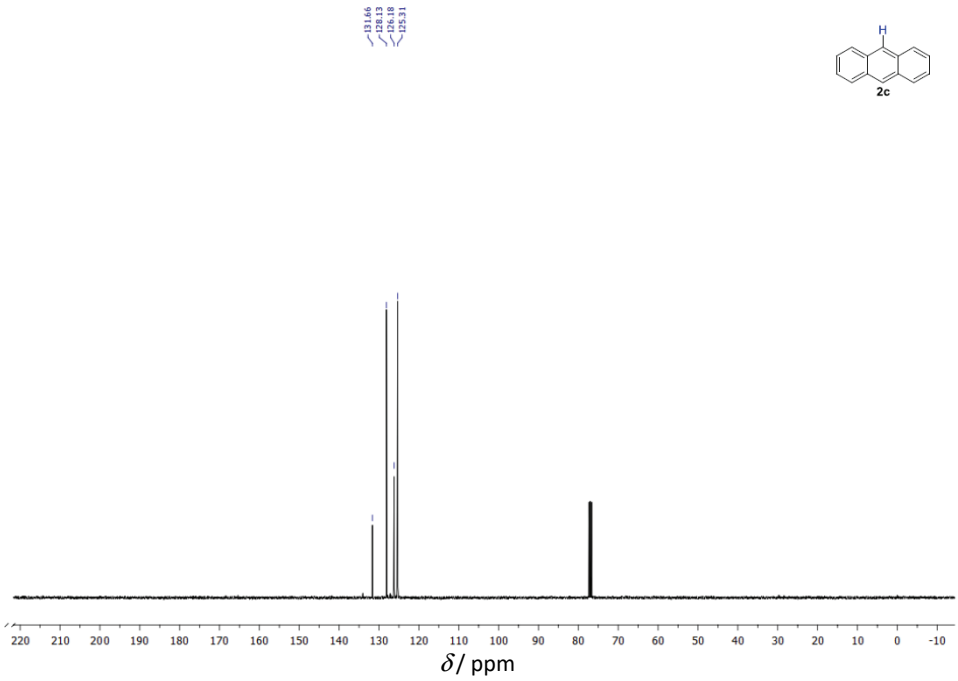

Fig. S-6. ^{13}C-NMR spectra of compound **2c**.

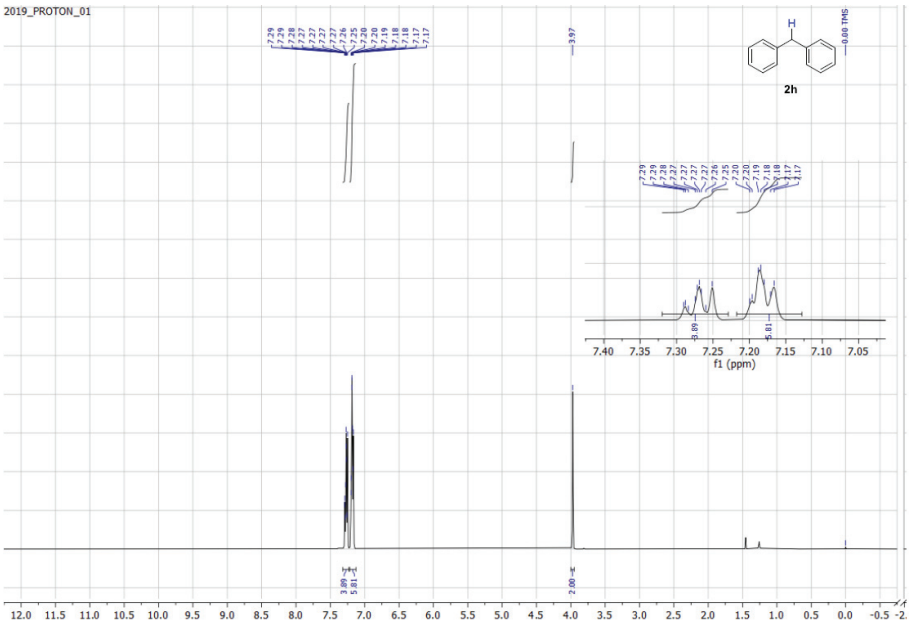

δ/ ppm

Fig. S-7. ^{1}H-NMR spectra of compound **2h**.

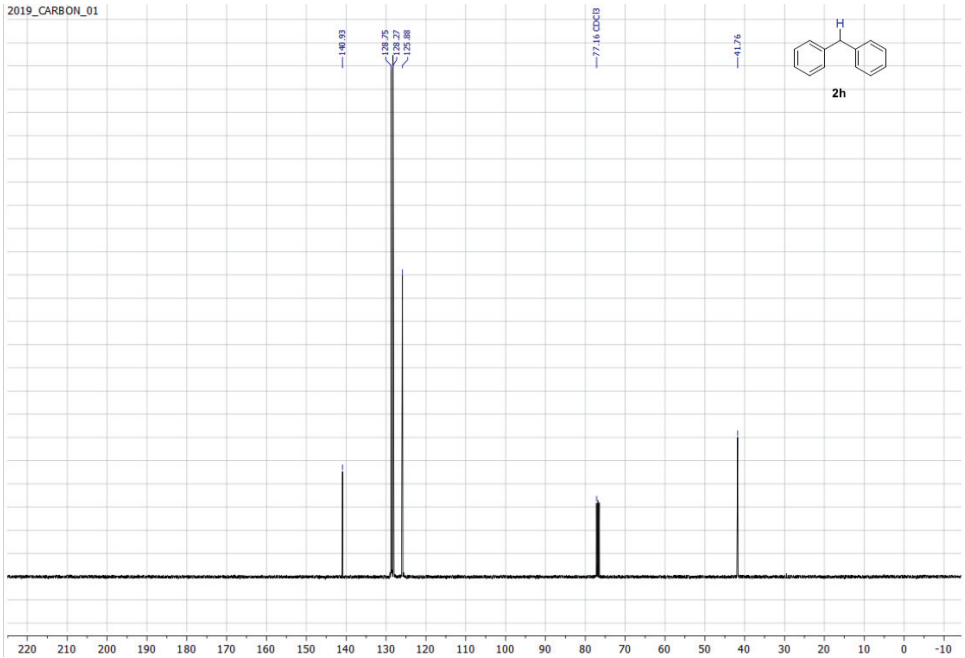

δ/ ppm

Fig. S-8. ^{13}C-NMR spectra of compound **2h**.

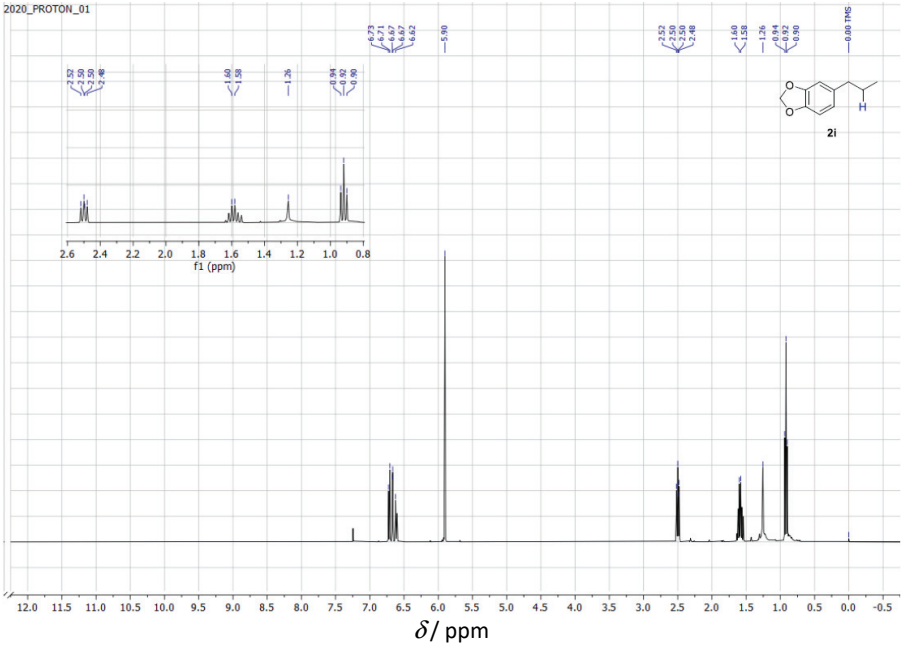

Fig. S-9. ^{1}H-NMR spectra of compound **2i**.

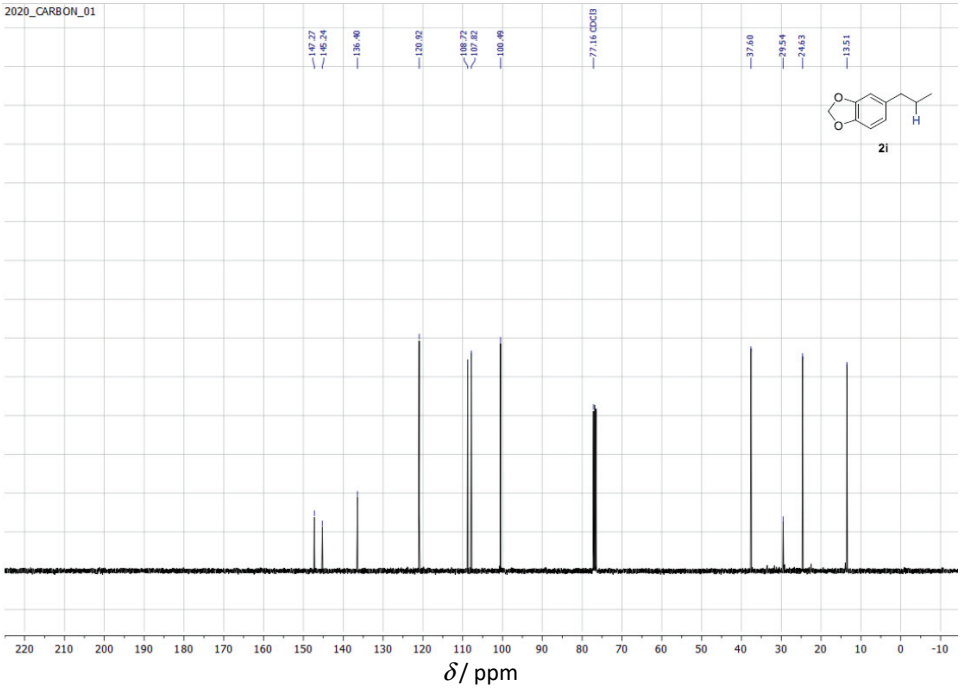

Fig. S-10. ^{13}C-NMR spectra of compound **2i**.

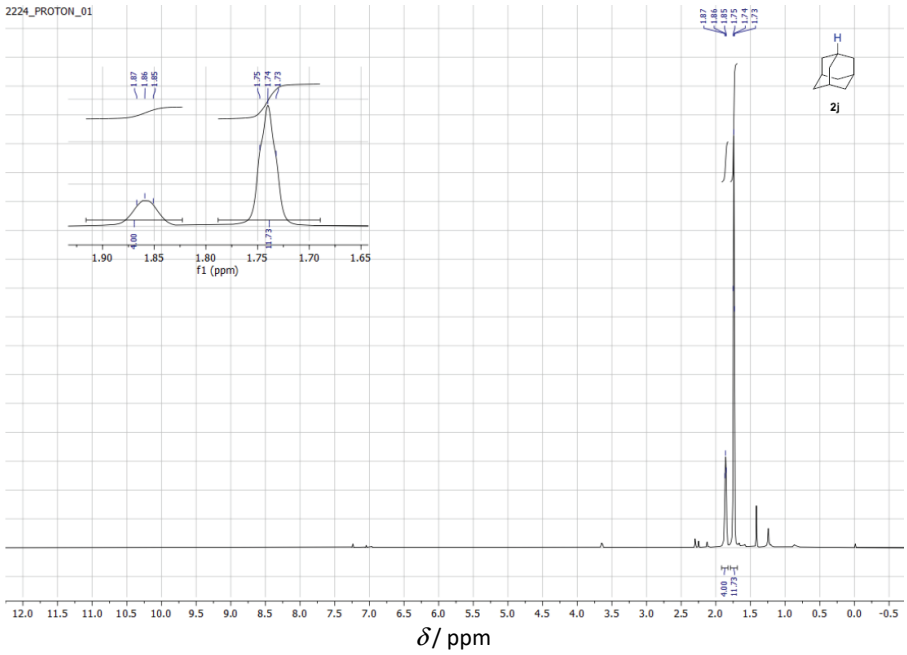

Fig. S-11. ^{1}H-NMR spectra of compound **2j**.

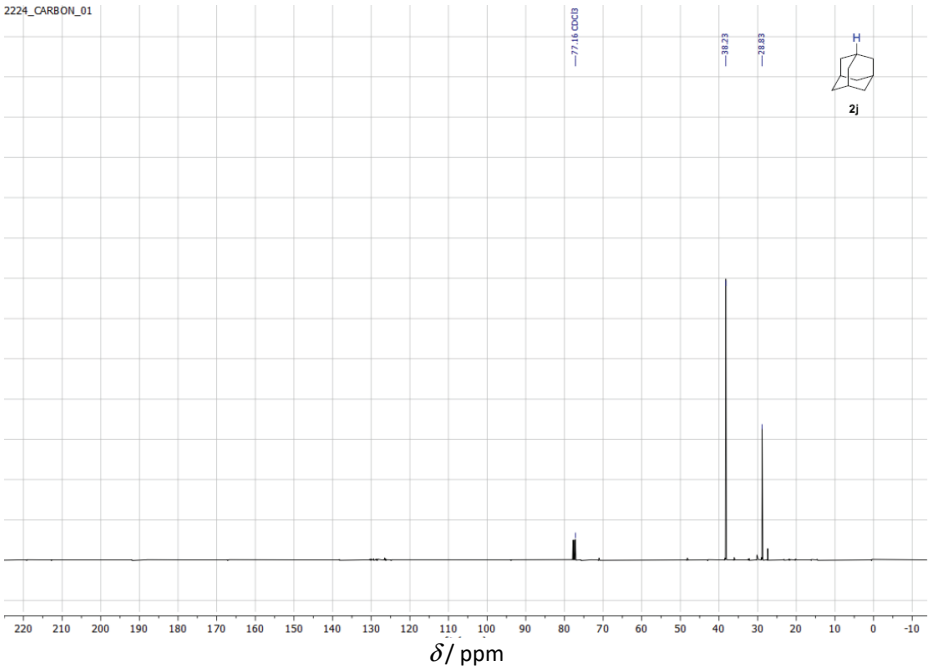

Fig. S-12. ^{13}C-NMR spectra of compound **2j**.

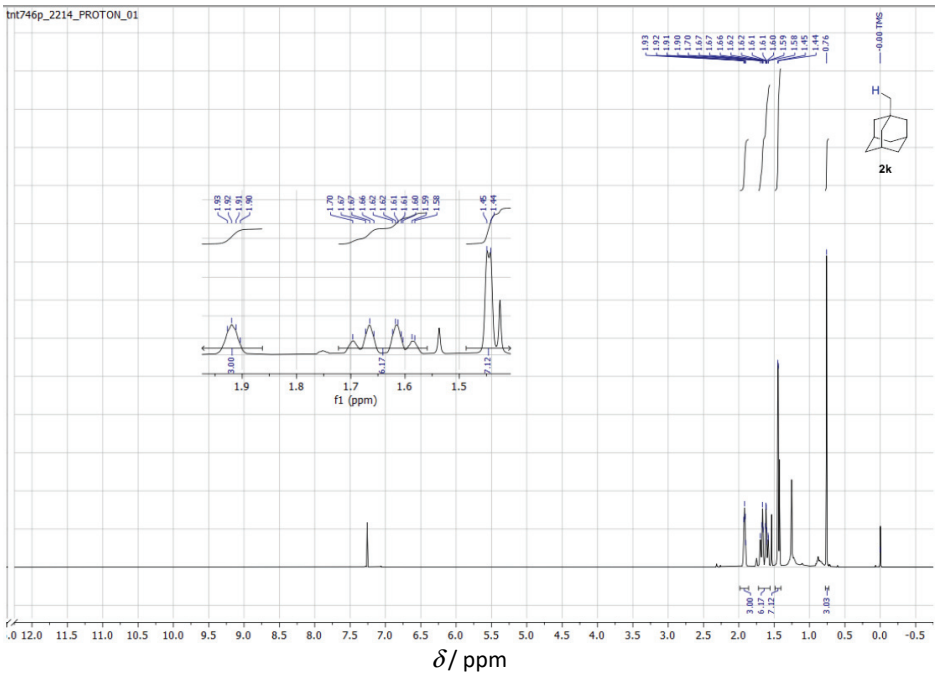

Fig. S-13. ^{1}H-NMR spectra of compound **2k**.

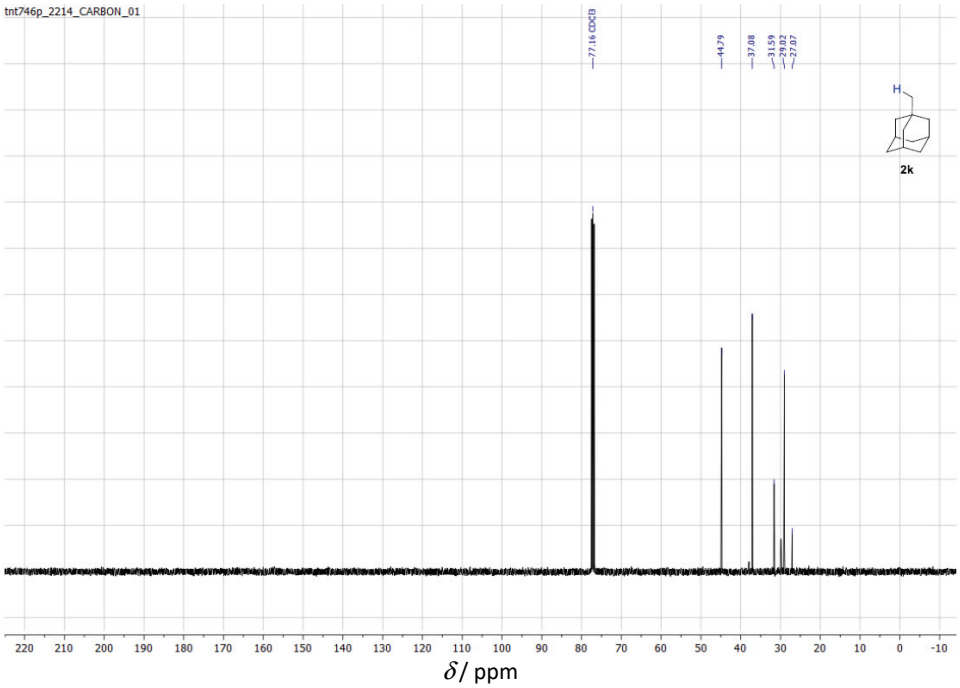

Fig. S-14. ^{13}C-NMR spectra of compound **2k**.

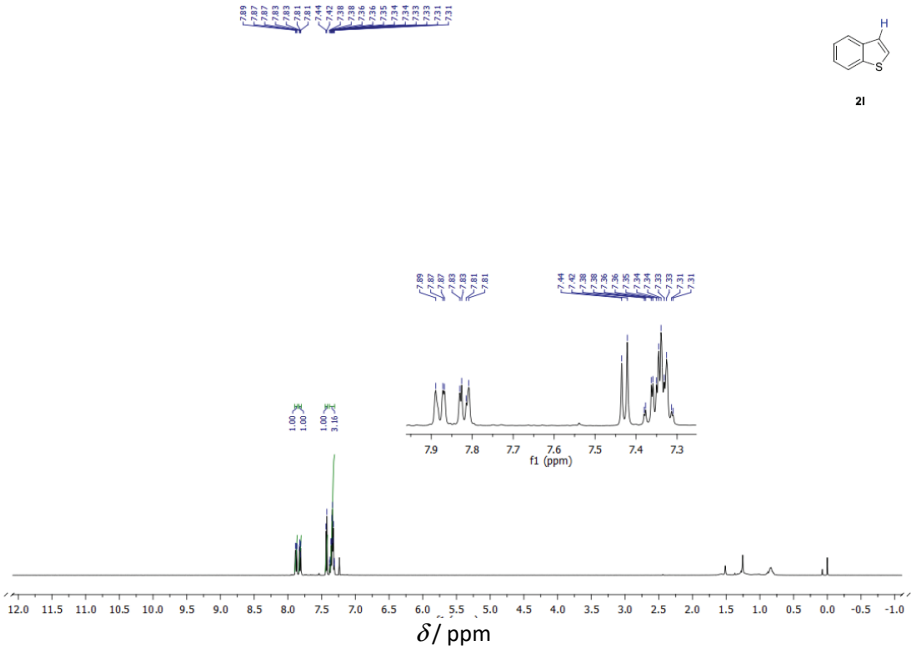

Fig. S-15. ^{1}H-NMR spectra of compound **2l**.

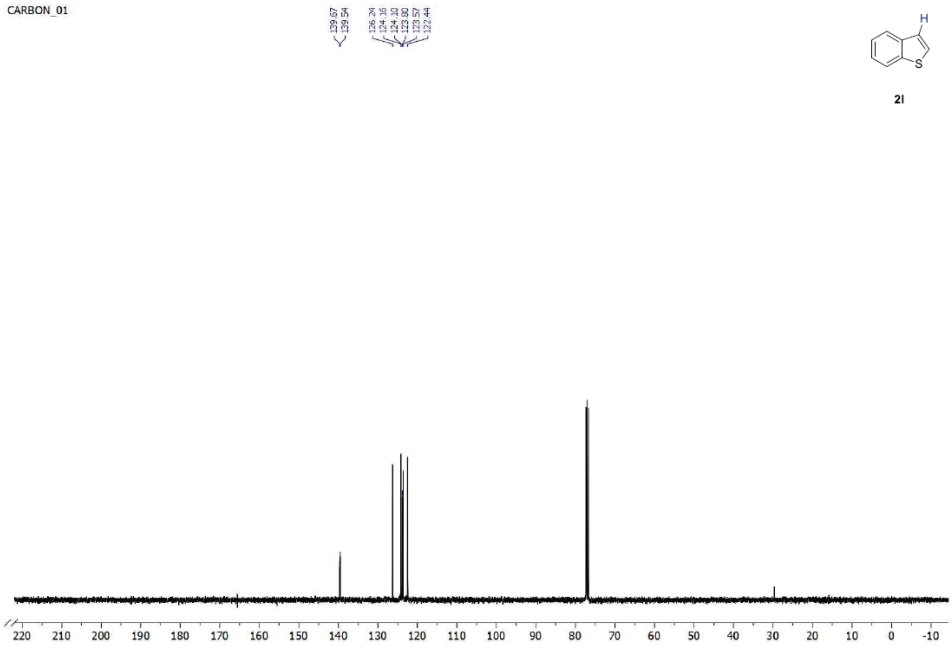

δ/ ppm

Fig. S-16. ^{13}C-NMR spectra of compound **2l**.

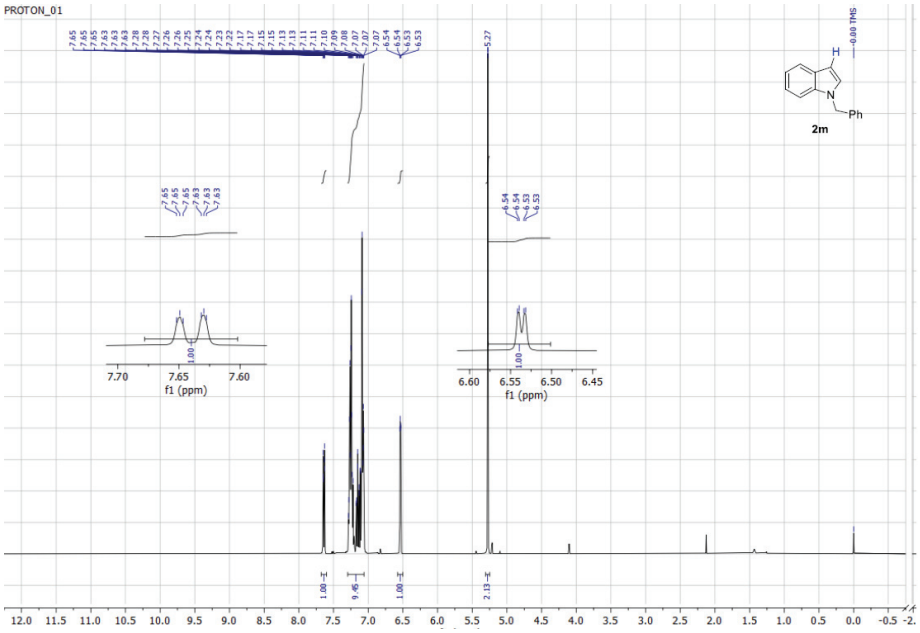

δ/ ppm

Fig. S-17. ^{1}H-NMR spectra of compound **2m**.

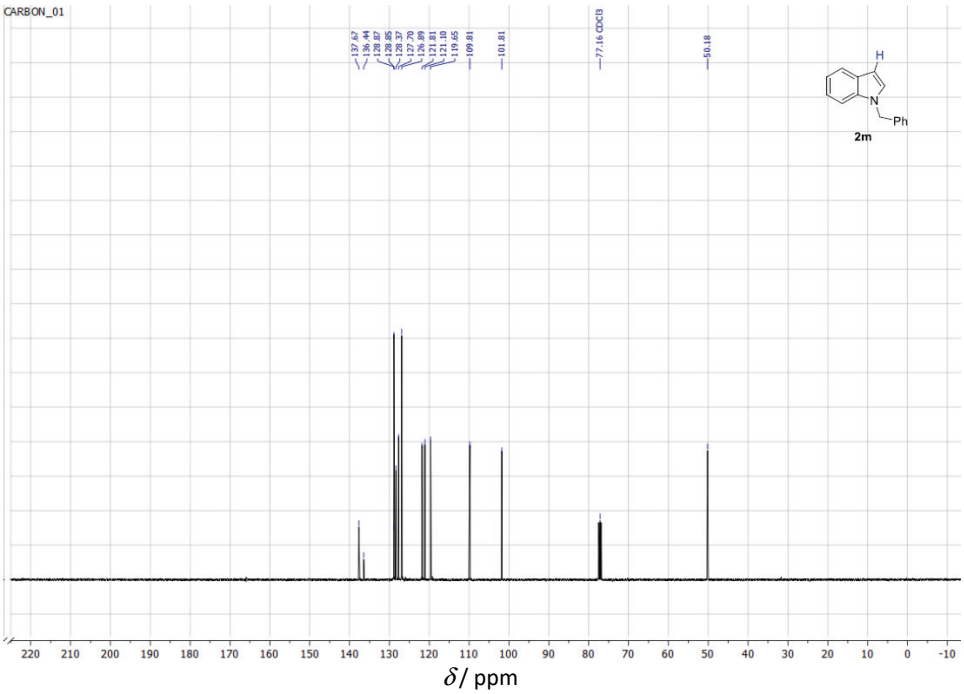

Fig. S-18. ^{13}C-NMR spectra of compound **2m**.

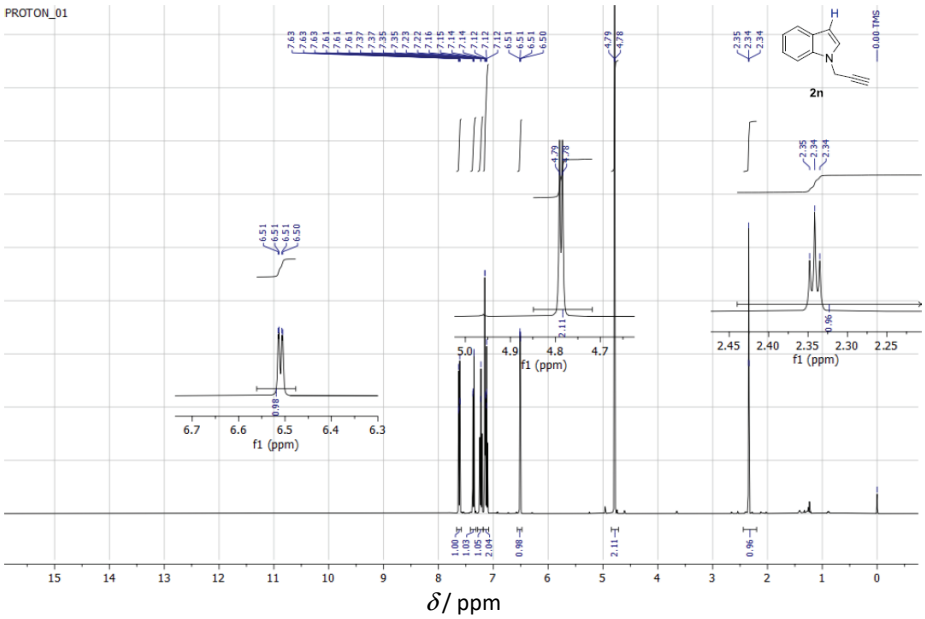

Fig. S-19. ^{1}H-NMR spectra of compound **2n**.

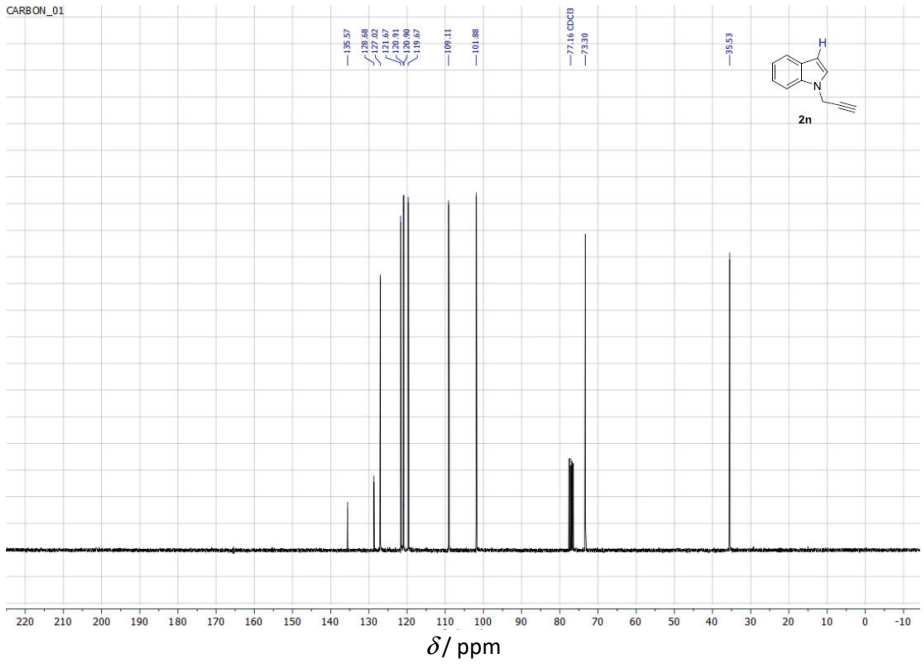

Fig. S-20. ^{13}C-NMR spectra of compound **2m**.

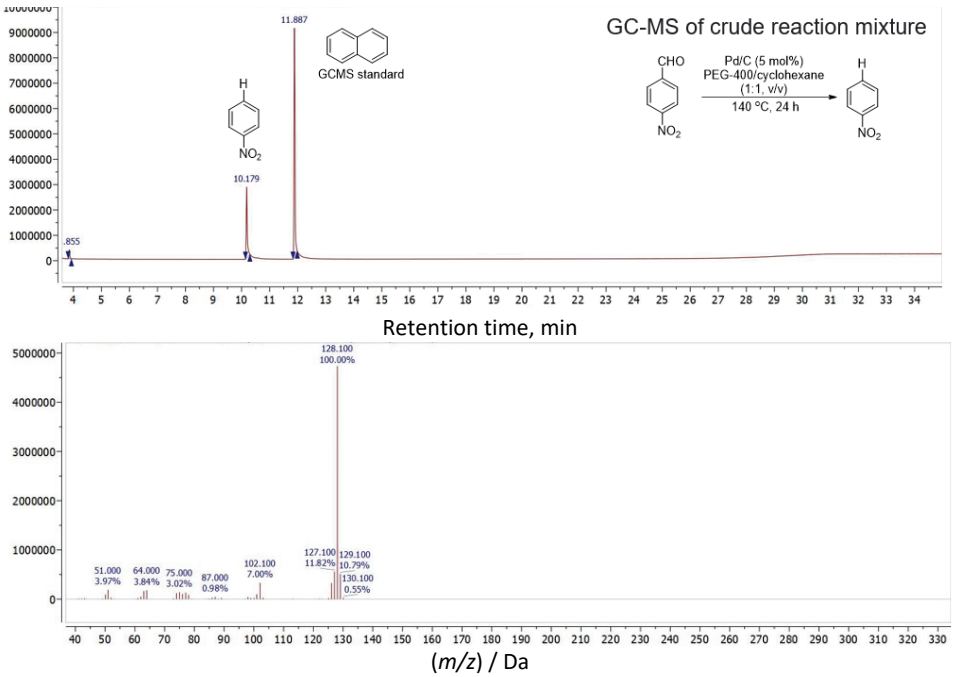

Fig. S-21. GC–MS Analysis.

Journal of the Serbian Chemical Society
JSCS-info@shd.org.rs • www.shd.org.rs/JSCS

J. Serb. Chem. Soc. 87 (6) 677–692 (2022)
JSCS–5550

Original scientific paper
Published 28 April 2022

Non-conventional expression of recombinant chitinase A originating from *Bacillus licheniformis* DSM8785, in *Saccharomyces cerevisiae* INVSc1

GHEORGHITA MENGHIU[1], RADIVOJE PRODANOVIĆ[2], MARIJA BLAŽIĆ[2], MANUELA MINCEA[1], CRISTINA MORARU[1] and VASILE OSTAFE[1]*

[1]*Advanced Environmental Research Laboratories, Department of Biology – Chemistry, West University of Timisoara, Oituz 4, 300086, Timisoara, Romania and* [2]*Faculty of Chemistry, University of Belgrade, Studentski trg 12, 11000 Belgrade, Serbia*

(Received 13 September, revised 29 December 2021, accepted 28 February 2022)

Abstract: Chitinases are glycosyl hydrolases, that cleave the *β*-1,4 linkage between *N*-acetyl glucosamines present in chitin chains. Chitin is the second most abundant polysaccharide on Earth after cellulose, and it is produced in the exoskeleton of crustaceans and insects, and in some parts of the cell walls of fungi. Enzymatic development and the extraction of superior derivatives from chitin wastes – such as chitooligosaccharides with vast importance in the medical and biofuels industry – lead to the necessity of creating chitinases using different strains of organisms. In this paper, the chiA gene from the *Bacillus licheniformis* DSM8785 encoding chitinase A (ChiA) with C-terminal hexahistidine tag was cloned and expressed in the extracellular expression system pYES2 from *Saccharomyces cerevisiae* INVSc1 as a hyperglycosylated enzyme. The production of recombinant ChiA was successfully confirmed by dot blotting, using anti-His antibodies. The optimal time of expression was identified to be 24 h when galactose was added only at the beginning of fermentation, the chitinase activity starting to decrease after this threshold. Nevertheless, in another experiment, when galactose was added every 24 h for 72 h, the expression continued for the entire period. The purified enzyme was detected, using sodium dodecyl sulphate–polyacrylamide gel electrophoresis (SDS-PAGE), as a heterogeneous diffuse band between 80 and 180 kDa. The molecular mass of the same ChiA enzyme expressed in *Pichia pastoris* KM71H and *Escherichia coli* BL21 (DE3) was compared using SDS-PAGE with ChiA expressed in *S. cerevisiae* INVSc1. The activity of ChiA was determined using the fluorogenic substrate, 4-methylumbelliferyl *β*-D-*N*,*N*,*N*-triacetylchitotrioside (4MUTC). Using a bioinformatics simulation, the number of the glycolsylation sites of the ChiA gene sequence and the proximity of these sites to the alpha factor sequ-

* Corresponding author. E-mail: vasile.ostafe@e-uvt.ro
https://doi.org/10.2298/JSC210913017M

ence were hypothesized to be a possible reason for which ChiA enzyme was internally expressed.

Keywords: chitinolytic enzymes; molecular cloning; dot blotting, fluorescent assay; glycosylation.

INTRODUCTION

Chitinases (EC 3.2.2.14) are glycosyl hydrolases that hydrolyze the β-1,4 linkage of the *N*-acetyl glucosamine group in chitin chains.[1] The production of chitinases is an important step in the bioconversion process of treating shellfish waste, resulting in proteins for animal and aquaculture feed and in valuable chito-oligomers. The production of chitinase enzymes is presently unprofitable due to the high prices of commercially available chitinases. A more efficient and economically reliable process is essential for chitin exploitation and the management of shellfish wastes.[2] Genetic engineering technology offers a method to approach this problem by using recombinant enzymes. Recombinant enzymes, which are used in biotechnology or in waste management, require high thermostability. The glycosylated proteins are more stable at higher temperatures compared to their non-glycosylated counterparts. As a general rule, when proteins are expressed by *Escherichia coli* and other types of bacteria, a glycosylation portion is not added to the protein. For eukaryotic cells, glycosylation constituents are usually added to the expressed proteins, helping secretion outside the cells. The glycosylation pattern is species dependent. For example, *Saccharomyces cerevisiae* usually creates a hyperglycosylation pattern that depends on the primary structure of the protein, while *Pichia pastoris* creates a rather frequent and repetitive glycosylation pattern, similar to all types of expressed proteins.[3] While glycosylation of *P. pastoris* can have 20 residues in length, *S. cerevisiae* exceeds 100 residues.

It is well known that glycosylated proteins and enzymes are more thermostable than less or aglycosylated variants, therefore strains with glycosylation pathways are often preferred for production of proteins. One of the most well-known strains that can create hyperglycosylated enzymes is *S. cerevisiae*. In contrast with other yeasts, such as *P. pastoris*, the endoplasmic reticulum (ER) of *S. cerevisiae* involved in the glycosylation process is dispersed differently in the cells.[4] This feature makes *S. cerevisiae* a model organism with regard to its mode of glycosylation. This yeast is also an attractive host for the production of recombinant proteins, enzymes and different pharmaceuticals.[5] Other advantages offered by these systems are well-defined DNA transformation and secretory system (the ability to secrete biologically active enzymes into the culture medium), rapid growth, and the simple and inexpensive culture media.[6] It is therefore a very attractive system for the production of industrial enzymes, such as chitinase, α-amylase, xylanase, β-glucanase and human therapeutic proteins.[7]

In the present paper, the chitinase A gene from *Bacillus licheniformis* DSM8785 was cloned and expressed in *S. cerevisiae* INVSc1. The optimal time of expression was investigated when galactose was added only at the beginning of induction or every day during fermentation. The ChiA was purified from *S. cerevisiae* INVSc1 cells and its molecular mass was compared to the same ChiA expressed by *P. pastoris* KM71H and *E. coli* BL21 (DE3).

EXPERIMENTAL

Chemicals, enzymes and antibodies

The chemicals were purchased from Carl Roth and Sigma-Aldrich, Germany. The restriction enzymes Kpn I and Bam HI, T4 DNA ligase, Dpn I; calf intestinal alkaline phosphatase (CIAP) and PNGase F kit were purchased from Thermo Fisher Scientific or New England Biolabs, Ipswich, MA, USA. The DNA purification kit, plasmid purification columns (NucleoSpin®) and PCR products were supplied by Macherey-Nagel, Germany. Pfu HF DNA polymerase and Taq DNA polymerase were bought from Agilent Technology, Santa Clara, CA, USA. Anti-6-His antibody produced in rabbit, goat anti-rabbit IgG antibody, (H+L) alkaline phosphatase conjugate and chromogenic phosphatase substrate solution (Nitro-Blue tetrazolium chloride (NBT)/5-bromo-4-chloro-3-indolylphosphate toluidine salt (BCIP)) were purchased from Sigma Aldrich.

Plasmids and genes

The synthetic ChiA gene from *Bacillus licheniformis* DSM8785 (GenBank Accession Number FJ465148) was provided by GenScript (USA) and used as a template for molecular cloning in the yeast expression system. The *S. cerevisiae* INVSc1 expression vector pYES2 (#V82520) was purchased from Invitrogen, USA. The ChiA gene was cloned as well in *Pichia pastoris* KM71H pPICZαA extracellular expression system[8] and *E. coli* BL21 (DE3) pET22b(+) periplasmic expression system (this research is the subject of another article).

Organisms and growth conditions

S. cerevisiae INVSc1 (#C81000, Invitrogen) was cultured in SC-U medium containing 2 vol. % glucose at 27 °C. The basal components of the SC-U medium were 0.67 % yeast nitrogen base, 0.12% amino acid mix without uracil (0.01 % adenine, arginine, cysteine, leucine, lysine, threonine, tryptophan; 0.005 % aspartic acid, histidine, isoleucine, methionine, phenylalanine, proline, serine, tyrosine, valine), 2 vol. % glucose or galactose. The SC-U medium and glucose solution were autoclaved at 120 °C for 20 min. The galactose solution was added to the medium in order to induce enzyme expression and was separately sterilized using a 0.2 µm PDVF filter. For the preparation of the solid medium, in addition, 2 % agar was added before autoclaving. After the yeast was transformed with ChiA_pYES2 or pYES2 plasmid, the cells were cultured on YPD medium containing chloramphenicol (50 µg mL^{-1}). Plasmids were also inserted and amplified into *E. coli* XL10 Gold ultra-competent cells and grown in LB medium.

Subcloning of ChiA gene into pYES2 expression vector

The ChiA gene was cloned by the classical PCR/restriction method using forward primer FP pro α Kpn I (5′ ATC <u>GGT ACC</u> ATG AGA TTT CCT TCA ATT TTT ACT GCT GTT TTA TTC-3′) and reverse primer RP his Bam HI (5′-ATT <u>GGA TCC</u> TCA GTG GTG GTG GTG GTG GTG TTC GCA GCC TCC GAT CAG CC-3′). The PCR reaction mixture consisted of 1 µL ChiA template (58.6 ng μL^{-1}), 2 µL forward primer (25 µM), 2 µL reverse pri-

mer (25 μM), 2 μL deoxynucleotide mixture (dNTP, 10 mM), 10 μL 10x Pfu buffer, 2.5 μL Pfu DNA polymerase (2.5 U/μL) and 80.5 μL ultrapure water. PCR amplification comprised an initial denaturation step at 95 °C for 3 min followed by 25 cycles at 95 °C for 30 s, 50 °C for 30 s, and 72 °C for 4 min, followed by a final extension step at 72 °C for 10 min. The reaction products (100 μL) were treated with 1 μL Dpn I (10 U μL^{-1}) for 1 h at 37 °C to eliminate the template, then purified on NucleoSpin Plasmid Columns.

The pYES2 vector and PCR products containing amplified ChiA were each double digested with Kpn I and Bam HI. The vector was treated with calf intestinal alkaline phosphatase and the components were ligated overnight at 17 °C using T4 DNA ligase. The ligated vector was inserted into *E. coli* XL10 Gold cells by heat-shock transformation.[9] The insert was verified by colony PCR and Sanger sequencing.[10] The verified ChiA_pYES2 and pYES2 plasmids were used to transform the *Saccharomyces cerevisiae* INVSc1 strain, using the lithium acetate/single-strand carrier DNA/poly(ethylene glycol) method.[11]

Chitin agar plate assay

Around 15 colonies of transformed *S. cerevisiae* INVSc1 containing ChiA_pYES2 or pYES2 were transferred on plates with a solid SC-U media containing 2 % galactose and 0.5 % colloidal chitin. The plates were incubated at 27 °C for 3 days. After this step, the *S. cerevisiae* INVSc1 cells were removed by washing the plate surface with water and the plate was subjected to staining with Congo Red.[8]

Dot blot analysis

A preculture (25 μL) of *S cerevisiae* INVSc1 containing ChiA-pYES2 or pYES2 was inoculated in an Elisa plate containing 85 μL well of SC-U with galactose and then the plate was incubated at 30 °C and 900 rpm for 48 h. The fermented cultures (18 μL) were transferred to a dot blot plate fitted with a nitrocellulose membrane and connected to a vacuum. After each 3 μL transferred in 6 rounds, the cultures were allowed to adsorb for a few minutes. Anti-6-His antibody produced in rabbit was used as the positive control. The nitrocellulose membrane was incubated for 30 min in 25 mL 5 % milk powder. The membrane was washed several times with PBS-T buffer. The anti-6-His antibody produced in rabbit was added (3 μL of 1 mg mL^{-1} antibody in 10 mL PBS-T) and incubated for 1 h under mild mixing. The membrane was washed several times and then the goat anti-rabbit IgG antibody, (H+L) alkaline phosphatase conjugate (3 μL of 0.6 mg mL^{-1} antibody in 10 mL PBS-T) was added. After 1 h, the second antibody was removed by washing with PBS-T. Then, 10 mL of NBT/BCIP (100 μL NBT (18.8 mg mL^{-1})/BCIP (9.4 mg mL^{-1})) in 67 % DMSO stock solution diluted in 10 mL alkaline phosphatase buffer) was added. After 5 min, the dots were observed and photographed.

Heterologous expression of ChiA

A volume of 6 mL of *S. cerevisiae* INVSc1 preculture containing the recombinant plasmid ChiA-pYES2 was diluted in 50 mL of SC-U medium supplemented with 2 % galactose contained in two different flasks. The cultures were incubated for 72 h at 27 °C and 160 rpm. In one culture, galactose was added at the beginning of the expression, in the other culture, 2.5 mL of 20 % galactose was added every 24 h, for 72 h. Cell culture samples (1.5 mL) were taken after 0, 4, 24, 48 and 72 h of expression. The samples were kept at –20 °C until use. Aliquots from samples (1 mL) were centrifuged at 11000 g for 5 min and the supernatant was separated from the cells in order to determine whether the expression of chitinase was intra- or extracellular. The cells were diluted with 1 mL of water to equalize the cell concentration to the supernatant concentration.

Chitinase activity assay

Chitinase activity was verified by fluorogenic substrate analysis using 4MUTC as follows: 25 µL of samples were rapidly mixed with 25 µL of 0.05 mg mL^{-1} 4MUTC and the fluorescence product was measured at an excitation of 355 nm and emission of 460 nm. The negative control comprised 25 µL distilled water mixed with 25 µL of 0.05 mg mL^{-1} 4MUTC.

Production of ChiA

A preculture of *S. cerevisiae* INVSc1 containing ChiA-pYES2 plasmid (5 mL) was diluted in 400 mL of SC-U medium supplemented with 2 % glucose (*OD* 600 start = 0.083). The culture was divided into two portions of 200 mL in two Erlenmeyer flasks (5 L). The cultures were incubated at 27 °C, 160 rpm for 24 h. After 24 h, the *OD* 600 of the culture was approximately 1.805. Chitinase expression was induced by the addition of 1 L of SC-U supplemented with 2 % galactose (six times dilution, *OD* 600 start = 0.608), to each 200 mL culture. The culture was incubated for 24 h at 27 °C, 160 rpm. After 24 h of incubation at 27 °C, the expression culture was centrifuged at 6200g, 4 °C for 20 min. The cells were resuspended in 70 mL of their own supernatant then passed through a French press four times at 10000 psi* (pound-force per square inch). After pressing, the cells were centrifuged again for 30 min at 4 °C at 27200*g*. The enzyme-containing supernatant was first filtered through a 0.2 µm membrane to remove cell debris and then filtered through centrifugation at 3000*g* using Millipore 50 kDa membrane filters. The concentrated enzyme was dialyzed in 4 L of 10 mM Tris-HCl buffer, pH 7.0, for 24 h at 4 °C.

Purification of ChiA

A sample of dialyzed enzyme (11 mL) was injected into a 20 mL DEAE Sepharose FF 16/10 HiPrep column. The column was equilibrated with 2 column volumes of 10 mM Tris--HCl buffer, pH 7.0. The elution gradient was operated from 0 to 100 % of 10 mM Tris-HCl/1 M NaCl buffer pH 7.0, over 20 column volumes. The injection flow and flow rate were 0.5 and 1 mL min^{-1}, respectively. The volume of each collected fraction was 2 mL.

The concentration of purified chitinase enzyme was determined using a spectrophotometric method at 280 nm adapted after Grimsley and Pace.[12] A solution of commercial chitinase from *Streptomyces griseus* with a known concentration was used as the standard.

Deglycosylation of purified ChiA

The deglycosylation reaction comprised of 40 µL ChiA (1.2 µg $µL^{-1}$) and 20 µL glycoprotein denaturing buffer was first incubated at 100 °C, after which 10 µL glycobuffer 2, 10 µL NP-40 (10 %), 3 µL PNGase F and 17 µL distilled water were added. The reaction mixture was incubated at 37 °C on a shaker platform. The same procedure was undertaken for the negative control, except for the presence of PNGase F.

SDS-PAGE analysis

Three different samples of the same purified recombinant ChiA produced in three different strains of *S. cerevisiae* INVSc1, *P. pastoris* KM71H[8], . *coli* BL21 (DE3, the purification of this strain will be the subject of another article) was exposed to polyacrylamide gel electrophoresis (PAGE) according to Laemmli, 1970.[13] Purified ChiA samples (30 µL, 1.0 mg mL^{-1}) were loaded into the gel. The samples were subjected to electrophoresis using a current of 120 V for 90 min. The proteins were stained with Comassie Brilliant Blue, then progressively

* 1 psi = 6896 Pa

decolorized with 10 % acetic acid solution. The deglycosylated sample was subjected to SDS--PAGE under the same conditions.

Bioinformatics analysis

For bioinformatic analysis, the DNA sequence of the ChiA was first translated in protein sequence using the Translate tool - Expasy. Based on the amino acids sequence, the theoretical molecular mass and isoelectric pH were calculated applying the Compute pI/Mw tool – Expasy. The amino acids sequence (Fasta format) was analyzed in a NetNGlyc - 1.0 server in order to predict the *N*-glycosylation sites and examine the sequence context of Asn-Xaa-Ser/ /Thr sequins, where Xaa is represented by any amino acid except for proline.[14] According to this bioinformatics protocol, the protein sequences of hexose oxidase (HOx), cellobiose dehydrogenase (CBDH), and glucose oxidase (GOx) were compared to chitinase A. The comparison was focused on the number of *N*-glycosylation points in the protein structures, and the distances between these points and *N*-glycosylation points from signal peptides attached to proteins. The results obtained were outlined in a schematic figure.

RESULTS AND DISCUSSIONS

Molecular cloning of chiA gene in pYES2 expression vector

The ChiA gene derived from *Bacillus licheniformis* DSM8785 was cloned into the extracellular expression vector pYES2, compatible with the expression system of *S. cerevisiae* INVSc1. The pYES2 vector is an extracellular expression vector that allows the cloning of the gene of interest and the selection of transformants on uracil deficient environments due to its *ura*3 gene construct for uracil-specific synthesis required for cell growth.[15] The *B. licheniformis* DSM8785 ChiA gene has an open reading frame (ORF) of 2023 bp, including *α* factor and 6x *his* tag sequences. The main genetic elements involved in gene cloning and expression are outlined in Fig. 1A. The presence of the GAL1 promoter induces the expression of chitinase in *S. cerevisiae* in the presence of galactose and acts as a repressor in the presence of glucose. For the extracellular expression of chitinase, the gene was cloned with the *α*-factor pro-peptide sequence.[16] The sequence encoding 6 histidines was introduced at the C end of the gene that allowed easy detection of recombinant chitinase A by dot blot analysis. Restriction endonucleases Bam HI and Kpn I were used in the gene and vector digestion step to create compatible sticky ends. The ChiA_pYES2 recombinant plasmid scheme was created using Vector NTI bioinformatics software, created by InforMax Inc., North Bethesda, MD, USA. The ChiA gene linked to 6 histidines sequence encodes an enzyme with a theoretical molecular mass of 64.77 kDa and an isoelectric pH in the acid range at 5.21, according to the Expasy Bioinformatics Resource Portal program.[17]

PCR amplification of the gene consisted of introducing restriction sites for Bam HI and Kpn I endonucleases at its ends, for ligation compatibility in the pYES2 vector. The ChiA gene amplified by PCR (Fig. 1B, line 1 and the vector pYES2 line 2) were digested with Bam HI and Kpn I restriction enzymes and

ligated to form the recombinant plasmid ChiA_pYES2. The ligation products were checked on a agarose gel and, as can be seen in Fig. 1B, line 3, there are several DNA fragments. The DNA fragments located at about 2.0 and 6.0 kbp correspond to the ChiA gene and pYES2, respectively, representing non-ligated fragments. The 8.0 kbp DNA fragment represents the recombinant ChiA_pYES2 plasmid, summing the vector and gene mass. At approximately 4.0 kbp, a band appears that could represent self-ligation of two ChiA genes, a situation created when several gene fragments are partially digested by one of the restriction enzymes, or not digested at all. By DNA sequencing, the correct insertion of the ChiA gene into the vector pYES2 was confirmed.[10]

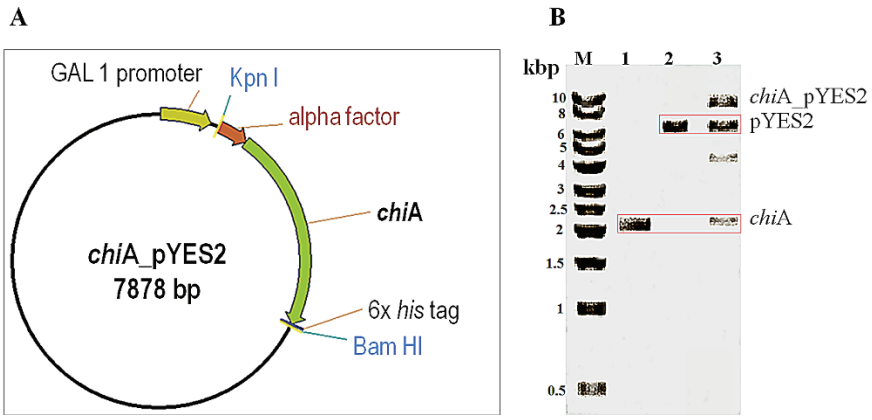

Fig. 1. Theoretical scheme of ChiA gene inserted into pYES2 vector and the main genetic elements used for cloning and expression (A). Agarose gel electrophoresis for the ChiA gene (B). Line M = DNA molecular marker, line 1 = PCR amplified ChiA gene, line 2 = pYES2 vector, line 3 = ligation products.

A fast chitin agar plate assay highlighted that there was no difference between cells that produce recombinant chitinase and those that did not produce (data not shown). The information obtained from this test is proof of chitinase activity. The negative control shows enzymatic activity coming from native chitinase in *S. cerevisiae*[18] located in the periplasmic space and allowing the enzyme to act on the secreted chitin in that space during cell septum formation. The function of native chitinase in cell division is suggested by the high concentration found during exponential growth, compared to the stationary phase, in yeast cells.[19] Additional experiments were performed to detect recombinant chitinase A. The ChiA gene was inserted into the expression vector pYES2 having six histidine residues at the C terminus, which allowed western blotting to detect it using rabbit anti-His antibody and goat anti-rabbit antibody coupled to alkaline phosphatase. Thus, a dot blot analysis was performed using samples from a culture of *S. cerevisiae* INVSc1 that expressed chitinase A. The negative control

consisted of yeast cells containing only the vector and not producing recombinant chitinase, and the positive control consisted of the rabbit anti-His antibody.

Following this assay, the presence of recombinant ChiA in the yeast culture containing the plasmid ChiA_pYES2 was demonstrated, as could be seen in Fig. 2 (lines 1 and 2). In the negative sample (line N) containing *S. cerevisiae* cells with pYES2, the peptide sequence of 6 histidines was not detected.

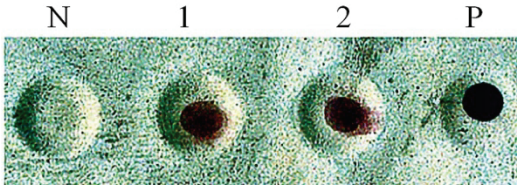

Fig 2. Dot blot analysis for recombinant chitinase expressed by *S. cerevisiae* INVSc1 cells. Line N = negative control – *S. cerevisiae* INVSc1 pYES2 cells, line 1–2 = *S. cerevisiae* INVSc1 ChiA_pYES2 cells, line P = positive control – rabbit anti His antibody.

Optimization of protein expression

Since each enzyme behaves differently, it is important to optimize the growth and expression conditions. The recombinant *B. licheniformis* ChiA gene was controlled by the GAL1 promoter in *S. cerevisiae* allowing the induction of gene expression on 2 % galactose. The coding sequence was also fused to the *α*--factor pro-peptide to ensure the secretion of the enzyme to the extracellular medium. The expression of ChiA in the *S. cerevisiae* strain INVSc1 was analyzed by growing the strain transformed with ChiA_pYES2 in a small volume of SC-U expression medium, and the culture samples were tested for the presence of ChiA over the next 72 h. This analysis was realized within two conditions: first, with the addition of galactose inductor only at the moment of the beginning of expression and second, with the addition of galactose every 24 h, for 72 h. The optimal chitinase expression time was found to be about 24 h after galactose induction. After 48 h, the relative activity of chitinase droped below 20 % (Fig. 3A). Surprisingly, when galactose was added to the expression medium on a daily basis, chitinase activity existed throughout the expression range (0–72 h), which translates to the fact that the recombinant enzyme was synthesized constantly (Fig. 3B). The consumption of galactose is the explanation for which the production of ChiA stagnates after 48 h, this fact being revealed by a decrease of the enzyme activity.

To determine whether recombinant chitinase A is produced as an intra- or extracellular enzyme, samples were taken after 24 h of expression and centrifuged to separate the supernatant from cells. Using 4MUTC fluorogenic substrate, the chitinase activity from the supernatant and cells of *S. cerevisiae* con-

taining ChiA_pYES2 or pYES2, was verified. Unexpectedly, only in the cell samples was chitinase activity observed, as could be seen in Fig. 4.

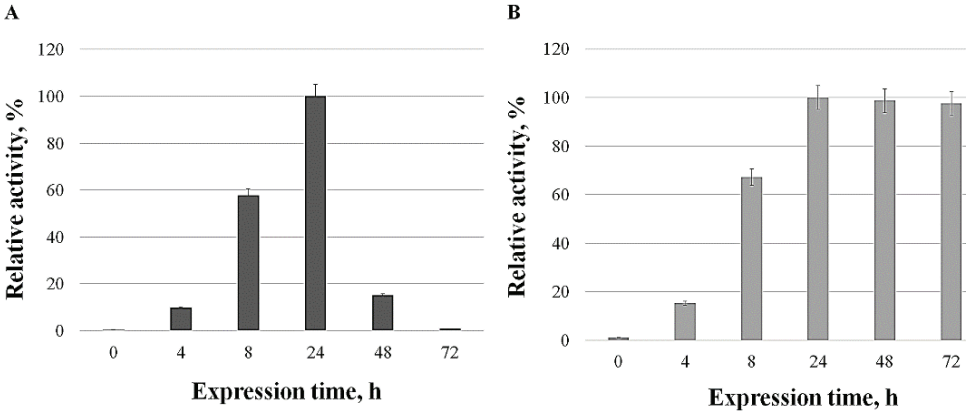

Fig. 3. Optimal expression time of recombinant chitinase A produced by *S. cerevisiae* INVSc1, on a 4 MUTC fluorogenic substrate, at different expression time intervals. A) Galactose was added only at the beginning of expression; B) galactose was added at every 24 h, for 72 h. Fluorescent assay was realized on culture samples.

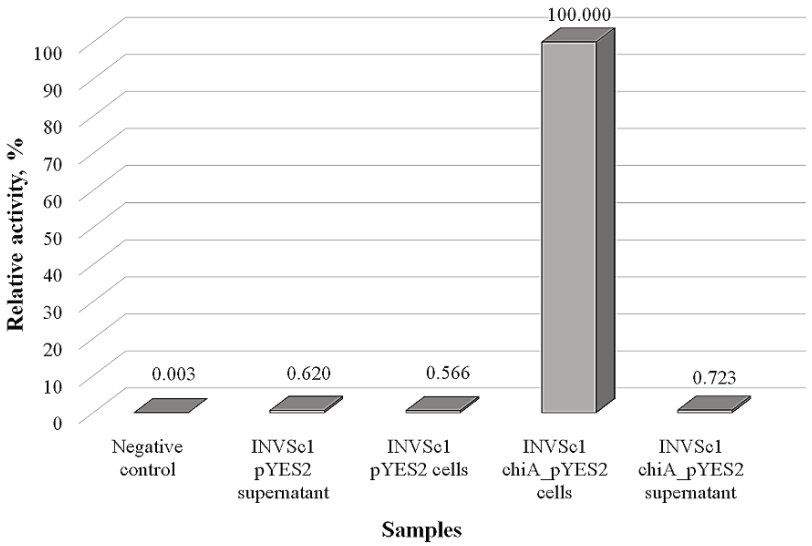

Fig. 4. Relative activity of recombinant chitinase from supernatant and cells of *S. cerevisiae* INVSc1, on a 4MUTC fluorogenic substrate. The negative control contained only distilled water and fluorogenic substrate.

Based on the optimized small-scale fermentation conditions, the recombinant ChiA was produced for 24 h at 27 °C. The enzyme was recovered from the cells and purified using anion exchange chromatography on a Sepharose/DEAE column.

From the fractions obtained, only those that showed chitinase activity on the fluorogenic substrate were collected. Purified recombinant chitinase A revealed on SDS protein electrophoresis to be a highly glycosylated enzyme.

In order to see the mode of expression, from a glycosylation point of view, ChiA produced in *S. cerevisiae* INVSc1 was compared to the same enzyme produced in *P. pastoris* KM71H[8] and *E. coli* BL21 (DE3) (purification of ChiA from this strain will be subject of another research article). As could be observed in Fig 5A, line 1, recombinant ChiA produced in *S. cerevisiae* is represented by a heterogeneous diffuse band between 80 and 180 kDa, which means strong glycosylation. In Fig 5A, line 2, ChiA produced in *P. pastoris* shows a visible lower molecular mass, being situated between 70–130 kDa. In contrast, in line 3, from the same figure, ChiA produced in *E. coli* is aglycosylated, having a molecular mass around 75 kDa.

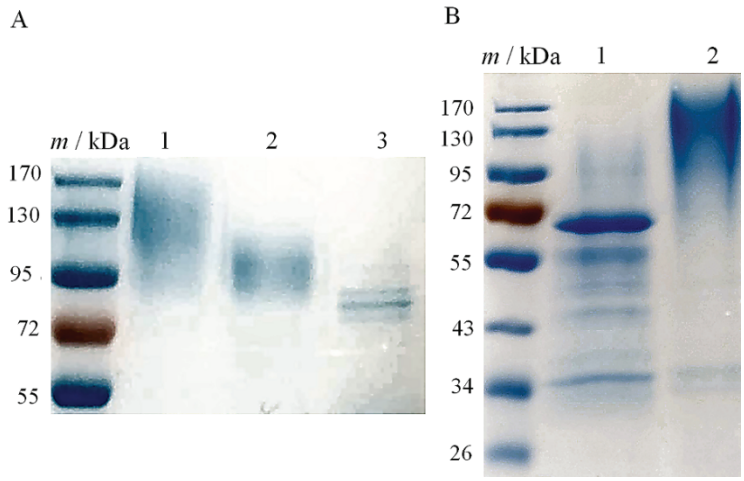

Fig. 5. SDS-PAGE (9 % gel) analysis of purified recombinant ChiA under reducing conditions. A) SDS-PAGE analysis of purified recombinant ChiA expressed by different strains. Line *m* / kDa = protein molecular marker, line 1 = ChiA expressed in *S. cerevisiae* INVSc1, line 2 = ChiA expressed in, line 3 = ChiA expressed in *E. coli* BL21 (DE3). B) SDS-PAGE analysis of deglycosylated ChiA produced in S. cerevisiae INVSc1. Line 1 = ChiA deglycosylated with PNGase F, line2 = ChiA hyperglycosylated.

Deglycosylation was performed using PNGase F, the most effective enzyme for removing completely N-linked oligosaccharides from glycoproteins,[20] in order to confirm the theoretical mass of ChiA. This reaction confirmed as well the hyperglycosylation of the recombinant ChiA in *S. cerevisiae* (Fig. 5B). In *S. cerevisiae* most proteins are synthesized in the extracellular medium as hyperglycosylated proteins.[21] Nevertheless, the recombinant ChiA, originated from *B. licheniformis* was not exported in extracellular space. In order to have a better

understanding on mode of expression of other proteins, in *S. cerevisiae* INVSc1, a synthetic view is presented in Table I. As could be seen, after expression, proteins have higher molecular mass, because of the glycosylation. Molecular mass of heterologous expressed proteins is even 3 times higher than mass of the same proteins produced in the organism of origin.

As it can be seen in Table I, extracellularly expressed proteins have relatively small mass even after glycosylation. Signal sequences are the strategic factors adjusting protein secretion. Introduction of a signal peptide improves the secretion of heterologous proteins in yeast. However, it is clear that even with *α*-factor signal peptide proteins can remain in the intracellular space. Some studies showed that the secretion efficiency of foreign proteins in recombinant microbes is strongly dependent on the combination of the signal peptides.[22,23] This could be a possible explanation for the case when some proteins are exported in extracellular space, some are not, when an α-factor signal peptide is used for secretion.

TABLE I. An overview of expression of different enzymes in *S. cerevisiae* INVSc1, by galactose induction

Organism of origin	Expression vector	Recomb. enzyme	*m* / kDa		Location of expressed enzyme	Peptide sequence	Ref.
			Native enzyme	Recomb. enzyme			
Bacillus licheniformis DSM8785	pYES2	Chitinase A	66.8	95-180	Intracellular	*α*-Factor signal peptide	This paper, [24]
Melanocarpus albomyces	pMS174 pMS175	Laccase	80	95	Intracellular (major part) and extracellular	*α*-Factor signal peptide and propeptide	[25]
Aspergillus oryzae	pYES/EXL, pYES3/CT	Cutinase	26	–	Intracellular (cell walls and/or between cell wall and cell membrane) and extracellular (traces), extracellular for protoplasts	-	[26]
Lentinula edodes	pYES2	Cytochrome P450	46.8	61	Intracellular (microsomes)	–	[27]
Insect-derived amylolytic enzyme	pYES2	Alpha-amylase	–	~53	Intracellular and extracellular (major part)	No	[22]

TABLE I. Continued

Organism of origin	Expression vector	Recomb. enzyme	*m* / kDa		Location of expressed enzyme	Peptide sequence	Ref.
			Native enzyme	Recomb. enzyme			
Acinetobacter sp. SM04	pYES2-alpha (pYα)	Peroxiredoxin	20	–	Extracellular	*α*-Factor signal peptide	28
Aspergillus niger	pYES2	Xylanase	27.2	–	Extracellular	*α*-Factor signal peptide	29
Dioscoreophyllum cumminsii	pYES2	Monellin (sweet protein)	11	~10.7	Extracellular	*α*-Factor signal peptide	30
Bombyx mori	pYES2/CT	Cecropin antibacterial peptide	4	6–10	Extracellular	*α*-Factor signal peptide	31
Phanerochaete chrysosporium	pYES2	Cellobiose dehydrogenase	≈90	120–150	Extracellular	*α*-Factor signal peptide	32

In 1982, Elango *et al.*[19] during the transformation of yeast cells into protoplasts observed as well that only about half of the yeast chitinase were released into the medium, indicating that part of the enzyme is located in the periplasmic space, and the other part remains in vacuoles or intracellular vesicles.

The capacity of the endoplasmic reticulum (ER) to fold and process foreign proteins is a significant factor restricting the expression of foreign proteins in *S. cerevisiae* and could represent another reason for which ChiA remain blocked in the cells.

A schematic overview representing glycosylation sites of different enzymes expressed with a pro-peptide signal in *S. cerevisiae* pYES2 system is presented in Fig. 6. Chitinase A (Fig. 6A) and hexose oxidase Fig. 6B) enzymes even though they are cloned with α factor signal peptide are not externally expressed in the culture medium. Nevertheless, cellobiose dehydrogenase (Fig. 6C) and glucose oxidase (Fig. 6D) are secreted in the culture medium.

The main hypothesis in this case was correlated with the glycosylated sites and the molecular mass at which the enzyme reaches after glycosylation. Chitinase A was expressed in the *P. pastoris* KM71H pPICZαA system as an external glycosylated enzyme with a molecular mass between 70 and 130 kDa.[8] In this case, the signal peptide was efficient and transported the enzyme out of the cell. Despite this fact, in *S. cerevisiae* INVSc1, the signal peptide is not efficient, chitinase A being blocked in the intracellular or periplasmic space of the cells. In *S. cerevisiae* INVSc1, ChiA was internally expressed as a hyperglycosylated enzyme, with a molecular mass between 80 and 180 kDa, 50 kDa higher than of ChiA expressed in *P. pastoris*. Number of glycosylation residues at S. *cerevisiae*

is higher than at *P. pastoris* and this could be a possible explanation for blocking the ChiA in the cell.

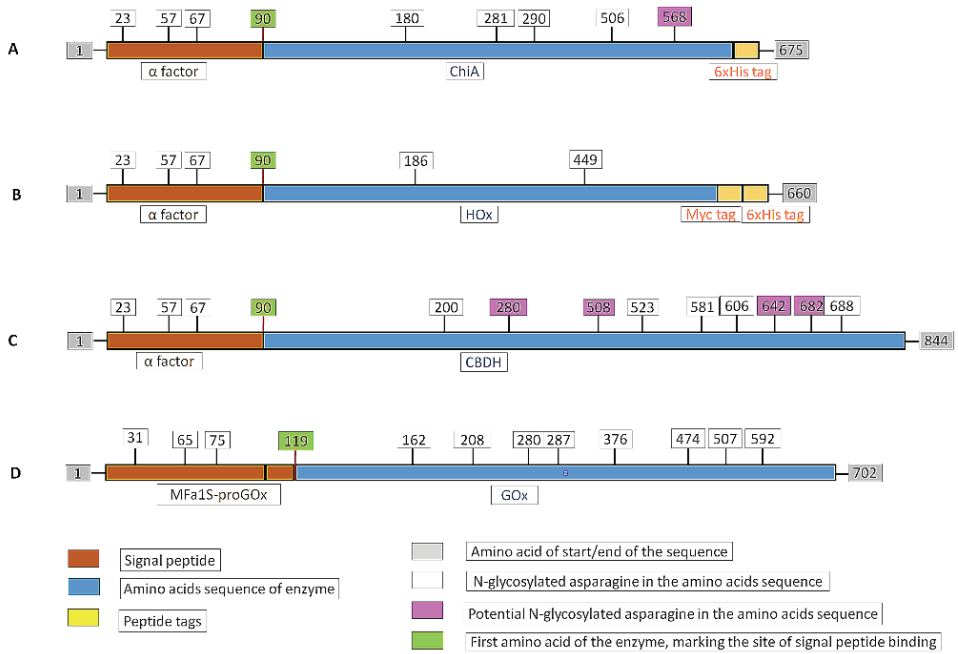

Fig. 6. Schematic representation of glycosylation sites in 4 different enzymes expressed in the *S. cerevisiae* pYES2 system. A) α factor_ChiA (chitinase A) 6xHis tag, B) *α*-factor_HOx (hexose oxidase) Myc_6xHis tags, C) *α*-factor_CBDH (cellobiose dehydrogenase), D) MFa1S-pro_GOx (glucose oxidase). The sequences were analyzed using Expasy Bioinformatics tools and NetNGlyc 1.0 Server – DTU.

CONCLUSIONS

The recombinant ChiA enzyme originating from *Bacillus licheniformis* has been successfully expressed in the *S. cerevisiae* INVSc1 expression platform. Unlike the native enzyme, the recombinant ChiA produced in *S. cerevisiae* INVSc1 was hyperglycosylated. Hyperglycosylation of ChiA was confirmed, as well, by a comparative analysis between the same recombinant ChiA produced in *P. pastoris* and *E. coli* systems. It was shown that by adding of galactose inductor, every day to culture medium, the expression of chitinase is constant, for 72 h. Production of hyperglycosylated ChiA into the yeast cells was confirmed by fluorescent activity assay. The number of the glycosylation sites of the ChiA gene sequence and the proximity of these sites to the α factor sequence were hypothesized to be a possible reason for which ChiA enzyme was internally expressed instead to be secreted by *S. cerevisiae* INVSc1 strain.

Acknowledgments. The authors thanks go to Dr. Raluca Ostafe from the Purdue Institute of Inflammation, Immunology and Infectious Disease, Molecular Evolution, Protein Engineering and Production, USA, and to Prof. Dr. Rainer Fischer from Department of Biological Sciences and Chemistry, Purdue University, USA, for valuable help in designing and training of the experimental part of the work. This work was supported by the strategic grant POSDRU/159/1.5/S/137750: Project "Doctoral and postdoctoral programs support for increased competitiveness in exact sciences research" co-financed by the European Social Fund within the Sectorial Operational Program Human Resources Development 2007–2013.

ИЗВОД

НЕКОНВЕНЦИОНАЛНА ЕКСПРЕСИЈА РЕКОМБИНАНТНЕ ХИТИНАЗЕ А ПОРЕКЛОМ ИЗ *Bacillus licheniformis* DSM8785 У *Saccharomyces cerevisiae* INVSC1

GHEORGHITA MENGHIU[1], РАДИВОЈЕ ПРОДАНОВИЋ[2], МАРИЈА БЛАЖИЋ[2], MANUELA MINCEA[1], CRISTINA MORARU[1] и VASILE OSTAFE[1]

[1]*Advanced Environmental Research Laboratories, Department of Biology – Chemistry, West University of Timisoara, Timisoara, Romania и* [2]*Хемијски факултет, Универзитет у Београду, Београд*

Хитиназе су гликозил-хидролазе које цепају β-1,4 везу између *N*-ацетил-глукозамина, који су присутни у хитинским ланцима. Хитин је други најраспрострањенији полисахарид на земљи након целулозе и формира се у егзоскелету ракова и инсеката, а налази се и у неким деловима ћелијских зидова печурака. Ензимско дејство и екстракција виших деривата из хитинског отпада (као што су хитоолигосахариди који имају важну улогу у медицинској и индустрији биогорива) доводе до потражње за хитиназом и њеном синтезом употребом различитих сојева организама. У овом раду је клониран ген ChiA из *Bacillus licheniformis* DSM8785 који кодира хитиназу А (ChiA) са С-терминалним хексахистидином, а експримиран је у ванћелијском експресионом систему pYES2 из *Saccharomyces cerevisiae* INVSc1 као хипергликозилован ензим. Производња рекомбинантног ензима ChiA је са успехом потврђена тачкастим блотом употребом анти-His антитела. Утврђено је да је оптимално време експресије 24 h када је додата галактоза само на почетку ферментације, односно да након тог времена активност хитиназе опада. У другом експерименту је утврђено да се експресија наставља 72 h, уколико се галактоза додаје свака 24 h. Пречишћен ензим је детектован применом SDS-PAGE као хетерогена дифузна трака између 80 и 180 kDa. Упоређивана је молекулска маса ензима ChiA експримираног у *Pichia pastoris* KM71H, *Escherichia coli* BL21 (DE3) и *Saccharomyces cerevisiae* INVSc1 методом SDS-PAGE. Активност ензима ChiA је утврђена употребом флуорогеног супстрата 4-метилумбелиферил β-D-*N*,*N*,*N*-триацетилхитотриозида (4MUTC). Користећи биоинформатичку симулацију, постављена је хипотеза о могућем разлогу унутарћелијске експресије ензима. Претпоставка је да су број места гликозиловања кодираних у ChiA гену и близина ових места секвенци алфа фактора могући разлог овакве експресије.

(Примљено 13. септембра, ревидирано 29. децембра 2021, прихваћено 28. фебруара 2022)

REFERENCES

1. P. Jolles, R. A. A. Muzzarelli, *Chitin and Chitinases*, Birkhäuser Basel, Basel, 1999
2. Y. M. Stoykov, A. Pavlov, A. Krastanov, *Eng. Life Sci.* **15** (2015) 30 (https://doi.org/10.1002/elsc.201400173)

3. R. K. Bretthauer, F. J. Castellino, *Biotechnol. Appl. Biochem.* **30** (1999) 193 (https://doi.org/10.1111/j.1470-8744.1999.tb00770.x)
4. O. W. Rossanese, J. Soderholm, B. J. Bevis, I. B. Sears, J. O'Connor, E. K. Williamson, B. S. Glick, *J. Cell Biol.* **145** (1999) 69 (https://doi.org/10.1083/jcb.145.1.69)
5. B. Huang, J. Guo, B. Yi, X. Yu, L. Sun, W. Chen, *Biotechnol. Lett.* **30** (2008) 1121 (https://doi.org/10.1007/s10529-008-9663-z)
6. H. Kim, S. J. Yoo, H. A. Kang, *FEMS Yeast Res.* **15** (2015) 1 (https://doi.org/10.1111/1567-1364.12195)
7. R. Mokdad-Gargouri, S. Abdelmoula-Soussi, N. Hadiji-Abbes, I. Y. Amor, I. Borchani--Chabchoub, A. Gargouri, *Methods Mol. Biol.* **824** (2012) 359 (https://doi.org/10.1007/978-1-61779-433-9_18)
8. G. Menghiu, V. Ostafe, R. Prodanovic, R. Fischer, R. Ostafe, *Protein Expression Purif.* **154** (2019) 25 (https://doi.org/10.1016/j.pep.2018.09.007)
9. H. Miller, D. S. Witherow, S. Carson, *Molecular Biology Techniques: A Classroom L-aboratory Manual*, Academic Press, Boston, MA, 2011, pp. 35–40 (ISBN 9780123855459)
10. F. Sanger, S. Nicklen, A. R. Coulson, *Proc. Natl. Acad. Sci. U.S.A.* **74** (1977) 5463 (https://doi.org/10.1073/pnas.74.12.5463)
11. D. R. Gietz, R. A. Woods, *Methods Enzymology*, *Transformation of yeast by lithium acetate/single-stranded carrier DNA/polyethylene glycol method*, Academic Press, New York, 2002, pp. 87–96 (https://doi.org/10.1016/S0076-6879(02)50957-5)
12. G. R. Grimsley, C. N. Pace, *Curr. Protoc. Protein Sci.* 33(2003 3.1.1- (https://doi.org/10.1002/0471140864.ps0301s33)
13. U. K. Laemmli, *Nature* **227** (1970) 680 (https://doi.org/10.1038/227680a0)
14. R. Gupta, S. Brunak, *Pac. Symp. Biocomput.* (2002) 310 (https://pubmed.ncbi.nlm.nih.gov/11928486/)
15. L. T. Invitrogen: pPICZalpha A, B, and C, *Pichia* expression vectors for selection on zeocin™ and purification of secreted, recombinant proteins, Cat. no. V195-20, MAN0000035. In *User Manual*, 2010 (https://www.fishersci.ca/shop/products/invitrogen-ppicz-a-b-c-i-pichia-i-vectors/v19520)
16. A. J. Brak,, J. P. Merryweather, D. G. Coit, U. A. Heberlein, F. R. Masiarz, G. T. Mullenbach, M. S. Urdea, P. Valenzuela, P. J. Barr, *Proc. Natl. Acad. Sci. U.S.A.* **81** (1984) 4642 (https://doi.org/10.1073/pnas.81.15.4642)
17. M. R. Wilkins, E. Gasteiger, A. Bairoch, J. C. Sanchez, K. L. Williams, R. D. Appel, D. F. Hochstrasser, *Methods Mol. Biol.* **112** (1999) 531 (https://doi.org/10.1385/1-59259-584-7:531)
18. J. U. Correa, N. Elango, I. Polacheck, E. Cabib, *J. Biol. Chem.* **257** (1982) 1392 (https://doi.org/10.1016/S0021-9258(19)68204-9)
19. N. Elango, J. U. Correa, E. Cabib, *J. Biol. Chem.* **257** (1982) 1398 (https://doi.org/10.1016/S0021-9258(19)68205-0)
20. M. Vilaj, G. Lauc, I. Trbojević-Akmačić, *Glycobiology* (2020) (https://doi.org/10.1093/glycob/cwaa047)
21. M. J. Kuranda, P. W. Robbins, *J. Biol. Chem.* **266** (1991) 19758 (https://doi.org/10.1016/S0021-9258(18)55057-2)
22. E. Celińska, M. Borkowska, W. Białas, *Appl. Microbiol. Biotechnol.* **100** (2016) 2693 (https://doi.org/10.1007/s00253-015-7098-8)

23. A. Mori, S. Hara, T. Sugahara, T. Kojima, Y. Iwasaki, Y. Kawarasaki, T. Sahara, S. Ohgiya, H. Nakano, *J. Biosci. Bioeng.* **120** (2015) 518 (https://doi.org/10.1016/j.jbiosc.2015.03.003)
24. C. Songsiriritthigul, S. Lapboonrueng, P. Pechsrichuang, P. Pesatcha, M. Yamabhai, *Biores. Technol.* **101** (2010) 4096 (http://dx.doi.org/10.1016/j.biortech.2010.01.036)
25. L. L. Kiiskinen, M. Saloheimo, *Appl. Environ. Microbiol.* **70** (2004) 137 (https://doi.org/10.1128/AEM.70.1.137-144.2004)
26. H. Aoyagi, Y. Katakura, A. Iwasaki, *Springer Plus* **5** (2016) 160 (https://doi.org/10.1186/s40064-016-1806-4)
27. R. Akiyama, S. Kajiwara, K. Shishido, *Biosci. Biotechnol. Biochem.* **68** (2004) 79 (https://doi.org/10.1271/bbb.68.79)
28. Y. Tang, J. Xiao, Y. Chen, Y. Yu, X. Xiao, Y. Yu, H. Wu, *Microbiol. Res.* **168** (2013) 6 (https://doi.org/10.1016/j.micres.2012.08.002)
29. C. Bao, J. Li, H. Chen, Y. Sun, G. Wang, G. Chen, S. Zhang, *Sci. Rep.* **10** (2020) 11686 (https://doi.org/10.1038/s41598-020-68570-6)
30. Z. Chen, Z. Li, N. Yu, L. Yan, *Biotechnol. Lett.* **33** (2010) 721 (https://doi.org/10.1007/s10529-010-0479-2)
31. L. Xia, Z. Liu, J. Ma, S. Sun, J. Yang, F. Zhang, *Protein Expression Purif.* **90** (2013) 47 (https://doi.org/10.1016/j.pep.2013.02.013)
32. M. Blažić, A. M. Balaž, V. Tadić, B. Draganić, R. Ostafe, R. Fischer, R. Prodanović, *Biochem. Eng. J.* **146** (2019) 179 (https://doi.org/10.1016/j.bej.2019.03.025).

Journal of the Serbian Chemical Society
JSCS@tmf.bg.ac.rs • www.shd.org.rs/JSCS

J. Serb. Chem. Soc. 87 (6) 693–706 (2022)
JSCS–5551

Original scientific paper
Published 28 April 2022

In silico identification of novel allosteric inhibitors of Dengue virus NS2B/NS3 serine protease

RENATO A. DA COSTA[1], JOÃO A. P. DA ROCHA[2]*, ALAN S. PINHEIRO[3], ANDRÉIA S. S. DA COSTA[4], ELAINE C. M. DA ROCHA[5], LUIZ P. C. JOSINO[3], ARLAN DA SILVA GONÇALVES[6], ANDERSON H. L. LIMA[3] and DAVI S. B. BRASIL[4]

[1]*Federal Institute of Education, Science and Technology of Pará - Campus Castanhal, 68740-970, Castanhal-PA, Brazil,* [2]*Federal Institute of Education, Science and Technology of Pará - Campus Bragança, 68600-000, Bragança-PA, Brazil,* [3]*Graduate Program in Chemistry, Institute of Exact and Natural Sciences, Federal University of Pará (UFPA), 66075-110 Belém-PA, Brazil,* [4]*Graduate Program in Science and Environment, Institute of Exact and Natural Sciences, Federal University of Pará (UFPA), 66075-110 Belém-PA, Brazil,* [5]*Federal Rural University of the Amazon Campus Capanema (UFRA), 68700-665 Capanema-PA, Brazil and* [6]*Federal Institute of Education, Science and Technology Technology of Espírito Santo Campus Vila Velha, 29106-010 Vila Velha-ES, Brazil*

(Received 29 September 2021, revised 20 January, accepted 17 February 2022)

Abstract: Although dengue is a disease that affects more than 100 countries and puts almost 400 million lives at risk each year, there is no approved antiviral in the treatment of this pathology. In this context, proteases are potential biological targets since they are essential in the replication process of this virus. In this study, a library of more than 3,000 structures was used to explore the allosteric inhibition of the NS2B/NS3 protease complex using consensual docking techniques. The results show four best ranked structures that were selected for molecular dynamics and free energy simulations. The present analysis corroborates with other studies (experimental and theoretical) presented in the literature. Thus, the computational approach used here proved to be useful for planning new inhibitors in the combat against Dengue disease.

Keywords: NS2B/NS3pro; consensual docking; molecular dynamics; binding free energy calculations.

INTRODUCTION

Dengue is a disease caused by the dengue virus (DENV), which affects the tropics and subtropics and is transmitted by the *Aedes aegypti*. In more than 100 countries, the virus causes approximately 390 million infections per year. DENV infections can result in several clinical conditions, even leading to death.[1–3] Not-

* Corresponding author. E-mail: joao.rocha@ifpa.edu.br
https://doi.org/10.2298/JSC210929011D

ably, there are no approved antiviral drugs for this disease and, currently, patients are treated with supportive care to relieve fever, pain, and dehydration.[4] Therefore, a new strategy is needed to discover potential antiviral agents for treating the dengue virus. The success of such research lies in finding protease enzymes that are indispensable for virus replication and for maintaining its infectivity. For this purpose, the NS2B/NS3 protease (NS2B/NS3pro) complex appears promising, as it is necessary for processing at the junctions of NS2A/NS2B, NS2B/NS3, NS3/NS4A and NS4B/NS5, NS3, NS2A and NS4A in dengue, and is therefore an important target for the development of drugs against dengue infection.[5,6] Most studies targeting NS2B-NS3pro by small-molecule inhibitors have focused on the active site, but unfortunately none of the drugs that inhibit the enzyme by binding to the active site have been approved to date. The flat and charged nature of the NS2B–NS3pro active site may be responsible for the difficulties in the development of inhibitors, which suggests that a strategy for exploring allosteric sites may be useful.[7]

A promising strategy is to design small molecules directed at the allosteric site.[8] Allosteric sites are defined as regions of a protein that, when linked to a small ligand, change the conformation or change the conformational balance, affecting the enzyme function. Allosteric sites have previously been considered important in proteases, making the exploration of allosteric sites in DENV NS2B–NS3pro promising.[9] Thus, in this work, the results of virtual screening (VS), consensual docking, molecular dynamics (MD), and free energy calculations for a bank of molecules that may be active against the DENV NS2B/ /NS3pro allosteric site are presented. This study is expected to contribute to the discovery of novel and potent anti-dengue agents. The use of molecular-scale methods for the discovery of new potential active ligands, as well as binding sites for unknown target proteins, is now an established reality. The literature offers many success stories of active compounds developed from insights obtained *in silico* and approved by the Food and Drug Administration (FDA). One of the most famous examples is raltegravir, an inhibitor of HIV integrase, developed after the discovery of a transient binding area through molecular dynamics simulations. These simulations in biomolecules and biomacromolecules are an interesting and fast method that is increasingly contributing to the fundamental understanding of living organisms, as well as having a profound impact on numerous diverse scientific endeavors, from biotechnological applications such as the manufacture of new intelligent biomaterials, DNA sequencing and the treatment of disease and drug development. Using computer modeling to complement experiments is helping to bridge the gap between atomic-level properties with whole-organism function, an effort that cannot be accomplished by either approach in isolation. A combination of several computational techniques, span-

ning a wide range of time and size scales, is ideal for capturing information at biological scales.[10,11]

EXPERIMENTAL

Virtual screenings and consensul docking

A library of 3940 compounds from the BaSe FilTer[12] (Part 1/20 of the total compounds present in the bank) were submitted to a VS and subsequently to a consensus analysis. The crystallographic coordinates of the DENV NS2B/NS3pro enzyme (PDB code: 2FOM)[13] retrieved from the Protein Data Bank (PDB) were used as a model of the biological target.

Consensual docking is an approach that consists of combining the results obtained by different scoring functions and ranking them, according to the combination of the results, improving the results obtained and compensating for the deficiencies found in each scoring function.[14] Thus, consensus analysis is considered more efficient than single scoring for molecular docking and represents an effective way to achieve better hit rates in various VS studies.[15,16] In both programs, fluctuations of the enzyme and the ligands were not allowed. Therefore, the docking results were analyzed using different protocols to obtain the most consistent binding affinity of the ligands. First, a VS was performed with the compounds in DENV NS2B/ /NS3pro using two programs: CSDGOLD[17] and DOCK6.[18] The CSDGOLD program uses the empirical fitness function called ChemPLP, which consists of applying hydrogen and metal bonding terms and piecewise linear potential (PLP) to model the steric complementarity between the protein and the ligand. The dimensionless scoring scale measures the success of the pose; higher scores indicate better docking positions.[17] The DOCK6 program is characterized by the use of an incremental construction algorithm. The scoring functions that guide the ligands to the target are based on a grid of potential energy, where van der Waals interactions are assessed by Lennard–Jones potentials, and the electrostatic interactions are evaluated through time-dependent dielectric functions.[18]

To perform molecular docking calculations, the coordinates for the search box were positioned based on the position of the allosteric binding site DENV NS2B/NS3pro according to.[19] For the CSD-GOLD protocol, the following parameters were set for the ChemPLP algorithm: all water molecules and ions were removed, then the coordinates for the search box were centered in $x = -10.004$, $y = -8.839$ and $z = 7.879$. For the DOCK6 protocol, the hydrogens were removed from the crystallographic model, and a box of 10 Å in size was generated and calculated by the dms, SPHGEN, grid and SHOWBOX programs.[20,21]

The consensual docking analysis was performed using the scaled-rank-by-number method. The scaled-rank-by-number is employed by scoring the energy values predicted for all compounds in the molecular docking with the different programs, according to Eq. (1):

$$X_{\text{ranked}} = (X - X_{\min})/(X_{\max} - X_{\min}) \quad (1)$$

where the scored value is obtained; $X_{\max}$ and $X_{\min}$ are, respectively, the maximum and minimum values of the utilized set. $X_{\max}$ corresponds to the most favorable affinity energy (lowest energy value), *i.e.*, X_{ranked} equals 1; the least favorable affinity energy value (highest energy value) is assigned 0, *i.e.*, X_{ranked} equals 0. The respective values scored for the compounds are then summed up in each program, and the final rank of the compounds that were best scored by different scoring functions is obtained.[22]

Molecular dynamics simulations

For analyze conformational changes in proteins and ligand structures, as well as the stability of ligand-receptor complexes, MD simulations were performed using the Amber18 pack-

age. Amber ff14SB and the amber general force field (GAFF) were applied to treat the structures of the protein and the four ligands best scored by the consensual dock, respectively.[23,24]

The atomic charges of the ligands were calculated using the restrained electrostatic potential (RESP) protocol at the HF/6-31G* level of theory[25] using the Gaussian 09 software[26] (see Supplementary material to this paper). First, the protonation states of the ionizable residues of the protein structures were analyzed by pK_a calculation at neutral pH using the H^{++} server.[27] All systems were solvated in the Leap module using a cubic water-box with the TIP3P model.[28] Na^+ was added to maintain the electroneutrality of the systems. All hydrogen atoms were minimized by 2000 steps of steepest descent, followed by 3000 steps of conjugate gradient algorithm. Next, the positions of the water molecules were relaxed using the same protocol. The whole system was energy-minimized for 5000 steps of the steepest descent plus 5000 steps of conjugate gradients. Thereafter, the system was heated from 0 to 300 K running 200 ps of MD and, next, 300 ps to density equilibration with position of the starting restraints on the protein-ligand atoms at a constant volume. Before performing the production step, all protein-ligand systems were equilibrated with 500 ps of MD without positional restraints at a constant pressure. The temperature was maintained at 300 K by coupling to a Langevin thermostat using a collision frequency of 2 cm^{-1}. A cutoff of 8 Å was employed for non-bonded interactions, the particle mesh Ewald (PME)[29] method and the Shake[30] algorithm were used to restrict the bond lengths involving the hydrogen atoms. Finally, the MD simulations (production) were performed using 100 ns at a temperature of 300 K without positional restraints. The generated trajectories were used to analyze the behavior of each complex to access the stability of the system in the explicit water environment. The deviations of the protein and protein–ligand complex system was analyzed by calculating root mean square deviation (*RMSD*), root mean square fluctuation (*RMSF*), radius of gyration (*RG*) and solvent accessible surface area (*SASA*).

Generalized Born and surface area continuum solvation (MM/GBSA)

End-point methods are strategies to perform binding free energy calculations in structure-based drug discovery, known for their accuracy/time consuming advantage, once it is considered the end of trajectory simulations as sample, where theoretically it should have a more stable structure, with lower *RMSD* fluctuation values through MD simulations. Therefore, using these methods to perform predictions about the strength of a receptor–ligand type of structure is advantageous, and usually more accurate than the scoring functions implemented in molecular docking.[31]

A widely used method in the literature is the molecular mechanics/generalized-Born surface area (MM/GBSA) method that was first implemented in studies with RNA and DNA complexes.[32]

The MM/GBSA method was applied to estimate the binding free energy change (ΔG_{bind}).[33] The last 10 ns of MD simulations of each system were used for binding free energy calculations.

ΔG_{bind} can be calculated according to the Eqs. (2)–(5):

$$\Delta G_{bind} = G_{complex} - (G_{protein} - G_{ligand}) \quad (2)$$

$$\Delta G_{bind} = \Delta H - T\Delta S \approx \Delta E_{MM} + \Delta G_{solv} - T\Delta S \quad (3)$$

$$\Delta E_{MM} = \Delta E_{internal} + \Delta E_{electrostatic} + \Delta H_{vd} \quad (4)$$

$$\Delta G_{solv} = \Delta G_{GB} + \Delta G_{nonpol} \quad (5)$$

where ΔG_{bind} is the inhibitor–protein binding free energy change resulting from the sum of the molecular mechanic energy (ΔE_{MM}), the desolvation free energy change (ΔG_{solv}) and the

entropic change term ($-T\Delta S$). The gas-phase molecular mechanic energy change (ΔE_{MM}) can be described by the sum of the internal energy contributions ($\Delta E_{internal}$), the sum of the energies due to the bonds, angles and dihedrals, electrostatic contributions ($\Delta E_{electrostatic}$), and the van der Waals term (ΔE_{vdw}). The desolvation free energy change (ΔG_{solv}) is the sum of the polar (ΔG_{GB}) and non-polar (ΔG_{nonpol}) contributions. The polar desolvation term was calculated using the implicit generalized Born (GB) approach. The entropic contribution explicit by the term $-T\Delta S$ in Eq. (3) is often disregarded when one is interested in relative and not absolute free energies, because it is significantly costly to compute entropic conformational changes.[31] In this work ligands with similar structures were analyzed, and for this reason a normal mode calculation was not used for this analysis because of computational cost and the tendency to have a large margin of error, introducing compelling uncertainty to the final result.

Per-residue energy decomposition

A per-residue energy decomposition method was used to determine the total energy contribution of each residue to the drug–receptor interaction and also to investigate the chemical nature of its interactions.[34]

MM/GBSA allows analysis of the contributions of individual residues or energetic terms by free energy decomposition analysis, which provides detailed energetic contributions to each specific amino acid residue sidechain to the binding state of the system, identifying the leading interactions in the binding process. That information can help further researchers to get a drug developed with the help of theoretical studies in the complex formation with proteins or another receptor type.

The interaction energy between an inhibitor and every residue in an enzyme could be described, according to Eq. (5), as the sum of of van der Waals (ΔE_{vdw} terms) and electrostatic (ΔE_{ele}) contributions in the gas phase, and polar (ΔG_{pol}) and nonpolar solvation (ΔG_{nonpol}) contributions:

$$\Delta G_{inhibitor\text{-}residue} = \Delta E_{vdw} + \Delta G_{ele} - \Delta G_{pol} + \Delta G_{nonpol} \quad (6)$$

RESULTS AND DISCUSSION

Analysis of selectivity of ligands to DENV-2 NS2B/NS3pro alosteric binding pockets

VS was performed for 3940 compounds and the efficacy of these compounds against DENV-2 NS2B/NS3pro was evaluated using consensual molecular docking, MD simulations, and binding free energy calculations. First, the docking scores obtained from GOLD and DOCK6, as well as the number of H-bond interactions formed with the amino acid residues from protein allosteric site, were analyzed. The consensual scoring values obtained for all 3940 compounds bound to the DENV-2 NS2B/NS3pro structure are given in Table S-I (Supplementary material). The results demonstrated that compounds 33-P5, 3-P5, 1466-P6 and 2645-P15 showed the best consensus docking rank. Thus, these ligands were selected for the MD simulation. The final ranks are listed in Table I.

Molecular docking is a powerful computational method used to investigate the selectivity and affinity of a ligand in a macromolecular receptor,[35] and has been widely applied in structure-based virtual screening approaches combined with *in silico* MD simulation techniques, and in calculating the free energy of

binding in the search for allosteric inhibitors of DENV-2 NS2B/NS3pro.[36–38] Based on the consensual docking results, the four best compounds were selected for analyzing the conformational dynamics of the complexes and their binding affinities.

TABLE I. Consensual docking rank final of four compounds docked against the DENV-2 NS2B/NS3pro structures

Compound ID	Rank final	Structure
Compound_33-P5	1.65	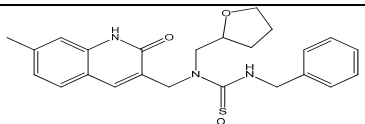
Compound_3-P5	1.64	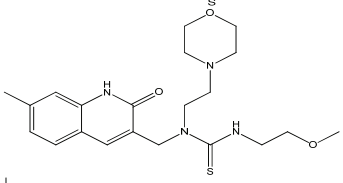
Compound_2645-P15	1.63	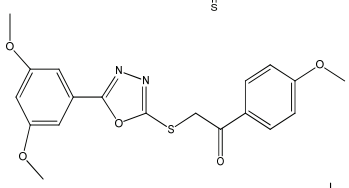
Compound_1466-P6	1.62	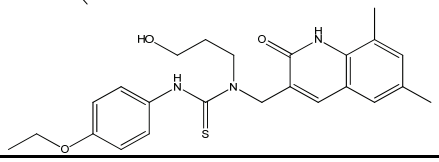

Molecular dynamics

The four best compounds were selected for MD simulation analysis to assess their stability and conformational changes, and to understand the dynamic characteristics of these ligands in relation to time in nanoseconds. Overall, the backbone *RMSD* values for Apo NS2B/NS3, NS2B/NS3pro-3-P5, NS2B/NS3pro-33--P5, NS2B/ /NS3pro-1466-P6 and NS2B/NS3pro-2645-P15 are < 3 Å throughout the 100 ns simulation time, reflecting the stability of the systems. Fluctuations between 1 and 3 Å within a reference protein structure are perfectly acceptable and indicate the stability of the complex.[39] Note that ligand 1466-P6 showed the highest *RMSD* value of ≈2.5 Å, lightly greater than the *RMSD* value for the free protein (Apo). We believe that this ligand is undergoing a process of reaccommodation in the allosteric site. The 3-P5 and 2645-P15 ligands showed the lowest *RMSD* values of 1.4 and 1.7 Å, respectively, even less than the value for free protein (Apo, Fig. 1). This fact may suggest that these two simulated ligands have high affinity for the protein.

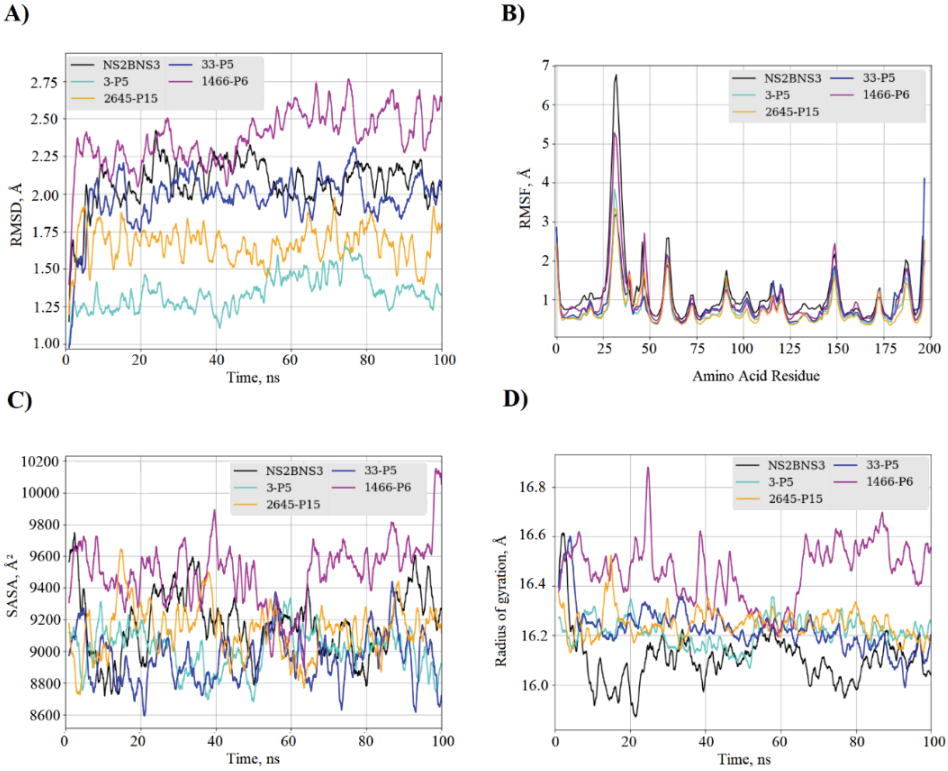

Fig. 1 Structural dynamics of NS2B/NS3pro enzyme-ligand complexes (3-P5 in cyan, 33-P5 in blue, 1466-P6 in mangeta and 264-P15 inhibitor in orange) and unbounded Apo (black) during 100 ns of MD simulations. A) Cα backbone *RMSD* in Å of all the selected compounds bound to the NS2B/NS3pro enzyme; B) *RMSF* values in Å plotted against the residue number for all the selected compounds bound to the NS2B/NS3pro enzyme; C) *SASA* values of the Cα backbone atoms; D) *Rg* values after compound binding.

The *RMSF* values (Fig. 1B) support this hypothesis. The highest fluctuations correspond to free protein and the 1466-P6 ligand, while the lowest values are attributed to systems complexed with ligands 3-P5 and 2645-P15, suggesting that these systems are more stable.

A solvent accessible surface area (*SASA*) analysis was performed to define the hydrophobicity of the protein in relation to the solvent. An *SASA* analysis is important for an energetic evaluation of biological macromolecules.[40] The *SASA* results for all systems during 100 ns of MD simulations are shown in Fig. 1C. The average *SASA* values for the APO protein and the complexes 3-P5-NS2B/ /NS3, 33-P5-NS2B/NS3, 1466-P6-NS2B/NS3 and 2645-P15-NS2B/NS3 were, respectively, 9176 (black), 9014 (cyan), 8955 (blue), 9499 (magenta) and 9132 $Å^2$ (orange), showing that the systems NS2B/NS3-ligands were relatively more stables.

A calculation of the radius of gyration (*Rg*) was performed to evaluate the stability of the protein–ligand systems by calculating the structural compactness along the MD trajectories.[41] After the MD simulation calculation, the calculation of *Rg* was also used to determine the stability of the folded and unfolded protein, and the complexes system. A graph of *Rg* as a function of time for the protein and all the protein-ligand complexes (NS2B/NS3pro-3-P5, NS2B/NS3pro-33-P5, NS2B/NS3pro-1466-P6 and NS2B/NS3pro-2645-P15) is shown in Fig. 1D. The average *Rg* value of the Apo protein was 16,10 Å (black). The average *Rg* value of the complexes were 16.21 (cyan), 16.22 (blue), 16.46 (magenta) and 116.24 Å (orange), respectively. It was found that all complexes exhibited relatively similar and consistent *Rg* values as compared to the Apo protein, which indicates that these are perfectively superimposed with each other and have good stability. Since the radius of gyration had a relatively consistent value throughout the MD simulation, it was regarded as stably folded.[42]

To further explore the binding mode of the complexes, the MMGBSA method was applied to the simulated systems, and the values of the free energies and their components for the complexes formed between DENV-2 NS2B/NS3pro ligands 3-P5, 33-P5, 1466-P6 and 2645-P15 indicated that the formation of the four complexes was favorable. The ΔG_{bind} and the values of the van der Waals energy change (ΔE_{vdW}), and the electrostatic (ΔE_{ele}), polar (ΔG_{GB}), and non-polar (ΔG_{nonpol}) contributions are summarized in Table II. Based on the binding free energy calculations, the complex of ligand 2645-P15 with DENV-2 NS2B/ /NS3pro showed the lowest affinity energy change (ΔG_{bind}) based on the MM/ /GBSA method.

TABLE II. Affinity energy values (J mol^{-1}) and energy components. ΔE_{vdw}, van der Waals contributions; ΔE_{ele}, electrostatic contributions; ΔG_{GB}, polar contributions; ΔG_{np}, non-polar contributions; ΔG_{bind}, affinity energy; the values ± correspond to the standard error of the mean

Ligand ID	ΔE_{vdW}	ΔE_{ele}	ΔG_{GB}	ΔG_{NP}	ΔG_{bind}
3-P5	–184765.44 ±376.56	–70165.68 ±962.32	158531.76 ±878.64	–23346.72 ±376.56	–120624.72 ±334.72
33-P5	–136440.24 ±418.4	–118323.52 ±962.32	175142.24 ±920.48	–15899.20 ±41.84	–95478.88 ±376.56
1466-P6	–174682.00 ±460.24	–66818.48 ±794.96	149619.84 ±711.28	–21296.56 ±41.84	–113135.36 ±418.40
2645-P15	–199200.24 ±292.88	–36066.08 ±627.60	117235.68 ±543.92	–24016.16 ±251.04	–140164.00 ±334.72

The main energetic contributions to the interaction of the DENV-2 NS2B/ /NS3pro receptor with the ligands are van der Waals contributions. It was observed that the energetic contribution of the hydrophobic residues of Leu106 (76), Trp113 (83), Ile153 (123), Val184 (154), Ala194 (164) and Ala196 (166), are present in the DENV NS2B/NS3pro allosteric site;[38,43] the numbers in paren-

theses indicate the numbering in the Erbel[16] model. In general, this is the preferred type of interaction observed between the complexes under study and protein residues.[44] To a lesser extent, electrostatic and nonpolar contributions also favored system formation.

The energy contributions in the simulations of each residue to the four complexes are shown in Fig. 2. This energy decomposition analysis shows the residues that contribute most significantly to the total interaction energy and, therefore, to the stabilization of the complexes.

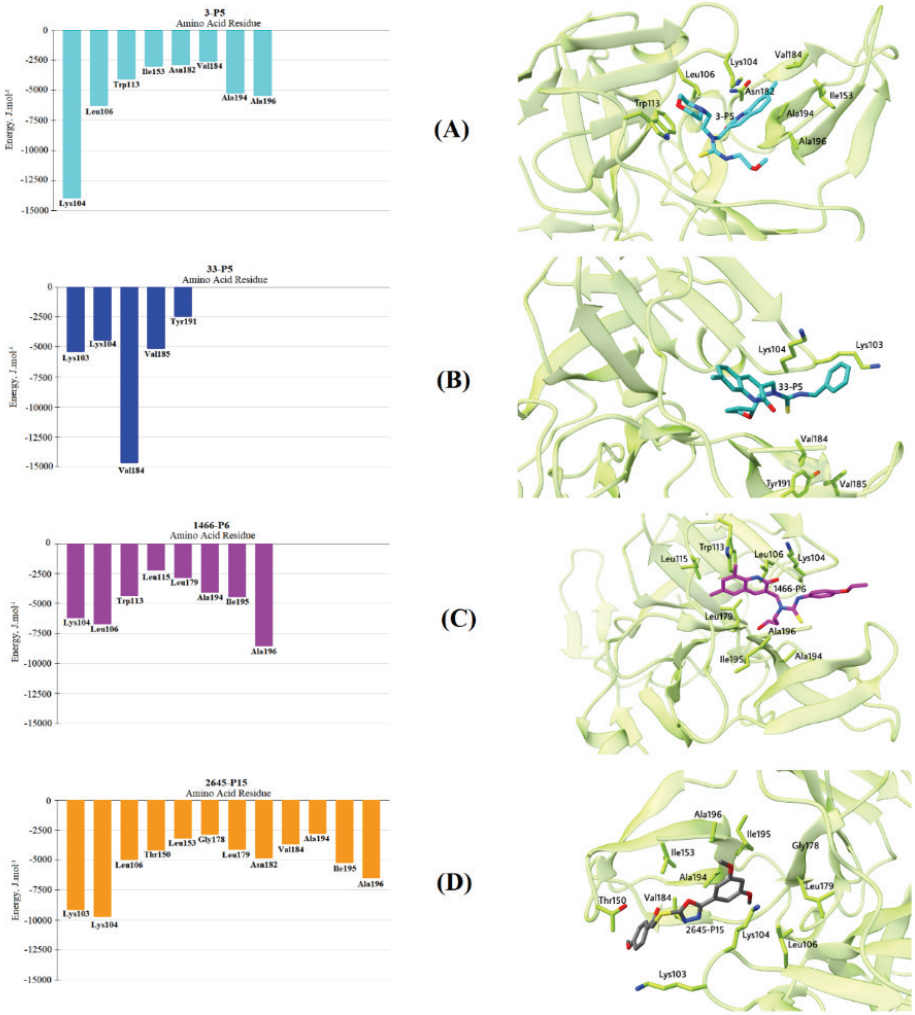

Fig. 2. Graphical representation of the interaction energy per residue (left) for the formed complexes: A) ligand 3-P5, B) ligand 33-P5, C) ligand 1466-P6 and D) ligand 2645-P15.

Analyzing the decomposition energy per residue of the NS2B/NS3pro structure complexed with ligand 2645-P15, it was observed that the residues Lys103 (73), Lys104 (74), Leu106 (76), Thr150 (120), Ile153 (123), Gly178 (148), Leu179 (149), Asn182 (152), Val184 (154), Ala194 (164), Ile195 (165) and Ala196 (166) from the NS2B/NS3pro allosteric site[43] formed favorable interactions with the aforementioned ligand, thus contributing to the stabilization of this complex. Of the other complex, 3-P5 presented the second lowest affinity energy and from an analysis of the residues that contribute favorably to the interaction with it, the influence of Lys104 (74), Leu106 (76), Trp113 (83), Ile153 (123), Asn182 (152), Val184 (154), Ala194 (164) and Ala196 (166). For the ligand 1466-P6, the residues Lys104 (74), Leu106 (76), Trp113 (83), Leu115 (85), Leu179 (149), Ala194 (164), Ile195 (165), Ala196 (166) were the main contributors to stability and to ligand 33-P5, the residues Lys103 (73), Lys104 (74), Val184 (154), Tyr191(161) and Val185(155) had favorable contributions. All ligands present favorable interactions that stabilized the complexes with residues from the NS2B/NS3pro allosteric site.[7,19,43] Therefore, inhibitors targeting this pocket may potentially be broad spectrum flavivirus inhibitors.

The residues Lys104(74) and Leu106(76) contribute significantly to the four simulated complexes. However, the interaction of Lys104(74) with the double benzene ring of the 3-P5 ligand is 1 kcal* mol^{-1} greater than that of the other systems, which is also well highlighted for the 2645-P15 ligand that also undergoes hydrogen bonding interaction with Thr150, is well highlighted. The triad of residues Ala194(164), Ile195(165), and Ala196(166) seems to contribute to the stabilization of the ligands at this site, especially in the systems of ligands 33-P5 and ligand 1466-P6. Based on this strong link with the triad, structural modifications to obtain more promising compounds are possible.

Although the two systems share similar bonds and interactions, which ensures that the inhibitors can bind tightly to the receptor protein, the existence of subtle discrepancies can be used in the future for designing drugs having these residues, with a high binding capacity.

The favorable interactions presented for the 3-P5 and 2645-P15 ligands corroborate the results observed in the literature that report NS2B/NS3pro allosteric inhibitors *in silico* and *in vitro* studies.[38,43,45,46] This fact suggests that these ligands may show inhibitory activity directed at the NS2B/NS3pro allosteric site.

In particular, analyzing the ligand 2645-P15, which showed the best binding affinities (ΔG_{bind}) based on the MM/GBSA method, it was possible to observe interactions with the residue Lys103 (73), Lys104 (74), Leu179 (149) and Asn182 (152), Val184(154) that, according to experimental and theoretical studies, are essential for protease inhibition.[19,38,43,45] Othman and collaborators[46] observed that interactions with residues Lys104 (74) and Leu179 (149) explained

* 1 kcal = 4184 J

the difference in the inhibition activity of non-competitive inhibitors in their studies. This interaction with Lys104 (74) is directly linked to Asp75 inducing a change in the region of the catalytic triad. This, presumably, could interrupt the electron transfer process necessary for the binding of the substrate at the active site, thus affecting the activity of the protease. Herein, the effects of the protein environment on the ligand binding could be highlighted. Some reports have considered the protonation pattern of the protein system determined by calculating the electrostatic energies from the solution of the linearized Poisson–Boltzmann Equation (LPBE).[47,48] The present results using an empirical approach (H++ server) indicate that the protonation states are in accordance with other studies, as mentioned above. Finally, it should be stressed that Leu179 (149) residue plays a role in the inhibition activity by blocking the entry of the ligand into the active site due to its position in the protease.[38,46]

CONCLUSIONS

In the present study, molecular docking, MD simulations and binding free energy calculations were used to investigate the binding affinity, selectivity and stability of candidates for allosteric inhibitors of the DENV NS2B/NS3pro enzyme. GOLD and DOCK6 programs were used to filter 3940 compounds through consensual docking, where the best positions were chosen based on the docking energies and hydrogen bonds. To estimate the dynamic behavior, MD simulations were performed for four protein–ligand complexes that proved to be promising in the consensual approach, and simulations of 100 ns each were performed using the AMBER package. The binding free energies were calculated for the simulated systems, highlighting the ligands 3-P5 and 2645-P15 that presented interactions with several residues of interest, these results are consistent with the results of other studies. Among them, the residues Lys103 (73), Asn182 (152), Lys104 (74) and Leu179 (149) are highlight. In addition, the triad of residues Ala194(164), Ile195(165), and Ala196(166) seems to be important in the stability of all systems and could be explored in the future when designing new compounds. The computational approach used herein proved to be useful for designing new inhibitors to combat Dengue.

SUPPLEMENTARY MATERIAL

Docking energy values for all compounds obtained by the GOLD and DOCK6 programs and their final classification values collected by the consensus platform Additional data and information are available electronically at the pages of journal website: https://www.shd-pub.org.rs/index.php/JSCS/article/view/11230, or from the corresponding author on request.

И З В О Д

IN SILICO ИДЕНТИФИКАЦИЈА НОВИЈИХ АЛОСТЕРИЧНИХ ИНХИБИТОРА СЕРИН ПРОТЕАЗЕ ДЕНГА ВИРУСА NS2B/NS3

RENATO A. DA COSTA[1], JOÃO A. P. DA ROCHA[2] , ALAN S. PINHEIRO[3], ANDRÉIA S. S. DA COSTA[4], ELAINE C. M. DA ROCHA[5], LUIZ P. C. JOSINO[3], ARLAN DA SILVA GONÇALVES[6], ANDERSON H. L. LIMA[3] и DAVI S. B. BRASIL[4]

[1]*Federal Institute of Education, Science and Technology of Pará - Campus Castanhal, 68740-970, Castanhal--PA, Brazil,* [2]*Federal Institute of Education, Science and Technology of Pará – Campus Bragança, 68600-000, Bragança-PA, Brazil,* [3]*Graduate Program in Chemistry, Institute of Exact and Natural Sciences, Federal University of Pará (UFPA), 66075-110 Belém-PA, Brazil,* [4]*Graduate Program in Science and Environment, Institute of Exact and Natural Sciences, Federal University of Pará (UFPA), 66075-110 Belém-PA, Brazil,* [5]*Federal Rural University of the Amazon Campus Capanema (UFRA), 68700-665 Capanema-PA, Brazil и* [6]*Federal Institute of Education, Science and Technology Technology of Espírito Santo Campus Vila Velha, 29106-010 Vila Velha-ES, Brazil*

Иако је Денга грозница болест која напада преко 100 земаља и сваке године излаже опасности скоро 400 милиона живота, нема одобреног антивирусног лека за третирање ове патологије. У том контексту, протеазе су потенцијални биолошки циљеви пошто су оне битне у процесу умножавања овог вируса. У овој студији је коришћена библиотека са више од 3000 структура да би се истражила алостеричка инхибиција NS2B/NS3 комплекса протеаза коришћењем техника сагласног докинга (consensual docking techniques). Резултати показују четири најбоље рангиране структуре које су одабране за симулације молекулске динамике и слободне енергије. Наша анализа је подржана другим студијама (експерименталним и теоријским) изнесеним у литератури. Тако је показано да овде коришћен рачунарски приступ може бити користан за планирање нових инхибитора у борби против Денга болести.

(Примљено 29. септембра 2021, ревидирано 20. јануара, прихваћено 17. фебруара 2022)

REFERENCES

1. A. Wilder-Smith, Murray, M. Quam, *Clin. Epidemiol.* (2013) 299 (https://doi.org/10.2147/CLEP.S34440)
2. M. G. Guzman E. Harris, *Lancet* **385** (2015) 453 (https://doi.org/10.1016/S0140-6736(14)60572-9)
3. S. Bhatt, P. W. Gething, O. J. Brady, J. P. Messina, A. W. Farlow, C. L. Moyes, J. M. Drake, J. S. Brownstein, A. G. Hoen, O. Sankoh, M. F. Myers, D. B. George, T. Jaenisch, G. R. W. Wint, C. P. Simmons, T. W. Scott, J. J. Farrar, S. I. Hay, *Nature* **496** (2013) 504 (https://doi.org/10.1038/nature12060)
4. C. P. Simmons, K. McPherson, N. Van Vinh Chau, D. T. Hoai Tam, P. Young, J. Mackenzie, B. Wills, *Vaccine* **33** (2015) 7061 (https://doi.org/10.1016/j.vaccine.2015.09.103)
5. K. V Pugachev, F. Guirakhoo, D. W. Trent, T. P. Monath, *Int. J. Parasitol.* **33** (2003) 567 (https://doi.org/10.1016/S0020-7519(03)00063-8)
6. D. Luo, S. G. Vasudevan, J. Lescar, *Antiviral Res.* **118** (2015) 148 (https://doi.org/10.1016/j.antiviral.2015.03.014)
7. M. Yildiz, S. Ghosh, J. A. Bell, W. Sherman, J. A. Hardy, *ACS Chem. Biol.* **8** (2013) 2744 (https://doi.org/10.1021/cb400612h)
8. B. Millies, F. von Hammerstein, A. Gellert, S. Hammerschmidt, F. Barthels, U. Göppel, M. Immerheiser, F. Elgner, N. Jung, M. Basic, C. Kersten, W. Kiefer, J. Bodem, E. Hildt, M. Windbergs, U. A. Hellmich, T. Schirmeister, *J. Med. Chem.* **62** (2019) 11359 (https://doi.org/10.1021/acs.jmedchem.9b01697)

9. M. Merdanovic, T. Mönig, M. Ehrmann, M. Kaiser, *ACS Chem. Biol.* **8** (2013) 19 (https://doi.org/10.1021/cb3005935)
10. M. Aminpour, C. Montemagno, J. A. Tuszynski, *Molecules* **24** (2019) 1693 (https://doi.org/10.3390/molecules24091693)
11. T. Casalini, *J. Control. Rel.* **332** (2021) 390 (https://doi.org/10.1016/j.jconrel.2021.03.005)
12. B. S. Kolte, S. R. Londhe, B. R. Solanki, R. N. Gacche, R. J. Meshram, *J. Mol. Graph. Model.* **80** (2018) 95 (https://doi.org/10.1016/j.jmgm.2017.12.020)
13. P. Erbel, N. Schiering, A. D'Arcy, M. Renatus, M. Kroemer, S. P. Lim, Z. Yin, T. H. Keller, S. G. Vasudevan, U. Hommel, *Nat. Struct. Mol. Biol.* **13** (2006) 372 (https://doi.org/10.1038/nsmb1073)
14. R. Perez-Pineiro, A. Burgos, D. C. Jones, L. C. Andrew, H. Rodriguez, M. Suarez, A. H. Fairlamb, D. S. Wishart, *J. Med. Chem.* **52** (2009) 1670 (https://doi.org/10.1021/jm801306g)
15. M. D. de Oliveira, J. de O. Araújo, J. M. P. Galúcio, K. Santana, A. H. Lima, *J. Mol. Graph. Model.* **101** (2020) 107735 (https://doi.org/10.1016/j.jmgm.2020.107735)
16. E. Harigua-Souiai, Y. Z. Abdelkrim, I. Bassoumi-Jamoussi, O. Zakraoui, G. Bouvier, K. Essafi-Benkhadir, J. Banroques, N. Desdouits, H. Munier-Lehmann, M. Barhoumi, N. K. Tanner, M. Nilges, A. Blondel, I. Guizani, *PLOS Negl. Trop. Dis.* **12** (2018) e0006160 (https://doi.org/10.1371/journal.pntd.0006160)
17. G. Jones, P. Willett, R. C. Glen, *J. Mol. Biol.* **245** (1995) 43 (https://doi.org/10.1016/s0022-2836(95)80037-9)
18. S. R. Brozell, S. Mukherjee, T. E. Balius, D. R. Roe, D. A. Case, R. C. Rizzo, *J. Comput. Aided Mol. Des.* **26** (2012) 749 (https://doi.org/10.1007/s10822-012-9565-y)
19. M. Brecher, Z. Li, B. Liu, J. Zhang, C. A. Koetzner, A. Alifarag, S. A. Jones, Q. Lin, L. D. Kramer, H. Li, *PLoS Pathog.* **13** (2017) e1006411 (https://doi.org/10.1371/journal.ppat.1006411)
20. E. C. Meng, B. K. Shoichet, I. D. Kuntz, *J. Comput. Chem.* **13** (1992) 505 (https://doi.org/10.1002/jcc.540130412)
21. I. D. Kuntz, J. M. Blaney, S. J. Oatley, R. Langridge, T. E. Ferrin, *J. Mol. Biol.* **161** (1982) 269 (https://doi.org/10.1016/0022-2836(82)90153-X)
22. A. S. Pinheiro, J. B. C. Duarte, C. N. Alves, F. A. de Molfetta, *Appl. Biochem. Biotechnol.* **176** (2015) 1709 (https://doi.org/10.1007/s12010-015-1672-5)
23. J. M. Wang, R. M. Wolf, J. W. Caldwell, P. a Kollman, D. a Case, *J. Comput. Chem.* **25** (2004) 1157 (https://doi.org/10.1002/jcc.20035)
24. J. A. Maier, C. Martinez, K. Kasavajhala, L. Wickstrom, K. E. Hauser, C. Simmerling, *J. Chem. Theory Comput.* **11** (2015) 3696 (https://doi.org/10.1021/acs.jctc.5b00255)
25. P. A. Kollman, I. Massova, C. Reyes, B. Kuhn, S. Huo, L. Chong, M. Lee, T. Lee, Y. Duan, W. Wang, O. Donini, P. Cieplak, J. Srinivasan, D. A. Case, T. E. Cheatham, *Acc. Chem. Res* **33** (2000) 889 (https://doi.org/10.1021/ar000033j)
26. *Gaussian 09 software*, Pittsburgh, PA, 2016
27. R. Anandakrishnan, B. Aguilar, A. V. Onufriev, *Nucleic Acids Res.* **40** (2012) W537 (https://doi.org/10.1093/nar/gks375)
28. W. L. Jorgensen, J. Chandrasekhar, J. D. Madura, R. W. Impey, M. L. Klein, *J. Chem. Phys.* **79** (1983) 926 (https://doi.org/10.1063/1.445869)
29. T. Darden, D. York, L. Pedersen, *J. Chem. Phys.* **98** (1993) 10089 (https://doi.org/10.1063/1.464397)
30. J. P. Ryckaert, G. Ciccotti, H. J. C. Berendsen, *J. Comput. Phys.* **23** (1977) 327 (https://doi.org/10.1016/0021-9991(77)90098-5)

31. E. Wang, H. Sun, J. Wang, Z. Wang, H. Liu, J. Z. H. Zhang, T. Hou, *Chem. Rev.* **119** (2019) 9478 (https://doi.org/10.1021/acs.chemrev.9b00055)
32. P. A. Kollman, I. Massova, C. Reyes, B. Kuhn, S. Huo, L. Chong, M. Lee, T. Lee, Y. Duan, W. Wang, O. Donini, P. Cieplak, J. Srinivasan, D. A. Case, T. E. Cheatham, *Acc. Chem. Res.* **33** (2000) 889 (https://doi.org/10.1021/ar000033j)
33. S. Genheden U. Ryde, *Expert Opin. Drug Discov.* **10** (2015) 449 (https://doi.org/10.1517/17460441.2015.1032936)
34. R. A. Costa, J. N. Cruz, F. C. A. Nascimento, S. G. Silva, S. O. Silva, M. C. Martelli, S. M. L. Carvalho, C. B. R. Santos, A. M. J. C. Neto, D. S. B. Brasil, *Med. Chem. Res.* **28** (2019) 246 (https://doi.org/10.1007/s00044-018-2280-z)
35. E. P. Semighini, J. A. Resende, P. de Andrade, P. A. B. Morais, I. Carvalho, C. A. Taft, C. H. T. P. Silva, *J. Biomol. Struct. Dyn.* **28** (2011) 787 (https://doi.org/10.1080/07391102.2011.10508606)
36. M. Hariono, S. B. Choi, R. F. Roslim, M. S. Nawi, M. L. Tan, E. E. Kamarulzaman, N. Mohamed, R. Yusof, S. Othman, N. Abd Rahman, R. Othman, H. A. Wahab, *PLOS One* **14** (2019) e0210869 (https://doi.org/10.1371/journal.pone.0210869)
37. A. J. Fathima, G. Murugaboopathi, P. Selvam, *Curr. Bioinform.* **13** (2018) 606 (https://doi.org/10.2174/1574893613666180118105659)
38. A. Mukhametov, E. I. Newhouse, N. A. Aziz, J. A. Saito, M. Alam, *J. Mol. Graph. Model.* **52** (2014) 103 (https://doi.org/10.1016/j.jmgm.2014.06.008)
39. F. A. D. M. Opo, M. M. Rahman, F. Ahammad, I. Ahmed, M. A. Bhuiyan, A. M. Asiri, *Sci. Rep.* **11** (2021) 4049 (https://doi.org/10.1038/s41598-021-83626-x)
40. A. Fornili, F. Autore, N. Chakroun, P. Martinez, F. Fraternali, *Computational Drug Discovery and Design*, Springer, New York, 2011, p. 375 (https://doi.org/10.1007/978-1-61779-465-0_23)
41. M. Shahbaaz, A. Nkaule, A. Christoffels, *Sci. Rep.* **9** (2019) 4405 (https://doi.org/10.1038/s41598-019-40621-7)
42. F. Ghasemi, A. Zomorodipour, A. A. Karkhane, M. R. Khorramizadeh, *J. Mol. Graph. Model* **68** (2016) 39 (https://doi.org/10.1016/j.jmgm.2016.05.011)
43. H. Wu, S. Bock, M. Snitko, T. Berger, T. Weidner, S. Holloway, M. Kanitz, W. E. Diederich, H. Steuber, C. Walter, D. Hofmann, B. Weißbrich, R. Spannaus, E. G. Acosta, R. Bartenschlager, B. Engels, T. Schirmeister, J. Bodem, *Antimicrob. Agents Chemother.* **59** (2015) 1100 (https://doi.org/10.1128/AAC.03543-14)
44. R. A. Costa, J. N. Cruz, F. C. A. Nascimento, S. G. Silva, S. O. Silva, M. C. Martelli, S. M. L. Carvalho, C. B. R. Santos, A. M. J. C. Neto, D. S. B. Brasil, *Med. Chem. Res.* **28** (2019) 246 (https://doi.org/10.1007/s00044-018-2280-z)
45. B. Millies, F. von Hammerstein, A. Gellert, S. Hammerschmidt, F. Barthels, U. Göppel, M. Immerheiser, F. Elgner, N. Jung, M. Basic, C. Kersten, W. Kiefer, J. Bodem, E. Hildt, M. Windbergs, U. A. Hellmich, T. Schirmeister, *J. Med. Chem.* **62** (2019) 11359 (https://doi.org/10.1021/acs.jmedchem.9b01697)
46. R. Othman, T. S. Kiat, N. Khalid, R. Yusof, E. Irene Newhouse, J. S. Newhouse, M. Alam, N. A. Rahman, *J. Chem. Inf. Model.* **48** (2008) 1582 (https://doi.org/10.1021/ci700388k)
47. D. Popovic I. Djordjevic, *J. Serb. Chem. Soc.* **85** (2020) 1429 (https://doi.org/10.2298/JSC200720047P)
48. D. M. Popović A. A. Stuchebrukhov, *J. Am. Chem. Soc.* **126** (2004) 1858 (https://doi.org/10.1021/ja038267w).

Journal of the Serbian Chemical Society
JSCS@tmf.bg.ac.rs • www.shd.org.rs/JSCS
J. Serb. Chem. Soc. 87 (6) S148–S234 (2022)
Supplementary material

SUPPLEMENTARY MATERIAL TO

In silico identification of novel allosteric inhibitors of Dengue virus NS2B/NS3 serine protease

RENATO A. DA COSTA[1], JOÃO A. P. DA ROCHA[2]*, ALAN S. PINHEIRO[3], ANDRÉIA S. S. DA COSTA[4], ELAINE C. M. DA ROCHA[5], LUIZ P. C. JOSINO[3], ARLAN DA SILVA GONÇALVES[6], ANDERSON H. L. LIMA[3] and DAVI S. B. BRASIL[4]

[1]Federal Institute of Education, Science and Technology of Pará - Campus Castanhal, 68740-970, Castanhal-PA, Brazil, [2]Federal Institute of Education, Science and Technology of Pará - Campus Bragança, 68600-000, Bragança-PA, Brazil, [3]Graduate Program in Chemistry, Institute of Exact and Natural Sciences, Federal University of Pará (UFPA), 66075-110 Belém-PA, Brazil, [4]Graduate Program in Science and Environment, Institute of Exact and Natural Sciences, Federal University of Pará (UFPA), 66075-110 Belém-PA, Brazil, [5]Federal Rural University of the Amazon Campus Capanema (UFRA), 68700-665 Capanema-PA, Brazil and [6]Federal Institute of Education, Science and Technology Technology of Espírito Santo Campus Vila Velha, 29106-010 Vila Velha-ES, Brazil

J. Serb. Chem. Soc. 87 (6) (2022) 693–706

TABLE S-I. Docking energy in final rank of all compounds

Compound	Docking energy, kJ mol^{-1}		
	GOLD	DOCK6	RANK
Compound_493-P10	55.0145	-40.4792	1.05
Compound_494-P10	48.3619	-40.6335	0.94
Compound_498-P10	47.2003	-33.1897	0.70
Compound_499-P10	42.4681	-32.8555	0.61
Compound_500-P10	49.1437	-35.1738	0.79
Compound_501-P10	45.8524	-35.1685	0.74
Compound_502-P10	42.9861	-34.5863	0.67
Compound_505-P10	43.5991	-35.0761	0.69
Compound_506-P10	35.3827	-34.7362	0.55
Compound_508-P10	49.0915	-37.4725	0.86
Compound_525-P10	43.4997	-34.5456	0.68
Compound_526-P10	39.5333	-34.9957	0.62
Compound_527-P10	53.3547	-36.2203	0.89
Compound_528-P10	46.6404	-37.0252	0.80
Compound_529-P10	43.2136	-37.0475	0.75
Compound_532-P10	51.9567	-41.3784	1.02
Compound_533-P10	66.5579	-45.3406	1.38

* Corresponding author. E-mail: joao.rocha@ifpa.edu.br

Compound	Docking energy, kJ mol^{-1}		
	GOLD	DOCK6	RANK
Compound_534-P10	66.3429	-44.8105	1.36
Compound_535-P10	54.8078	-46.4996	1.22
Compound_555-P10	47.1294	-42.0086	0.96
Compound_559-P10	72.8622	-43.7078	1.44
Compound_560-P10	53.2122	-43.6176	1.11
Compound_660-P10	43.7724	-42.6863	0.92
Compound_661-P10	51.1173	-43.8134	1.08
Compound_662-P10	37.5227	-43.0681	0.82
Compound_663-P10	48.0049	-41.0775	0.94
Compound_667-P10	60.6392	-44.2672	1.25
Compound_669-P10	59.9525	-44.3928	1.24
Compound_671-P10	43.0997	-44.2358	0.95
Compound_808-P10	47.4178	-44.9295	1.05
Compound_814-P10	43.6496	-38.7764	0.80
Compound_817-P10	48.6523	-40.2933	0.93
Compound_818-P10	53.1156	-44.8452	1.14
Compound_822-P10	52.9414	-40.9323	1.02
Compound_833-P10	63.2860	-41.3482	1.21
Compound_834-P10	53.6338	-37.4700	0.93
Compound_846-P10	40.7596	-36.3473	0.68
Compound_1267-P10	36.9559	-38.9872	0.70
Compound_1277-P10	64.6098	-42.0334	1.25
Compound_1301-P10	59.8522	-41.5171	1.16
Compound_1302-P10	54.2002	-42.6608	1.10
Compound_1314-P10	57.7154	-44.2496	1.20
Compound_1316-P10	41.4238	-43.2699	0.90
Compound_1320-P10	57.0063	-42.7086	1.14
Compound_1321-P10	46.9147	-42.1110	0.96
Compound_1323-P10	53.5591	-34.9115	0.86
Compound_1325-P10	60.4689	-41.5155	1.17
Compound_1326-P10	49.1343	-41.4219	0.97
Compound_1330-P10	53.6180	-44.0684	1.13
Compound_1632-P10	53.8111	-45.7540	1.18
Compound_1833-P10	42.6250	-31.3776	0.57
Compound_2036-P10	61.8467	-37.5276	1.08
Compound_2037-P10	50.6276	-31.6351	0.71
Compound_2038-P10	60.7469	-36.6313	1.03
Compound_2061-P10	69.9754	-43.6064	1.39
Compound_2092-P10	57.9794	-44.8444	1.22
Compound_2093-P10	40.4366	-46.7546	0.98
Compound_2094-P10	61.2447	-44.7289	1.27
Compound_2095-P10	60.2489	-45.1089	1.27
Compound_2096-P10	45.0966	-44.4462	0.99
Compound_2097-P10	59.4450	-43.3326	1.20
Compound_2100-P10	51.1354	-41.5047	1.01
Compound_2105-P10	48.4534	-33.6467	0.74

Compound	Docking energy, kJ mol^{-1}		
	GOLD	DOCK6	RANK
Compound_2106-P10	48.1227	-35.4610	0.78
Compound_2109-P10	44.1434	-43.4043	0.95
Compound_2114-P10	50.9913	-43.1084	1.05
Compound_2115-P10	67.3150	-43.6992	1.35
Compound_2118-P10	34.3255	-42.4298	0.75
Compound_2119-P10	54.3968	-43.9169	1.13
Compound_2121-P10	53.7670	-39.4133	0.99
Compound_2122-P10	42.4321	-40.5701	0.83
Compound_2125-P10	38.0393	-33.2455	0.55
Compound_2131-P10	44.0794	-45.0650	0.99
Compound_2136-P10	48.9384	-46.9752	1.13
Compound_2137-P10	42.4597	-42.3731	0.89
Compound_2138-P10	40.7445	-35.0601	0.65
Compound_2139-P10	60.8563	-45.3153	1.29
Compound_2140-P10	34.9478	-46.1151	0.87
Compound_2144-P10	38.3626	-46.3833	0.93
Compound_2145-P10	53.1406	-46.4414	1.19
Compound_2146-P10	36.3688	-43.3671	0.81
Compound_2147-P10	38.3319	-46.8173	0.95
Compound_2155-P10	39.4951	-46.2351	0.95
Compound_2159-P10	48.3234	-47.2788	1.13
Compound_2160-P10	39.0845	-45.1868	0.91
Compound_2180-P10	32.8939	-30.8277	0.39
Compound_2219-P10	41.3088	-34.5854	0.64
Compound_2254-P10	55.0989	-35.7801	0.91
Compound_2278-P10	49.1206	-39.4010	0.91
Compound_2339-P10	53.8117	-43.1300	1.10
Compound_2359-P10	60.1688	-36.6478	1.02
Compound_2424-P10	56.7177	-42.6482	1.14
Compound_2565-P10	68.5571	-42.2957	1.33
Compound_2577-P10	66.5549	-47.4789	1.44
Compound_2579-P10	41.1970	-41.3316	0.84
Compound_2583-P10	54.2175	-46.0503	1.19
Compound_2616-P10	57.9462	-42.7637	1.16
Compound_2664-P10	67.7664	-40.7089	1.27
Compound_2727-P10	65.7697	-44.9486	1.36
Compound_2737-P10	59.7896	-43.1793	1.21
Compound_2766-P10	46.2643	-35.6101	0.76
Compound_2767-P10	51.5390	-36.7953	0.88
Compound_2776-P10	51.2687	-37.9631	0.91
Compound_2440-P11	39.7743	-32.3569	0.55
Compound_2441-P11	50.1818	-32.1041	0.72
Compound_2463-P11	48.3836	-36.9779	0.83
Compound_2539-P11	53.3664	-37.9739	0.94
Compound_2546-P11	45.2918	-38.4890	0.82
Compound_2547-P11	63.4939	-39.4801	1.16

Compound	Docking energy, kJ mol^{-1}		
	GOLD	DOCK6	RANK
Compound_2548-P11	51.8828	-40.3744	0.99
Compound_2550-P11	41.3962	-43.2997	0.90
Compound_2551-P11	39.1605	-42.6747	0.84
Compound_2552-P11	55.3679	-41.9173	1.09
Compound_2554-P11	59.3719	-45.4047	1.26
Compound_2555-P11	45.2353	-45.6473	1.03
Compound_2569-P11	44.5374	-35.2276	0.72
Compound_2570-P11	42.4711	-37.3101	0.74
Compound_2571-P11	54.3922	-40.1765	1.03
Compound_2572-P11	49.8883	-40.0611	0.95
Compound_2573-P11	49.3663	-40.3050	0.94
Compound_2574-P11	67.9678	-44.0928	1.37
Compound_2584-P11	38.6052	-39.0160	0.72
Compound_2585-P11	49.7889	-43.4295	1.04
Compound_2586-P11	52.5446	-42.5088	1.06
Compound_2588-P11	57.9195	-44.7613	1.22
Compound_2589-P11	58.5917	-43.6817	1.20
Compound_2591-P11	53.3422	-46.7401	1.20
Compound_2592-P11	62.6974	-39.6109	1.15
Compound_2593-P11	52.2059	-40.6821	1.00
Compound_2594-P11	60.2085	-46.9019	1.32
Compound_2595-P11	45.6377	-45.2476	1.02
Compound_2596-P11	53.1575	-42.0078	1.06
Compound_2598-P11	54.1807	-42.3687	1.09
Compound_2599-P11	54.0687	-46.4592	1.20
Compound_2652-P11	31.5918	-38.9124	0.60
Compound_2657-P11	44.9156	-38.7006	0.82
Compound_2665-P11	43.7432	-40.3750	0.85
Compound_2667-P11	65.9916	-40.7361	1.24
Compound_2668-P11	52.5808	-39.2773	0.97
Compound_2669-P11	56.2488	-40.9469	1.08
Compound_2670-P11	44.6478	-43.0276	0.94
Compound_2689-P11	37.4111	-37.7554	0.67
Compound_2690-P11	41.7158	-40.8678	0.83
Compound_2691-P11	44.4737	-42.7648	0.93
Compound_2692-P11	46.0591	-41.3822	0.92
Compound_2693-P11	61.5882	-42.0828	1.20
Compound_2695-P11	41.9024	-41.6596	0.86
Compound_2696-P11	66.3707	-44.0720	1.34
Compound_2698-P11	43.7714	-39.8152	0.84
Compound_2699-P11	44.4826	-39.8318	0.85
Compound_2700-P11	45.5816	-45.3305	1.03
Compound_2701-P11	64.5427	-45.6295	1.36
Compound_2703-P11	62.0708	-48.1437	1.39
Compound_2714-P11	44.5524	-36.0907	0.74
Compound_2715-P11	61.4006	-40.9367	1.17

Compound	Docking energy, kJ mol^{-1}		
	GOLD	DOCK6	RANK
Compound_2716-P11	48.4413	-42.1222	0.98
Compound_2717-P11	39.0429	-41.6999	0.81
Compound_2718-P11	50.2161	-42.3834	1.02
Compound_2720-P11	70.4130	-45.8771	1.46
Compound_2734-P11	63.5645	-44.2241	1.30
Compound_2735-P11	48.2251	-44.6284	1.05
Compound_2736-P11	64.2626	-46.7529	1.38
Compound_2743-P11	49.5718	-41.4932	0.98
Compound_2744-P11	41.9503	-44.4549	0.94
Compound_2745-P11	67.8441	-45.6421	1.41
Compound_2746-P11	60.8689	-42.2971	1.20
Compound_2747-P11	54.1800	-41.2640	1.05
Compound_2748-P11	51.7120	-47.0152	1.18
Compound_2750-P11	54.9374	-46.3364	1.21
Compound_2751-P11	43.5952	-45.1259	0.99
Compound_2818-P11	38.3860	-38.5915	0.71
Compound_2926-P11	63.1888	-42.1957	1.23
Compound_2939-P11	67.1451	-40.8512	1.26
Compound_2947-P11	79.2870	-43.8454	1.56
Compound_2948-P11	43.0468	-41.9508	0.88
Compound_2950-P11	66.7275	-41.3116	1.27
Compound_2951-P11	62.4857	-42.7354	1.24
Compound_2952-P11	59.7380	-42.4072	1.18
Compound_2960-P11	63.5794	-41.7107	1.23
Compound_2961-P11	60.0337	-41.6643	1.17
Compound_2963-P11	43.2168	-43.8173	0.94
Compound_2977-P11	38.9457	-39.8107	0.75
Compound_2978-P11	58.2777	-41.4194	1.13
Compound_2987-P11	54.3138	-42.0076	1.08
Compound_2988-P11	48.8261	-45.7669	1.09
Compound_2989-P11	63.9906	-45.9240	1.36
Compound_2990-P11	55.9811	-44.1223	1.17
Compound_2991-P11	54.2087	-44.0480	1.14
Compound_2992-P11	57.2201	-43.9059	1.18
Compound_2993-P11	49.6923	-45.3260	1.10
Compound_7-P12	58.1285	-41.2478	1.12
Compound_11-P12	39.2064	-43.7520	0.87
Compound_16-P12	64.3475	-46.0334	1.37
Compound_17-P12	62.3227	-43.6602	1.26
Compound_18-P12	50.2518	-43.8827	1.06
Compound_19-P12	47.6999	-44.1428	1.03
Compound_20-P12	45.6626	-45.8612	1.04
Compound_21-P12	53.6205	-45.2832	1.16
Compound_22-P12	45.4960	-46.5368	1.06
Compound_23-P12	49.0648	-45.1276	1.08
Compound_24-P12	44.6797	-44.9049	1.00

Compound	Docking energy, kJ mol^{-1}		
	GOLD	DOCK6	RANK
Compound_25-P12	47.3316	-44.8282	1.04
Compound_34-P12	44.8141	-45.1385	1.01
Compound_35-P12	57.1023	-48.3877	1.31
Compound_36-P12	48.1950	-42.3645	0.98
Compound_42-P12	43.9065	-44.7252	0.98
Compound_43-P12	46.8825	-45.9323	1.07
Compound_44-P12	43.6752	-46.7260	1.03
Compound_69-P12	44.6811	-43.9480	0.97
Compound_73-P12	50.2951	-43.2508	1.05
Compound_74-P12	64.9289	-47.9564	1.43
Compound_82-P12	60.9698	-44.9682	1.28
Compound_83-P12	65.7484	-47.5668	1.43
Compound_87-P12	34.7672	-45.9655	0.86
Compound_88-P12	51.4550	-46.9608	1.17
Compound_126-P12	45.2388	-43.5365	0.97
Compound_129-P12	45.4882	-44.4994	1.00
Compound_136-P12	42.7748	-44.3435	0.95
Compound_137-P12	58.1166	-43.9229	1.20
Compound_138-P12	51.4574	-45.2706	1.12
Compound_146-P12	53.2765	-42.2250	1.07
Compound_147-P12	53.6617	-44.1477	1.13
Compound_150-P12	41.2204	-42.0893	0.86
Compound_151-P12	52.7339	-46.6455	1.19
Compound_152-P12	79.9672	-42.3993	1.53
Compound_153-P12	52.5741	-43.9431	1.10
Compound_155-P12	70.1897	-45.3428	1.44
Compound_156-P12	53.7179	-47.0722	1.21
Compound_157-P12	48.5293	-43.7938	1.03
Compound_183-P12	66.5172	-42.4638	1.30
Compound_220-P12	48.2077	-37.4034	0.84
Compound_221-P12	47.5117	-39.0119	0.88
Compound_222-P12	38.0102	-38.4851	0.70
Compound_223-P12	62.4553	-41.2578	1.19
Compound_224-P12	62.2008	-46.5198	1.34
Compound_225-P12	56.9408	-44.6311	1.20
Compound_232-P12	42.5467	-35.8072	0.70
Compound_233-P12	47.0232	-40.1599	0.90
Compound_234-P12	50.5868	-40.4429	0.97
Compound_235-P12	33.7772	-41.1330	0.70
Compound_237-P12	29.4502	-43.2434	0.69
Compound_238-P12	66.1052	-44.4000	1.35
Compound_239-P12	46.4590	-43.8220	1.00
Compound_260-P12	47.1868	-41.9991	0.96
Compound_261-P12	61.1859	-42.7580	1.22
Compound_263-P12	43.6539	-42.3964	0.91
Compound_264-P12	55.7679	-43.5930	1.15

Compound	Docking energy, kJ mol^{-1}		
	GOLD	DOCK6	RANK
Compound_265-P12	55.9379	-46.3870	1.23
Compound_266-P12	46.9191	-43.5543	1.00
Compound_267-P12	59.0686	-43.6316	1.21
Compound_268-P12	60.4902	-39.6845	1.12
Compound_269-P12	50.9549	-39.7859	0.96
Compound_270-P12	52.8004	-39.8881	0.99
Compound_271-P12	43.1304	-42.5918	0.90
Compound_272-P12	50.7148	-44.0636	1.08
Compound_275-P12	64.5592	-45.7428	1.36
Compound_317-P12	45.2689	-39.4437	0.85
Compound_318-P12	38.1824	-38.0762	0.69
Compound_319-P12	47.3405	-41.1609	0.93
Compound_320-P12	33.5390	-41.5117	0.71
Compound_321-P12	39.7915	-38.5122	0.73
Compound_322-P12	50.0678	-39.9441	0.95
Compound_323-P12	49.0724	-40.4058	0.94
Compound_324-P12	52.7995	-43.0872	1.08
Compound_326-P12	37.1693	-39.4723	0.71
Compound_327-P12	53.4869	-44.0562	1.12
Compound_328-P12	46.0680	-39.2524	0.86
Compound_329-P12	61.8525	-40.9092	1.17
Compound_330-P12	42.1432	-45.6131	0.98
Compound_331-P12	43.7936	-45.4231	1.00
Compound_339-P12	52.7022	-41.6552	1.04
Compound_340-P12	38.5761	-43.5686	0.86
Compound_341-P12	47.4463	-39.0420	0.88
Compound_342-P12	51.1874	-41.4556	1.01
Compound_343-P12	61.6994	-42.6910	1.22
Compound_344-P12	47.6461	-44.4160	1.03
Compound_345-P12	68.7693	-45.5231	1.43
Compound_346-P12	39.0499	-43.5352	0.86
Compound_347-P12	47.8762	-44.4228	1.04
Compound_362-P12	45.5614	-42.9589	0.96
Compound_363-P12	56.5986	-42.3588	1.13
Compound_364-P12	70.3903	-42.7190	1.37
Compound_365-P12	47.8858	-41.5470	0.96
Compound_366-P12	49.6425	-42.9748	1.03
Compound_367-P12	52.1089	-40.0191	0.98
Compound_368-P12	50.7542	-40.3889	0.97
Compound_369-P12	58.6640	-38.7588	1.06
Compound_370-P12	71.6724	-40.1290	1.32
Compound_371-P12	50.0969	-40.0148	0.95
Compound_372-P12	57.3259	-42.9412	1.16
Compound_373-P12	60.5865	-40.4950	1.14
Compound_374-P12	45.9589	-41.1502	0.91
Compound_375-P12	55.4855	-45.8678	1.21

Compound	Docking energy, kJ mol^{-1}		
	GOLD	DOCK6	RANK
Compound_376-P12	46.9243	-43.8303	1.01
Compound_377-P12	50.6913	-42.9026	1.04
Compound_378-P12	55.7973	-40.1780	1.05
Compound_379-P12	59.6804	-42.4551	1.18
Compound_380-P12	51.6952	-45.1844	1.13
Compound_381-P12	55.4237	-40.6277	1.06
Compound_382-P12	39.4086	-43.1960	0.86
Compound_383-P12	46.4308	-42.8481	0.97
Compound_384-P12	51.9058	-47.4080	1.19
Compound_718-P12	51.8337	-40.0717	0.98
Compound_720-P12	59.4739	-46.5939	1.30
Compound_739-P12	49.0808	-34.7179	0.78
Compound_741-P12	43.0800	-38.9961	0.80
Compound_742-P12	61.0861	-44.0639	1.25
Compound_743-P12	68.0726	-43.5887	1.36
Compound_747-P12	47.2582	-38.2264	0.85
Compound_748-P12	45.7214	-34.9126	0.73
Compound_780-P12	41.1400	-26.5671	0.41
Compound_782-P12	50.2483	-35.4410	0.82
Compound_783-P12	44.0104	-37.0640	0.76
Compound_785-P12	46.5577	-41.6131	0.93
Compound_789-P12	51.0346	-35.9160	0.85
Compound_814-P12	56.5264	-39.7178	1.05
Compound_815-P12	53.2572	-37.0403	0.92
Compound_822-P12	56.2107	-41.0110	1.08
Compound_824-P12	55.4603	-36.9822	0.95
Compound_842-P12	43.5716	-33.9995	0.66
Compound_846-P12	41.9325	-34.3117	0.64
Compound_847-P12	49.1093	-38.8561	0.90
Compound_850-P12	43.0629	-37.8122	0.77
Compound_868-P12	49.2019	-36.5176	0.83
Compound_869-P12	46.6886	-38.1351	0.84
Compound_870-P12	68.1718	-41.4734	1.30
Compound_875-P12	43.3789	-40.2097	0.84
Compound_883-P12	52.9995	-39.8665	0.99
Compound_884-P12	64.3404	-43.4453	1.29
Compound_885-P12	45.2835	-41.7532	0.92
Compound_889-P12	42.8562	-39.7402	0.82
Compound_896-P12	48.0709	-38.5519	0.87
Compound_899-P12	54.2277	-42.7077	1.10
Compound_900-P12	40.5952	-39.5418	0.77
Compound_901-P12	33.6413	-41.1663	0.70
Compound_902-P12	48.1626	-42.2867	0.98
Compound_909-P12	66.0470	-47.6562	1.44
Compound_910-P12	58.5755	-40.8439	1.12
Compound_911-P12	61.2639	-42.1278	1.20

Compound	Docking energy, kJ mol^{-1}		
	GOLD	DOCK6	RANK
Compound_912-P12	46.5436	-44.3495	1.01
Compound_914-P12	65.3786	-42.8472	1.29
Compound_915-P12	40.1401	-45.8248	0.95
Compound_934-P12	55.1278	-46.6926	1.23
Compound_943-P12	57.9137	-44.7958	1.22
Compound_946-P12	35.3749	-36.9199	0.61
Compound_958-P12	69.5183	-42.6556	1.36
Compound_961-P12	63.2124	-43.4353	1.27
Compound_966-P12	54.2059	-39.6576	1.01
Compound_968-P12	45.4178	-39.6811	0.86
Compound_970-P12	52.6497	-41.9318	1.05
Compound_975-P12	36.8547	-39.0582	0.70
Compound_978-P12	65.2279	-40.5311	1.22
Compound_982-P12	55.5538	-41.3965	1.08
Compound_983-P12	63.1675	-44.9975	1.32
Compound_984-P12	46.9892	-41.5429	0.94
Compound_986-P12	66.2708	-43.7086	1.33
Compound_1004-P12	50.4445	-39.8501	0.95
Compound_1005-P12	60.6039	-41.1211	1.16
Compound_1007-P12	52.5963	-38.5765	0.95
Compound_1064-P12	53.5345	-42.3624	1.08
Compound_1070-P12	54.0613	-36.2323	0.91
Compound_1086-P12	57.7422	-35.7439	0.95
Compound_1088-P12	46.9075	-39.3295	0.87
Compound_1098-P12	57.1922	-35.1776	0.93
Compound_1109-P12	53.5266	-36.2018	0.90
Compound_1116-P12	51.2038	-43.1477	1.06
Compound_1119-P12	46.8142	-40.3522	0.90
Compound_1122-P12	58.1418	-44.0157	1.20
Compound_1229-P12	40.8363	-39.6448	0.78
Compound_1230-P12	41.1799	-32.6199	0.58
Compound_1238-P12	57.0396	-49.1078	1.33
Compound_1746-P12	38.8517	-46.3792	0.94
Compound_1748-P12	67.8588	-44.8080	1.39
Compound_1751-P12	57.7686	-48.8908	1.34
Compound_1757-P12	66.6318	-44.1677	1.35
Compound_1769-P12	42.4267	-44.5245	0.95
Compound_1770-P12	47.0593	-39.7181	0.89
Compound_2313-P12	36.2422	-44.2302	0.84
Compound_2321-P12	46.4107	-42.6761	0.96
Compound_2324-P12	44.8323	-42.7807	0.94
Compound_2327-P12	52.8229	-42.8714	1.08
Compound_2339-P12	59.3147	-43.9784	1.22
Compound_2428-P12	34.2659	-44.0945	0.80
Compound_2430-P12	35.8132	-43.9411	0.82
Compound_2444-P12	48.8790	-45.4703	1.09

Compound	Docking energy, kJ mol^{-1}		
	GOLD	DOCK6	RANK
Compound_2477-P12	35.0684	-45.9967	0.87
Compound_2513-P12	57.7514	-40.8408	1.10
Compound_2516-P12	41.5891	-40.3276	0.81
Compound_2519-P12	58.0976	-43.4975	1.19
Compound_2576-P12	45.1658	-41.7509	0.92
Compound_2579-P12	58.8898	-43.0667	1.19
Compound_2582-P12	62.9167	-42.9882	1.25
Compound_2593-P12	33.4096	-42.8882	0.75
Compound_2614-P12	37.7373	-44.7578	0.88
Compound_2634-P12	42.8016	-45.6161	0.99
Compound_2686-P12	46.7598	-40.2014	0.90
Compound_2689-P12	58.0220	-42.0360	1.14
Compound_2692-P12	44.0234	-44.3581	0.97
Compound_2702-P12	41.1141	-43.9412	0.91
Compound_2797-P12	64.3679	-44.7752	1.33
Compound_2800-P12	52.6577	-44.8663	1.13
Compound_2803-P12	48.2608	-45.5384	1.08
Compound_2814-P12	38.7355	-45.1140	0.90
Compound_2882-P12	49.5151	-44.6195	1.07
Compound_2883-P12	36.2996	-43.4463	0.81
Compound_2886-P12	63.2164	-44.9135	1.31
Compound_2948-P12	24.8651	-43.4045	0.62
Compound_11-P13	50.8179	-42.7679	1.04
Compound_12-P13	44.0068	-41.3465	0.88
Compound_15-P13	60.5646	-39.1283	1.10
Compound_2452-P13	68.8033	-45.8146	1.43
Compound_2454-P13	54.0255	-43.0710	1.10
Compound_2455-P13	53.1834	-44.9230	1.14
Compound_2460-P13	54.5596	-41.1024	1.06
Compound_2463-P13	57.4093	-42.4225	1.14
Compound_2507-P13	57.8295	-35.9483	0.96
Compound_2511-P13	46.1377	-33.8329	0.70
Compound_2513-P13	45.3246	-40.4507	0.88
Compound_2518-P13	47.5901	-36.5015	0.80
Compound_2520-P13	44.3699	-38.5697	0.81
Compound_2524-P13	51.5027	-38.8883	0.94
Compound_2529-P13	60.6094	-39.3514	1.11
Compound_2530-P13	46.6495	-33.1950	0.69
Compound_2532-P13	56.5132	-39.8657	1.05
Compound_2540-P13	42.9762	-36.2652	0.72
Compound_2542-P13	54.2782	-38.7066	0.98
Compound_2549-P13	62.5866	-39.4564	1.14
Compound_2550-P13	48.7098	-37.6657	0.86
Compound_2558-P13	46.1899	-34.6363	0.73
Compound_2601-P13	79.3081	-44.3116	1.57
Compound_2602-P13	52.7671	-46.3412	1.18

Compound	Docking energy, kJ mol^{-1}		
	GOLD	DOCK6	RANK
Compound_2667-P13	39.0287	-43.8395	0.87
Compound_2704-P13	47.9596	-33.7660	0.73
Compound_2706-P13	50.2584	-36.2616	0.84
Compound_2719-P13	52.3933	-40.2722	1.00
Compound_2721-P13	47.6982	-41.2643	0.94
Compound_2731-P13	43.4613	-34.8812	0.69
Compound_2771-P13	68.3343	-41.1504	1.29
Compound_2772-P13	69.7717	-42.3348	1.35
Compound_2789-P13	54.0643	-34.8607	0.87
Compound_2806-P13	49.1660	-33.3193	0.74
Compound_2807-P13	56.4184	-36.2483	0.95
Compound_2820-P13	37.0031	-44.6431	0.86
Compound_2821-P13	54.7284	-46.4566	1.21
Compound_2822-P13	57.7087	-45.0919	1.23
Compound_2829-P13	45.1063	-43.0206	0.95
Compound_2833-P13	29.7739	-45.7938	0.77
Compound_2834-P13	50.4251	-43.3978	1.05
Compound_2835-P13	48.9238	-44.6719	1.06
Compound_2836-P13	55.6036	-42.6940	1.12
Compound_2837-P13	32.8043	-43.3681	0.75
Compound_2844-P13	75.9887	-43.9979	1.50
Compound_2851-P13	39.8603	-48.3251	1.02
Compound_2854-P13	55.6174	-43.1775	1.13
Compound_2857-P13	52.0878	-46.0637	1.16
Compound_2858-P13	60.4387	-45.6487	1.29
Compound_2859-P13	55.8397	-46.8769	1.25
Compound_2861-P13	57.8992	-41.7518	1.13
Compound_2862-P13	55.8713	-46.1819	1.23
Compound_2863-P13	49.5151	-47.0837	1.14
Compound_2865-P13	43.6891	-44.6283	0.97
Compound_2868-P13	50.7243	-41.9483	1.02
Compound_2870-P13	57.0489	-41.3935	1.11
Compound_2871-P13	45.2534	-43.1990	0.96
Compound_2878-P13	34.7022	-39.0567	0.66
Compound_2879-P13	52.3703	-43.1414	1.08
Compound_2880-P13	62.1641	-42.0084	1.21
Compound_2881-P13	53.9229	-41.9310	1.07
Compound_2894-P13	62.5096	-44.3977	1.29
Compound_2909-P13	46.3798	-51.4962	1.22
Compound_2911-P13	42.1408	-49.1917	1.08
Compound_2916-P13	41.1081	-44.1473	0.92
Compound_2921-P13	55.0710	-50.5722	1.34
Compound_2928-P13	53.5942	-42.6343	1.08
Compound_2938-P13	55.8512	-47.3414	1.26
Compound_2970-P13	66.0422	-45.8864	1.39
Compound_42-P14	55.3744	-32.6016	0.82

Compound	Docking energy, kJ mol^{-1}		
	GOLD	DOCK6	RANK
Compound_65-P14	41.2803	-34.6891	0.64
Compound_90-P14	62.7892	-35.2004	1.02
Compound_116-P14	75.0843	-40.9241	1.40
Compound_140-P14	51.2651	-34.8180	0.82
Compound_143-P14	49.2783	-35.1801	0.79
Compound_177-P14	44.8657	-37.1976	0.78
Compound_244-P14	45.3575	-39.0454	0.84
Compound_258-P14	40.2202	-35.6684	0.65
Compound_271-P14	50.5715	-38.4632	0.91
Compound_272-P14	50.1430	-40.8325	0.97
Compound_330-P14	57.0592	-36.0526	0.95
Compound_341-P14	61.0548	-36.2365	1.03
Compound_342-P14	31.0110	-33.2370	0.43
Compound_343-P14	46.1652	-36.7920	0.79
Compound_1577-P14	61.4422	-42.4758	1.21
Compound_2140-P14	52.7434	-44.2709	1.12
Compound_2141-P14	54.8068	-45.3000	1.18
Compound_2143-P14	47.1215	-50.1559	1.19
Compound_2144-P14	46.7221	-45.9093	1.06
Compound_2146-P14	44.1755	-45.6099	1.01
Compound_2147-P14	56.7071	-46.2304	1.24
Compound_2148-P14	40.3410	-47.3501	1.00
Compound_2149-P14	53.0775	-43.2231	1.09
Compound_2150-P14	60.6179	-48.4633	1.37
Compound_2152-P14	36.3999	-44.3614	0.84
Compound_2155-P14	52.9803	-47.3252	1.21
Compound_2156-P14	32.8452	-50.1278	0.95
Compound_2160-P14	41.0716	-44.0075	0.91
Compound_2161-P14	51.8595	-44.8165	1.12
Compound_2172-P14	31.8272	-50.2355	0.93
Compound_2175-P14	41.5615	-45.0386	0.95
Compound_2176-P14	66.8294	-48.7733	1.49
Compound_2181-P14	58.5780	-43.9837	1.21
Compound_2182-P14	54.1331	-45.7173	1.18
Compound_2187-P14	38.0742	-46.3311	0.93
Compound_2189-P14	46.7889	-47.5741	1.11
Compound_2190-P14	54.3031	-48.4801	1.27
Compound_2199-P14	35.9274	-44.9020	0.85
Compound_2203-P14	57.8520	-47.8872	1.31
Compound_2208-P14	64.8630	-42.1623	1.26
Compound_2209-P14	32.6154	-44.4828	0.78
Compound_2210-P14	48.1178	-43.6813	1.02
Compound_2211-P14	60.8221	-51.5269	1.46
Compound_2213-P14	51.9480	-47.6416	1.20
Compound_2217-P14	63.1143	-47.6602	1.39
Compound_2315-P14	49.3407	-45.2599	1.09

Compound	Docking energy, kJ mol^{-1}		
	GOLD	DOCK6	RANK
Compound_60-P15	32.3295	-44.9280	0.79
Compound_67-P15	30.6566	-42.7533	0.70
Compound_68-P15	39.0790	-45.1744	0.91
Compound_71-P15	33.5893	-49.7783	0.95
Compound_78-P15	46.0844	-46.9450	1.08
Compound_79-P15	42.7280	-47.2661	1.03
Compound_85-P15	32.2533	-47.6859	0.87
Compound_93-P15	37.4089	-48.1520	0.97
Compound_94-P15	47.3043	-45.1388	1.05
Compound_97-P15	48.3480	-49.3361	1.19
Compound_100-P15	51.3545	-48.0847	1.20
Compound_109-P15	49.9687	-46.1713	1.12
Compound_135-P15	37.4457	-46.7330	0.93
Compound_169-P15	32.9391	-48.6293	0.91
Compound_175-P15	31.4659	-44.5367	0.76
Compound_186-P15	34.5471	-49.2542	0.95
Compound_193-P15	42.9731	-48.1355	1.06
Compound_252-P15	37.2600	-45.2948	0.88
Compound_256-P15	34.9926	-43.9475	0.81
Compound_257-P15	45.6171	-43.1089	0.96
Compound_258-P15	49.9877	-45.7923	1.11
Compound_264-P15	33.1361	-44.8677	0.80
Compound_265-P15	45.6921	-43.9153	0.99
Compound_268-P15	54.2503	-46.1010	1.20
Compound_274-P15	45.9556	-47.0223	1.08
Compound_275-P15	47.8914	-46.2281	1.09
Compound_277-P15	52.9905	-50.5947	1.30
Compound_279-P15	28.0927	-44.4183	0.70
Compound_306-P15	45.9079	-47.4787	1.09
Compound_331-P15	46.8655	-47.3582	1.11
Compound_337-P15	26.8009	-44.6027	0.69
Compound_338-P15	22.9179	-43.7928	0.60
Compound_342-P15	32.3415	-46.1482	0.82
Compound_346-P15	46.4526	-43.4514	0.99
Compound_347-P15	52.5922	-46.4871	1.18
Compound_350-P15	38.0346	-46.4183	0.93
Compound_358-P15	30.4845	-47.3617	0.83
Compound_359-P15	63.7881	-45.4389	1.34
Compound_360-P15	45.9847	-50.9792	1.20
Compound_362-P15	60.0864	-48.4227	1.36
Compound_370-P15	61.5580	-46.6328	1.34
Compound_392-P15	46.6412	-46.9900	1.09
Compound_422-P15	26.4722	-46.8790	0.75
Compound_428-P15	42.5447	-43.8131	0.93
Compound_430-P15	31.7284	-46.5914	0.83
Compound_439-P15	30.8850	-45.6602	0.79

Compound	Docking energy, kJ mol^{-1}		
	GOLD	DOCK6	RANK
Compound_442-P15	49.6041	-45.4664	1.10
Compound_487-P15	38.2995	-45.9030	0.92
Compound_516-P15	32.3646	-47.3933	0.86
Compound_523-P15	34.0456	-47.3401	0.89
Compound_524-P15	25.0075	-47.3510	0.73
Compound_526-P15	54.9836	-48.1793	1.27
Compound_535-P15	53.9476	-48.6813	1.27
Compound_538-P15	38.2954	-48.7358	1.00
Compound_546-P15	28.8341	-47.2486	0.80
Compound_579-P15	59.1526	-49.7576	1.39
Compound_605-P15	51.5081	-46.9275	1.17
Compound_610-P15	32.5445	-46.8332	0.85
Compound_613-P15	29.4016	-47.9031	0.83
Compound_632-P15	53.9406	-48.2980	1.25
Compound_670-P15	41.7274	-50.3554	1.11
Compound_692-P15	39.3112	-41.1517	0.80
Compound_693-P15	44.0866	-45.0908	0.99
Compound_695-P15	57.6035	-45.1391	1.22
Compound_702-P15	47.7467	-44.4198	1.04
Compound_706-P15	61.8490	-44.6390	1.28
Compound_773-P15	27.2407	-46.5854	0.75
Compound_780-P15	26.3601	-44.6025	0.68
Compound_781-P15	43.6357	-44.2313	0.96
Compound_782-P15	54.5992	-48.1450	1.26
Compound_784-P15	28.8929	-47.3242	0.80
Compound_792-P15	48.8650	-47.1912	1.14
Compound_799-P15	55.9166	-45.1213	1.20
Compound_1181-P15	51.0767	-41.7666	1.02
Compound_1182-P15	35.3816	-45.0646	0.84
Compound_1183-P15	36.4037	-44.0670	0.83
Compound_1208-P15	44.2462	-44.1954	0.97
Compound_1209-P15	43.4463	-44.3126	0.96
Compound_1235-P15	64.1974	-44.2686	1.31
Compound_1241-P15	49.1386	-45.2867	1.09
Compound_1243-P15	62.5753	-45.4635	1.32
Compound_1256-P15	58.8681	-45.4229	1.25
Compound_1301-P15	51.3504	-46.2105	1.15
Compound_1303-P15	47.0571	-40.3263	0.91
Compound_1306-P15	45.7446	-41.9908	0.93
Compound_1307-P15	41.9399	-40.4053	0.82
Compound_1309-P15	60.1089	-43.9201	1.23
Compound_1311-P15	55.9244	-44.2489	1.17
Compound_1313-P15	58.8805	-38.0490	1.04
Compound_1320-P15	59.3806	-41.7253	1.16
Compound_1321-P15	65.6545	-43.6465	1.32
Compound_1323-P15	58.3101	-37.4927	1.02

Compound	Docking energy, kJ mol^{-1}		
	GOLD	DOCK6	RANK
Compound_1644-P15	60.8990	-43.6940	1.24
Compound_1645-P15	47.6756	-41.9188	0.96
Compound_1648-P15	50.7563	-38.6211	0.92
Compound_1649-P15	56.5494	-31.4920	0.81
Compound_1685-P15	48.8819	-43.7566	1.04
Compound_1712-P15	38.5345	-42.3829	0.82
Compound_1728-P15	57.5719	-38.7876	1.04
Compound_1729-P15	49.5271	-36.7886	0.85
Compound_1732-P15	65.0854	-35.2740	1.07
Compound_1733-P15	35.6220	-30.3358	0.42
Compound_1750-P15	57.5548	-40.1350	1.08
Compound_1762-P15	57.2331	-40.6421	1.09
Compound_1785-P15	67.5036	-41.1095	1.28
Compound_1857-P15	41.7836	-29.7616	0.51
Compound_1859-P15	47.8030	-32.4814	0.69
Compound_1860-P15	39.0058	-30.6567	0.49
Compound_1932-P15	49.5756	-41.6036	0.99
Compound_1934-P15	50.6396	-40.5538	0.97
Compound_1957-P15	52.9920	-42.7341	1.08
Compound_1977-P15	70.0229	-44.2620	1.41
Compound_1993-P15	58.3564	-39.3281	1.07
Compound_2005-P15	48.9091	-34.1063	0.76
Compound_2057-P15	53.9821	-42.7896	1.10
Compound_2065-P15	63.7709	-43.7793	1.29
Compound_2076-P15	41.1918	-46.0370	0.97
Compound_2077-P15	63.4482	-41.7132	1.22
Compound_2078-P15	54.2703	-43.4468	1.12
Compound_2079-P15	54.6507	-41.7211	1.08
Compound_2095-P15	53.3392	-42.1439	1.07
Compound_2103-P15	49.1762	-40.1984	0.94
Compound_2110-P15	54.1972	-41.4947	1.06
Compound_2111-P15	56.1692	-43.0690	1.14
Compound_2112-P15	57.0978	-38.7341	1.03
Compound_2113-P15	54.7997	-39.1574	1.00
Compound_2114-P15	60.0865	-43.8622	1.23
Compound_2118-P15	52.2012	-38.4421	0.94
Compound_2121-P15	59.1667	-43.7910	1.21
Compound_2125-P15	51.8480	-39.1995	0.95
Compound_2163-P15	38.3008	-32.3324	0.53
Compound_2164-P15	33.9065	-31.3917	0.42
Compound_2177-P15	48.1718	-37.0025	0.83
Compound_2178-P15	39.5657	-36.8605	0.68
Compound_2206-P15	42.6848	-38.9908	0.79
Compound_2214-P15	42.8826	-40.0391	0.83
Compound_2215-P15	48.3048	-37.3888	0.84
Compound_2218-P15	38.9508	-37.9610	0.70

Compound	Docking energy, kJ mol^{-1}		
	GOLD	DOCK6	RANK
Compound_2221-P15	64.1949	-37.6293	1.12
Compound_2225-P15	41.6237	-32.3240	0.58
Compound_2227-P15	40.8592	-39.8476	0.79
Compound_2427-P15	37.3116	-31.4091	0.48
Compound_2554-P15	44.0038	-42.2172	0.91
Compound_2555-P15	46.0343	-41.7871	0.93
Compound_2556-P15	48.2442	-40.6091	0.93
Compound_2557-P15	49.5253	-35.3491	0.80
Compound_2558-P15	52.1322	-37.1202	0.90
Compound_2560-P15	60.5354	-47.9124	1.36
Compound_2561-P15	58.7299	-47.4359	1.31
Compound_2562-P15	46.0176	-44.6051	1.01
Compound_2565-P15	59.1507	-47.6397	1.32
Compound_2566-P15	63.7380	-43.7822	1.29
Compound_2568-P15	52.8986	-41.4391	1.04
Compound_2571-P15	61.0430	-44.6434	1.27
Compound_2572-P15	59.1238	-42.7411	1.18
Compound_2574-P15	57.3728	-45.4308	1.23
Compound_2575-P15	43.1054	-44.5721	0.96
Compound_2576-P15	58.8568	-45.9396	1.27
Compound_2577-P15	58.7662	-45.3395	1.25
Compound_2578-P15	52.4911	-44.9423	1.13
Compound_2581-P15	50.2484	-46.0829	1.13
Compound_2584-P15	51.8196	-42.4146	1.05
Compound_2592-P15	71.7780	-45.0486	1.46
Compound_2593-P15	53.4809	-47.4443	1.22
Compound_2595-P15	55.5752	-45.2087	1.19
Compound_2596-P15	54.1647	-42.6255	1.09
Compound_2601-P15	42.6830	-35.2035	0.68
Compound_2604-P15	50.1052	-39.8099	0.94
Compound_2607-P15	70.0806	-43.2477	1.38
Compound_2608-P15	51.5240	-39.3056	0.95
Compound_2617-P15	51.6089	-40.7447	1.00
Compound_2619-P15	42.8593	-40.0761	0.83
Compound_2627-P15	50.5989	-37.6181	0.89
Compound_2631-P15	49.3238	-39.5076	0.92
Compound_2642-P15	56.3187	-38.3923	1.01
Compound_2643-P15	45.7776	-33.2832	0.68
Compound_2644-P15	50.4238	-44.3790	1.08
Compound_2645-P15	81.3018	-45.3161	1.63
Compound_2646-P15	53.9802	-43.0922	1.10
Compound_2648-P15	70.3747	-46.1624	1.47
Compound_2652-P15	75.4642	-43.2966	1.48
Compound_2654-P15	61.3965	-42.6950	1.22
Compound_2657-P15	48.8215	-44.6131	1.06
Compound_2658-P15	43.9239	-43.4404	0.94

Compound	Docking energy, kJ mol^{-1}		
	GOLD	DOCK6	RANK
Compound_2661-P15	50.2732	-43.7017	1.06
Compound_2664-P15	72.6534	-43.6379	1.44
Compound_2669-P15	52.4027	-40.3921	1.00
Compound_2677-P15	48.1132	-43.8065	1.02
Compound_2678-P15	45.7188	-45.8239	1.04
Compound_2680-P15	57.1952	-44.0820	1.19
Compound_2682-P15	47.0028	-40.4378	0.91
Compound_2837-P15	47.6584	-42.0570	0.97
Compound_2892-P15	48.6865	-42.5318	1.00
Compound_2977-P15	55.1704	-43.2227	1.13
Compound_2979-P15	67.2393	-43.0887	1.33
Compound_2981-P15	49.7755	-43.9746	1.06
Compound_124-P16	52.4495	-44.9170	1.13
Compound_131-P16	60.1977	-44.4027	1.25
Compound_140-P16	52.0827	-42.2185	1.05
Compound_142-P16	57.7677	-41.0080	1.11
Compound_144-P16	48.9522	-41.4201	0.97
Compound_159-P16	47.6440	-44.2410	1.03
Compound_171-P16	58.5275	-43.3978	1.19
Compound_177-P16	57.6102	-43.8220	1.19
Compound_317-P16	45.7847	-40.8902	0.90
Compound_321-P16	37.8708	-45.2762	0.89
Compound_334-P16	53.9178	-39.7262	1.01
Compound_337-P16	62.9704	-40.4457	1.18
Compound_348-P16	38.0308	-42.8054	0.82
Compound_351-P16	44.1183	-45.1353	1.00
Compound_454-P16	52.4464	-40.5505	1.00
Compound_455-P16	41.3746	-39.2035	0.78
Compound_463-P16	61.3136	-42.7951	1.22
Compound_489-P16	50.7249	-43.2933	1.05
Compound_558-P16	31.8131	-42.3571	0.71
Compound_570-P16	59.5072	-46.8233	1.31
Compound_663-P16	55.5288	-44.8932	1.18
Compound_667-P16	37.4258	-43.0287	0.82
Compound_683-P16	51.7006	-44.9901	1.12
Compound_769-P16	49.9098	-42.3585	1.01
Compound_1357-P16	66.1906	-41.2510	1.26
Compound_1377-P16	57.3907	-43.8614	1.18
Compound_1391-P16	52.0908	-45.7779	1.15
Compound_1437-P16	45.4896	-45.3549	1.03
Compound_1479-P16	31.9536	-45.5066	0.80
Compound_1492-P16	60.6088	-47.7705	1.35
Compound_2123-P16	51.9581	-34.6681	0.83
Compound_2124-P16	42.2631	-31.3513	0.56
Compound_2125-P16	42.8302	-32.3024	0.60
Compound_2126-P16	41.1547	-32.7854	0.59

Compound	Docking energy, kJ mol^{-1}		
	GOLD	DOCK6	RANK
Compound_2127-P16	39.3869	-31.6594	0.52
Compound_2128-P16	41.5567	-31.8395	0.57
Compound_2129-P16	50.2926	-32.1875	0.72
Compound_2130-P16	40.4039	-32.4652	0.56
Compound_2131-P16	47.9443	-32.4849	0.69
Compound_2132-P16	44.6951	-33.7888	0.68
Compound_2133-P16	35.4693	-28.6157	0.37
Compound_2352-P16	64.6752	-38.3925	1.15
Compound_2357-P16	53.7315	-37.3640	0.93
Compound_2358-P16	53.7148	-36.2203	0.90
Compound_2360-P16	44.6103	-36.2844	0.75
Compound_2455-P16	50.0787	-42.2774	1.01
Compound_2457-P16	47.7185	-43.3636	1.01
Compound_2458-P16	56.9074	-42.2748	1.13
Compound_2459-P16	48.6665	-44.2148	1.05
Compound_2460-P16	53.9491	-45.1302	1.16
Compound_2461-P16	43.7045	-43.2457	0.93
Compound_2462-P16	54.1436	-45.4115	1.17
Compound_2472-P16	48.2059	-41.0919	0.95
Compound_2475-P16	52.6139	-43.2361	1.08
Compound_2627-P16	66.8982	-36.4001	1.13
Compound_2630-P16	46.6629	-37.6086	0.82
Compound_2631-P16	51.7221	-39.3665	0.96
Compound_2651-P16	49.9435	-37.6244	0.88
Compound_2652-P16	46.2248	-37.5736	0.81
Compound_2654-P16	49.7225	-37.9376	0.88
Compound_2659-P16	36.5227	-30.5166	0.44
Compound_2660-P16	51.1211	-37.5821	0.90
Compound_2661-P16	54.5194	-36.1991	0.91
Compound_2662-P16	47.7907	-36.5050	0.81
Compound_2707-P16	49.4028	-41.0740	0.97
Compound_2708-P16	39.4753	-40.7519	0.79
Compound_2717-P16	51.2964	-42.6839	1.05
Compound_2719-P16	47.1152	-44.7233	1.03
Compound_2722-P16	55.6537	-44.8379	1.18
Compound_2784-P16	49.4411	-42.0685	1.00
Compound_2787-P16	49.1795	-42.4673	1.00
Compound_533-P17	51.2692	-42.3004	1.03
Compound_534-P17	64.9323	-39.1565	1.18
Compound_535-P17	53.6961	-39.9897	1.01
Compound_605-P17	53.5001	-38.5964	0.97
Compound_608-P17	43.9293	-35.5325	0.71
Compound_623-P17	49.4270	-39.5870	0.92
Compound_634-P17	60.7085	-40.7726	1.15
Compound_721-P17	49.0744	-42.0801	0.99
Compound_772-P17	42.3118	-43.9820	0.93

Compound	Docking energy, kJ mol^{-1}		
	GOLD	DOCK6	RANK
Compound_773-P17	47.6912	-42.8445	0.99
Compound_774-P17	41.8753	-37.5698	0.74
Compound_775-P17	67.9827	-45.1521	1.40
Compound_776-P17	71.4452	-47.1162	1.52
Compound_777-P17	47.5593	-46.2752	1.09
Compound_779-P17	55.2081	-48.9935	1.30
Compound_780-P17	47.6416	-45.3834	1.06
Compound_781-P17	73.0370	-46.0913	1.52
Compound_787-P17	37.6163	-45.2412	0.89
Compound_789-P17	50.4900	-49.3306	1.23
Compound_790-P17	61.7092	-47.3133	1.36
Compound_791-P17	70.7876	-47.9107	1.53
Compound_792-P17	45.1031	-46.7589	1.06
Compound_795-P17	51.2514	-47.8907	1.20
Compound_797-P17	53.1722	-48.7654	1.25
Compound_808-P17	43.8569	-46.0572	1.02
Compound_810-P17	44.2197	-45.7135	1.01
Compound_811-P17	49.9819	-47.7311	1.17
Compound_816-P17	64.9593	-47.6965	1.42
Compound_968-P17	47.8106	-40.9960	0.94
Compound_987-P17	65.3041	-42.1414	1.27
Compound_1009-P17	40.8505	-42.2598	0.86
Compound_1010-P17	56.3070	-41.2587	1.09
Compound_1015-P17	51.8829	-44.1294	1.10
Compound_1021-P17	53.7931	-41.7998	1.06
Compound_1022-P17	59.7375	-40.4266	1.12
Compound_1023-P17	50.8909	-42.5343	1.04
Compound_1024-P17	52.5244	-44.1059	1.11
Compound_1025-P17	39.4157	-41.4701	0.81
Compound_1031-P17	65.4147	-38.9928	1.18
Compound_1101-P17	57.9656	-41.4027	1.12
Compound_1420-P17	53.6367	-41.8422	1.06
Compound_1434-P17	51.3604	-38.2585	0.92
Compound_1461-P17	62.7630	-36.7154	1.07
Compound_1499-P17	47.4332	-38.8108	0.87
Compound_1500-P17	56.5873	-41.4155	1.10
Compound_1922-P17	39.4114	-35.3593	0.63
Compound_1939-P17	32.0445	-36.4906	0.54
Compound_1956-P17	34.0169	-36.6275	0.58
Compound_2023-P17	39.6930	-37.5380	0.70
Compound_2035-P17	44.5120	-35.2791	0.72
Compound_2043-P17	36.5173	-36.7516	0.62
Compound_2074-P17	59.7928	-35.9209	0.99
Compound_2688-P17	62.6735	-40.5096	1.18
Compound_2754-P17	59.4220	-43.0009	1.19
Compound_2982-P17	50.2026	-45.2009	1.10

Compound	Docking energy, kJ mol^{-1}		
	GOLD	DOCK6	RANK
Compound_2983-P17	38.1697	-42.4606	0.82
Compound_2984-P17	38.9068	-43.5795	0.86
Compound_2985-P17	48.7949	-42.8186	1.01
Compound_2990-P17	57.9452	-44.8733	1.22
Compound_7-P18	48.1272	-45.1446	1.06
Compound_12-P18	65.7802	-43.0451	1.30
Compound_703-P18	53.9190	-38.3648	0.97
Compound_705-P18	41.7242	-42.6024	0.88
Compound_709-P18	54.8831	-42.2655	1.10
Compound_713-P18	50.7650	-37.8667	0.90
Compound_714-P18	53.4571	-39.7973	1.00
Compound_715-P18	25.8035	-38.8792	0.50
Compound_716-P18	40.6429	-37.9756	0.73
Compound_717-P18	37.3795	-39.5573	0.72
Compound_718-P18	58.4892	-39.8162	1.09
Compound_719-P18	39.4414	-38.6070	0.73
Compound_720-P18	48.6751	-39.7485	0.92
Compound_721-P18	46.8555	-41.1915	0.93
Compound_723-P18	59.6604	-40.9862	1.14
Compound_724-P18	55.2125	-41.3037	1.07
Compound_735-P18	50.7487	-42.5265	1.03
Compound_736-P18	61.3985	-42.2070	1.20
Compound_742-P18	61.6744	-42.3897	1.21
Compound_743-P18	29.6019	-43.4504	0.70
Compound_744-P18	55.9017	-42.8997	1.13
Compound_745-P18	49.9978	-40.8856	0.97
Compound_746-P18	60.4094	-42.8778	1.21
Compound_782-P18	52.5304	-46.3234	1.17
Compound_818-P18	58.2595	-39.9032	1.08
Compound_819-P18	52.6216	-38.6911	0.95
Compound_820-P18	43.1711	-38.1142	0.78
Compound_840-P18	43.8606	-38.5295	0.80
Compound_841-P18	47.8748	-39.1663	0.89
Compound_848-P18	47.6013	-39.8695	0.90
Compound_849-P18	38.8294	-40.0181	0.76
Compound_865-P18	31.2535	-44.0680	0.75
Compound_867-P18	44.1860	-37.6432	0.78
Compound_868-P18	38.4658	-37.3854	0.67
Compound_871-P18	48.7854	-37.9044	0.87
Compound_873-P18	25.1743	-37.4437	0.45
Compound_879-P18	47.8473	-36.6262	0.81
Compound_885-P18	47.7792	-38.1566	0.86
Compound_888-P18	53.9354	-37.8858	0.95
Compound_945-P18	43.6949	-43.5656	0.94
Compound_947-P18	25.4351	-44.6409	0.66
Compound_952-P18	36.4785	-47.2050	0.93

Compound	Docking energy, kJ mol^{-1}		
	GOLD	DOCK6	RANK
Compound_957-P18	42.6647	-44.8725	0.96
Compound_959-P18	42.3601	-45.5220	0.98
Compound_961-P18	23.3454	-41.8400	0.55
Compound_962-P18	39.9807	-41.3895	0.82
Compound_963-P18	58.8655	-40.5795	1.11
Compound_971-P18	43.6614	-43.2640	0.93
Compound_972-P18	49.3106	-49.8042	1.22
Compound_977-P18	48.8926	-45.0998	1.08
Compound_987-P18	35.1285	-48.7679	0.95
Compound_996-P18	55.3720	-44.0286	1.15
Compound_997-P18	40.6848	-47.8666	1.02
Compound_1042-P18	41.1127	-39.4130	0.78
Compound_1047-P18	50.8675	-40.2877	0.97
Compound_1048-P18	54.1436	-41.8955	1.07
Compound_1057-P18	69.3621	-42.4581	1.35
Compound_1059-P18	33.3993	-42.7991	0.75
Compound_1082-P18	51.5548	-41.8388	1.03
Compound_1085-P18	51.9438	-36.9464	0.89
Compound_1086-P18	36.4177	-40.4483	0.73
Compound_1087-P18	51.9892	-43.2757	1.08
Compound_1088-P18	29.5077	-43.6467	0.70
Compound_1091-P18	37.7620	-45.3097	0.89
Compound_1093-P18	59.4624	-44.2239	1.23
Compound_1108-P18	56.1209	-31.6580	0.81
Compound_1110-P18	41.4434	-31.1492	0.54
Compound_1111-P18	44.9902	-30.2159	0.58
Compound_1114-P18	48.0206	-36.8853	0.82
Compound_1118-P18	44.4421	-29.8637	0.56
Compound_1120-P18	45.8803	-29.0904	0.56
Compound_1123-P18	43.1116	-37.0432	0.74
Compound_1125-P18	49.9017	-35.7130	0.82
Compound_1126-P18	42.6408	-29.3065	0.51
Compound_2373-P18	52.8613	-34.3359	0.83
Compound_2661-P18	44.3483	-41.5203	0.89
Compound_2664-P18	46.9535	-32.9651	0.69
Compound_2665-P18	50.3171	-30.7221	0.68
Compound_2667-P18	46.4664	-35.3501	0.75
Compound_2668-P18	53.1194	-34.8296	0.85
Compound_2669-P18	46.2173	-32.3664	0.66
Compound_2670-P18	37.5517	-29.2327	0.42
Compound_2671-P18	33.8878	-32.1066	0.44
Compound_2672-P18	31.6705	-26.8557	0.25
Compound_2673-P18	43.9961	-33.4592	0.65
Compound_2678-P18	54.0282	-34.1937	0.85
Compound_2680-P18	49.0198	-39.5344	0.92
Compound_2681-P18	48.6102	-34.4593	0.76

Compound	Docking energy, kJ mol^{-1}		
	GOLD	DOCK6	RANK
Compound_2683-P18	44.7049	-33.1393	0.66
Compound_2684-P18	41.3823	-43.7072	0.91
Compound_2685-P18	41.3245	-37.6868	0.73
Compound_2686-P18	47.8214	-38.1406	0.86
Compound_2687-P18	33.1189	-35.9685	0.54
Compound_2688-P18	47.9522	-40.0911	0.91
Compound_2691-P18	58.5036	-41.5314	1.14
Compound_2693-P18	39.4441	-41.5193	0.81
Compound_2694-P18	41.3051	-37.7864	0.73
Compound_2695-P18	40.9183	-33.9117	0.62
Compound_2696-P18	56.8132	-39.4019	1.05
Compound_2697-P18	52.8807	-33.7136	0.81
Compound_2698-P18	47.5149	-33.5569	0.72
Compound_2700-P18	53.3278	-38.7362	0.97
Compound_2701-P18	49.0645	-41.9010	0.99
Compound_2726-P18	57.3266	-34.8446	0.92
Compound_2734-P18	42.7746	-37.3884	0.75
Compound_2737-P18	48.2100	-39.9646	0.92
Compound_2740-P18	43.5814	-37.4258	0.76
Compound_2741-P18	38.5688	-29.7682	0.46
Compound_2742-P18	63.9009	-37.1037	1.10
Compound_2743-P18	42.4683	-35.1000	0.68
Compound_2744-P18	54.2458	-40.6883	1.04
Compound_2747-P18	57.5007	-37.9556	1.01
Compound_2748-P18	38.9087	-41.6218	0.80
Compound_2757-P18	38.7761	-34.0572	0.58
Compound_2765-P18	38.9456	-39.9749	0.76
Compound_2767-P18	37.1455	-34.6151	0.57
Compound_2772-P18	39.0484	-31.7681	0.52
Compound_2773-P18	43.4703	-28.4667	0.50
Compound_2774-P18	26.5100	-28.0408	0.20
Compound_2775-P18	36.8545	-23.2490	0.24
Compound_2776-P18	31.2249	-31.8513	0.39
Compound_2777-P18	34.8815	-27.9856	0.34
Compound_2778-P18	46.2998	-31.6880	0.64
Compound_2779-P18	43.7258	-30.9712	0.58
Compound_2780-P18	38.8679	-28.3339	0.42
Compound_2791-P18	37.8782	-33.2534	0.54
Compound_2792-P18	51.3478	-30.8954	0.71
Compound_2793-P18	41.4913	-35.6056	0.67
Compound_2800-P18	48.0613	-35.1340	0.77
Compound_2801-P18	38.8983	-39.7673	0.75
Compound_2805-P18	42.5077	-33.0831	0.62
Compound_2808-P18	50.0865	-34.5618	0.79
Compound_2813-P18	44.9705	-33.0059	0.66
Compound_2814-P18	37.2571	-34.8121	0.58

Compound	Docking energy, kJ mol^{-1}		
	GOLD	DOCK6	RANK
Compound_2816-P18	51.7890	-35.2531	0.84
Compound_2817-P18	37.6119	-33.6597	0.55
Compound_2819-P18	33.9733	-38.7617	0.64
Compound_2821-P18	45.1838	-36.4662	0.76
Compound_2823-P18	48.5255	-33.1486	0.72
Compound_2824-P18	48.8884	-37.1275	0.84
Compound_2825-P18	45.5927	-41.0466	0.90
Compound_2836-P18	44.1235	-39.8603	0.84
Compound_2837-P18	44.5509	-35.9233	0.74
Compound_2943-P18	40.0764	-45.7037	0.94
Compound_2946-P18	48.2217	-40.6703	0.94
Compound_2947-P18	37.0229	-40.6138	0.74
Compound_2948-P18	44.4439	-39.5095	0.84
Compound_2972-P18	63.3247	-50.5631	1.48
Compound_2999-P18	59.5477	-40.9061	1.14
Compound_3000-P18	65.1723	-43.8721	1.32
Compound_6-P19	44.3074	-44.5106	0.98
Compound_7-P19	35.2933	-45.3531	0.85
Compound_9-P19	65.0941	-46.5354	1.39
Compound_138-P19	45.8869	-35.2536	0.74
Compound_139-P19	49.4719	-36.6764	0.84
Compound_150-P19	47.2633	-37.3139	0.82
Compound_156-P19	52.9781	-38.4495	0.95
Compound_163-P19	47.0599	-38.2792	0.85
Compound_180-P19	38.1420	-37.5590	0.67
Compound_187-P19	40.1973	-38.0297	0.72
Compound_191-P19	51.1396	-35.9205	0.85
Compound_348-P19	49.8115	-39.5414	0.93
Compound_349-P19	33.2567	-39.2863	0.64
Compound_350-P19	36.7458	-38.2978	0.67
Compound_351-P19	53.3319	-36.7740	0.91
Compound_353-P19	34.8623	-33.6476	0.50
Compound_357-P19	55.4755	-42.1813	1.10
Compound_359-P19	47.8868	-44.3044	1.04
Compound_360-P19	38.6299	-41.8870	0.81
Compound_363-P19	40.2338	-46.4591	0.97
Compound_364-P19	54.3007	-41.8593	1.07
Compound_366-P19	45.5168	-42.1410	0.93
Compound_368-P19	52.6406	-45.5691	1.15
Compound_377-P19	49.8562	-41.3665	0.98
Compound_378-P19	53.5929	-43.7447	1.12
Compound_379-P19	54.7375	-43.5894	1.13
Compound_380-P19	65.0321	-42.2134	1.27
Compound_381-P19	42.9079	-42.1550	0.89
Compound_382-P19	49.5514	-42.0562	1.00
Compound_384-P19	66.3114	-44.2590	1.35

Compound	Docking energy, kJ mol^{-1}		
	GOLD	DOCK6	RANK
Compound_388-P19	62.9252	-47.0196	1.37
Compound_392-P19	49.7143	-39.0531	0.91
Compound_396-P19	46.4255	-41.9484	0.94
Compound_397-P19	54.5856	-41.5966	1.07
Compound_402-P19	45.7707	-43.1309	0.97
Compound_403-P19	48.7414	-42.9119	1.01
Compound_404-P19	61.4852	-44.2437	1.26
Compound_406-P19	58.0569	-42.7491	1.16
Compound_408-P19	51.2843	-39.5322	0.95
Compound_413-P19	52.2200	-45.7202	1.15
Compound_414-P19	47.1290	-43.1244	0.99
Compound_654-P19	61.9789	-45.9705	1.32
Compound_655-P19	57.8314	-40.8139	1.10
Compound_692-P19	53.1820	-37.9619	0.94
Compound_693-P19	55.8534	-40.1468	1.05
Compound_694-P19	47.0840	-40.4775	0.91
Compound_711-P19	52.7027	-40.7125	1.01
Compound_712-P19	41.2678	-39.3768	0.78
Compound_727-P19	44.9386	-43.2542	0.95
Compound_742-P19	58.7186	-40.7332	1.12
Compound_749-P19	55.3089	-35.2595	0.90
Compound_751-P19	41.1812	-36.1155	0.68
Compound_756-P19	50.0977	-35.8771	0.83
Compound_767-P19	48.0756	-34.2355	0.75
Compound_768-P19	50.8859	-33.2033	0.76
Compound_771-P19	59.0929	-38.1013	1.05
Compound_772-P19	47.5089	-37.5411	0.83
Compound_784-P19	54.4735	-35.3938	0.89
Compound_788-P19	59.0346	-35.1613	0.96
Compound_790-P19	42.1735	-34.6326	0.66
Compound_799-P19	53.6600	-36.2690	0.90
Compound_804-P19	53.2965	-33.1012	0.80
Compound_811-P19	53.5804	-43.7337	1.12
Compound_823-P19	45.5421	-34.7739	0.72
Compound_835-P19	48.4364	-38.5315	0.88
Compound_836-P19	45.8590	-38.1765	0.82
Compound_837-P19	48.6907	-37.5119	0.85
Compound_840-P19	39.5688	-31.5952	0.53
Compound_854-P19	34.1498	-32.6718	0.46
Compound_862-P19	49.9185	-37.0740	0.86
Compound_863-P19	55.7602	-40.1102	1.05
Compound_864-P19	48.9547	-36.8476	0.84
Compound_867-P19	47.0354	-39.7645	0.89
Compound_868-P19	40.3310	-40.9032	0.81
Compound_869-P19	46.1659	-39.4092	0.86
Compound_873-P19	44.8826	-33.2144	0.66

Compound	Docking energy, kJ mol^{-1}		
	GOLD	DOCK6	RANK
Compound_874-P19	44.3529	-34.8560	0.70
Compound_876-P19	37.4223	-30.8314	0.47
Compound_878-P19	46.5360	-29.0431	0.57
Compound_888-P19	45.0754	-38.1268	0.81
Compound_893-P19	49.9788	-32.5239	0.73
Compound_894-P19	47.9031	-30.9960	0.65
Compound_897-P19	55.9827	-28.0014	0.70
Compound_900-P19	48.8830	-34.3000	0.76
Compound_902-P19	50.3124	-32.0555	0.72
Compound_903-P19	40.3077	-27.7988	0.43
Compound_905-P19	44.8586	-34.5649	0.70
Compound_911-P19	53.7554	-35.7985	0.89
Compound_912-P19	40.7090	-33.5434	0.60
Compound_933-P19	45.3791	-38.9924	0.84
Compound_951-P19	63.5275	-40.0152	1.18
Compound_958-P19	54.9209	-34.8170	0.88
Compound_959-P19	46.8039	-34.0570	0.72
Compound_964-P19	45.4306	-36.6807	0.77
Compound_965-P19	42.2932	-35.3341	0.68
Compound_966-P19	47.6798	-33.8220	0.73
Compound_975-P19	55.7516	-37.8758	0.98
Compound_976-P19	49.5146	-35.4944	0.81
Compound_979-P19	51.9169	-35.9787	0.86
Compound_980-P19	43.3741	-34.0677	0.66
Compound_985-P19	44.6039	-36.5865	0.76
Compound_986-P19	51.0791	-34.8250	0.81
Compound_994-P19	52.2508	-33.9653	0.81
Compound_995-P19	53.8626	-34.0651	0.84
Compound_996-P19	49.8827	-33.6874	0.76
Compound_1000-P19	54.2383	-34.9787	0.87
Compound_1001-P19	43.8734	-33.7084	0.66
Compound_1011-P19	49.8949	-38.2766	0.89
Compound_1012-P19	46.0276	-38.4556	0.83
Compound_1017-P19	55.1627	-35.5567	0.91
Compound_1018-P19	43.5936	-33.4179	0.65
Compound_1019-P19	44.9945	-33.2032	0.66
Compound_1034-P19	48.9689	-31.5827	0.68
Compound_1052-P19	47.9186	-35.7912	0.79
Compound_1053-P19	55.6747	-35.3573	0.91
Compound_1056-P19	40.2838	-32.4244	0.56
Compound_1081-P19	51.2181	-41.9048	1.02
Compound_1082-P19	54.3931	-41.0739	1.05
Compound_1083-P19	44.2686	-40.5334	0.86
Compound_1087-P19	54.2213	-38.1415	0.96
Compound_1088-P19	46.2163	-36.6740	0.79
Compound_1093-P19	50.2417	-32.2778	0.73

Compound	Docking energy, kJ mol^{-1}		
	GOLD	DOCK6	RANK
Compound_1094-P19	54.0245	-33.1573	0.82
Compound_1096-P19	41.2786	-33.5010	0.61
Compound_1105-P19	50.0705	-39.1624	0.92
Compound_1111-P19	61.3292	-32.7504	0.93
Compound_1112-P19	44.4731	-32.4586	0.63
Compound_1114-P19	37.7098	-30.7275	0.47
Compound_1117-P19	60.9053	-31.6603	0.89
Compound_1120-P19	42.1654	-29.3942	0.51
Compound_1122-P19	47.4651	-37.3467	0.83
Compound_1123-P19	48.7371	-37.4366	0.85
Compound_1124-P19	58.7640	-34.0345	0.92
Compound_1127-P19	49.5807	-33.5966	0.75
Compound_1128-P19	45.0447	-33.6904	0.68
Compound_1150-P19	40.1852	-36.2042	0.67
Compound_1175-P19	46.7146	-40.6346	0.91
Compound_1188-P19	43.3506	-34.2727	0.67
Compound_1190-P19	41.0564	-28.3900	0.46
Compound_1195-P19	50.3015	-38.8191	0.92
Compound_1196-P19	43.3101	-34.3217	0.67
Compound_1197-P19	45.7354	-25.7859	0.46
Compound_1208-P19	44.1975	-35.2433	0.71
Compound_1260-P19	55.1546	-46.6992	1.23
Compound_1263-P19	53.2898	-43.8229	1.11
Compound_1348-P19	62.0831	-40.6267	1.17
Compound_1349-P19	63.9169	-40.9800	1.21
Compound_1350-P19	32.7956	-43.6419	0.76
Compound_1351-P19	54.9087	-40.2681	1.04
Compound_1369-P19	48.5091	-37.3771	0.85
Compound_1411-P19	46.8608	-34.9670	0.75
Compound_1420-P19	37.9236	-37.2662	0.66
Compound_1443-P19	44.7146	-28.5593	0.52
Compound_1705-P19	59.3836	-44.4411	1.23
Compound_1709-P19	53.7171	-47.1859	1.22
Compound_1712-P19	53.2987	-40.4852	1.02
Compound_1716-P19	51.3835	-42.9556	1.06
Compound_1725-P19	36.9072	-46.0693	0.90
Compound_1842-P19	60.0227	-31.9646	0.88
Compound_2191-P19	48.9228	-31.0282	0.67
Compound_2989-P19	38.9140	-31.1741	0.50
Compound_188-P1	45.7733	-38.0209	0.82
Compound_189-P1	52.5142	-43.8409	1.10
Compound_370-P1	46.7556	-42.1784	0.95
Compound_530-P1	41.4861	-41.9434	0.86
Compound_672-P1	32.7816	-32.5210	0.44
Compound_751-P1	49.4778	-37.3502	0.86
Compound_771-P1	55.9456	-38.6238	1.01

Compound	Docking energy, kJ mol^{-1}		
	GOLD	DOCK6	RANK
Compound_851-P1	51.2702	-39.1796	0.94
Compound_853-P1	52.5064	-37.1493	0.91
Compound_865-P1	37.6504	-32.3977	0.52
Compound_890-P1	47.2072	-36.9125	0.81
Compound_891-P1	44.8696	-35.7664	0.74
Compound_892-P1	40.3265	-35.1897	0.64
Compound_894-P1	41.1637	-37.4576	0.72
Compound_985-P1	51.0694	-43.2225	1.06
Compound_986-P1	41.4665	-34.2860	0.64
Compound_1027-P1	50.2264	-39.3076	0.93
Compound_1066-P1	41.3851	-39.5438	0.79
Compound_1166-P1	45.2830	-37.5549	0.80
Compound_1192-P1	41.3554	-33.0645	0.60
Compound_1221-P1	49.4055	-34.9437	0.79
Compound_1336-P1	45.8612	-41.3780	0.92
Compound_1337-P1	54.0925	-43.8430	1.13
Compound_1385-P1	48.2290	-36.1998	0.81
Compound_1407-P1	51.3227	-37.9468	0.91
Compound_1469-P1	47.0385	-38.2233	0.84
Compound_1472-P1	42.3044	-31.9142	0.58
Compound_1474-P1	40.1100	-32.1383	0.55
Compound_1606-P1	47.7148	-42.5239	0.98
Compound_1607-P1	50.2809	-37.3254	0.87
Compound_1636-P1	49.2539	-35.4009	0.80
Compound_1651-P1	61.0846	-43.1661	1.23
Compound_1715-P1	49.3389	-37.6323	0.87
Compound_1725-P1	41.8657	-27.8953	0.46
Compound_1754-P1	43.6031	-37.4005	0.76
Compound_1784-P1	52.8471	-40.5714	1.01
Compound_1785-P1	42.1036	-39.6049	0.80
Compound_1786-P1	50.3460	-38.2159	0.90
Compound_1794-P1	38.1559	-33.975	0.57
Compound_1795-P1	46.8089	-36.4657	0.79
Compound_1796-P1	49.9783	-39.3874	0.93
Compound_1797-P1	38.8844	-36.7301	0.66
Compound_1804-P1	55.6323	-37.5051	0.97
Compound_1805-P1	56.8035	-37.4806	0.99
Compound_1873-P1	46.8691	-36.0224	0.78
Compound_1924-P1	29.8855	-44.2065	0.73
Compound_1938-P1	51.0436	-43.4280	1.06
Compound_1939-P1	49.8509	-46.8226	1.14
Compound_1940-P1	48.2612	-41.4959	0.96
Compound_1955-P1	43.1855	-42.5290	0.90
Compound_1962-P1	47.6298	-40.8750	0.93
Compound_1986-P1	41.7985	-46.4207	0.99
Compound_2090-P1	56.3740	-39.1430	1.03

Compound	Docking energy, kJ mol^{-1}		
	GOLD	DOCK6	RANK
Compound_2147-P1	55.2153	-39.2223	1.01
Compound_2151-P1	48.4837	-37.9815	0.86
Compound_2155-P1	46.0551	-35.8144	0.76
Compound_2274-P1	47.3442	-38.5784	0.86
Compound_2275-P1	42.9640	-36.7927	0.73
Compound_2276-P1	38.7735	-37.1531	0.67
Compound_2279-P1	40.1856	-38.6084	0.74
Compound_2280-P1	47.6738	-39.7615	0.90
Compound_2287-P1	46.6132	-38.1428	0.84
Compound_2288-P1	45.8882	-36.1515	0.76
Compound_2295-P1	56.4527	-40.8720	1.08
Compound_2299-P1	50.3383	-34.7932	0.80
Compound_2300-P1	39.8669	-33.9974	0.60
Compound_2301-P1	55.1002	-38.0583	0.98
Compound_2317-P1	50.8961	-32.3080	0.74
Compound_2384-P1	48.5193	-37.4172	0.85
Compound_2389-P1	43.0082	-35.2004	0.69
Compound_2390-P1	51.8695	-37.0355	0.89
Compound_2391-P1	48.2416	-38.6694	0.88
Compound_2399-P1	51.4178	-39.6501	0.96
Compound_2400-P1	45.8709	-40.5779	0.89
Compound_2409-P1	45.1807	-35.5990	0.74
Compound_2414-P1	45.4891	-34.6046	0.71
Compound_2415-P1	49.7350	-36.3606	0.84
Compound_2421-P1	48.2003	-38.2169	0.86
Compound_2422-P1	49.9433	-39.1626	0.92
Compound_2453-P1	48.0252	-35.7347	0.79
Compound_2695-P1	43.1010	-34.9401	0.68
Compound_2810-P1	55.4221	-44.1011	1.16
Compound_2812-P1	50.1788	-37.5453	0.88
Compound_2813-P1	52.8589	-44.3778	1.12
Compound_2819-P1	56.1674	-39.8642	1.05
Compound_2820-P1	43.9184	-41.1261	0.88
Compound_2821-P1	55.2055	-42.0001	1.09
Compound_2822-P1	62.4376	-40.9447	1.19
Compound_2823-P1	52.9541	-38.0968	0.94
Compound_2824-P1	58.2865	-39.9983	1.09
Compound_2825-P1	54.0658	-38.2005	0.96
Compound_2827-P1	40.4912	-41.4373	0.83
Compound_2828-P1	48.6306	-39.8172	0.92
Compound_2835-P1	62.2363	-44.4676	1.28
Compound_2905-P1	57.6916	-40.3382	1.09
Compound_2985-P1	56.9140	-44.8783	1.21
Compound_4-P20	47.2373	-37.5831	0.83
Compound_8-P20	52.2456	-36.2770	0.88
Compound_18-P20	54.4898	-39.8425	1.02

Compound	Docking energy, kJ mol^{-1}		
	GOLD	DOCK6	RANK
Compound_19-P20	39.4755	-34.9926	0.62
Compound_21-P20	48.2209	-35.9581	0.80
Compound_40-P20	49.9410	-38.9077	0.91
Compound_41-P20	54.9698	-35.5985	0.90
Compound_43-P20	49.9768	-38.1576	0.89
Compound_44-P20	58.2847	-37.7453	1.02
Compound_45-P20	45.7981	-36.7932	0.78
Compound_48-P20	42.9312	-38.5150	0.78
Compound_50-P20	47.3909	-37.6691	0.83
Compound_64-P20	55.7161	-32.8364	0.84
Compound_75-P20	47.2395	-36.5848	0.80
Compound_76-P20	43.0483	-38.3223	0.78
Compound_88-P20	39.5176	-31.8613	0.53
Compound_100-P20	50.9323	-43.1232	1.05
Compound_118-P20	53.3136	-42.2320	1.07
Compound_120-P20	47.1924	-36.6702	0.80
Compound_128-P20	50.9761	-39.0669	0.94
Compound_129-P20	55.2128	-39.0490	1.01
Compound_130-P20	47.1924	-37.8846	0.84
Compound_134-P20	46.2483	-38.8362	0.85
Compound_135-P20	37.2670	-37.8499	0.67
Compound_139-P20	56.4995	-43.4741	1.16
Compound_141-P20	61.5949	-39.7043	1.14
Compound_736-P20	47.1548	-38.0939	0.84
Compound_742-P20	53.8893	-36.8363	0.92
Compound_743-P20	54.6919	-40.1230	1.03
Compound_744-P20	54.6562	-43.8956	1.14
Compound_748-P20	52.1262	-37.9993	0.92
Compound_787-P20	48.5125	-38.3731	0.87
Compound_788-P20	38.7202	-39.5314	0.74
Compound_789-P20	50.4095	-40.8466	0.98
Compound_790-P20	42.1697	-37.9980	0.76
Compound_800-P20	48.3315	-41.1332	0.95
Compound_802-P20	49.9569	-43.6114	1.05
Compound_804-P20	61.3303	-44.0072	1.26
Compound_864-P20	48.1587	-39.5842	0.90
Compound_866-P20	25.0719	-38.0390	0.47
Compound_868-P20	48.5298	-40.5310	0.94
Compound_898-P20	39.1607	-32.3247	0.54
Compound_900-P20	38.7676	-43.1134	0.85
Compound_901-P20	37.0507	-30.6419	0.45
Compound_902-P20	37.8428	-33.6363	0.56
Compound_903-P20	42.2485	-35.9948	0.70
Compound_904-P20	32.6209	-39.3472	0.63
Compound_905-P20	40.2484	-37.8880	0.72
Compound_906-P20	56.6482	-35.7666	0.94

Compound	Docking energy, kJ mol^{-1}		
	GOLD	DOCK6	RANK
Compound_907-P20	55.3290	-37.7977	0.97
Compound_908-P20	39.2947	-36.6559	0.67
Compound_909-P20	36.3065	-34.1416	0.54
Compound_910-P20	34.7343	-34.0624	0.51
Compound_911-P20	43.7893	-37.4319	0.77
Compound_913-P20	40.5744	-39.5917	0.77
Compound_915-P20	48.0120	-37.6511	0.84
Compound_916-P20	46.2088	-37.8146	0.82
Compound_933-P20	57.0508	-38.7602	1.03
Compound_934-P20	51.5258	-40.7731	0.99
Compound_935-P20	53.5548	-44.9848	1.15
Compound_936-P20	38.7576	-45.9705	0.93
Compound_938-P20	55.1472	-36.0139	0.92
Compound_939-P20	47.4134	-34.5338	0.74
Compound_940-P20	46.4727	-34.5534	0.73
Compound_941-P20	62.9269	-38.8224	1.13
Compound_943-P20	55.1663	-42.3451	1.10
Compound_953-P20	39.8264	-36.6816	0.68
Compound_955-P20	49.7221	-40.5529	0.96
Compound_956-P20	37.2109	-28.7686	0.40
Compound_957-P20	44.1767	-32.9350	0.64
Compound_960-P20	41.4051	-35.7321	0.68
Compound_968-P20	63.2407	-40.7471	1.19
Compound_972-P20	41.1019	-32.9714	0.59
Compound_981-P20	45.2392	-42.8393	0.95
Compound_982-P20	50.0335	-36.3658	0.84
Compound_988-P20	41.5113	-33.0425	0.60
Compound_989-P20	41.7070	-33.0803	0.60
Compound_990-P20	43.5727	-34.6274	0.68
Compound_991-P20	43.1329	-36.8295	0.74
Compound_992-P20	45.2134	-36.3690	0.76
Compound_1005-P20	34.2049	-33.7888	0.50
Compound_1006-P20	43.4794	-37.3573	0.76
Compound_1007-P20	32.7415	-33.6963	0.47
Compound_1008-P20	35.1082	-34.2604	0.53
Compound_1009-P20	51.1905	-35.6619	0.84
Compound_1010-P20	61.0697	-37.2607	1.06
Compound_1012-P20	52.8861	-42.5919	1.07
Compound_1014-P20	56.6650	-38.8221	1.03
Compound_1016-P20	48.0607	-36.4743	0.81
Compound_1039-P20	35.1842	-33.4781	0.51
Compound_1040-P20	42.3744	-36.3041	0.71
Compound_1041-P20	47.8614	-37.0537	0.82
Compound_1042-P20	25.6296	-29.3219	0.22
Compound_1043-P20	33.0862	-34.6831	0.50
Compound_1050-P20	63.7649	-44.0363	1.30

Compound	Docking energy, kJ mol^{-1}		
	GOLD	DOCK6	RANK
Compound_1086-P20	40.4423	-46.7327	0.98
Compound_1093-P20	51.8696	-37.1846	0.90
Compound_1094-P20	53.7561	-42.8220	1.09
Compound_1095-P20	47.0708	-37.0197	0.81
Compound_1097-P20	51.1108	-42.2384	1.03
Compound_1101-P20	60.6178	-44.8460	1.27
Compound_1103-P20	35.5308	-37.3624	0.62
Compound_1104-P20	35.5043	-33.4754	0.51
Compound_1105-P20	38.5386	-34.7593	0.60
Compound_1106-P20	51.3025	-33.3902	0.78
Compound_1108-P20	49.6975	-37.6050	0.87
Compound_1110-P20	36.7866	-33.6733	0.54
Compound_1111-P20	38.2891	-34.6834	0.59
Compound_1113-P20	42.9141	-40.8382	0.85
Compound_1114-P20	46.0229	-33.8141	0.70
Compound_1123-P20	47.3492	-40.0615	0.90
Compound_1125-P20	42.2151	-40.1559	0.82
Compound_1185-P20	35.4616	-43.8363	0.81
Compound_1187-P20	47.6967	-44.0974	1.03
Compound_1193-P20	59.0395	-43.5560	1.20
Compound_1261-P20	41.6968	-45.9409	0.98
Compound_1262-P20	36.6163	-43.1475	0.81
Compound_1290-P20	47.8853	-40.7867	0.93
Compound_1291-P20	52.2645	-44.2484	1.11
Compound_1311-P20	30.0768	-39.7482	0.60
Compound_1322-P20	45.6856	-35.1867	0.73
Compound_1326-P20	54.4994	-36.8929	0.93
Compound_1327-P20	41.3433	-34.8881	0.65
Compound_1328-P20	47.5949	-34.3418	0.74
Compound_1329-P20	51.0505	-39.3329	0.95
Compound_1334-P20	46.2608	-37.7071	0.82
Compound_1337-P20	35.2979	-33.3913	0.50
Compound_1417-P20	57.6220	-40.8189	1.10
Compound_1418-P20	38.3346	-37.2462	0.67
Compound_1421-P20	44.1931	-39.0777	0.82
Compound_1439-P20	62.7599	-43.7083	1.27
Compound_1455-P20	65.1042	-42.4724	1.28
Compound_1459-P20	62.8124	-42.2647	1.23
Compound_1462-P20	62.0588	-43.1627	1.24
Compound_1464-P20	50.3724	-43.4750	1.05
Compound_1465-P20	64.1062	-43.0453	1.27
Compound_1495-P20	57.0610	-38.8148	1.03
Compound_1501-P20	58.4298	-41.3646	1.13
Compound_1503-P20	47.0229	-40.6064	0.91
Compound_1504-P20	52.6580	-41.0202	1.02
Compound_1506-P20	55.7860	-40.7974	1.07

Compound	Docking energy, kJ mol^{-1}		
	GOLD	DOCK6	RANK
Compound_1508-P20	55.6971	-41.8094	1.10
Compound_1544-P20	60.2396	-41.4775	1.16
Compound_1662-P20	46.8395	-41.2498	0.93
Compound_1668-P20	36.6564	-47.2668	0.93
Compound_1669-P20	66.2982	-43.7038	1.33
Compound_1670-P20	59.2275	-44.4737	1.23
Compound_1671-P20	61.3081	-42.5833	1.21
Compound_1764-P20	53.3124	-33.6836	0.82
Compound_1766-P20	54.1464	-39.8037	1.01
Compound_1767-P20	61.1432	-38.1590	1.08
Compound_1770-P20	44.3317	-38.9390	0.82
Compound_1776-P20	46.6417	-40.1366	0.89
Compound_1777-P20	36.9439	-41.0954	0.76
Compound_1778-P20	52.1695	-41.5365	1.03
Compound_1782-P20	52.1088	-37.0285	0.90
Compound_1783-P20	40.1960	-41.4939	0.82
Compound_1784-P20	42.8503	-40.0084	0.83
Compound_1789-P20	59.5260	-39.9101	1.11
Compound_1791-P20	47.4126	-40.1249	0.91
Compound_1792-P20	37.2035	-41.8176	0.78
Compound_1795-P20	54.7666	-41.4768	1.07
Compound_1796-P20	51.9281	-44.5724	1.11
Compound_1798-P20	51.1196	-38.7129	0.93
Compound_1799-P20	50.0267	-37.6472	0.88
Compound_1833-P20	55.6795	-43.0723	1.13
Compound_1834-P20	33.1493	-43.8321	0.77
Compound_1835-P20	47.6039	-42.9787	0.99
Compound_1836-P20	40.4522	-38.9515	0.75
Compound_1837-P20	45.2165	-40.1505	0.87
Compound_1846-P20	40.9976	-37.7203	0.73
Compound_1847-P20	55.1244	-37.4314	0.96
Compound_1853-P20	39.1061	-38.9025	0.73
Compound_1854-P20	45.5418	-40.4389	0.88
Compound_1865-P20	52.6835	-39.9931	0.99
Compound_1866-P20	47.6847	-42.1448	0.97
Compound_1869-P20	52.8948	-40.5046	1.01
Compound_1889-P20	64.8486	-43.0385	1.29
Compound_1890-P20	59.4902	-42.2794	1.17
Compound_1899-P20	44.7253	-38.6712	0.82
Compound_1900-P20	47.1703	-40.6245	0.92
Compound_1911-P20	46.7001	-39.7667	0.88
Compound_1912-P20	49.4574	-40.8834	0.96
Compound_1917-P20	46.0342	-39.8914	0.88
Compound_1918-P20	52.0909	-38.6772	0.94
Compound_1919-P20	56.2928	-38.0288	1.00
Compound_1920-P20	53.0737	-38.7453	0.96

Compound	Docking energy, kJ mol^{-1}		
	GOLD	DOCK6	RANK
Compound_1921-P20	52.4948	-40.6234	1.01
Compound_1925-P20	62.0506	-43.6445	1.26
Compound_1926-P20	53.7117	-40.6719	1.03
Compound_1930-P20	41.3891	-36.3827	0.70
Compound_1937-P20	44.4917	-38.6927	0.81
Compound_1939-P20	46.9295	-37.5647	0.82
Compound_1940-P20	41.4992	-36.6272	0.70
Compound_1941-P20	41.0335	-41.0912	0.83
Compound_1944-P20	61.2642	-39.8674	1.13
Compound_1945-P20	61.5886	-39.4240	1.13
Compound_1950-P20	46.8587	-37.3562	0.82
Compound_1974-P20	54.5598	-41.7479	1.07
Compound_1975-P20	43.2308	-43.0071	0.92
Compound_1976-P20	67.1734	-41.5208	1.28
Compound_1979-P20	38.8333	-39.2272	0.73
Compound_1980-P20	53.9995	-41.5778	1.06
Compound_1988-P20	41.0484	-38.5647	0.75
Compound_1989-P20	63.7526	-40.6108	1.20
Compound_1991-P20	58.8442	-41.9440	1.15
Compound_1995-P20	62.0584	-39.6983	1.14
Compound_1996-P20	52.8185	-40.3744	1.01
Compound_2008-P20	53.0026	-40.2162	1.00
Compound_2009-P20	55.1120	-41.5028	1.08
Compound_2013-P20	42.2243	-41.2654	0.85
Compound_2014-P20	49.0981	-40.5044	0.95
Compound_2024-P20	43.3753	-44.6582	0.97
Compound_2025-P20	48.4383	-41.9249	0.98
Compound_2030-P20	46.0566	-39.2977	0.86
Compound_2031-P20	57.9856	-42.3691	1.15
Compound_2037-P20	48.0534	-40.0889	0.92
Compound_2040-P20	37.3627	-39.6138	0.72
Compound_2041-P20	31.5315	-40.2709	0.64
Compound_2042-P20	38.5870	-37.4337	0.68
Compound_2047-P20	54.9237	-37.3698	0.95
Compound_2048-P20	48.9983	-36.5413	0.83
Compound_2049-P20	60.8614	-38.5957	1.09
Compound_2050-P20	44.7106	-38.4175	0.81
Compound_2051-P20	56.9392	-41.5393	1.11
Compound_2057-P20	47.7987	-38.8330	0.88
Compound_2058-P20	45.3166	-39.9968	0.87
Compound_2059-P20	49.2034	-41.5309	0.98
Compound_2060-P20	42.6464	-41.7792	0.87
Compound_2061-P20	54.2473	-41.4250	1.06
Compound_2063-P20	51.3565	-33.8150	0.79
Compound_2064-P20	59.6600	-36.0208	1.00
Compound_2065-P20	45.8178	-40.3901	0.89

Compound	Docking energy, kJ mol^{-1}		
	GOLD	DOCK6	RANK
Compound_2066-P20	54.6862	-39.5302	1.01
Compound_2069-P20	34.2227	-39.3566	0.66
Compound_2070-P20	51.8876	-40.0315	0.98
Compound_2071-P20	45.7058	-41.0240	0.90
Compound_2072-P20	36.8466	-40.7402	0.74
Compound_2077-P20	56.7363	-41.2678	1.10
Compound_2078-P20	61.6675	-42.3239	1.21
Compound_2079-P20	50.6615	-44.1706	1.08
Compound_2080-P20	45.7835	-35.5593	0.75
Compound_2081-P20	60.1745	-39.9495	1.12
Compound_2084-P20	44.9425	-39.5686	0.85
Compound_2087-P20	43.0768	-38.5208	0.79
Compound_2092-P20	39.6129	-42.1005	0.83
Compound_2093-P20	38.4286	-41.7239	0.80
Compound_2094-P20	41.7703	-42.3771	0.88
Compound_2095-P20	50.8339	-35.5530	0.83
Compound_2096-P20	51.9070	-37.3471	0.90
Compound_2097-P20	34.2944	-41.7104	0.73
Compound_2099-P20	63.1917	-41.7047	1.22
Compound_2100-P20	51.3382	-41.4486	1.01
Compound_2101-P20	52.6780	-38.9220	0.96
Compound_2105-P20	46.4973	-39.5948	0.88
Compound_2106-P20	54.8318	-40.8760	1.05
Compound_2108-P20	40.9246	-42.4679	0.86
Compound_2112-P20	44.8146	-37.6125	0.79
Compound_2113-P20	47.7471	-41.9587	0.96
Compound_2128-P20	41.5196	-42.4736	0.87
Compound_2130-P20	45.7366	-43.5349	0.98
Compound_2134-P20	49.6503	-42.9900	1.03
Compound_2135-P20	43.4970	-42.9508	0.92
Compound_2138-P20	48.4097	-39.1152	0.89
Compound_2139-P20	49.9014	-40.0395	0.95
Compound_2140-P20	34.3418	-41.4644	0.72
Compound_2141-P20	55.4306	-41.8926	1.09
Compound_2142-P20	47.1080	-40.1773	0.90
Compound_2143-P20	46.0869	-42.0539	0.94
Compound_2149-P20	57.7322	-39.6219	1.07
Compound_2150-P20	44.4876	-42.9204	0.94
Compound_2151-P20	51.7468	-41.3269	1.01
Compound_2154-P20	51.7576	-39.2785	0.96
Compound_2155-P20	46.2823	-40.9488	0.91
Compound_2166-P20	34.8253	-44.1919	0.81
Compound_2168-P20	44.8483	-40.2969	0.87
Compound_2169-P20	42.5350	-41.8737	0.87
Compound_2171-P20	41.5520	-38.7447	0.77
Compound_2172-P20	41.7339	-41.0473	0.84

Compound	Docking energy, kJ mol^{-1}		
	GOLD	DOCK6	RANK
Compound_2183-P20	56.2545	-41.6955	1.10
Compound_2184-P20	58.0324	-42.8440	1.17
Compound_2185-P20	67.8677	-42.3419	1.32
Compound_2192-P20	61.2011	-38.7465	1.10
Compound_2193-P20	50.5935	-40.8976	0.98
Compound_2200-P20	53.8695	-40.4379	1.03
Compound_2204-P20	52.0480	-39.7767	0.97
Compound_2207-P20	43.7845	-39.7073	0.83
Compound_2208-P20	56.1962	-39.6687	1.04
Compound_2209-P20	42.9411	-40.4515	0.84
Compound_2210-P20	62.7111	-39.8886	1.16
Compound_2214-P20	51.4698	-35.7576	0.85
Compound_2215-P20	47.8897	-38.0605	0.85
Compound_2218-P20	43.1822	-42.1067	0.89
Compound_2219-P20	51.7244	-42.4641	1.05
Compound_2222-P20	42.7810	-42.0953	0.88
Compound_2223-P20	45.8189	-39.6974	0.87
Compound_2230-P20	51.6863	-39.8597	0.97
Compound_2233-P20	51.8606	-36.8298	0.89
Compound_2234-P20	46.2380	-40.4727	0.90
Compound_2235-P20	47.8241	-43.4129	1.01
Compound_2238-P20	42.0623	-40.4964	0.83
Compound_2239-P20	75.3779	-43.4974	1.48
Compound_2255-P20	68.5071	-45.1179	1.41
Compound_2256-P20	41.6689	-44.2828	0.93
Compound_2257-P20	52.6019	-44.2303	1.11
Compound_2264-P20	44.4206	-39.7962	0.85
Compound_2265-P20	50.5031	-42.0209	1.01
Compound_2269-P20	45.6076	-41.3622	0.91
Compound_2270-P20	60.0763	-38.8687	1.09
Compound_2280-P20	28.0228	-45.9083	0.74
Compound_2283-P20	52.6815	-42.0062	1.05
Compound_2284-P20	51.6036	-43.5254	1.08
Compound_2287-P20	50.6985	-40.6441	0.98
Compound_2288-P20	53.0094	-42.9799	1.08
Compound_2302-P20	54.9517	-40.9521	1.06
Compound_2303-P20	56.1798	-43.0132	1.14
Compound_2307-P20	59.0296	-41.2494	1.14
Compound_2308-P20	52.7870	-37.5051	0.92
Compound_2309-P20	51.8253	-38.5068	0.93
Compound_2311-P20	44.4172	-37.5936	0.78
Compound_2312-P20	30.8006	-38.7066	0.58
Compound_2313-P20	45.0748	-38.7811	0.83
Compound_2318-P20	53.5334	-34.4157	0.84
Compound_2319-P20	55.6671	-35.3954	0.91
Compound_2323-P20	37.0303	-40.6920	0.75

Compound	Docking energy, kJ mol^{-1}		
	GOLD	DOCK6	RANK
Compound_2328-P20	38.2381	-36.5919	0.65
Compound_2330-P20	48.4147	-40.9305	0.95
Compound_2331-P20	43.1801	-40.2455	0.84
Compound_2336-P20	32.2742	-35.4194	0.51
Compound_2337-P20	46.1068	-36.4985	0.78
Compound_2339-P20	54.8363	-41.9866	1.09
Compound_2340-P20	58.0980	-39.6967	1.08
Compound_2343-P20	58.5008	-40.9924	1.12
Compound_2345-P20	49.0782	-36.5190	0.83
Compound_2346-P20	38.7279	-37.6272	0.69
Compound_2363-P20	42.4406	-40.8809	0.84
Compound_2365-P20	48.5773	-41.2990	0.96
Compound_2368-P20	52.3573	-44.6349	1.12
Compound_2370-P20	37.7360	-38.4379	0.69
Compound_2371-P20	60.3305	-42.3751	1.19
Compound_2376-P20	41.9904	-39.4740	0.79
Compound_2378-P20	37.4372	-41.0037	0.76
Compound_2388-P20	52.5724	-40.4651	1.00
Compound_2391-P20	49.9655	-44.2550	1.07
Compound_2396-P20	46.3500	-40.7132	0.91
Compound_2405-P20	46.5935	-38.2597	0.84
Compound_2406-P20	49.8264	-37.6098	0.87
Compound_2409-P20	37.3003	-44.1776	0.85
Compound_2415-P20	46.1044	-38.9846	0.85
Compound_2416-P20	33.4095	-41.6022	0.71
Compound_2417-P20	44.4062	-35.7987	0.73
Compound_2418-P20	50.4811	-38.6211	0.91
Compound_2420-P20	47.1613	-41.4818	0.94
Compound_2421-P20	46.8811	-41.8984	0.95
Compound_2422-P20	46.6664	-41.9250	0.95
Compound_2425-P20	46.8667	-41.2638	0.93
Compound_2426-P20	42.1588	-43.3449	0.91
Compound_2427-P20	36.3856	-42.9205	0.80
Compound_2428-P20	37.2468	-42.0404	0.79
Compound_2434-P20	56.8162	-44.1448	1.18
Compound_2435-P20	56.0653	-43.7206	1.16
Compound_2436-P20	42.5377	-38.7110	0.78
Compound_2437-P20	53.1946	-39.4543	0.98
Compound_2438-P20	55.1826	-42.4213	1.10
Compound_2439-P20	50.3089	-43.2028	1.04
Compound_2441-P20	49.7795	-37.2383	0.86
Compound_2442-P20	32.2811	-39.5798	0.63
Compound_2444-P20	42.8857	-42.0334	0.88
Compound_2446-P20	45.6453	-37.8555	0.81
Compound_2447-P20	45.6206	-38.7284	0.84
Compound_2449-P20	42.3145	-42.3208	0.88

Compound	Docking energy, kJ mol^{-1}		
	GOLD	DOCK6	RANK
Compound_2450-P20	50.5618	-44.4376	1.08
Compound_2451-P20	46.8829	-42.5238	0.97
Compound_2453-P20	60.3772	-42.3802	1.19
Compound_2454-P20	52.1756	-43.6856	1.09
Compound_2458-P20	48.5926	-39.5652	0.91
Compound_2459-P20	48.9583	-41.1455	0.96
Compound_2483-P20	32.3273	-46.7898	0.84
Compound_2484-P20	39.1000	-46.9158	0.96
Compound_2486-P20	38.6578	-42.4338	0.82
Compound_2487-P20	46.9934	-44.0738	1.01
Compound_2489-P20	41.4154	-44.3254	0.93
Compound_2490-P20	48.3376	-44.6652	1.05
Compound_2493-P20	62.6533	-40.6192	1.18
Compound_2494-P20	55.7760	-41.9151	1.10
Compound_2498-P20	50.8971	-41.7902	1.01
Compound_2499-P20	53.8329	-43.1124	1.10
Compound_2510-P20	32.7193	-40.7777	0.68
Compound_2526-P20	60.6222	-40.8084	1.15
Compound_2527-P20	45.0699	-42.8887	0.95
Compound_2529-P20	50.0703	-41.2802	0.98
Compound_2530-P20	61.9276	-42.1644	1.21
Compound_2531-P20	47.8621	-40.6083	0.93
Compound_2533-P20	42.0606	-40.5928	0.83
Compound_2534-P20	55.5328	-41.2223	1.08
Compound_2535-P20	54.3247	-42.1969	1.08
Compound_2542-P20	60.2846	-42.0712	1.18
Compound_2543-P20	51.5187	-37.2278	0.89
Compound_2544-P20	60.9812	-38.3942	1.09
Compound_2546-P20	36.7415	-40.3610	0.73
Compound_2550-P20	51.1993	-39.9930	0.97
Compound_2551-P20	39.5081	-39.2563	0.75
Compound_2557-P20	37.7314	-35.8314	0.62
Compound_2558-P20	47.7286	-37.1571	0.83
Compound_2564-P20	34.8365	-35.2032	0.55
Compound_2565-P20	30.8959	-36.4412	0.52
Compound_2566-P20	41.6868	-39.2353	0.78
Compound_2569-P20	49.4959	-38.5332	0.90
Compound_2571-P20	34.3131	-44.4463	0.81
Compound_2572-P20	63.7537	-38.2888	1.13
Compound_2573-P20	56.0141	-40.1590	1.05
Compound_2590-P20	35.4080	-41.5822	0.74
Compound_2591-P20	53.2701	-40.6822	1.02
Compound_2599-P20	54.2608	-38.4120	0.97
Compound_2600-P20	49.2665	-40.3457	0.94
Compound_2602-P20	57.0597	-42.4615	1.14
Compound_2603-P20	48.0228	-41.8076	0.97

Compound	Docking energy, kJ mol^{-1}		
	GOLD	DOCK6	RANK
Compound_2613-P20	60.1746	-43.5899	1.22
Compound_2616-P20	47.9872	-44.9737	1.06
Compound_2631-P20	49.5947	-45.0039	1.08
Compound_2636-P20	53.9330	-40.5066	1.03
Compound_2640-P20	51.2475	-40.3634	0.98
Compound_2643-P20	52.9772	-40.6465	1.02
Compound_2644-P20	39.2803	-41.8984	0.82
Compound_2649-P20	48.1839	-35.0458	0.77
Compound_2654-P20	24.9414	-36.9540	0.43
Compound_2655-P20	51.7612	-39.0107	0.95
Compound_2657-P20	47.5894	-40.6997	0.93
Compound_2658-P20	47.8391	-39.9446	0.91
Compound_2659-P20	58.7360	-45.4741	1.25
Compound_2660-P20	62.0732	-45.7128	1.32
Compound_2661-P20	41.3586	-42.2060	0.86
Compound_2672-P20	29.3482	-45.6107	0.76
Compound_2675-P20	57.2938	-39.9112	1.07
Compound_2676-P20	51.1162	-41.1858	1.00
Compound_2678-P20	48.2153	-43.8341	1.03
Compound_2683-P20	46.7592	-40.2224	0.90
Compound_2684-P20	30.5087	-43.1504	0.71
Compound_2697-P20	47.0001	-43.1345	0.99
Compound_2701-P20	53.3451	-41.6223	1.05
Compound_2702-P20	37.9133	-42.0519	0.80
Compound_2717-P20	57.0880	-41.1643	1.10
Compound_2725-P20	59.0604	-45.7349	1.27
Compound_2730-P20	54.8740	-36.9105	0.94
Compound_2731-P20	53.2472	-38.0170	0.94
Compound_2732-P20	33.0719	-39.8222	0.65
Compound_2740-P20	38.6503	-35.4302	0.62
Compound_2741-P20	39.8412	-39.5159	0.76
Compound_2744-P20	49.7199	-34.7759	0.79
Compound_2745-P20	50.4153	-34.6399	0.80
Compound_2746-P20	41.0427	-41.5217	0.84
Compound_2749-P20	55.8703	-38.8723	1.01
Compound_2750-P20	48.0936	-35.4785	0.78
Compound_2751-P20	49.3530	-38.5381	0.89
Compound_2763-P20	40.0523	-42.3867	0.85
Compound_2764-P20	49.2972	-36.0784	0.82
Compound_2771-P20	55.8050	-35.2836	0.91
Compound_2772-P20	43.1117	-37.0858	0.74
Compound_2773-P20	47.9112	-40.0828	0.91
Compound_2782-P20	39.3098	-41.1261	0.80
Compound_2784-P20	44.3741	-42.0452	0.91
Compound_2795-P20	45.3835	-37.0950	0.78
Compound_2796-P20	68.1320	-40.8568	1.28

Compound	Docking energy, kJ mol^{-1}		
	GOLD	DOCK6	RANK
Compound_2798-P20	60.5011	-39.4322	1.11
Compound_2800-P20	54.1514	-42.9674	1.10
Compound_2803-P20	44.5115	-38.1391	0.80
Compound_2804-P20	44.1127	-41.4173	0.89
Compound_2811-P20	40.5254	-43.5847	0.89
Compound_2812-P20	38.6924	-40.4369	0.77
Compound_2816-P20	56.7695	-43.7863	1.17
Compound_2818-P20	46.1659	-37.9595	0.82
Compound_2822-P20	60.8497	-38.7500	1.09
Compound_2824-P20	54.4909	-39.9321	1.02
Compound_2832-P20	38.3162	-39.6510	0.74
Compound_2838-P20	48.8312	-37.5309	0.85
Compound_2841-P20	51.6045	-37.6873	0.91
Compound_2845-P20	47.7608	-41.2271	0.94
Compound_2863-P20	56.9436	-42.1684	1.13
Compound_2866-P20	33.8354	-45.1391	0.82
Compound_2867-P20	47.9376	-40.6511	0.93
Compound_2869-P20	54.2137	-39.4403	1.00
Compound_2871-P20	55.1501	-44.7662	1.17
Compound_2873-P20	66.3993	-36.5893	1.13
Compound_2874-P20	55.3653	-38.9314	1.01
Compound_2894-P20	59.5290	-39.8102	1.10
Compound_2895-P20	37.2975	-44.3245	0.86
Compound_2906-P20	50.8415	-46.1295	1.14
Compound_2913-P20	44.7081	-43.4897	0.96
Compound_2914-P20	52.2120	-43.9610	1.10
Compound_2917-P20	60.5291	-39.0770	1.10
Compound_2926-P20	56.8378	-42.0827	1.12
Compound_2930-P20	45.9377	-43.0360	0.97
Compound_2931-P20	59.8000	-41.5908	1.16
Compound_2934-P20	42.0213	-42.5522	0.88
Compound_2935-P20	43.2191	-41.8190	0.88
Compound_2936-P20	59.6786	-44.9079	1.25
Compound_2937-P20	56.9473	-37.6587	1.00
Compound_2938-P20	60.6126	-40.0444	1.13
Compound_2943-P20	43.6097	-38.6411	0.80
Compound_2946-P20	48.7175	-42.7870	1.01
Compound_2947-P20	44.4019	-43.0146	0.94
Compound_2949-P20	44.9274	-41.2155	0.90
Compound_2963-P20	51.5463	-42.7902	1.05
Compound_2965-P20	42.4670	-41.4828	0.86
Compound_2970-P20	38.8775	-45.5296	0.92
Compound_2974-P20	63.0047	-39.3148	1.15
Compound_2975-P20	48.4616	-42.1787	0.98
Compound_2979-P20	51.7337	-40.0263	0.98
Compound_2980-P20	45.0788	-42.6923	0.94

Compound	Docking energy, kJ mol^{-1}		
	GOLD	DOCK6	RANK
Compound_2995-P20	53.4670	-42.1637	1.07
Compound_2996-P20	45.9670	-43.9964	0.99
Compound_2998-P20	37.1226	-43.0113	0.81
Compound_9-P2	55.2653	-44.7582	1.17
Compound_22-P2	41.2397	-43.5645	0.90
Compound_24-P2	46.1508	-45.4218	1.04
Compound_110-P2	53.1964	-34.7250	0.85
Compound_112-P2	47.4644	-42.2660	0.97
Compound_113-P2	46.2341	-41.0134	0.91
Compound_118-P2	46.8434	-42.8512	0.98
Compound_120-P2	38.5798	-35.1944	0.61
Compound_122-P2	49.3046	-39.0021	0.91
Compound_123-P2	41.4380	-37.9708	0.74
Compound_129-P2	41.7378	-36.7641	0.71
Compound_131-P2	37.3168	-41.9137	0.79
Compound_142-P2	53.9650	-32.3761	0.79
Compound_143-P2	51.6997	-33.4637	0.79
Compound_147-P2	38.5198	-27.9737	0.40
Compound_150-P2	58.9588	-37.6252	1.03
Compound_156-P2	45.3552	-39.1067	0.84
Compound_160-P2	48.2470	-33.8176	0.74
Compound_166-P2	56.4127	-34.5775	0.90
Compound_209-P2	50.1403	-39.1654	0.92
Compound_210-P2	50.0800	-38.3564	0.90
Compound_230-P2	45.2953	-37.5568	0.80
Compound_234-P2	60.1448	-41.7892	1.17
Compound_328-P2	60.4353	-40.9585	1.15
Compound_333-P2	47.1658	-34.5049	0.74
Compound_341-P2	55.3774	-38.0279	0.98
Compound_430-P2	44.2333	-29.6579	0.55
Compound_463-P2	47.2158	-39.6697	0.89
Compound_466-P2	30.5912	-39.0835	0.59
Compound_470-P2	51.0755	-43.9973	1.08
Compound_473-P2	51.8213	-44.3024	1.10
Compound_475-P2	59.5938	-41.9150	1.17
Compound_476-P2	49.9768	-40.3047	0.95
Compound_478-P2	56.1760	-44.1138	1.17
Compound_497-P2	42.2531	-43.6377	0.92
Compound_498-P2	55.2655	-40.2258	1.04
Compound_503-P2	60.7608	-42.9657	1.22
Compound_511-P2	65.3407	-42.5305	1.28
Compound_514-P2	52.1467	-40.7620	1.01
Compound_515-P2	46.2021	-35.7633	0.76
Compound_548-P2	63.5626	-42.0082	1.24
Compound_589-P2	53.9779	-40.7805	1.04
Compound_612-P2	36.5516	-50.9958	1.04

Compound	Docking energy, kJ mol^{-1}		
	GOLD	DOCK6	RANK
Compound_619-P2	66.4298	-46.1925	1.41
Compound_622-P2	63.1300	-37.2779	1.09
Compound_723-P2	63.2842	-42.5811	1.25
Compound_745-P2	37.1222	-42.7961	0.81
Compound_747-P2	47.4629	-42.7842	0.98
Compound_764-P2	45.6719	-44.0303	0.99
Compound_776-P2	64.6085	-43.2070	1.29
Compound_846-P2	45.3191	-44.6434	1.00
Compound_947-P2	59.4647	-44.0085	1.22
Compound_948-P2	51.7558	-42.3395	1.04
Compound_949-P2	44.4432	-40.3243	0.86
Compound_952-P2	38.5339	-46.3370	0.94
Compound_1020-P2	56.5300	-45.1857	1.21
Compound_1023-P2	54.3292	-44.9802	1.16
Compound_1072-P2	41.8648	-39.5667	0.80
Compound_1073-P2	49.8048	-39.5665	0.93
Compound_1089-P2	37.7552	-40.7328	0.76
Compound_1091-P2	36.3674	-35.0488	0.57
Compound_1092-P2	54.8765	-40.1982	1.04
Compound_1093-P2	44.5843	-43.4346	0.95
Compound_1103-P2	45.8569	-39.9308	0.87
Compound_1104-P2	36.1701	-40.4850	0.73
Compound_1117-P2	53.5569	-41.5691	1.05
Compound_1119-P2	53.1302	-45.0865	1.15
Compound_1125-P2	41.9972	-34.3285	0.65
Compound_1126-P2	36.5210	-32.4523	0.50
Compound_1129-P2	32.5827	-44.0136	0.77
Compound_1130-P2	55.2567	-39.8426	1.03
Compound_1131-P2	35.0896	-41.4862	0.74
Compound_1151-P2	55.4872	-42.3484	1.11
Compound_1153-P2	38.6614	-37.3289	0.68
Compound_1164-P2	48.7131	-36.7129	0.83
Compound_1165-P2	42.6935	-34.0675	0.65
Compound_1166-P2	42.3792	-35.6382	0.69
Compound_1173-P2	43.9900	-38.8769	0.81
Compound_1182-P2	38.1026	-34.6323	0.59
Compound_1244-P2	55.4161	-43.6182	1.14
Compound_1246-P2	58.3536	-49.1160	1.35
Compound_1394-P2	44.4020	-40.7070	0.87
Compound_1396-P2	51.5752	-38.9659	0.94
Compound_1397-P2	40.8691	-40.7717	0.81
Compound_1398-P2	37.8556	-30.9075	0.48
Compound_1399-P2	39.5882	-37.9256	0.71
Compound_1400-P2	54.7730	-40.9177	1.05
Compound_1409-P2	48.8841	-35.5741	0.80
Compound_1435-P2	43.0699	-40.4570	0.84

Compound	Docking energy, kJ mol^{-1}		
	GOLD	DOCK6	RANK
Compound_1447-P2	48.8540	-31.4717	0.68
Compound_1455-P2	44.6498	-31.2212	0.60
Compound_1546-P2	47.9023	-41.6371	0.96
Compound_1547-P2	69.8251	-45.5243	1.44
Compound_1606-P2	44.3452	-44.3909	0.98
Compound_1809-P2	62.9775	-46.6216	1.36
Compound_1828-P2	47.4243	-44.3539	1.03
Compound_1832-P2	46.0262	-39.9295	0.88
Compound_1842-P2	51.2745	-42.8205	1.05
Compound_1851-P2	46.7041	-34.3643	0.73
Compound_1855-P2	52.2443	-39.3671	0.97
Compound_1857-P2	46.5851	-39.0246	0.86
Compound_1863-P2	49.5324	-41.1981	0.97
Compound_1978-P2	40.8616	-38.5986	0.75
Compound_2028-P2	39.6926	-39.1667	0.75
Compound_2174-P2	41.2540	-40.9200	0.82
Compound_2175-P2	49.9404	-39.4581	0.93
Compound_2177-P2	45.3667	-45.0981	1.02
Compound_2182-P2	52.4605	-44.0678	1.11
Compound_2193-P2	48.8114	-42.9310	1.01
Compound_2194-P2	56.5924	-39.7800	1.05
Compound_2244-P2	64.1343	-44.3433	1.31
Compound_2263-P2	52.0155	-39.2207	0.96
Compound_2264-P2	52.7445	-43.7705	1.10
Compound_2353-P2	51.5283	-38.1098	0.92
Compound_2368-P2	65.7495	-46.0764	1.39
Compound_2371-P2	67.2480	-46.9933	1.44
Compound_2372-P2	48.5103	-43.0831	1.01
Compound_2374-P2	43.0768	-44.3294	0.95
Compound_2375-P2	47.4112	-48.1953	1.14
Compound_2391-P2	41.7257	-47.4531	1.02
Compound_2392-P2	50.5350	-47.3056	1.17
Compound_2394-P2	37.9301	-47.1841	0.95
Compound_2411-P2	52.9866	-41.2910	1.03
Compound_2412-P2	52.5620	-46.1588	1.17
Compound_2414-P2	37.0041	-52.2249	1.08
Compound_2448-P2	38.3916	-42.3894	0.82
Compound_2517-P2	50.7271	-41.5953	1.01
Compound_2522-P2	48.8318	-44.9158	1.07
Compound_2531-P2	52.2662	-35.6993	0.86
Compound_2532-P2	58.8413	-44.4437	1.23
Compound_2533-P2	58.0308	-44.3953	1.21
Compound_2616-P2	45.7688	-39.3945	0.86
Compound_2721-P2	55.1269	-43.0005	1.12
Compound_2723-P2	43.5502	-42.5240	0.91
Compound_2786-P2	42.8761	-39.8269	0.82

Compound	Docking energy, kJ mol^{-1}		
	GOLD	DOCK6	RANK
Compound_2787-P2	46.3103	-40.8670	0.91
Compound_2788-P2	46.7562	-36.1581	0.78
Compound_2789-P2	57.3871	-41.5185	1.12
Compound_2791-P2	50.2076	-36.5387	0.85
Compound_2792-P2	61.4160	-49.5119	1.42
Compound_2820-P2	48.1275	-41.5088	0.96
Compound_2821-P2	51.3970	-43.8518	1.08
Compound_2822-P2	44.5361	-32.4341	0.63
Compound_2823-P2	62.4160	-41.2394	1.19
Compound_2852-P2	45.4143	-31.8115	0.63
Compound_2854-P2	47.4291	-34.7189	0.75
Compound_2856-P2	39.6198	-32.4772	0.55
Compound_2861-P2	50.1237	-43.2838	1.04
Compound_2867-P2	43.5306	-35.5902	0.71
Compound_2868-P2	52.0374	-36.6872	0.89
Compound_2869-P2	51.0459	-39.4449	0.95
Compound_2870-P2	47.2751	-38.6886	0.86
Compound_2907-P2	44.7120	-43.5481	0.96
Compound_2925-P2	30.3815	-27.0788	0.24
Compound_2926-P2	43.0538	-37.5758	0.76
Compound_2941-P2	41.9792	-31.9010	0.58
Compound_2942-P2	52.3818	-32.6381	0.77
Compound_2949-P2	25.7030	-25.1083	0.10
Compound_2950-P2	46.2701	-25.3758	0.46
Compound_2951-P2	30.7584	-27.8851	0.27
Compound_2952-P2	34.7939	-27.6349	0.33
Compound_2953-P2	38.7039	-27.4849	0.39
Compound_2954-P2	35.3172	-26.5562	0.31
Compound_2955-P2	35.5159	-29.1544	0.39
Compound_2956-P2	31.4698	-28.3726	0.29
Compound_2957-P2	36.2478	-30.8706	0.45
Compound_3-P4	64.8396	-41.8643	1.25
Compound_34-P4	35.1408	-38.5929	0.65
Compound_43-P4	44.8774	-35.3229	0.72
Compound_44-P4	42.8558	-34.4959	0.67
Compound_45-P4	52.5763	-36.5612	0.89
Compound_46-P4	47.8773	-36.7727	0.82
Compound_84-P4	43.3467	-37.6203	0.76
Compound_86-P4	49.4063	-39.2242	0.91
Compound_90-P4	47.3623	-39.7788	0.90
Compound_391-P4	55.9498	-44.1598	1.17
Compound_392-P4	35.7724	-43.2654	0.80
Compound_393-P4	51.7638	-47.8267	1.20
Compound_396-P4	52.2459	-44.7974	1.12
Compound_397-P4	38.2379	-44.3156	0.87
Compound_398-P4	59.8581	-46.1690	1.29

Compound	Docking energy, kJ mol^{-1}		
	GOLD	DOCK6	RANK
Compound_405-P4	48.7911	-40.9687	0.95
Compound_424-P4	43.2388	-38.7308	0.79
Compound_427-P4	52.1795	-45.2714	1.14
Compound_455-P4	42.3026	-41.4418	0.86
Compound_457-P4	42.1628	-38.8949	0.78
Compound_514-P4	50.7049	-35.6579	0.83
Compound_529-P4	39.6904	-32.3732	0.55
Compound_621-P4	42.5315	-47.7133	1.04
Compound_623-P4	36.1954	-42.3638	0.78
Compound_628-P4	54.0081	-47.5665	1.23
Compound_676-P4	50.5759	-42.7368	1.04
Compound_677-P4	50.2263	-43.7986	1.06
Compound_698-P4	56.9422	-45.4387	1.22
Compound_699-P4	35.2207	-40.5453	0.71
Compound_708-P4	37.9417	-34.3708	0.58
Compound_721-P4	49.9226	-40.9443	0.97
Compound_725-P4	42.7958	-43.1067	0.91
Compound_726-P4	48.1453	-42.9922	1.00
Compound_728-P4	56.5104	-44.1085	1.18
Compound_957-P4	44.9744	-40.2148	0.87
Compound_962-P4	57.3223	-45.4819	1.23
Compound_991-P4	51.5424	-44.4777	1.10
Compound_992-P4	49.8424	-42.8239	1.03
Compound_993-P4	40.4780	-45.2554	0.94
Compound_994-P4	55.9599	-37.3483	0.97
Compound_995-P4	46.4700	-43.1942	0.98
Compound_999-P4	61.1665	-40.6328	1.15
Compound_1160-P4	44.5154	-42.0208	0.91
Compound_1161-P4	49.3359	-43.9000	1.05
Compound_1162-P4	40.9367	-43.3998	0.89
Compound_1163-P4	39.7497	-50.0681	1.06
Compound_1166-P4	48.7200	-42.8007	1.01
Compound_1167-P4	52.4006	-38.2477	0.94
Compound_1169-P4	48.6625	-46.8934	1.12
Compound_1176-P4	55.8167	-42.7526	1.13
Compound_1177-P4	38.1200	-38.0263	0.69
Compound_1181-P4	53.5731	-42.7639	1.09
Compound_1183-P4	46.7899	-41.5695	0.94
Compound_1184-P4	57.9176	-43.4204	1.18
Compound_1222-P4	47.0546	-34.5120	0.74
Compound_1223-P4	45.7119	-39.7514	0.87
Compound_1229-P4	58.0825	-40.0292	1.08
Compound_1230-P4	38.4174	-35.8689	0.63
Compound_1242-P4	54.6107	-41.2791	1.06
Compound_1243-P4	49.7547	-39.9635	0.94
Compound_1245-P4	53.7566	-38.3779	0.96

Compound	Docking energy, kJ mol^{-1}		
	GOLD	DOCK6	RANK
Compound_1247-P4	46.6590	-41.6424	0.94
Compound_1251-P4	52.9296	-43.5040	1.10
Compound_1253-P4	55.0565	-40.2190	1.04
Compound_1255-P4	70.9198	-43.0144	1.39
Compound_1260-P4	50.7472	-40.4363	0.97
Compound_1261-P4	46.1446	-41.6075	0.93
Compound_1263-P4	60.8911	-46.5662	1.32
Compound_1278-P4	54.7742	-40.5639	1.04
Compound_1279-P4	49.5799	-39.2958	0.92
Compound_1280-P4	55.6884	-41.0141	1.07
Compound_1281-P4	58.5202	-38.2166	1.04
Compound_1282-P4	52.5101	-41.5027	1.03
Compound_1283-P4	50.0610	-30.8856	0.68
Compound_1288-P4	40.1303	-42.3511	0.85
Compound_1290-P4	46.3151	-39.7881	0.88
Compound_1291-P4	56.7440	-43.5972	1.17
Compound_1292-P4	54.7256	-44.7010	1.16
Compound_1293-P4	57.1668	-47.2251	1.28
Compound_1296-P4	42.9606	-33.6094	0.64
Compound_1299-P4	53.6746	-37.4307	0.93
Compound_1300-P4	52.4333	-41.6470	1.04
Compound_1303-P4	68.1046	-40.2834	1.26
Compound_1304-P4	41.9075	-40.2285	0.82
Compound_1305-P4	54.2735	-37.0532	0.93
Compound_1306-P4	51.3084	-40.4878	0.98
Compound_1307-P4	47.5185	-31.9356	0.67
Compound_1308-P4	49.4747	-30.3534	0.66
Compound_1312-P4	47.0433	-42.2575	0.96
Compound_1313-P4	38.7049	-43.9013	0.87
Compound_1315-P4	58.7582	-41.1243	1.13
Compound_1318-P4	56.0773	-42.6518	1.13
Compound_1320-P4	72.5038	-46.3616	1.51
Compound_1321-P4	66.3441	-46.1531	1.40
Compound_1322-P4	45.0911	-41.1785	0.90
Compound_1324-P4	49.3214	-32.2603	0.71
Compound_1326-P4	48.6279	-36.6961	0.83
Compound_1327-P4	51.0655	-41.7116	1.01
Compound_1328-P4	55.7923	-37.7429	0.98
Compound_1329-P4	59.9370	-40.4538	1.13
Compound_1332-P4	64.4020	-41.1249	1.22
Compound_1333-P4	43.2280	-40.1171	0.83
Compound_1334-P4	46.3811	-43.0096	0.97
Compound_1335-P4	44.1123	-38.3881	0.80
Compound_1336-P4	48.2341	-33.7950	0.74
Compound_1337-P4	46.8008	-30.8633	0.63
Compound_1342-P4	50.7846	-41.6918	1.01

Compound	Docking energy, kJ mol^{-1}		
	GOLD	DOCK6	RANK
Compound_1343-P4	53.1073	-42.8981	1.08
Compound_1345-P4	49.9691	-47.7974	1.17
Compound_1347-P4	37.4611	-38.5327	0.69
Compound_1348-P4	45.9722	-37.6753	0.81
Compound_1349-P4	45.2244	-39.1792	0.84
Compound_1353-P4	44.7903	-39.9238	0.86
Compound_1354-P4	37.1166	-41.4137	0.77
Compound_1355-P4	55.1301	-35.7098	0.91
Compound_1356-P4	45.7881	-41.7557	0.93
Compound_1357-P4	43.5694	-38.1443	0.78
Compound_1359-P4	39.0405	-33.8627	0.58
Compound_1360-P4	44.6897	-32.4048	0.64
Compound_1368-P4	42.3879	-41.9675	0.87
Compound_1370-P4	43.5283	-38.9883	0.81
Compound_1372-P4	53.5965	-41.8191	1.06
Compound_1373-P4	42.1747	-43.2747	0.91
Compound_1375-P4	53.1847	-33.4957	0.81
Compound_1378-P4	46.8351	-37.7155	0.83
Compound_1379-P4	38.7476	-39.1844	0.73
Compound_1450-P4	49.1950	-41.4019	0.97
Compound_1451-P4	33.9352	-40.1768	0.68
Compound_1452-P4	61.3817	-40.5301	1.16
Compound_1453-P4	35.9869	-42.6054	0.78
Compound_1454-P4	50.5686	-35.4567	0.82
Compound_1457-P4	53.2844	-43.9944	1.12
Compound_1461-P4	48.3152	-43.4954	1.02
Compound_1462-P4	55.1740	-48.1113	1.27
Compound_1464-P4	47.5909	-42.4415	0.98
Compound_1465-P4	38.6454	-40.7794	0.78
Compound_1468-P4	52.5291	-42.0476	1.05
Compound_1469-P4	45.1014	-43.3616	0.96
Compound_1470-P4	48.3787	-40.7274	0.94
Compound_1471-P4	53.6530	-44.1429	1.13
Compound_1472-P4	51.3192	-38.3767	0.92
Compound_1473-P4	46.4168	-37.4980	0.81
Compound_1477-P4	40.4579	-44.2904	0.91
Compound_1479-P4	59.0527	-44.3485	1.23
Compound_1481-P4	42.7480	-37.2267	0.74
Compound_1483-P4	60.3982	-42.2795	1.19
Compound_1484-P4	39.2777	-43.4469	0.86
Compound_1553-P4	46.8519	-40.2420	0.90
Compound_1555-P4	52.1259	-44.6131	1.12
Compound_1556-P4	49.9801	-42.2106	1.01
Compound_1558-P4	43.5489	-44.1419	0.96
Compound_1559-P4	54.8696	-43.6420	1.13
Compound_1560-P4	53.1644	-45.9706	1.17

Compound	Docking energy, kJ mol^{-1}		
	GOLD	DOCK6	RANK
Compound_1562-P4	57.5095	-43.5080	1.18
Compound_1563-P4	50.1186	-44.7398	1.09
Compound_1565-P4	54.0870	-40.4273	1.03
Compound_1566-P4	42.5727	-40.9659	0.85
Compound_1567-P4	60.8653	-43.1023	1.22
Compound_1568-P4	57.9583	-43.8787	1.19
Compound_1570-P4	61.1500	-44.0336	1.25
Compound_1571-P4	62.0724	-45.4361	1.31
Compound_1572-P4	48.1641	-45.2930	1.07
Compound_1573-P4	39.2575	-40.3922	0.78
Compound_1574-P4	49.7983	-40.4956	0.96
Compound_1575-P4	55.6365	-44.6076	1.18
Compound_1576-P4	74.0539	-47.0347	1.56
Compound_1577-P4	53.8425	-45.5121	1.17
Compound_1579-P4	38.5607	-42.6510	0.83
Compound_1580-P4	52.9020	-46.2713	1.18
Compound_1583-P4	50.1295	-42.5809	1.02
Compound_1586-P4	51.0613	-39.1192	0.94
Compound_1587-P4	68.4840	-42.3231	1.33
Compound_1590-P4	56.6619	-44.7564	1.20
Compound_1594-P4	47.4786	-44.4655	1.03
Compound_1595-P4	52.8482	-45.2243	1.15
Compound_1597-P4	59.2344	-46.6137	1.30
Compound_1598-P4	51.9690	-46.3821	1.17
Compound_1600-P4	54.8253	-45.8941	1.20
Compound_1603-P4	43.3834	-44.1781	0.96
Compound_1607-P4	39.6197	-39.0822	0.74
Compound_1608-P4	47.4663	-40.0037	0.90
Compound_1613-P4	54.2144	-38.5349	0.98
Compound_1614-P4	47.4265	-38.6852	0.86
Compound_1621-P4	50.3469	-43.0010	1.04
Compound_1622-P4	50.9257	-42.0635	1.02
Compound_1682-P4	50.8647	-39.8069	0.96
Compound_1683-P4	40.6868	-38.6724	0.75
Compound_1684-P4	63.6591	-39.0154	1.15
Compound_1685-P4	46.6192	-38.9345	0.86
Compound_1686-P4	54.4201	-41.0134	1.05
Compound_1687-P4	47.0157	-38.6472	0.86
Compound_1691-P4	50.1081	-39.6955	0.94
Compound_1717-P4	55.7154	-39.6172	1.03
Compound_1722-P4	49.4059	-37.7106	0.87
Compound_1723-P4	48.6438	-37.7271	0.86
Compound_1724-P4	33.6288	-34.8455	0.52
Compound_1725-P4	44.6506	-32.2867	0.63
Compound_1796-P4	40.2086	-42.5825	0.85
Compound_1797-P4	45.8542	-40.1611	0.88

Compound	Docking energy, kJ mol^{-1}		
	GOLD	DOCK6	RANK
Compound_1798-P4	48.7802	-38.8192	0.89
Compound_1799-P4	44.3908	-40.0405	0.85
Compound_1800-P4	43.1898	-38.2718	0.78
Compound_1801-P4	37.8841	-38.0866	0.68
Compound_1802-P4	44.2290	-39.4203	0.83
Compound_1803-P4	33.3616	-37.9477	0.60
Compound_1806-P4	50.5455	-42.8202	1.04
Compound_1826-P4	48.7858	-42.7723	1.01
Compound_1831-P4	45.2964	-39.2994	0.85
Compound_1832-P4	42.9362	-35.7109	0.70
Compound_1833-P4	44.0457	-37.2159	0.76
Compound_1834-P4	33.7373	-38.9214	0.64
Compound_1835-P4	40.6549	-38.7868	0.75
Compound_1836-P4	39.1013	-34.3265	0.60
Compound_1837-P4	46.2963	-35.8333	0.76
Compound_1838-P4	40.9736	-38.0857	0.74
Compound_1841-P4	40.1099	-36.3618	0.67
Compound_1844-P4	33.5500	-35.0059	0.52
Compound_1845-P4	41.3507	-37.3205	0.72
Compound_1846-P4	50.1780	-42.9483	1.04
Compound_1883-P4	53.7150	-38.7923	0.97
Compound_1886-P4	61.3802	-40.2562	1.15
Compound_1898-P4	61.8682	-38.1925	1.10
Compound_1899-P4	53.5348	-38.8137	0.97
Compound_1900-P4	53.1504	-42.0040	1.06
Compound_2003-P4	42.7755	-40.1476	0.83
Compound_2004-P4	35.2888	-38.7606	0.66
Compound_2009-P4	45.5491	-43.4474	0.97
Compound_2011-P4	45.4722	-48.1904	1.11
Compound_2014-P4	43.3663	-49.7047	1.12
Compound_2016-P4	39.5825	-45.0216	0.91
Compound_2022-P4	42.6503	-40.8646	0.85
Compound_2023-P4	42.0405	-44.2359	0.93
Compound_2024-P4	40.9123	-45.1518	0.94
Compound_2025-P4	46.3980	-47.6410	1.11
Compound_2028-P4	50.7817	-46.2146	1.14
Compound_2030-P4	47.9754	-49.0606	1.17
Compound_2033-P4	35.8685	-50.6124	1.01
Compound_2080-P4	54.6273	-39.3000	1.00
Compound_2081-P4	52.0896	-42.1022	1.04
Compound_2089-P4	43.3842	-44.4139	0.96
Compound_2091-P4	66.3032	-47.3571	1.44
Compound_2117-P4	54.0288	-43.4021	1.11
Compound_2118-P4	48.3983	-42.4276	0.99
Compound_2123-P4	64.1809	-46.8474	1.39
Compound_2125-P4	45.4061	-47.1303	1.08

Compound	Docking energy, kJ mol^{-1}		
	GOLD	DOCK6	RANK
Compound_2128-P4	50.1467	-48.1581	1.19
Compound_2131-P4	33.4585	-41.6958	0.71
Compound_2132-P4	56.8461	-46.8574	1.26
Compound_2133-P4	57.7937	-48.6395	1.33
Compound_2134-P4	33.0025	-37.9317	0.60
Compound_2135-P4	42.5853	-39.6755	0.81
Compound_2136-P4	42.8285	-44.1783	0.95
Compound_2137-P4	55.1004	-46.4951	1.22
Compound_2138-P4	67.1081	-46.8034	1.43
Compound_2139-P4	64.0940	-44.9093	1.33
Compound_2140-P4	57.3536	-46.1236	1.25
Compound_2151-P4	38.4933	-37.4440	0.68
Compound_2152-P4	52.5681	-38.8963	0.96
Compound_2155-P4	43.7776	-43.3893	0.94
Compound_2157-P4	48.0119	-44.4854	1.04
Compound_2160-P4	46.8027	-45.2795	1.05
Compound_2166-P4	42.1285	-42.7328	0.89
Compound_2167-P4	36.5834	-43.2411	0.81
Compound_2168-P4	56.6917	-47.1238	1.27
Compound_2173-P4	51.4238	-46.2763	1.15
Compound_2180-P4	40.8223	-46.3117	0.97
Compound_2314-P4	34.2845	-33.0871	0.48
Compound_2315-P4	37.2828	-28.4651	0.40
Compound_2371-P4	53.4385	-47.0057	1.21
Compound_2372-P4	37.5626	-45.6671	0.90
Compound_2377-P4	43.1331	-42.5496	0.90
Compound_2378-P4	44.6380	-42.9963	0.94
Compound_2379-P4	46.0620	-42.4138	0.95
Compound_2380-P4	38.6706	-43.6165	0.86
Compound_2381-P4	37.8001	-45.6111	0.90
Compound_2382-P4	56.1160	-45.3342	1.21
Compound_2653-P4	65.9770	-39.4781	1.20
Compound_2657-P4	45.3024	-41.4858	0.91
Compound_2659-P4	42.9155	-36.2111	0.72
Compound_2663-P4	46.7489	-36.9540	0.80
Compound_2669-P4	56.8967	-38.3031	1.01
Compound_2679-P4	55.8411	-39.7994	1.04
Compound_2696-P4	50.2721	-36.6761	0.85
Compound_2697-P4	51.3207	-36.4222	0.87
Compound_2698-P4	45.6292	-38.0340	0.82
Compound_2700-P4	49.3852	-38.0764	0.88
Compound_2741-P4	39.3740	-54.7273	1.19
Compound_2743-P4	40.5606	-34.5158	0.63
Compound_2745-P4	48.2048	-37.6243	0.85
Compound_2751-P4	48.3303	-36.9094	0.83
Compound_2754-P4	42.2264	-35.1774	0.67

Compound	Docking energy, kJ mol^{-1}		
	GOLD	DOCK6	RANK
Compound_2756-P4	56.2616	-39.5942	1.04
Compound_2758-P4	47.6676	-39.8452	0.90
Compound_2779-P4	56.0812	-43.5328	1.15
Compound_2794-P4	60.4013	-38.6582	1.08
Compound_2800-P4	46.6625	-40.1538	0.89
Compound_2876-P4	35.3833	-45.1179	0.85
Compound_2877-P4	47.8093	-46.3575	1.09
Compound_2889-P4	45.6986	-43.2878	0.97
Compound_2891-P4	55.1729	-42.5653	1.11
Compound_2893-P4	50.2159	-46.5270	1.14
Compound_2894-P4	48.2016	-47.2498	1.13
Compound_2896-P4	54.5995	-41.4752	1.07
Compound_2897-P4	53.7311	-43.5776	1.11
Compound_2898-P4	55.7255	-42.8226	1.13
Compound_2899-P4	61.2710	-46.1960	1.32
Compound_2900-P4	64.5871	-46.1375	1.37
Compound_2901-P4	55.4712	-48.7930	1.29
Compound_2903-P4	60.3972	-46.8923	1.32
Compound_2905-P4	52.3028	-45.9515	1.16
Compound_2908-P4	51.4424	-47.1259	1.18
Compound_2909-P4	41.1266	-44.3335	0.92
Compound_2910-P4	53.9262	-45.6568	1.18
Compound_2917-P4	51.7524	-37.7412	0.91
Compound_2918-P4	56.8506	-40.7251	1.08
Compound_2924-P4	65.2797	-42.5369	1.28
Compound_2926-P4	41.7955	-43.4656	0.91
Compound_2927-P4	47.0122	-47.3023	1.11
Compound_2929-P4	47.2537	-45.7527	1.07
Compound_2931-P4	50.0217	-42.1048	1.01
Compound_2932-P4	43.7152	-42.0594	0.90
Compound_2933-P4	51.1196	-44.3410	1.09
Compound_2935-P4	31.1730	-39.7081	0.62
Compound_2936-P4	64.3870	-40.6084	1.21
Compound_2937-P4	62.7215	-44.5098	1.29
Compound_2938-P4	47.6632	-47.1987	1.12
Compound_2939-P4	69.2399	-48.6792	1.53
Compound_2940-P4	55.1414	-46.7122	1.23
Compound_2942-P4	51.8905	-45.2026	1.13
Compound_2944-P4	56.7918	-45.6392	1.23
Compound_2946-P4	50.9874	-45.9844	1.14
Compound_2947-P4	48.7430	-44.8538	1.07
Compound_2948-P4	35.8922	-47.0134	0.91
Compound_2949-P4	39.2538	-40.9193	0.79
Compound_2951-P4	51.9817	-44.7726	1.12
Compound_2952-P4	42.8958	-43.2260	0.92
Compound_2953-P4	55.4342	-46.7473	1.23

Compound	Docking energy, kJ mol^{-1}		
	GOLD	DOCK6	RANK
Compound_2954-P4	56.6655	-39.7670	1.05
Compound_2955-P4	45.6682	-40.5815	0.89
Compound_2956-P4	56.5035	-43.1577	1.15
Compound_2957-P4	81.0314	-42.5339	1.55
Compound_2958-P4	50.0491	-44.6677	1.08
Compound_2960-P4	54.9285	-44.1309	1.15
Compound_2962-P4	54.6272	-44.6485	1.16
Compound_2963-P4	57.2218	-48.5572	1.32
Compound_2965-P4	39.2056	-45.4320	0.92
Compound_2966-P4	53.6360	-43.0639	1.10
Compound_2967-P4	49.5127	-42.9369	1.02
Compound_2972-P4	41.1540	-41.7526	0.85
Compound_2978-P4	44.3810	-44.9418	0.99
Compound_2980-P4	51.0935	-45.2592	1.12
Compound_2983-P4	46.1072	-45.7275	1.05
Compound_2984-P4	54.4354	-41.4305	1.06
Compound_2985-P4	50.3303	-44.7293	1.09
Compound_2991-P4	56.1446	-43.4777	1.15
Compound_2992-P4	48.1392	-44.3723	1.04
Compound_2993-P4	53.6253	-47.4065	1.22
Compound_2998-P4	51.7928	-47.3983	1.19
Compound_2-P5	40.4799	-45.0664	0.93
Compound_3-P5	73.3080	-50.0978	1.64
Compound_10-P5	42.8506	-43.2061	0.92
Compound_11-P5	38.4490	-45.6078	0.91
Compound_12-P5	57.9826	-47.3254	1.29
Compound_24-P5	60.3688	-44.3826	1.25
Compound_25-P5	55.9169	-46.6615	1.24
Compound_27-P5	61.9207	-48.5159	1.40
Compound_28-P5	47.0937	-47.9874	1.13
Compound_30-P5	50.0907	-39.2070	0.93
Compound_31-P5	67.8346	-40.2421	1.26
Compound_32-P5	54.5447	-45.0408	1.17
Compound_33-P5	76.9626	-48.4025	1.65
Compound_34-P5	53.3445	-48.4883	1.25
Compound_35-P5	61.1948	-47.6792	1.36
Compound_37-P5	55.5826	-46.9374	1.24
Compound_39-P5	53.9618	-48.7174	1.27
Compound_42-P5	62.5841	-47.2883	1.37
Compound_43-P5	46.5313	-42.1676	0.95
Compound_44-P5	59.4122	-45.5692	1.27
Compound_51-P5	52.8071	-38.6758	0.96
Compound_52-P5	32.7595	-40.4604	0.67
Compound_58-P5	58.1447	-43.3433	1.18
Compound_60-P5	53.2720	-44.2074	1.12
Compound_61-P5	60.1981	-49.9015	1.41

Compound	Docking energy, kJ mol^{-1}		
	GOLD	DOCK6	RANK
Compound_63-P5	42.5509	-43.5243	0.92
Compound_65-P5	43.5981	-44.3731	0.96
Compound_69-P5	51.1257	-40.4852	0.98
Compound_70-P5	54.7070	-40.7664	1.05
Compound_74-P5	67.0215	-46.7196	1.43
Compound_76-P5	45.1461	-45.0017	1.01
Compound_79-P5	43.4350	-46.9259	1.04
Compound_81-P5	45.1087	-44.3023	0.99
Compound_103-P5	49.2023	-42.0978	0.99
Compound_104-P5	34.7205	-42.1047	0.75
Compound_106-P5	59.5949	-46.0615	1.29
Compound_107-P5	43.6168	-44.8696	0.98
Compound_109-P5	56.4977	-41.9924	1.11
Compound_110-P5	38.6820	-42.1488	0.82
Compound_111-P5	36.5764	-46.2549	0.90
Compound_112-P5	46.2182	-45.6770	1.05
Compound_113-P5	53.9656	-47.4672	1.23
Compound_114-P5	40.6887	-48.0226	1.02
Compound_116-P5	63.1109	-47.3176	1.38
Compound_118-P5	51.2778	-45.7736	1.14
Compound_121-P5	47.5834	-46.7166	1.10
Compound_122-P5	52.6081	-43.9007	1.10
Compound_123-P5	34.4510	-45.6823	0.85
Compound_124-P5	50.3888	-40.7382	0.97
Compound_125-P5	55.8954	-43.8938	1.16
Compound_126-P5	41.5311	-39.5551	0.79
Compound_128-P5	40.8590	-43.1917	0.88
Compound_129-P5	45.8889	-42.9615	0.96
Compound_130-P5	41.7789	-44.6405	0.94
Compound_131-P5	34.5220	-36.7159	0.59
Compound_132-P5	47.1587	-38.0250	0.84
Compound_133-P5	41.9327	-40.2123	0.82
Compound_134-P5	46.3439	-41.8564	0.94
Compound_135-P5	52.4827	-42.0476	1.05
Compound_136-P5	58.1602	-44.3281	1.21
Compound_139-P5	26.2221	-43.0346	0.63
Compound_140-P5	51.1534	-45.5507	1.13
Compound_142-P5	51.9802	-43.3501	1.08
Compound_143-P5	55.9774	-41.8720	1.10
Compound_144-P5	43.5300	-41.7710	0.89
Compound_145-P5	44.1167	-41.7100	0.90
Compound_146-P5	37.2128	-41.8575	0.78
Compound_148-P5	50.9771	-45.0876	1.11
Compound_149-P5	42.8780	-43.8695	0.94
Compound_150-P5	56.0432	-45.9184	1.22
Compound_151-P5	45.9821	-39.8223	0.87

Compound	Docking energy, kJ mol^{-1}		
	GOLD	DOCK6	RANK
Compound_152-P5	46.6931	-41.0108	0.92
Compound_153-P5	50.2256	-41.8796	1.00
Compound_154-P5	43.0917	-44.9124	0.97
Compound_155-P5	40.3501	-45.0136	0.93
Compound_156-P5	40.2018	-46.4097	0.97
Compound_158-P5	40.8406	-44.9715	0.93
Compound_164-P5	64.9247	-41.9668	1.26
Compound_167-P5	51.0975	-41.5322	1.01
Compound_168-P5	46.0196	-38.6617	0.84
Compound_174-P5	58.4288	-44.1452	1.21
Compound_176-P5	48.3839	-45.6130	1.08
Compound_178-P5	47.0532	-44.3760	1.02
Compound_179-P5	40.7799	-42.4218	0.86
Compound_180-P5	44.9260	-45.2271	1.01
Compound_186-P5	41.1485	-41.2279	0.83
Compound_187-P5	49.4445	-43.8545	1.05
Compound_188-P5	50.7279	-46.3907	1.14
Compound_193-P5	54.1547	-47.9984	1.25
Compound_199-P5	58.5493	-48.4961	1.34
Compound_200-P5	58.9677	-46.8934	1.30
Compound_207-P5	60.9423	-44.9913	1.28
Compound_208-P5	43.3978	-45.2777	0.99
Compound_209-P5	50.3704	-47.8472	1.18
Compound_222-P5	48.0295	-43.3256	1.01
Compound_223-P5	56.3713	-45.1164	1.20
Compound_225-P5	51.5265	-47.0803	1.18
Compound_226-P5	47.7416	-46.2624	1.09
Compound_228-P5	42.8128	-38.6811	0.79
Compound_229-P5	39.5821	-43.5299	0.87
Compound_230-P5	68.4123	-43.9286	1.37
Compound_231-P5	51.0410	-46.0128	1.14
Compound_232-P5	68.4364	-45.1292	1.41
Compound_233-P5	73.5798	-47.5240	1.57
Compound_235-P5	69.8391	-45.9459	1.46
Compound_239-P5	57.5506	-45.2669	1.23
Compound_240-P5	41.1676	-42.7695	0.88
Compound_241-P5	49.7668	-44.0768	1.06
Compound_247-P5	34.7152	-38.1543	0.63
Compound_248-P5	39.0731	-41.4817	0.80
Compound_254-P5	51.5685	-45.8028	1.14
Compound_256-P5	42.2385	-43.9623	0.93
Compound_257-P5	45.0243	-46.2938	1.04
Compound_259-P5	55.5468	-45.0744	1.19
Compound_261-P5	55.2298	-44.2667	1.16
Compound_265-P5	47.4001	-40.8107	0.93
Compound_266-P5	45.3443	-42.7965	0.95

Compound	Docking energy, kJ mol^{-1}		
	GOLD	DOCK6	RANK
Compound_271-P5	56.1760	-46.4395	1.24
Compound_273-P5	55.3269	-46.9777	1.24
Compound_276-P5	51.9491	-47.9317	1.21
Compound_278-P5	53.8563	-46.2525	1.19
Compound_300-P5	33.9699	-45.1431	0.82
Compound_301-P5	47.1354	-44.5879	1.03
Compound_303-P5	44.3079	-45.2061	1.00
Compound_304-P5	35.2433	-46.9295	0.90
Compound_305-P5	59.0213	-47.3939	1.31
Compound_306-P5	48.1068	-39.9674	0.91
Compound_307-P5	34.9992	-40.0354	0.69
Compound_308-P5	53.7818	-43.1904	1.10
Compound_309-P5	46.9950	-47.2307	1.11
Compound_310-P5	59.7847	-46.1881	1.29
Compound_311-P5	55.2883	-48.1222	1.27
Compound_312-P5	40.9707	-44.3149	0.92
Compound_314-P5	47.0531	-50.6705	1.21
Compound_315-P5	46.7144	-47.3676	1.10
Compound_316-P5	53.6081	-45.4622	1.17
Compound_317-P5	55.0648	-44.9473	1.18
Compound_320-P5	56.1079	-40.0275	1.05
Compound_326-P5	55.0941	-35.6331	0.91
Compound_327-P5	51.0107	-35.3571	0.83
Compound_331-P5	49.1322	-36.2684	0.82
Compound_360-P5	38.8158	-31.0422	0.50
Compound_363-P5	50.5423	-37.3681	0.88
Compound_365-P5	56.2222	-39.7196	1.04
Compound_366-P5	53.6292	-39.0633	0.98
Compound_578-P5	49.2361	-36.4673	0.83
Compound_581-P5	45.3371	-33.7885	0.69
Compound_685-P5	46.3201	-39.1703	0.86
Compound_686-P5	42.5681	-42.6200	0.90
Compound_734-P5	55.7011	-42.8275	1.13
Compound_738-P5	46.9505	-40.5126	0.91
Compound_743-P5	56.7710	-44.6501	1.20
Compound_750-P5	46.6732	-42.3114	0.96
Compound_752-P5	64.2460	-46.0005	1.36
Compound_753-P5	46.4858	-40.3088	0.90
Compound_760-P5	46.6440	-45.0071	1.03
Compound_761-P5	51.6921	-41.2305	1.01
Compound_763-P5	70.6863	-43.2598	1.39
Compound_768-P5	55.6140	-46.6724	1.24
Compound_769-P5	47.1584	-39.5244	0.88
Compound_770-P5	41.9009	-41.6524	0.86
Compound_771-P5	37.7792	-31.2564	0.49
Compound_772-P5	47.2692	-32.5921	0.69

Compound	Docking energy, kJ mol^{-1}		
	GOLD	DOCK6	RANK
Compound_778-P5	60.9020	-40.0407	1.13
Compound_786-P5	49.4677	-42.5369	1.01
Compound_793-P5	33.3068	-31.0297	0.40
Compound_794-P5	39.1815	-34.5651	0.60
Compound_882-P5	53.3321	-46.3812	1.19
Compound_883-P5	52.5986	-46.4243	1.18
Compound_884-P5	47.4617	-44.5343	1.03
Compound_896-P5	46.3656	-48.3423	1.13
Compound_898-P5	54.9235	-50.3225	1.33
Compound_903-P5	50.9155	-48.5939	1.21
Compound_909-P5	42.5553	-48.3538	1.06
Compound_922-P5	72.2317	-48.9625	1.58
Compound_929-P5	54.2439	-47.7438	1.24
Compound_954-P5	46.5957	-35.4873	0.76
Compound_968-P5	48.0017	-31.5160	0.67
Compound_969-P5	50.3639	-34.0084	0.78
Compound_1007-P5	44.0113	-42.9447	0.93
Compound_1008-P5	43.5492	-43.5727	0.94
Compound_1039-P5	47.1754	-41.6341	0.95
Compound_1041-P5	55.7439	-42.3185	1.11
Compound_1042-P5	47.7070	-38.7574	0.87
Compound_1044-P5	43.9553	-41.0389	0.87
Compound_1058-P5	49.0337	-45.6764	1.09
Compound_1059-P5	52.9447	-40.4071	1.01
Compound_1064-P5	45.2330	-46.6665	1.06
Compound_1065-P5	43.4695	-44.6442	0.97
Compound_1078-P5	45.0487	-44.7492	1.00
Compound_1111-P5	71.5005	-40.5855	1.33
Compound_1112-P5	45.4010	-41.0664	0.90
Compound_1113-P5	54.4409	-42.2894	1.09
Compound_1114-P5	42.9298	-43.9216	0.94
Compound_1115-P5	50.3552	-39.4523	0.94
Compound_1116-P5	55.9959	-34.6850	0.89
Compound_1117-P5	39.9356	-32.5834	0.56
Compound_1121-P5	53.7296	-44.3871	1.14
Compound_1123-P5	62.5683	-43.9180	1.27
Compound_1126-P5	45.9825	-45.0286	1.02
Compound_1127-P5	42.4210	-48.1396	1.05
Compound_1130-P5	42.7218	-38.7525	0.79
Compound_1132-P5	56.2104	-41.4647	1.09
Compound_1133-P5	50.7714	-41.4585	1.00
Compound_1136-P5	51.7903	-37.8502	0.91
Compound_1137-P5	55.0474	-42.4779	1.10
Compound_1138-P5	45.2039	-37.0256	0.78
Compound_1139-P5	41.2826	-32.2927	0.57
Compound_1146-P5	40.6848	-43.9863	0.90

Compound	Docking energy, kJ mol^{-1}		
	GOLD	DOCK6	RANK
Compound_1149-P5	49.0489	-43.3667	1.03
Compound_1150-P5	45.2098	-41.0139	0.89
Compound_1152-P5	39.4279	-47.9891	1.00
Compound_1153-P5	39.3786	-41.7568	0.82
Compound_1158-P5	40.6239	-41.0484	0.82
Compound_1159-P5	46.5018	-43.3983	0.99
Compound_1162-P5	48.5072	-43.0819	1.01
Compound_1163-P5	50.5992	-40.8283	0.98
Compound_1164-P5	37.6430	-39.1259	0.71
Compound_1165-P5	40.7456	-35.7133	0.66
Compound_1169-P5	63.6556	-44.1151	1.30
Compound_1171-P5	53.4023	-45.1575	1.15
Compound_1173-P5	49.7500	-47.3569	1.16
Compound_1174-P5	58.6710	-48.2654	1.33
Compound_1177-P5	47.2297	-38.4063	0.85
Compound_1185-P5	53.3093	-41.4697	1.05
Compound_1186-P5	36.5509	-40.6167	0.74
Compound_1187-P5	46.9507	-41.7902	0.95
Compound_1188-P5	52.5556	-43.4057	1.09
Compound_1189-P5	49.7112	-39.2874	0.92
Compound_1190-P5	38.1808	-34.2151	0.58
Compound_1202-P5	37.6204	-44.6923	0.87
Compound_1205-P5	36.0750	-45.2756	0.86
Compound_1207-P5	59.4473	-46.5424	1.30
Compound_1208-P5	35.7806	-48.3565	0.95
Compound_1212-P5	55.3589	-38.0083	0.98
Compound_1213-P5	43.3510	-35.2204	0.69
Compound_1215-P5	52.4646	-38.9732	0.96
Compound_1217-P5	45.5987	-39.0415	0.84
Compound_1218-P5	37.5371	-40.8593	0.76
Compound_1292-P5	40.4061	-43.0651	0.87
Compound_1293-P5	65.4879	-40.1566	1.21
Compound_1294-P5	56.7240	-43.6090	1.17
Compound_1295-P5	38.6428	-42.0146	0.81
Compound_1296-P5	53.8152	-37.1327	0.93
Compound_1297-P5	55.5348	-34.5481	0.88
Compound_1300-P5	48.7405	-44.3501	1.05
Compound_1302-P5	62.5695	-42.2606	1.23
Compound_1305-P5	55.8117	-48.6641	1.30
Compound_1307-P5	57.6247	-35.9446	0.96
Compound_1310-P5	41.5466	-42.3989	0.87
Compound_1315-P5	41.5464	-42.9342	0.89
Compound_1316-P5	51.3826	-40.6815	0.99
Compound_1317-P5	46.7329	-41.7658	0.94
Compound_1318-P5	52.9514	-38.9757	0.97
Compound_1325-P5	60.1382	-46.3654	1.30

Compound	Docking energy, kJ mol^{-1}		
	GOLD	DOCK6	RANK
Compound_1326-P5	41.5877	-42.6775	0.88
Compound_1328-P5	47.0467	-49.9331	1.18
Compound_1333-P5	46.7019	-43.3353	0.99
Compound_1348-P5	57.8882	-44.7270	1.22
Compound_1349-P5	57.7442	-40.6018	1.10
Compound_1351-P5	46.5659	-41.5295	0.93
Compound_1354-P5	51.4619	-36.7308	0.88
Compound_1384-P5	53.2378	-42.6699	1.08
Compound_1385-P5	53.3156	-43.5346	1.11
Compound_1398-P5	36.0160	-45.5073	0.87
Compound_1412-P5	43.5427	-44.9643	0.98
Compound_1416-P5	47.8538	-39.7105	0.90
Compound_1468-P5	42.4811	-49.3864	1.09
Compound_1470-P5	35.1816	-46.4673	0.88
Compound_1498-P5	46.9248	-46.8858	1.09
Compound_1499-P5	70.3351	-48.4254	1.54
Compound_1502-P5	49.7349	-47.4591	1.16
Compound_1503-P5	47.2068	-43.0559	0.99
Compound_1506-P5	57.8578	-39.6244	1.07
Compound_1522-P5	55.4131	-41.9227	1.09
Compound_1523-P5	57.5638	-41.8844	1.13
Compound_1525-P5	36.8099	-42.9154	0.81
Compound_1526-P5	67.3227	-43.4746	1.34
Compound_1530-P5	50.2977	-44.1743	1.07
Compound_1541-P5	61.2076	-44.3491	1.26
Compound_1545-P5	48.3143	-44.7506	1.06
Compound_1546-P5	52.7151	-44.8651	1.13
Compound_1553-P5	54.2046	-41.5940	1.06
Compound_1555-P5	52.5157	-40.2412	1.00
Compound_1557-P5	56.8176	-42.8188	1.14
Compound_1560-P5	43.1823	-45.6819	1.00
Compound_1561-P5	51.2729	-40.6325	0.99
Compound_1563-P5	40.4396	-43.9529	0.90
Compound_1569-P5	53.3739	-46.4255	1.19
Compound_1572-P5	51.4193	-43.7817	1.08
Compound_1581-P5	56.4135	-44.4856	1.19
Compound_1582-P5	54.0297	-41.9402	1.07
Compound_1588-P5	34.3010	-41.0870	0.71
Compound_1589-P5	53.6078	-44.9213	1.15
Compound_1594-P5	55.1991	-49.4713	1.31
Compound_1601-P5	52.6451	-47.3525	1.20
Compound_1622-P5	46.8891	-45.2300	1.05
Compound_1628-P5	39.8770	-42.2998	0.84
Compound_1629-P5	42.9470	-44.8493	0.97
Compound_1630-P5	46.6229	-46.5507	1.08
Compound_1633-P5	54.1216	-48.3686	1.26

Compound	Docking energy, kJ mol^{-1}		
	GOLD	DOCK6	RANK
Compound_1640-P5	46.3231	-45.8279	1.05
Compound_1641-P5	66.0964	-41.2892	1.26
Compound_1642-P5	50.1123	-42.8098	1.03
Compound_1644-P5	67.7068	-44.4102	1.38
Compound_1645-P5	29.1007	-43.9583	0.71
Compound_1646-P5	49.9206	-45.7135	1.11
Compound_1647-P5	39.7208	-40.6115	0.79
Compound_1648-P5	54.9028	-41.6218	1.08
Compound_1649-P5	38.9492	-42.2105	0.82
Compound_1650-P5	37.1726	-44.4490	0.86
Compound_1651-P5	50.8008	-44.7957	1.10
Compound_1652-P5	61.9703	-45.9708	1.32
Compound_1654-P5	44.5271	-42.9852	0.94
Compound_1660-P5	38.2798	-43.8368	0.86
Compound_1661-P5	60.3380	-43.8913	1.24
Compound_1662-P5	53.1422	-45.0845	1.15
Compound_1663-P5	47.6691	-43.8727	1.02
Compound_1665-P5	43.2824	-46.6846	1.03
Compound_1666-P5	37.3402	-45.7824	0.90
Compound_1668-P5	52.5727	-39.7069	0.98
Compound_1669-P5	51.0932	-42.5778	1.04
Compound_1670-P5	54.9243	-44.1776	1.15
Compound_1671-P5	52.1183	-47.0454	1.19
Compound_1672-P5	69.2117	-46.9718	1.48
Compound_1675-P5	56.8145	-45.8560	1.23
Compound_1680-P5	51.9372	-45.2937	1.13
Compound_1685-P5	48.9439	-37.8676	0.87
Compound_1693-P5	38.9481	-44.5487	0.89
Compound_1697-P5	50.8341	-48.1195	1.20
Compound_1704-P5	42.3155	-43.2731	0.91
Compound_1705-P5	34.8485	-45.3127	0.84
Compound_1706-P5	36.4002	-47.5113	0.93
Compound_1723-P5	38.9467	-45.6172	0.92
Compound_1724-P5	42.3095	-46.3391	1.00
Compound_1735-P5	48.9862	-42.8787	1.01
Compound_1741-P5	47.9579	-43.6844	1.02
Compound_1742-P5	54.1197	-45.4857	1.18
Compound_1743-P5	54.0389	-43.9094	1.13
Compound_1744-P5	50.7757	-48.0453	1.19
Compound_1748-P5	50.8627	-46.8225	1.16
Compound_1755-P5	54.5270	-46.8520	1.22
Compound_1761-P5	36.7710	-38.6492	0.68
Compound_1762-P5	44.6850	-40.1291	0.86
Compound_1768-P5	45.3244	-44.8004	1.01
Compound_1770-P5	34.6063	-46.4898	0.87
Compound_1773-P5	39.3847	-46.9654	0.97

Compound	Docking energy, kJ mol^{-1}		
	GOLD	DOCK6	RANK
Compound_1775-P5	42.4084	-44.2036	0.94
Compound_1801-P5	45.4592	-31.7044	0.63
Compound_1837-P5	49.3850	-39.0214	0.91
Compound_1848-P5	43.0344	-38.4109	0.78
Compound_1849-P5	41.4877	-37.1012	0.72
Compound_1850-P5	50.8645	-35.4917	0.83
Compound_1851-P5	66.8465	-38.3699	1.19
Compound_1852-P5	51.0373	-38.3689	0.92
Compound_1853-P5	42.9288	-37.4799	0.75
Compound_1861-P5	45.7499	-36.3736	0.77
Compound_1862-P5	52.2038	-38.3394	0.94
Compound_1863-P5	49.5927	-32.9516	0.74
Compound_1886-P5	45.0446	-36.5560	0.76
Compound_1975-P5	63.5885	-43.4039	1.28
Compound_1976-P5	54.5414	-42.5529	1.10
Compound_1977-P5	65.7635	-43.4240	1.31
Compound_1978-P5	68.6725	-43.7712	1.37
Compound_1979-P5	43.4721	-44.4866	0.97
Compound_1980-P5	48.2134	-43.0379	1.00
Compound_1985-P5	57.3361	-46.1887	1.25
Compound_1992-P5	44.6658	-38.4862	0.81
Compound_1993-P5	44.1682	-40.5949	0.86
Compound_1994-P5	61.0255	-41.4841	1.18
Compound_1995-P5	54.9185	-39.5243	1.02
Compound_1997-P5	55.2601	-39.6818	1.03
Compound_1998-P5	41.0012	-42.7832	0.87
Compound_2048-P5	51.0506	-33.1821	0.77
Compound_2109-P5	47.2566	-32.3932	0.68
Compound_2148-P5	33.6557	-33.4230	0.48
Compound_2250-P5	51.0774	-43.6636	1.07
Compound_2271-P5	54.1736	-43.0412	1.11
Compound_2272-P5	63.4586	-41.1395	1.21
Compound_2275-P5	47.2784	-45.0524	1.05
Compound_2287-P5	57.0384	-45.5006	1.23
Compound_2289-P5	63.6547	-43.5271	1.28
Compound_2292-P5	67.0451	-45.4917	1.40
Compound_2294-P5	46.2405	-34.2165	0.71
Compound_2295-P5	50.0192	-34.5654	0.79
Compound_2298-P5	54.0114	-44.8883	1.16
Compound_2305-P5	61.0604	-43.9419	1.25
Compound_2325-P5	52.1697	-35.1093	0.84
Compound_2326-P5	51.6397	-41.9718	1.03
Compound_2342-P5	51.7325	-41.5378	1.02
Compound_2343-P5	40.2525	-41.7727	0.83
Compound_2345-P5	44.9252	-40.1465	0.86
Compound_2355-P5	51.9398	-46.0995	1.16

Compound	Docking energy, kJ mol^{-1}		
	GOLD	DOCK6	RANK
Compound_2356-P5	57.7635	-43.4514	1.18
Compound_2360-P5	44.9223	-32.6895	0.65
Compound_2361-P5	45.8766	-33.8631	0.70
Compound_2363-P5	48.3274	-48.7553	1.17
Compound_2364-P5	57.6031	-42.1575	1.14
Compound_2366-P5	40.8728	-40.6236	0.81
Compound_2372-P5	57.6945	-46.6770	1.27
Compound_2387-P5	64.6946	-43.4511	1.30
Compound_2400-P5	47.7145	-41.4251	0.95
Compound_2406-P5	68.5700	-47.3240	1.47
Compound_2409-P5	55.3495	-45.5356	1.20
Compound_2412-P5	60.7488	-45.9796	1.30
Compound_2413-P5	61.0984	-43.6082	1.24
Compound_2414-P5	56.7382	-33.9447	0.89
Compound_2415-P5	61.9121	-44.6612	1.28
Compound_2418-P5	49.1126	-47.0248	1.14
Compound_2419-P5	41.8056	-45.5415	0.97
Compound_2653-P5	48.7400	-43.8164	1.04
Compound_2655-P5	41.6806	-41.7970	0.86
Compound_2661-P5	47.2977	-34.7183	0.75
Compound_2673-P5	48.1002	-43.0344	1.00
Compound_2674-P5	55.1440	-41.7014	1.08
Compound_2675-P5	43.3029	-39.9987	0.83
Compound_2676-P5	46.7136	-40.3679	0.90
Compound_2679-P5	45.4279	-34.3726	0.71
Compound_2690-P5	44.3773	-47.5447	1.07
Compound_2692-P5	37.7797	-42.1780	0.80
Compound_2695-P5	63.9478	-46.3534	1.37
Compound_2696-P5	52.4796	-48.8669	1.25
Compound_2697-P5	70.7623	-45.9253	1.47
Compound_2699-P5	51.1130	-43.0946	1.06
Compound_2706-P5	50.6867	-41.8064	1.01
Compound_2707-P5	37.7840	-41.6297	0.79
Compound_2712-P5	58.4960	-46.3784	1.28
Compound_2719-P5	48.3060	-43.8949	1.03
Compound_2721-P5	49.3766	-36.1624	0.82
Compound_2728-P5	57.3348	-48.3502	1.31
Compound_2730-P5	47.8459	-45.2372	1.06
Compound_2733-P5	49.4623	-46.6155	1.13
Compound_2734-P5	54.3246	-41.6539	1.07
Compound_2738-P5	55.0175	-47.9282	1.26
Compound_2739-P5	52.2264	-50.3962	1.29
Compound_2740-P5	57.5978	-47.7960	1.30
Compound_2744-P5	50.7963	-40.4502	0.97
Compound_2745-P5	41.1266	-45.2430	0.95
Compound_2748-P5	53.1932	-45.4869	1.16

Compound	Docking energy, kJ mol^{-1}		
	GOLD	DOCK6	RANK
Compound_2750-P5	52.3637	-46.1098	1.16
Compound_2755-P5	51.7107	-43.0837	1.07
Compound_2765-P5	58.8948	-49.3943	1.37
Compound_2769-P5	41.8108	-46.2488	0.99
Compound_51-P6	50.4464	-44.6464	1.09
Compound_60-P6	45.2243	-47.1530	1.07
Compound_97-P6	39.9459	-41.7794	0.83
Compound_99-P6	56.1093	-45.6552	1.21
Compound_112-P6	61.3602	-39.2664	1.12
Compound_116-P6	50.5681	-41.3995	1.00
Compound_120-P6	43.6167	-42.1042	0.90
Compound_151-P6	63.1773	-44.3950	1.30
Compound_165-P6	55.8268	-41.3409	1.08
Compound_171-P6	30.3903	-40.6505	0.63
Compound_293-P6	58.0073	-47.4506	1.30
Compound_299-P6	41.5593	-42.2017	0.87
Compound_300-P6	62.7522	-44.5477	1.30
Compound_301-P6	50.6694	-45.0428	1.10
Compound_302-P6	43.6003	-49.1364	1.10
Compound_306-P6	65.6874	-46.4082	1.40
Compound_308-P6	55.6688	-47.7453	1.27
Compound_311-P6	45.2769	-49.0770	1.13
Compound_313-P6	48.7929	-47.5400	1.14
Compound_314-P6	55.6742	-47.5767	1.26
Compound_321-P6	43.0572	-40.7953	0.85
Compound_322-P6	41.1691	-42.5978	0.87
Compound_328-P6	46.4051	-45.7544	1.05
Compound_330-P6	44.5651	-47.0357	1.06
Compound_333-P6	37.3959	-46.5899	0.92
Compound_335-P6	27.0547	-46.1973	0.74
Compound_479-P6	49.9384	-41.8468	1.00
Compound_480-P6	47.2195	-40.5943	0.92
Compound_481-P6	50.1435	-42.6716	1.03
Compound_482-P6	58.0918	-41.8754	1.14
Compound_483-P6	47.8874	-43.0377	1.00
Compound_484-P6	51.6902	-42.0171	1.03
Compound_491-P6	48.9227	-39.9429	0.93
Compound_503-P6	47.7601	-38.6887	0.87
Compound_504-P6	63.4299	-41.1098	1.21
Compound_726-P6	39.1830	-40.4303	0.77
Compound_727-P6	45.1490	-39.9779	0.86
Compound_732-P6	63.2549	-43.2229	1.27
Compound_734-P6	51.3500	-48.7099	1.22
Compound_736-P6	55.1071	-45.8663	1.20
Compound_738-P6	31.1933	-46.8285	0.82
Compound_760-P6	53.5832	-46.1667	1.19

Compound	Docking energy, kJ mol^{-1}		
	GOLD	DOCK6	RANK
Compound_765-P6	49.7470	-39.1204	0.92
Compound_766-P6	48.9969	-41.4774	0.97
Compound_767-P6	51.5408	-44.3499	1.10
Compound_768-P6	41.2397	-46.9122	1.00
Compound_772-P6	57.0199	-45.2082	1.22
Compound_774-P6	34.1856	-49.2218	0.94
Compound_777-P6	42.6035	-47.0123	1.02
Compound_779-P6	37.9115	-46.1888	0.92
Compound_780-P6	51.8116	-40.4524	0.99
Compound_781-P6	58.0704	-40.9717	1.11
Compound_782-P6	56.9545	-42.3176	1.13
Compound_783-P6	54.4938	-41.4184	1.06
Compound_784-P6	53.8753	-43.1890	1.10
Compound_785-P6	37.1390	-37.2342	0.65
Compound_786-P6	44.8764	-39.0528	0.83
Compound_787-P6	34.6463	-40.3040	0.69
Compound_788-P6	58.5163	-41.1290	1.12
Compound_789-P6	42.4238	-42.7858	0.90
Compound_790-P6	54.7003	-43.1056	1.12
Compound_792-P6	57.4329	-44.7208	1.21
Compound_794-P6	50.9387	-42.9447	1.05
Compound_795-P6	46.0883	-46.8414	1.08
Compound_797-P6	43.4548	-43.7644	0.94
Compound_798-P6	60.8150	-41.0164	1.16
Compound_799-P6	45.9311	-40.5796	0.89
Compound_800-P6	52.8726	-42.0156	1.05
Compound_801-P6	49.0784	-42.6064	1.01
Compound_802-P6	58.2600	-43.6497	1.19
Compound_803-P6	27.3434	-45.1232	0.71
Compound_804-P6	44.0660	-39.1426	0.82
Compound_805-P6	48.7103	-39.5080	0.91
Compound_806-P6	59.5982	-41.4564	1.15
Compound_807-P6	42.2788	-45.1411	0.96
Compound_808-P6	50.2744	-45.9844	1.12
Compound_810-P6	58.7128	-43.4333	1.19
Compound_815-P6	52.9987	-41.6413	1.05
Compound_816-P6	55.6012	-43.5764	1.15
Compound_822-P6	54.3674	-40.1554	1.03
Compound_823-P6	38.2708	-39.0644	0.72
Compound_831-P6	58.7400	-46.9013	1.30
Compound_834-P6	58.3037	-44.9807	1.23
Compound_836-P6	29.7462	-44.0335	0.72
Compound_843-P6	48.9998	-40.6747	0.95
Compound_844-P6	38.1141	-42.4139	0.81
Compound_845-P6	48.0342	-45.4214	1.07
Compound_856-P6	66.3551	-46.2762	1.41

Compound	Docking energy, kJ mol^{-1}		
	GOLD	DOCK6	RANK
Compound_862-P6	38.1656	-42.8514	0.83
Compound_863-P6	37.1613	-44.8710	0.87
Compound_864-P6	53.0795	-47.6399	1.22
Compound_876-P6	58.3312	-43.8906	1.20
Compound_881-P6	34.6680	-39.3945	0.67
Compound_882-P6	46.1036	-41.6318	0.93
Compound_883-P6	55.9002	-43.0013	1.13
Compound_884-P6	58.7698	-45.2571	1.25
Compound_888-P6	59.9289	-44.9800	1.26
Compound_890-P6	64.8469	-45.4194	1.36
Compound_893-P6	57.8888	-44.6294	1.21
Compound_895-P6	53.0834	-44.9984	1.14
Compound_901-P6	43.0008	-38.3846	0.78
Compound_902-P6	29.5707	-38.9036	0.57
Compound_908-P6	63.1825	-43.7910	1.28
Compound_910-P6	37.0118	-46.4463	0.91
Compound_913-P6	52.9514	-46.4463	1.18
Compound_915-P6	56.5836	-42.9668	1.14
Compound_969-P6	49.7072	-45.6896	1.11
Compound_970-P6	28.7941	-46.3626	0.77
Compound_971-P6	35.4003	-46.3508	0.88
Compound_972-P6	45.3993	-45.8403	1.04
Compound_973-P6	53.2140	-50.2033	1.30
Compound_974-P6	55.5982	-40.7305	1.06
Compound_975-P6	48.2208	-41.9725	0.97
Compound_976-P6	57.6311	-46.2159	1.26
Compound_977-P6	67.1099	-45.4562	1.40
Compound_978-P6	53.1439	-49.6677	1.28
Compound_979-P6	53.3794	-47.2209	1.21
Compound_981-P6	62.5783	-45.8531	1.33
Compound_985-P6	48.5479	-42.9542	1.01
Compound_986-P6	56.6337	-45.4417	1.22
Compound_992-P6	50.7492	-40.7630	0.98
Compound_993-P6	45.3965	-41.6186	0.92
Compound_1001-P6	50.9344	-46.4834	1.15
Compound_1003-P6	58.0818	-45.7922	1.25
Compound_1005-P6	39.5064	-41.9967	0.83
Compound_1012-P6	33.3123	-42.4892	0.73
Compound_1013-P6	47.2749	-45.5227	1.06
Compound_1032-P6	39.1264	-44.5913	0.89
Compound_1033-P6	41.1279	-47.4160	1.01
Compound_1034-P6	48.9822	-47.9953	1.16
Compound_1046-P6	69.5502	-48.0028	1.51
Compound_1051-P6	55.4010	-41.5582	1.08
Compound_1052-P6	45.5526	-44.0384	0.99
Compound_1053-P6	62.8403	-43.9457	1.28

Compound	Docking energy, kJ mol^{-1}		
	GOLD	DOCK6	RANK
Compound_1054-P6	63.4844	-50.2235	1.47
Compound_1058-P6	54.9846	-46.2595	1.21
Compound_1060-P6	54.5985	-48.6323	1.28
Compound_1063-P6	57.2868	-48.1113	1.31
Compound_1065-P6	49.8374	-47.8103	1.17
Compound_1072-P6	51.8146	-38.9495	0.95
Compound_1073-P6	43.7179	-43.2362	0.93
Compound_1079-P6	61.4289	-47.8049	1.37
Compound_1081-P6	40.9999	-46.2771	0.98
Compound_1084-P6	50.7324	-47.6442	1.18
Compound_1331-P6	49.8654	-46.4896	1.13
Compound_1332-P6	31.5297	-45.2419	0.78
Compound_1333-P6	51.5287	-47.3719	1.19
Compound_1334-P6	56.3390	-44.3139	1.18
Compound_1335-P6	47.3041	-46.0053	1.07
Compound_1336-P6	44.5251	-42.0894	0.91
Compound_1337-P6	54.1005	-43.3568	1.11
Compound_1338-P6	72.5805	-42.7308	1.41
Compound_1339-P6	60.2624	-41.1936	1.16
Compound_1340-P6	38.1405	-42.0365	0.80
Compound_1341-P6	41.4365	-42.8746	0.88
Compound_1342-P6	46.3957	-43.9845	1.00
Compound_1344-P6	55.0333	-44.0411	1.15
Compound_1345-P6	53.3708	-44.2444	1.13
Compound_1346-P6	55.8194	-46.6348	1.24
Compound_1347-P6	47.0096	-41.3780	0.94
Compound_1351-P6	53.3699	-46.7229	1.20
Compound_1353-P6	37.8285	-47.2344	0.95
Compound_1354-P6	38.3075	-49.5809	1.03
Compound_1355-P6	38.1711	-50.0056	1.04
Compound_1362-P6	48.6578	-44.0038	1.04
Compound_1363-P6	46.8902	-47.2648	1.10
Compound_1364-P6	51.4221	-46.0964	1.15
Compound_1365-P6	44.9591	-44.2408	0.98
Compound_1366-P6	62.3652	-46.2181	1.34
Compound_1367-P6	58.0784	-44.9274	1.23
Compound_1369-P6	43.2536	-42.7881	0.91
Compound_1371-P6	50.5201	-44.3840	1.08
Compound_1372-P6	52.1946	-43.2979	1.08
Compound_1379-P6	54.8729	-45.7447	1.20
Compound_1385-P6	47.2221	-49.2449	1.17
Compound_1387-P6	53.7537	-48.6826	1.26
Compound_1390-P6	43.8729	-47.2841	1.05
Compound_1392-P6	49.8894	-46.4135	1.13
Compound_1417-P6	46.1290	-47.4769	1.10
Compound_1424-P6	34.4100	-43.3389	0.78

Compound	Docking energy, kJ mol^{-1}		
	GOLD	DOCK6	RANK
Compound_1425-P6	44.2530	-46.8170	1.05
Compound_1426-P6	52.3842	-45.4414	1.14
Compound_1427-P6	54.7752	-47.7218	1.25
Compound_1431-P6	52.7185	-50.3784	1.29
Compound_1433-P6	43.5480	-47.2166	1.05
Compound_1436-P6	32.8650	-48.5968	0.90
Compound_1438-P6	36.3763	-47.4615	0.93
Compound_1439-P6	53.0719	-47.3038	1.21
Compound_1440-P6	49.6324	-41.3798	0.98
Compound_1441-P6	49.9649	-43.9460	1.06
Compound_1443-P6	49.1321	-45.6854	1.10
Compound_1444-P6	44.6460	-44.8394	1.00
Compound_1445-P6	49.1759	-46.9509	1.13
Compound_1446-P6	47.9443	-39.0591	0.88
Compound_1447-P6	41.7756	-40.3844	0.82
Compound_1448-P6	46.7770	-43.5878	1.00
Compound_1449-P6	47.8696	-44.2552	1.03
Compound_1450-P6	47.9834	-45.9072	1.08
Compound_1452-P6	45.1673	-44.3731	0.99
Compound_1454-P6	59.3630	-45.6760	1.27
Compound_1455-P6	43.5250	-48.3905	1.08
Compound_1457-P6	50.5180	-44.9264	1.10
Compound_1458-P6	50.0490	-43.5100	1.05
Compound_1459-P6	36.4804	-43.1963	0.81
Compound_1460-P6	60.1024	-42.8884	1.20
Compound_1461-P6	53.8543	-44.0098	1.13
Compound_1462-P6	56.4942	-45.6726	1.22
Compound_1464-P6	61.3845	-45.4174	1.30
Compound_1465-P6	41.8391	-46.0986	0.98
Compound_1466-P6	74.1660	-48.9269	1.62
Compound_1467-P6	49.9668	-41.2516	0.98
Compound_1468-P6	43.4099	-44.5804	0.97
Compound_1469-P6	57.8990	-46.8077	1.28
Compound_1470-P6	57.9500	-48.3207	1.32
Compound_1472-P6	45.7238	-45.7289	1.04
Compound_1476-P6	46.1221	-45.8825	1.05
Compound_1477-P6	39.8187	-43.6334	0.88
Compound_1478-P6	46.5908	-45.7837	1.06
Compound_1484-P6	46.2400	-41.1452	0.92
Compound_1485-P6	48.0662	-42.0548	0.97
Compound_1493-P6	45.0588	-48.6571	1.11
Compound_1496-P6	47.2350	-44.8485	1.04
Compound_1498-P6	36.1937	-43.3423	0.81
Compound_1506-P6	41.9781	-44.7919	0.95
Compound_1507-P6	37.7842	-44.7927	0.88
Compound_1508-P6	29.8843	-46.8959	0.80

Compound	Docking energy, kJ mol^{-1}		
	GOLD	DOCK6	RANK
Compound_1520-P6	43.9628	-49.8216	1.13
Compound_1521-P6	46.3800	-48.7942	1.14
Compound_1529-P6	26.9003	-47.7499	0.78
Compound_1530-P6	53.2425	-48.9772	1.26
Compound_1531-P6	34.7370	-49.5228	0.96
Compound_1551-P6	36.6521	-29.7434	0.42
Compound_1610-P6	43.9454	-37.8876	0.78
Compound_1621-P6	57.8002	-39.0244	1.05
Compound_1624-P6	48.0808	-37.1505	0.83
Compound_1639-P6	40.6384	-39.1761	0.76
Compound_1642-P6	49.2691	-44.9198	1.08
Compound_1643-P6	48.9159	-45.8339	1.10
Compound_1644-P6	66.1156	-38.0017	1.16
Compound_1657-P6	57.9108	-47.0329	1.29
Compound_1663-P6	46.0716	-43.6766	0.99
Compound_1665-P6	60.7189	-44.5762	1.26
Compound_1668-P6	67.4993	-47.1055	1.45
Compound_1670-P6	42.2411	-42.3437	0.88
Compound_1671-P6	51.1958	-43.8944	1.08
Compound_1675-P6	57.3188	-47.1114	1.28
Compound_1676-P6	48.6605	-46.5834	1.11
Compound_1678-P6	53.6614	-41.8420	1.06
Compound_1679-P6	43.2555	-44.2824	0.96
Compound_1684-P6	57.2643	-47.0006	1.27
Compound_1686-P6	48.7111	-43.4511	1.02
Compound_1689-P6	57.3012	-42.4334	1.14
Compound_1690-P6	47.6794	-45.7948	1.08
Compound_1691-P6	41.9843	-45.1843	0.96
Compound_1693-P6	50.4283	-45.1780	1.10
Compound_1708-P6	46.7089	-38.7095	0.85
Compound_1709-P6	57.7860	-44.2559	1.20
Compound_1748-P6	46.8392	-41.1496	0.93
Compound_1749-P6	43.8941	-43.2657	0.94
Compound_1750-P6	46.9460	-36.9812	0.81
Compound_1751-P6	42.5913	-34.7594	0.67
Compound_1752-P6	39.6692	-33.0841	0.57
Compound_1755-P6	56.3480	-39.0074	1.03
Compound_1756-P6	51.7021	-43.9399	1.09
Compound_1757-P6	58.6636	-44.0936	1.21
Compound_1764-P6	62.4800	-48.7616	1.41
Compound_1765-P6	41.6347	-40.7907	0.83
Compound_1766-P6	60.3491	-42.5657	1.20
Compound_1767-P6	39.1611	-35.5713	0.63
Compound_1768-P6	44.1998	-34.5234	0.69
Compound_1771-P6	52.6640	-44.0506	1.11
Compound_1772-P6	45.5447	-45.0455	1.02

Compound	Docking energy, kJ mol^{-1}		
	GOLD	DOCK6	RANK
Compound_1773-P6	49.7359	-44.3025	1.07
Compound_1788-P6	49.0654	-46.1072	1.11
Compound_1799-P6	46.6521	-42.2928	0.96
Compound_1800-P6	48.7384	-41.8816	0.98
Compound_1801-P6	45.6810	-34.2342	0.71
Compound_1807-P6	48.0715	-43.2544	1.01
Compound_1809-P6	54.6670	-44.8931	1.17
Compound_1817-P6	44.6714	-48.4664	1.10
Compound_1823-P6	50.3549	-42.1575	1.02
Compound_1824-P6	49.5354	-39.1649	0.91
Compound_1825-P6	49.3856	-39.3309	0.92
Compound_1826-P6	50.1794	-33.7706	0.77
Compound_1830-P6	47.1595	-40.9590	0.93
Compound_1831-P6	53.8438	-44.4161	1.14
Compound_1832-P6	53.3143	-45.0179	1.15
Compound_1833-P6	70.2428	-46.9745	1.49
Compound_1834-P6	52.2382	-43.2175	1.08
Compound_1837-P6	65.2615	-47.3054	1.42
Compound_1840-P6	52.3870	-45.9167	1.16
Compound_1842-P6	57.5841	-48.7327	1.33
Compound_1845-P6	54.9612	-48.4048	1.27
Compound_1847-P6	56.5359	-50.0444	1.35
Compound_2134-P6	45.0349	-44.1511	0.98
Compound_2135-P6	50.4100	-43.0569	1.04
Compound_2136-P6	53.3177	-45.4808	1.16
Compound_2138-P6	58.1119	-42.5580	1.16
Compound_2172-P6	63.5886	-42.7498	1.26
Compound_2173-P6	65.1871	-41.1293	1.24
Compound_2174-P6	44.3719	-42.7091	0.93
Compound_2175-P6	51.1823	-42.3139	1.03
Compound_2176-P6	66.1535	-43.9635	1.34
Compound_2177-P6	63.2243	-46.2888	1.35
Compound_2187-P6	59.4059	-41.7919	1.16
Compound_2216-P6	59.7434	-40.3137	1.12
Compound_2217-P6	39.1817	-41.3381	0.80
Compound_2218-P6	54.5459	-39.4260	1.01
Compound_2221-P6	54.8399	-43.4413	1.13
Compound_2230-P6	41.3499	-37.5091	0.73
Compound_2231-P6	51.0841	-38.7195	0.93
Compound_2232-P6	39.1164	-41.5813	0.81
Compound_2234-P6	74.4927	-42.9391	1.45
Compound_2336-P6	62.7301	-42.8023	1.24
Compound_2359-P6	42.5867	-45.5805	0.98
Compound_2366-P6	49.7240	-42.4237	1.01
Compound_2367-P6	43.1073	-43.4179	0.93
Compound_2368-P6	51.5847	-45.8044	1.14

Compound	Docking energy, kJ mol^{-1}		
	GOLD	DOCK6	RANK
Compound_2369-P6	38.1999	-48.5113	0.99
Compound_2372-P6	51.2030	-47.5318	1.19
Compound_2374-P6	36.2429	-47.7442	0.94
Compound_2376-P6	45.3437	-49.7471	1.15
Compound_2378-P6	52.5137	-48.2705	1.23
Compound_2379-P6	36.0774	-41.3555	0.75
Compound_2380-P6	54.5962	-42.8072	1.11
Compound_2383-P6	47.0036	-45.3011	1.05
Compound_2384-P6	38.9226	-43.7292	0.87
Compound_2385-P6	63.2745	-45.8639	1.34
Compound_2386-P6	48.4059	-38.6258	0.88
Compound_2387-P6	55.6064	-40.1175	1.05
Compound_2388-P6	57.3318	-41.7120	1.12
Compound_2389-P6	65.4981	-44.6551	1.35
Compound_2390-P6	58.0433	-45.6537	1.25
Compound_2392-P6	45.0123	-43.7127	0.97
Compound_2394-P6	42.0215	-43.3685	0.91
Compound_2395-P6	53.4870	-46.3779	1.19
Compound_2397-P6	51.9905	-43.9930	1.10
Compound_2398-P6	47.6521	-42.1769	0.97
Compound_2399-P6	42.1351	-44.2736	0.94
Compound_2400-P6	28.5443	-42.6247	0.66
Compound_2401-P6	52.7936	-43.3405	1.09
Compound_2402-P6	41.2170	-43.5690	0.90
Compound_2405-P6	59.0628	-44.6009	1.23
Compound_2406-P6	51.2349	-45.4141	1.12
Compound_2407-P6	54.3701	-47.0442	1.23
Compound_2408-P6	31.9370	-39.7971	0.63
Compound_2409-P6	44.8943	-41.5158	0.90
Compound_2410-P6	44.0949	-42.8349	0.93
Compound_2411-P6	66.6133	-45.6356	1.39
Compound_2412-P6	56.2100	-45.5691	1.21
Compound_2413-P6	58.2214	-47.4112	1.30
Compound_2415-P6	70.2745	-45.8801	1.46
Compound_2420-P6	51.7483	-43.7959	1.09
Compound_2421-P6	53.0547	-45.9756	1.17
Compound_2422-P6	39.1994	-44.2900	0.89
Compound_2427-P6	44.0012	-39.0373	0.82
Compound_2428-P6	38.0348	-39.6664	0.73
Compound_2435-P6	47.8549	-44.2968	1.03
Compound_2438-P6	32.5637	-45.3202	0.80
Compound_2439-P6	47.8679	-42.8591	0.99
Compound_2446-P6	58.6531	-45.3953	1.25
Compound_2447-P6	53.8319	-46.7593	1.21
Compound_2448-P6	43.3977	-47.1213	1.04
Compound_2458-P6	58.2577	-47.8182	1.31

Compound	Docking energy, kJ mol^{-1}		
	GOLD	DOCK6	RANK
Compound_2466-P6	35.4375	-44.7302	0.84
Compound_2467-P6	50.6360	-49.1373	1.22
Compound_2468-P6	63.4655	-46.3407	1.36
Compound_2480-P6	52.7151	-46.8799	1.19
Compound_2487-P6	44.4375	-42.1343	0.91
Compound_2488-P6	47.1434	-45.6255	1.06
Compound_2489-P6	55.4144	-48.2990	1.28
Compound_2493-P6	41.6094	-46.3752	0.99
Compound_2495-P6	64.8917	-48.0992	1.43
Compound_2498-P6	58.3738	-48.9769	1.35
Compound_2500-P6	43.0768	-46.9613	1.03
Compound_2501-P6	51.9080	-46.4530	1.17
Compound_2507-P6	65.5177	-39.8242	1.21
Compound_2508-P6	52.4057	-43.0718	1.08
Compound_2513-P6	71.3994	-46.3243	1.49
Compound_2515-P6	67.6183	-45.6979	1.41
Compound_2518-P6	42.9403	-44.2777	0.95
Compound_2520-P6	44.1034	-44.0369	0.96
Compound_2563-P6	45.5901	-39.8988	0.87
Compound_2564-P6	53.5802	-40.6951	1.03
Compound_2569-P6	39.4710	-46.2030	0.95
Compound_2571-P6	52.2288	-43.8670	1.10
Compound_2574-P6	50.9330	-46.0304	1.14
Compound_2576-P6	50.4824	-44.2869	1.08
Compound_2601-P6	46.7664	-42.7037	0.97
Compound_2608-P6	55.7355	-39.4863	1.03
Compound_2609-P6	45.4806	-41.2287	0.91
Compound_2610-P6	43.2468	-43.4362	0.93
Compound_2611-P6	56.5976	-43.7154	1.17
Compound_2615-P6	56.8246	-45.6827	1.23
Compound_2617-P6	47.0505	-44.5543	1.03
Compound_2620-P6	40.5700	-44.2004	0.91
Compound_2622-P6	52.8200	-43.4582	1.09
Compound_2623-P6	52.3945	-43.1142	1.08
Compound_2624-P6	56.2089	-36.9598	0.96
Compound_2625-P6	55.8578	-38.1197	0.99
Compound_2628-P6	52.2332	-41.6073	1.03
Compound_2629-P6	57.3466	-40.9553	1.10
Compound_2630-P6	48.3184	-45.7091	1.08
Compound_2631-P6	44.1220	-35.8216	0.73
Compound_2632-P6	52.8900	-38.1505	0.94
Compound_2633-P6	42.7019	-39.5847	0.81
Compound_2634-P6	51.6706	-40.9101	1.00
Compound_2635-P6	50.9261	-43.0196	1.05
Compound_2636-P6	47.4943	-43.7167	1.01
Compound_2638-P6	46.0721	-43.5301	0.98

Compound	Docking energy, kJ mol^{-1}		
	GOLD	DOCK6	RANK
Compound_2640-P6	49.5560	-43.0921	1.03
Compound_2641-P6	50.3298	-45.8005	1.12
Compound_2643-P6	44.1002	-42.2936	0.91
Compound_2644-P6	53.0905	-40.4392	1.01
Compound_2645-P6	44.3586	-42.3762	0.92
Compound_2646-P6	51.2614	-39.5683	0.96
Compound_2647-P6	55.7309	-40.1056	1.05
Compound_2650-P6	63.6777	-41.4938	1.22
Compound_2651-P6	50.2163	-42.1954	1.01
Compound_2652-P6	53.1214	-44.8713	1.14
Compound_2653-P6	45.7528	-39.2285	0.85
Compound_2654-P6	50.0775	-37.8074	0.88
Compound_2655-P6	50.3290	-42.3059	1.02
Compound_2656-P6	49.0027	-41.3366	0.97
Compound_2657-P6	54.0290	-42.6606	1.09
Compound_2658-P6	43.9424	-45.4759	1.00
Compound_2660-P6	56.4411	-43.0310	1.14
Compound_2665-P6	48.3460	-44.3903	1.05
Compound_2666-P6	44.4377	-43.1657	0.94
Compound_2667-P6	46.5363	-42.7073	0.97
Compound_2670-P6	47.9782	-37.6449	0.84
Compound_2671-P6	47.6430	-38.3888	0.86
Compound_2679-P6	44.6964	-41.3723	0.90
Compound_2682-P6	40.8739	-46.6378	0.98
Compound_2683-P6	29.3743	-41.0746	0.63
Compound_2689-P6	48.6946	-43.5111	1.03
Compound_2690-P6	64.5142	-41.7891	1.25
Compound_2691-P6	49.7811	-43.8721	1.06
Compound_2703-P6	53.4279	-42.2012	1.07
Compound_2704-P6	49.9536	-44.9878	1.09
Compound_2712-P6	48.6538	-47.1522	1.13
Compound_2713-P6	60.0110	-41.8142	1.17
Compound_2714-P6	42.7129	-45.5786	0.98
Compound_2727-P6	70.9962	-40.0377	1.30
Compound_2734-P6	50.0731	-38.0892	0.89
Compound_2735-P6	54.5046	-40.0956	1.03
Compound_2736-P6	53.9942	-40.8059	1.04
Compound_2737-P6	62.8412	-42.9370	1.25
Compound_2741-P6	61.0317	-44.0760	1.25
Compound_2743-P6	51.6358	-49.2391	1.24
Compound_2746-P6	46.2018	-43.9120	1.00
Compound_2748-P6	50.7618	-42.2378	1.02
Compound_2749-P6	55.0388	-42.8368	1.11
Compound_2755-P6	46.4314	-37.0166	0.80
Compound_2756-P6	49.1439	-38.5343	0.89
Compound_2762-P6	42.1179	-44.0763	0.93

Compound	Docking energy, kJ mol^{-1}		
	GOLD	DOCK6	RANK
Compound_2764-P6	34.7611	-42.6164	0.76
Compound_2767-P6	42.0166	-41.7195	0.86
Compound_2769-P6	51.5455	-41.7859	1.02
Compound_2817-P6	50.7404	-43.3889	1.06
Compound_2818-P6	65.7862	-44.2814	1.34
Compound_2819-P6	65.4044	-45.8220	1.38
Compound_2820-P6	51.3518	-43.3648	1.07
Compound_2821-P6	60.4955	-43.3729	1.22
Compound_2842-P6	40.2198	-29.7428	0.48
Compound_2843-P6	36.2021	-31.3494	0.46
Compound_2887-P6	53.7702	-37.6527	0.94
Compound_47-P7	61.8755	-42.9410	1.23
Compound_48-P7	43.6514	-45.8497	1.01
Compound_63-P7	57.9493	-48.8234	1.34
Compound_70-P7	51.8349	-46.8244	1.18
Compound_71-P7	50.8437	-45.5807	1.12
Compound_72-P7	42.6438	-48.4208	1.07
Compound_84-P7	38.5424	-43.1026	0.84
Compound_85-P7	43.5337	-43.6958	0.94
Compound_88-P7	60.8070	-46.8732	1.33
Compound_89-P7	54.6031	-45.7743	1.19
Compound_91-P7	50.9865	-41.2154	1.00
Compound_92-P7	63.0303	-42.6940	1.25
Compound_93-P7	30.9479	-45.0055	0.77
Compound_94-P7	47.4531	-47.0964	1.11
Compound_97-P7	73.4931	-45.7643	1.51
Compound_103-P7	55.0877	-46.0915	1.21
Compound_106-P7	60.7930	-43.9610	1.24
Compound_107-P7	51.0736	-43.5744	1.07
Compound_112-P7	49.9584	-44.6845	1.08
Compound_113-P7	53.7700	-43.1781	1.10
Compound_124-P7	51.0181	-46.1299	1.14
Compound_131-P7	37.2220	-41.9500	0.79
Compound_132-P7	41.3889	-45.2200	0.95
Compound_138-P7	59.0413	-47.6961	1.32
Compound_151-P7	44.6865	-45.0706	1.00
Compound_152-P7	53.5934	-46.0789	1.18
Compound_173-P7	55.7339	-47.1185	1.25
Compound_188-P7	52.5551	-45.8819	1.16
Compound_195-P7	54.3727	-42.6789	1.10
Compound_196-P7	48.0436	-45.8900	1.08
Compound_197-P7	69.4811	-47.0461	1.48
Compound_202-P7	67.1843	-48.8797	1.50
Compound_208-P7	59.3863	-47.7759	1.33
Compound_216-P7	54.4183	-43.5846	1.13
Compound_217-P7	56.7802	-43.7733	1.17

Compound	Docking energy, kJ mol^{-1}		
	GOLD	DOCK6	RANK
Compound_218-P7	58.6574	-45.3853	1.25
Compound_223-P7	64.4202	-46.6939	1.39
Compound_229-P7	52.5132	-44.8437	1.13
Compound_230-P7	50.1921	-47.4301	1.17
Compound_282-P7	48.9524	-42.8780	1.01
Compound_283-P7	43.5952	-41.4295	0.88
Compound_284-P7	54.1433	-45.5645	1.18
Compound_289-P7	54.8432	-44.4055	1.16
Compound_296-P7	41.0421	-46.5911	0.99
Compound_297-P7	44.4024	-46.2205	1.03
Compound_298-P7	60.6413	-43.7811	1.24
Compound_299-P7	51.7654	-46.7936	1.17
Compound_305-P7	42.7782	-44.8143	0.96
Compound_306-P7	46.3618	-49.2895	1.15
Compound_310-P7	57.1940	-46.2092	1.25
Compound_313-P7	40.1338	-44.7752	0.92
Compound_314-P7	49.0286	-42.3826	1.00
Compound_315-P7	54.1867	-41.9478	1.07
Compound_318-P7	42.5344	-47.4822	1.04
Compound_319-P7	59.7270	-45.4947	1.27
Compound_320-P7	50.9504	-46.5025	1.15
Compound_321-P7	48.5441	-40.4111	0.93
Compound_322-P7	37.9116	-39.3828	0.72
Compound_323-P7	51.8383	-43.6303	1.08
Compound_324-P7	55.6086	-48.9604	1.30
Compound_325-P7	48.5144	-44.6440	1.06
Compound_327-P7	46.9796	-46.4611	1.08
Compound_333-P7	71.0834	-42.5380	1.38
Compound_334-P7	55.0384	-43.6896	1.14
Compound_335-P7	56.3812	-42.1630	1.12
Compound_336-P7	42.2563	-46.1024	0.99
Compound_339-P7	39.7453	-49.5577	1.05
Compound_340-P7	58.5732	-48.5191	1.34
Compound_342-P7	40.9529	-42.0708	0.85
Compound_343-P7	54.1325	-43.4812	1.12
Compound_344-P7	57.1287	-43.3495	1.16
Compound_345-P7	71.0577	-48.8984	1.56
Compound_348-P7	57.2438	-47.4928	1.29
Compound_353-P7	52.5812	-43.6599	1.10
Compound_362-P7	43.2056	-44.2119	0.95
Compound_363-P7	53.7203	-46.3518	1.19
Compound_364-P7	38.8999	-45.7555	0.92
Compound_383-P7	55.4987	-45.7105	1.21
Compound_384-P7	50.9824	-48.1120	1.20
Compound_396-P7	51.2548	-46.1300	1.15
Compound_397-P7	51.2244	-42.3470	1.04

Compound	Docking energy, kJ mol^{-1}		
	GOLD	DOCK6	RANK
Compound_403-P7	47.1635	-42.4813	0.97
Compound_404-P7	56.7815	-42.0000	1.12
Compound_405-P7	55.4553	-43.4231	1.14
Compound_406-P7	51.0742	-43.1046	1.05
Compound_410-P7	63.2271	-49.2774	1.44
Compound_416-P7	53.8381	-44.8445	1.15
Compound_417-P7	55.3687	-48.0488	1.27
Compound_418-P7	44.1689	-47.7923	1.07
Compound_419-P7	41.1193	-42.9188	0.88
Compound_423-P7	49.7050	-41.9523	1.00
Compound_424-P7	46.0735	-45.5293	1.04
Compound_426-P7	34.2426	-38.0964	0.62
Compound_427-P7	51.0134	-42.5845	1.04
Compound_428-P7	47.0479	-45.9601	1.07
Compound_429-P7	49.9917	-43.9303	1.06
Compound_433-P7	50.0393	-45.3116	1.10
Compound_435-P7	34.9448	-48.3269	0.93
Compound_438-P7	67.2594	-48.7786	1.49
Compound_440-P7	41.7704	-42.8927	0.89
Compound_441-P7	50.7287	-46.6395	1.15
Compound_491-P7	60.0033	-43.3995	1.22
Compound_492-P7	53.6260	-46.0269	1.18
Compound_497-P7	42.0318	-50.1116	1.10
Compound_503-P7	45.0105	-46.4631	1.05
Compound_504-P7	54.4168	-47.1932	1.23
Compound_505-P7	27.8368	-44.1594	0.69
Compound_506-P7	59.5712	-46.1338	1.29
Compound_512-P7	63.3786	-41.6824	1.22
Compound_513-P7	44.7969	-45.4168	1.02
Compound_514-P7	63.0252	-49.2109	1.44
Compound_515-P7	42.5631	-48.9451	1.08
Compound_519-P7	58.8225	-47.5591	1.32
Compound_525-P7	36.6566	-47.2137	0.93
Compound_526-P7	38.8735	-48.9553	1.02
Compound_527-P7	63.6320	-48.0952	1.41
Compound_528-P7	55.7065	-42.5877	1.12
Compound_529-P7	55.0275	-43.7948	1.14
Compound_532-P7	48.0804	-44.5346	1.05
Compound_533-P7	36.8649	-43.3708	0.82
Compound_534-P7	57.5201	-46.5198	1.26
Compound_535-P7	28.4751	-39.1946	0.56
Compound_536-P7	47.8897	-40.7104	0.93
Compound_537-P7	40.3546	-42.8663	0.87
Compound_538-P7	51.8337	-44.6102	1.11
Compound_539-P7	59.2676	-45.2622	1.26
Compound_540-P7	62.6605	-46.9015	1.36

Compound	Docking energy, kJ mol^{-1}		
	GOLD	DOCK6	RANK
Compound_542-P7	53.2690	-44.4052	1.13
Compound_547-P7	39.1288	-42.8016	0.84
Compound_548-P7	55.6706	-44.2329	1.17
Compound_549-P7	40.8567	-42.6019	0.87
Compound_550-P7	57.5311	-44.1264	1.19
Compound_551-P7	48.5801	-43.6281	1.03
Compound_554-P7	55.1745	-46.4190	1.22
Compound_555-P7	55.8267	-45.9231	1.22
Compound_557-P7	51.8231	-46.1747	1.16
Compound_558-P7	52.4433	-46.1038	1.17
Compound_559-P7	58.8429	-48.1063	1.33
Compound_562-P7	44.2092	-45.8203	1.02
Compound_567-P7	45.1722	-45.7881	1.03
Compound_575-P7	36.3140	-40.1496	0.72
Compound_576-P7	54.1816	-41.4414	1.06
Compound_582-P7	50.6838	-46.2138	1.14
Compound_587-P7	52.2550	-45.3085	1.14
Compound_596-P7	34.7073	-44.4974	0.82
Compound_597-P7	42.3632	-48.3040	1.06
Compound_598-P7	65.0987	-48.2946	1.44
Compound_616-P7	44.9856	-46.7043	1.06
Compound_617-P7	35.4250	-48.5027	0.95
Compound_631-P7	60.5947	-46.4641	1.31
Compound_632-P7	51.8732	-43.2625	1.07
Compound_638-P7	58.0488	-41.7640	1.13
Compound_639-P7	48.0521	-46.5003	1.10
Compound_640-P7	44.9445	-46.7717	1.06
Compound_641-P7	60.3131	-49.3209	1.39
Compound_645-P7	54.7256	-48.8541	1.28
Compound_651-P7	55.9006	-45.7770	1.21
Compound_652-P7	53.7272	-48.5893	1.26
Compound_653-P7	64.6774	-46.9398	1.40
Compound_654-P7	49.4077	-41.7048	0.99
Compound_658-P7	61.6856	-43.6430	1.25
Compound_659-P7	33.9288	-46.7147	0.87
Compound_661-P7	57.4340	-38.7755	1.04
Compound_662-P7	58.0144	-42.6120	1.16
Compound_663-P7	60.5544	-43.5015	1.23
Compound_664-P7	51.6558	-45.7524	1.14
Compound_668-P7	48.5560	-44.4393	1.05
Compound_670-P7	35.5997	-46.3179	0.88
Compound_672-P7	52.0472	-46.8103	1.18
Compound_674-P7	47.4989	-45.0857	1.05
Compound_675-P7	45.4854	-44.4555	1.00
Compound_988-P7	63.1445	-44.8086	1.31
Compound_989-P7	46.0425	-43.2745	0.97

Compound	Docking energy, kJ mol^{-1}		
	GOLD	DOCK6	RANK
Compound_990-P7	68.7976	-44.8573	1.41
Compound_991-P7	43.0879	-39.0598	0.80
Compound_992-P7	43.4406	-41.2573	0.87
Compound_993-P7	47.8244	-43.7736	1.02
Compound_994-P7	48.2157	-45.5070	1.08
Compound_995-P7	54.1487	-44.7404	1.15
Compound_996-P7	61.7700	-46.4941	1.34
Compound_998-P7	51.0344	-44.7981	1.10
Compound_1003-P7	56.0963	-45.0925	1.20
Compound_1004-P7	49.8601	-46.4468	1.13
Compound_1005-P7	41.4557	-44.4094	0.93
Compound_1006-P7	51.4131	-43.4204	1.07
Compound_1007-P7	44.6485	-46.6340	1.05
Compound_1010-P7	24.2092	-45.6451	0.67
Compound_1011-P7	50.0060	-47.4394	1.16
Compound_1013-P7	49.0411	-40.3595	0.94
Compound_1014-P7	31.3983	-44.0779	0.75
Compound_1015-P7	53.4778	-44.6068	1.14
Compound_1016-P7	43.0958	-45.9149	1.00
Compound_1017-P7	76.9825	-46.3706	1.59
Compound_1020-P7	56.4577	-46.0486	1.23
Compound_1025-P7	49.2571	-44.8950	1.08
Compound_1027-P7	41.0732	-45.5809	0.96
Compound_1030-P7	35.1609	-48.2846	0.93
Compound_1031-P7	61.5070	-45.1770	1.29
Compound_1032-P7	34.2633	-44.4699	0.81
Compound_1033-P7	38.7333	-40.1340	0.76
Compound_1034-P7	48.1150	-40.3839	0.93
Compound_1035-P7	50.0398	-44.9141	1.09
Compound_1036-P7	49.0007	-48.0321	1.16
Compound_1037-P7	57.8175	-49.3548	1.35
Compound_1039-P7	56.5373	-48.1990	1.30
Compound_1040-P7	43.4134	-43.3160	0.93
Compound_1046-P7	27.3222	-46.8431	0.76
Compound_1047-P7	62.2649	-43.4808	1.26
Compound_1048-P7	60.9192	-44.4013	1.26
Compound_1049-P7	48.5697	-41.0781	0.95
Compound_1050-P7	48.2960	-43.8128	1.03
Compound_1053-P7	56.7662	-46.2670	1.24
Compound_1054-P7	47.6393	-45.9481	1.08
Compound_1055-P7	34.5225	-46.3250	0.87
Compound_1056-P7	28.0052	-39.5815	0.56
Compound_1057-P7	45.7558	-41.9460	0.93
Compound_1058-P7	49.4618	-42.5955	1.01
Compound_1059-P7	48.8295	-43.9761	1.04
Compound_1060-P7	54.4170	-45.9272	1.19

Compound	Docking energy, kJ mol^{-1}		
	GOLD	DOCK6	RANK
Compound_1061-P7	58.0496	-47.1278	1.29
Compound_1063-P7	55.4802	-45.0427	1.19
Compound_1069-P7	58.7877	-43.3827	1.19
Compound_1070-P7	53.2698	-44.9882	1.15
Compound_1071-P7	42.0649	-43.5490	0.91
Compound_1072-P7	55.1345	-43.1295	1.12
Compound_1073-P7	40.6190	-41.9544	0.84
Compound_1076-P7	52.0019	-44.3496	1.11
Compound_1077-P7	47.8801	-44.5240	1.04
Compound_1079-P7	46.1192	-40.0443	0.88
Compound_1080-P7	45.1577	-40.5355	0.88
Compound_1081-P7	49.9214	-43.0975	1.03
Compound_1082-P7	53.1543	-46.2784	1.18
Compound_1083-P7	55.2366	-45.6333	1.20
Compound_1084-P7	55.2415	-45.2812	1.19
Compound_1086-P7	53.5856	-44.3207	1.13
Compound_1092-P7	45.6870	-43.5625	0.98
Compound_1093-P7	48.7179	-44.8023	1.06
Compound_1094-P7	37.5584	-43.8543	0.85
Compound_1095-P7	56.5508	-46.3014	1.24
Compound_1100-P7	63.6211	-44.7881	1.32
Compound_1101-P7	42.1680	-47.1739	1.02
Compound_1102-P7	43.5070	-45.8370	1.01
Compound_1103-P7	42.3697	-44.3443	0.94
Compound_1106-P7	54.7315	-45.8848	1.20
Compound_1107-P7	48.7362	-47.0811	1.13
Compound_1109-P7	41.8113	-41.2703	0.84
Compound_1110-P7	43.0842	-43.0079	0.92
Compound_1111-P7	56.1495	-47.5263	1.27
Compound_1112-P7	57.4736	-46.6771	1.27
Compound_1113-P7	59.8331	-49.9864	1.40
Compound_1114-P7	26.0823	-50.2973	0.84
Compound_1116-P7	50.4961	-43.8373	1.07
Compound_1119-P7	55.5477	-47.5485	1.26
Compound_1120-P7	42.8729	-46.7575	1.02
Compound_1122-P7	35.4879	-41.3346	0.74
Compound_1123-P7	45.1618	-41.9521	0.92
Compound_1124-P7	53.8451	-43.8525	1.12
Compound_1125-P7	47.2094	-45.4283	1.06
Compound_1126-P7	50.0000	-48.2437	1.19
Compound_1127-P7	57.8107	-48.3901	1.32
Compound_1129-P7	53.8421	-45.9842	1.19
Compound_1134-P7	54.8289	-44.6972	1.16
Compound_1135-P7	47.2085	-44.2273	1.02
Compound_1136-P7	49.3701	-45.3852	1.09
Compound_1137-P7	49.3998	-49.0433	1.20

Compound	Docking energy, kJ mol^{-1}		
	GOLD	DOCK6	RANK
Compound_1142-P7	46.4063	-47.3593	1.10
Compound_1143-P7	55.4273	-44.9920	1.18
Compound_1144-P7	40.3648	-47.2221	0.99
Compound_1145-P7	39.7674	-44.4527	0.90
Compound_1148-P7	44.6979	-47.2099	1.07
Compound_1149-P7	46.4771	-50.3345	1.19
Compound_1151-P7	55.3563	-42.5174	1.11
Compound_1152-P7	53.0437	-43.5705	1.10
Compound_1153-P7	47.2235	-44.1946	1.02
Compound_1154-P7	47.7456	-49.8509	1.19
Compound_1155-P7	46.5206	-47.7123	1.11
Compound_1156-P7	43.4202	-47.4515	1.05
Compound_1158-P7	40.7167	-39.6695	0.78
Compound_1159-P7	44.5861	-40.5479	0.87
Compound_1162-P7	44.0260	-42.8209	0.93
Compound_1163-P7	35.3629	-42.5079	0.77
Compound_1165-P7	57.5551	-38.2776	1.03
Compound_1166-P7	40.0313	-38.9921	0.75
Compound_1167-P7	67.2561	-42.3947	1.31
Compound_1168-P7	54.0735	-42.4415	1.09
Compound_1169-P7	58.7526	-44.2039	1.22
Compound_1170-P7	57.2003	-44.0451	1.19
Compound_1172-P7	53.6726	-41.2468	1.05
Compound_1178-P7	54.7105	-41.5541	1.07
Compound_1179-P7	43.6681	-41.4372	0.88
Compound_1180-P7	39.8248	-41.4595	0.82
Compound_1181-P7	37.5349	-43.6808	0.84
Compound_1182-P7	46.5579	-45.6844	1.05
Compound_1185-P7	37.6943	-47.5357	0.96
Compound_1186-P7	48.7876	-45.8498	1.10
Compound_1188-P7	41.8693	-41.1316	0.84
Compound_1189-P7	55.4273	-42.3838	1.11
Compound_1190-P7	49.2750	-44.9783	1.08
Compound_1191-P7	60.1238	-47.2304	1.33
Compound_1192-P7	47.6756	-49.4890	1.18
Compound_1195-P7	60.7008	-47.9932	1.36
Compound_1201-P7	54.1487	-46.2430	1.20
Compound_1210-P7	56.7450	-47.3211	1.27
Compound_1213-P7	63.0518	-45.8191	1.34
Compound_1214-P7	39.5158	-48.2963	1.01
Compound_1220-P7	37.5482	-42.6021	0.81
Compound_1221-P7	42.5073	-43.5469	0.92
Compound_1227-P7	46.6020	-47.5940	1.11
Compound_1228-P7	38.6451	-48.3347	1.00
Compound_1231-P7	48.9072	-51.0712	1.25
Compound_1232-P7	44.2712	-44.6155	0.98

Compound	Docking energy, kJ mol^{-1}		
	GOLD	DOCK6	RANK
Compound_1234-P7	48.7559	-42.2682	0.99
Compound_1235-P7	48.7508	-43.7393	1.03
Compound_1236-P7	44.4323	-42.2195	0.92
Compound_1237-P7	36.2023	-47.5739	0.93
Compound_1238-P7	47.1771	-47.5981	1.12
Compound_1241-P7	52.3447	-49.4171	1.26
Compound_1246-P7	51.7953	-44.3638	1.10
Compound_1248-P7	34.7258	-45.0281	0.83
Compound_1255-P7	52.0308	-41.9064	1.04
Compound_1256-P7	53.8280	-45.0526	1.16
Compound_1283-P7	52.7780	-43.2154	1.09
Compound_1289-P7	39.7204	-48.3789	1.01
Compound_1296-P7	52.2646	-42.2400	1.05
Compound_1297-P7	50.8190	-43.8688	1.07
Compound_1317-P7	57.0612	-45.6242	1.23
Compound_1324-P7	47.9153	-42.5070	0.98
Compound_1325-P7	42.2873	-44.2302	0.94
Compound_1347-P7	47.1938	-41.1026	0.93
Compound_1348-P7	33.1047	-42.6453	0.74
Compound_1361-P7	32.7711	-45.1943	0.80
Compound_1362-P7	46.6821	-45.9872	1.06
Compound_1393-P7	34.2026	-44.1673	0.80
Compound_1394-P7	41.1329	-46.2514	0.98
Compound_1407-P7	42.5194	-44.0975	0.94
Compound_1408-P7	52.5174	-45.4862	1.15
Compound_1438-P7	41.4382	-40.9327	0.83
Compound_1439-P7	40.6237	-42.5290	0.86
Compound_1452-P7	38.8575	-43.0128	0.84
Compound_1468-P7	50.8079	-35.1998	0.82
Compound_1469-P7	52.9611	-33.9433	0.82
Compound_1470-P7	41.0046	-36.7307	0.70
Compound_1482-P7	44.3074	-35.9517	0.73
Compound_1487-P7	52.3339	-40.9762	1.01
Compound_1498-P7	46.3969	-39.5598	0.87
Compound_1516-P7	55.9473	-39.6403	1.04
Compound_1517-P7	58.8236	-44.2129	1.22
Compound_1603-P7	56.2907	-43.0720	1.14
Compound_1605-P7	64.7256	-44.4147	1.33
Compound_1673-P7	63.4099	-42.5593	1.25
Compound_1676-P7	47.5411	-41.4944	0.95
Compound_1677-P7	70.2605	-41.6239	1.34
Compound_1683-P7	52.3164	-41.7790	1.04
Compound_1689-P7	44.8381	-41.7303	0.91
Compound_1690-P7	47.1889	-42.1786	0.96
Compound_1691-P7	57.9028	-35.3415	0.95
Compound_1932-P7	39.2067	-35.3415	0.63

Compound	Docking energy, kJ mol^{-1}		
	GOLD	DOCK6	RANK
Compound_1939-P7	40.0871	-34.7056	0.62
Compound_1940-P7	36.9839	-33.3327	0.53
Compound_1948-P7	52.1477	-37.0139	0.90
Compound_1960-P7	27.8331	-32.9491	0.36
Compound_1969-P7	49.7203	-38.8223	0.91
Compound_2061-P7	40.6638	-42.3440	0.86
Compound_2062-P7	41.2426	-40.3393	0.81
Compound_2072-P7	50.0487	-37.6967	0.88
Compound_2075-P7	46.3665	-35.9147	0.77
Compound_2076-P7	41.1939	-36.2081	0.69
Compound_2077-P7	46.9229	-36.1600	0.78
Compound_2078-P7	50.2389	-37.1335	0.87
Compound_2219-P7	59.5093	-40.6528	1.13
Compound_2220-P7	48.5288	-41.5994	0.97
Compound_2222-P7	47.6792	-41.7915	0.96
Compound_2227-P7	43.7923	-39.2945	0.82
Compound_2233-P7	40.4422	-44.3447	0.91
Compound_2242-P7	57.1746	-41.1733	1.10
Compound_2261-P7	56.7244	-38.9581	1.03
Compound_2265-P7	32.7492	-39.9376	0.65
Compound_2266-P7	59.9447	-41.9562	1.17
Compound_2278-P7	42.3927	-44.2449	0.94
Compound_2284-P7	60.5630	-42.0874	1.19
Compound_2285-P7	54.1704	-42.0606	1.08
Compound_2286-P7	36.1607	-31.9691	0.48
Compound_2287-P7	51.5041	-32.4825	0.75
Compound_2289-P7	49.9213	-41.5895	0.99
Compound_2290-P7	49.5830	-40.2178	0.95
Compound_2295-P7	54.0634	-43.3870	1.11
Compound_2305-P7	58.6462	-40.3183	1.10
Compound_2306-P7	46.9475	-39.2798	0.87
Compound_2307-P7	49.7782	-45.4078	1.10
Compound_2338-P7	53.2778	-42.0251	1.06
Compound_2339-P7	38.3655	-48.1124	0.98
Compound_2345-P7	53.5066	-44.9871	1.15
Compound_2355-P7	55.6342	-42.4232	1.11
Compound_2357-P7	46.1940	-49.5161	1.16
Compound_2368-P7	52.2255	-52.0756	1.33
Compound_2374-P7	39.0901	-45.9000	0.93
Compound_2381-P7	45.3531	-43.1673	0.96
Compound_2382-P7	62.1530	-48.4448	1.40
Compound_2383-P7	59.9251	-50.5526	1.42
Compound_2391-P7	49.7859	-49.0996	1.21
Compound_2607-P7	29.1869	-35.6849	0.47
Compound_234-P8	66.7581	-43.3612	1.33
Compound_237-P8	51.2558	-35.2606	0.83

Compound	Docking energy, kJ mol^{-1}		
	GOLD	DOCK6	RANK
Compound_240-P8	48.3391	-39.1128	0.89
Compound_243-P8	43.7400	-34.1086	0.67
Compound_244-P8	52.2728	-43.5814	1.09
Compound_246-P8	49.5481	-39.0218	0.91
Compound_249-P8	63.1840	-39.4945	1.16
Compound_250-P8	41.1584	-38.2479	0.75
Compound_259-P8	47.3578	-35.5044	0.77
Compound_262-P8	64.8024	-39.8954	1.20
Compound_263-P8	40.0950	-38.9988	0.75
Compound_264-P8	48.7694	-41.4295	0.97
Compound_272-P8	48.6872	-35.5710	0.80
Compound_275-P8	39.6869	-34.3407	0.61
Compound_278-P8	47.2153	-44.0243	1.02
Compound_282-P8	50.9901	-41.3969	1.00
Compound_283-P8	52.8280	-38.0479	0.94
Compound_291-P8	43.7792	-37.7157	0.77
Compound_293-P8	49.1161	-34.8500	0.78
Compound_294-P8	49.8831	-36.8479	0.85
Compound_295-P8	46.8560	-34.8590	0.74
Compound_297-P8	50.9596	-37.8196	0.90
Compound_300-P8	62.0727	-41.9628	1.21
Compound_301-P8	56.6347	-38.9740	1.03
Compound_302-P8	58.9669	-38.4138	1.05
Compound_309-P8	50.1680	-36.3394	0.84
Compound_310-P8	49.7774	-34.9892	0.80
Compound_311-P8	47.3688	-36.9788	0.81
Compound_356-P8	53.4808	-42.9691	1.09
Compound_360-P8	48.4684	-37.7017	0.85
Compound_364-P8	43.3320	-37.8874	0.77
Compound_365-P8	51.8931	-36.8620	0.89
Compound_366-P8	41.6550	-36.7185	0.71
Compound_367-P8	39.8893	-38.4484	0.73
Compound_368-P8	46.6480	-35.2284	0.75
Compound_369-P8	52.1840	-41.5860	1.03
Compound_370-P8	53.9022	-42.9437	1.10
Compound_373-P8	54.3560	-36.4802	0.92
Compound_374-P8	63.3215	-44.7287	1.31
Compound_377-P8	47.8563	-44.6944	1.05
Compound_379-P8	47.1400	-40.0088	0.90
Compound_380-P8	42.5206	-40.0128	0.82
Compound_381-P8	41.8349	-40.3424	0.82
Compound_383-P8	45.9202	-42.4180	0.95
Compound_499-P8	45.1889	-38.5822	0.82
Compound_502-P8	37.6133	-36.8247	0.64
Compound_506-P8	53.5357	-40.8220	1.03
Compound_507-P8	54.9782	-44.7738	1.17

Compound	Docking energy, kJ mol^{-1}		
	GOLD	DOCK6	RANK
Compound_580-P8	50.9781	-39.5543	0.95
Compound_595-P8	48.0214	-31.7714	0.67
Compound_596-P8	48.5997	-42.0152	0.98
Compound_597-P8	60.5640	-40.7418	1.15
Compound_611-P8	35.0713	-39.7403	0.69
Compound_616-P8	50.2853	-36.8033	0.86
Compound_636-P8	51.8386	-41.9582	1.03
Compound_637-P8	56.7927	-42.2312	1.13
Compound_638-P8	44.2565	-43.2905	0.94
Compound_641-P8	47.8816	-44.8940	1.05
Compound_741-P8	59.5267	-34.5549	0.95
Compound_799-P8	44.6625	-40.7156	0.88
Compound_810-P8	48.3540	-30.3269	0.64
Compound_820-P8	49.9588	-35.6467	0.82
Compound_821-P8	41.5550	-38.7559	0.77
Compound_906-P8	62.6327	-40.6224	1.18
Compound_927-P8	42.1238	-37.9173	0.75
Compound_928-P8	44.1423	-38.4696	0.80
Compound_929-P8	32.6839	-37.8176	0.59
Compound_930-P8	30.5247	-35.4441	0.48
Compound_931-P8	38.0321	-35.7559	0.62
Compound_932-P8	35.3340	-30.2779	0.42
Compound_933-P8	48.3145	-38.2636	0.87
Compound_934-P8	35.9008	-35.6987	0.58
Compound_935-P8	44.8941	-32.1905	0.63
Compound_936-P8	38.7300	-35.8318	0.63
Compound_937-P8	56.0910	-40.1107	1.05
Compound_938-P8	48.6016	-37.1475	0.84
Compound_939-P8	45.4500	-36.2572	0.76
Compound_940-P8	47.9712	-34.3684	0.75
Compound_945-P8	47.3202	-35.6250	0.77
Compound_946-P8	38.9769	-34.1023	0.59
Compound_947-P8	47.8052	-38.6357	0.87
Compound_952-P8	47.2836	-37.9630	0.84
Compound_954-P8	58.2165	-37.4743	1.01
Compound_955-P8	53.6321	-38.4914	0.96
Compound_956-P8	45.8146	-40.0473	0.88
Compound_960-P8	44.5847	-36.1536	0.74
Compound_961-P8	40.9954	-35.5142	0.66
Compound_962-P8	42.2871	-35.4578	0.68
Compound_963-P8	39.6413	-39.5175	0.76
Compound_965-P8	45.8753	-36.0580	0.76
Compound_967-P8	39.2451	-34.5654	0.61
Compound_968-P8	34.1728	-34.1753	0.51
Compound_969-P8	36.5298	-34.7004	0.56
Compound_971-P8	53.2566	-38.5804	0.96

Compound	Docking energy, kJ mol^{-1}		
	GOLD	DOCK6	RANK
Compound_972-P8	45.6230	-36.7384	0.78
Compound_1008-P8	60.8023	-43.0194	1.22
Compound_1009-P8	47.4767	-43.1303	0.99
Compound_1022-P8	69.6801	-45.7845	1.45
Compound_1029-P8	47.4867	-45.5367	1.06
Compound_1030-P8	43.7360	-45.3438	0.99
Compound_1052-P8	51.8200	-42.6611	1.05
Compound_1053-P8	48.4235	-42.8833	1.00
Compound_1062-P8	61.2329	-46.9038	1.34
Compound_1075-P8	64.2151	-42.6068	1.26
Compound_1076-P8	54.8990	-44.2344	1.15
Compound_1085-P8	38.9881	-47.6185	0.98
Compound_1098-P8	43.2054	-42.0926	0.89
Compound_1099-P8	56.0493	-42.9997	1.14
Compound_1108-P8	56.4600	-46.2937	1.24
Compound_1119-P8	48.9683	-44.4081	1.06
Compound_1120-P8	52.0397	-47.8346	1.21
Compound_1128-P8	29.8796	-49.1313	0.87
Compound_1137-P8	49.9720	-45.2743	1.10
Compound_1138-P8	47.1697	-45.2544	1.05
Compound_1147-P8	56.3803	-50.7134	1.37
Compound_1159-P8	33.1459	-44.1839	0.78
Compound_1160-P8	48.7034	-44.2964	1.05
Compound_1169-P8	50.0077	-46.8630	1.15
Compound_1183-P8	44.9881	-42.9751	0.95
Compound_1184-P8	37.8612	-42.1564	0.80
Compound_1193-P8	46.5732	-45.6206	1.05
Compound_1207-P8	38.3617	-45.0213	0.89
Compound_1208-P8	30.6709	-45.3912	0.77
Compound_1209-P8	59.8290	-47.2808	1.32
Compound_1231-P8	30.6124	-49.1296	0.88
Compound_1232-P8	51.3203	-47.0736	1.17
Compound_1255-P8	45.0792	-43.6716	0.97
Compound_1256-P8	56.2279	-46.0730	1.23
Compound_1257-P8	31.1806	-46.2615	0.81
Compound_1582-P8	39.0920	-44.0604	0.88
Compound_1604-P8	29.9325	-45.3797	0.76
Compound_1605-P8	76.8056	-43.8847	1.52
Compound_1606-P8	48.7200	-44.6315	1.06
Compound_1612-P8	30.4653	-47.2524	0.82
Compound_1614-P8	63.0598	-43.2741	1.26
Compound_1615-P8	46.3273	-43.5493	0.99
Compound_1616-P8	45.7255	-43.5357	0.98
Compound_1617-P8	55.4224	-43.8335	1.15
Compound_1618-P8	52.2124	-42.9689	1.07
Compound_1619-P8	40.2125	-44.7658	0.92

Compound	Docking energy, kJ mol^{-1}		
	GOLD	DOCK6	RANK
Compound_1620-P8	48.0125	-36.9973	0.83
Compound_1621-P8	39.7003	-44.3787	0.90
Compound_1622-P8	38.5066	-44.4851	0.88
Compound_1623-P8	50.2636	-42.9684	1.04
Compound_1624-P8	37.1187	-43.9392	0.84
Compound_1625-P8	52.3956	-43.9544	1.10
Compound_1626-P8	46.7194	-46.0731	1.07
Compound_1627-P8	46.4625	-44.7853	1.03
Compound_1628-P8	53.1812	-45.1513	1.15
Compound_1629-P8	61.8198	-41.9734	1.20
Compound_1630-P8	42.4086	-44.1176	0.94
Compound_1631-P8	41.1979	-45.1861	0.95
Compound_1651-P8	50.4131	-42.3743	1.02
Compound_1653-P8	56.3467	-43.8525	1.17
Compound_1654-P8	55.9789	-44.9659	1.19
Compound_1660-P8	53.7903	-45.7219	1.18
Compound_1677-P8	55.1174	-43.0060	1.12
Compound_1678-P8	49.6692	-45.3543	1.10
Compound_1679-P8	35.8870	-42.1969	0.77
Compound_1680-P8	54.5600	-43.1169	1.11
Compound_1681-P8	39.7469	-45.0686	0.92
Compound_1682-P8	53.6332	-43.7158	1.12
Compound_1683-P8	50.2368	-42.5862	1.03
Compound_1684-P8	34.3412	-46.4047	0.87
Compound_1713-P8	38.5986	-41.4477	0.79
Compound_1714-P8	56.2865	-44.8722	1.19
Compound_1715-P8	41.0827	-42.3735	0.86
Compound_1716-P8	35.5314	-41.7717	0.75
Compound_1717-P8	43.6846	-43.0485	0.93
Compound_1718-P8	35.9507	-42.9935	0.79
Compound_1719-P8	57.3505	-37.7274	1.01
Compound_1720-P8	44.8007	-43.1045	0.95
Compound_1721-P8	42.7316	-44.5330	0.95
Compound_1722-P8	40.3361	-44.2291	0.90
Compound_1723-P8	51.9612	-46.0525	1.16
Compound_1724-P8	39.6201	-41.5765	0.82
Compound_1725-P8	46.3607	-46.3702	1.07
Compound_1726-P8	45.1584	-45.2790	1.02
Compound_1727-P8	55.0489	-46.9348	1.23
Compound_1728-P8	58.3488	-42.7117	1.17
Compound_1729-P8	48.2737	-46.4172	1.10
Compound_1730-P8	51.3169	-48.2427	1.21
Compound_1731-P8	57.6523	-45.8649	1.25
Compound_1782-P8	53.2232	-42.4581	1.07
Compound_1783-P8	53.6952	-46.5468	1.20
Compound_1784-P8	52.7307	-42.4129	1.06

Compound	Docking energy, kJ mol^{-1}		
	GOLD	DOCK6	RANK
Compound_1787-P8	44.7249	-45.7317	1.02
Compound_1821-P8	41.5617	-46.8208	1.00
Compound_1822-P8	37.8108	-43.9275	0.85
Compound_1823-P8	38.7755	-46.0004	0.93
Compound_1824-P8	49.6990	-44.5159	1.07
Compound_1825-P8	39.9135	-41.9044	0.83
Compound_1828-P8	55.1100	-46.8770	1.23
Compound_2154-P8	41.8642	-36.4461	0.71
Compound_2159-P8	51.6423	-39.5086	0.96
Compound_2162-P8	33.6694	-31.5508	0.42
Compound_2163-P8	37.1513	-33.3939	0.54
Compound_2165-P8	34.6978	-32.6078	0.47
Compound_2167-P8	44.3774	-33.2440	0.65
Compound_2173-P8	44.0840	-35.2711	0.71
Compound_6-P9	56.6723	-35.4705	0.93
Compound_35-P9	51.8540	-37.8461	0.92
Compound_59-P9	58.5436	-43.0203	1.18
Compound_60-P9	50.1989	-31.2840	0.70
Compound_85-P9	53.5339	-44.3993	1.13
Compound_86-P9	49.3914	-41.8339	0.99
Compound_87-P9	44.8840	-45.2601	1.01
Compound_92-P9	53.5161	-44.5448	1.14
Compound_93-P9	61.7821	-44.3497	1.27
Compound_102-P9	40.8128	-44.5186	0.92
Compound_105-P9	59.3451	-44.4403	1.23
Compound_108-P9	43.4862	-42.9345	0.92
Compound_109-P9	46.7786	-42.0374	0.95
Compound_110-P9	46.4726	-43.0904	0.98
Compound_111-P9	32.0345	-44.8822	0.78
Compound_117-P9	66.2463	-43.9321	1.34
Compound_132-P9	38.4395	-45.3696	0.91
Compound_133-P9	40.7431	-45.6136	0.95
Compound_134-P9	66.0641	-43.2382	1.31
Compound_139-P9	54.9778	-46.2290	1.21
Compound_169-P9	56.0238	-42.4957	1.12
Compound_170-P9	51.2486	-42.5217	1.04
Compound_171-P9	53.8857	-46.8513	1.21
Compound_184-P9	53.3823	-45.1516	1.15
Compound_187-P9	56.2059	-46.7496	1.25
Compound_190-P9	60.1112	-41.6768	1.17
Compound_191-P9	39.9297	-44.2897	0.90
Compound_192-P9	44.5439	-45.5641	1.02
Compound_197-P9	48.2938	-43.6699	1.02
Compound_211-P9	44.2379	-42.3409	0.92
Compound_212-P9	66.3741	-46.1872	1.40
Compound_213-P9	53.9485	-47.1849	1.22

Compound	Docking energy, kJ mol^{-1}		
	GOLD	DOCK6	RANK
Compound_219-P9	60.1285	-46.4408	1.31
Compound_249-P9	44.1133	-43.1929	0.94
Compound_250-P9	48.1389	-40.5958	0.93
Compound_251-P9	55.7430	-42.3900	1.11
Compound_255-P9	47.4842	-44.2210	1.03
Compound_267-P9	54.6465	-42.1503	1.09
Compound_285-P9	45.8549	-44.5520	1.01
Compound_286-P9	51.8638	-42.4697	1.05
Compound_287-P9	53.1295	-44.8534	1.14
Compound_326-P9	31.6662	-44.2477	0.76
Compound_327-P9	51.4042	-46.6229	1.16
Compound_328-P9	39.0728	-46.7401	0.96
Compound_347-P9	55.7397	-46.0147	1.22
Compound_348-P9	58.5378	-43.3956	1.19
Compound_349-P9	45.8451	-47.9201	1.11
Compound_367-P9	62.4658	-44.9364	1.30
Compound_368-P9	45.6230	-48.2249	1.11
Compound_1637-P9	47.0912	-42.0385	0.96
Compound_1638-P9	48.7201	-41.4095	0.97
Compound_1639-P9	52.7153	-37.6972	0.93
Compound_1641-P9	46.9770	-37.6918	0.83
Compound_1643-P9	58.6849	-37.1289	1.01
Compound_1644-P9	50.6211	-35.6836	0.83
Compound_1645-P9	41.4088	-35.2710	0.66
Compound_1646-P9	38.7933	-36.0257	0.64
Compound_1647-P9	51.4704	-38.5231	0.93
Compound_1655-P9	54.2538	-37.7755	0.95
Compound_1657-P9	51.7163	-36.1179	0.86
Compound_1659-P9	58.1652	-37.3293	1.01
Compound_1660-P9	59.7533	-38.7719	1.08
Compound_1739-P9	48.7904	-43.3774	1.02
Compound_1763-P9	61.3436	-38.7019	1.10
Compound_1764-P9	56.2121	-39.6824	1.04
Compound_1765-P9	58.6354	-41.1602	1.13
Compound_1766-P9	60.1777	-40.0006	1.12
Compound_1767-P9	68.6311	-39.4588	1.25
Compound_1769-P9	44.9763	-40.8157	0.88
Compound_1777-P9	44.1812	-33.6788	0.66
Compound_1778-P9	42.9588	-35.5958	0.70
Compound_1779-P9	50.7943	-42.0577	1.02
Compound_1781-P9	45.5567	-39.1373	0.85
Compound_1782-P9	50.7745	-40.4750	0.97
Compound_1789-P9	65.0951	-42.1232	1.26
Compound_1790-P9	60.4844	-42.6247	1.20
Compound_1791-P9	66.2567	-39.9695	1.22
Compound_1805-P9	46.3417	-47.5761	1.10

Compound	Docking energy, kJ mol^{-1}		
	GOLD	DOCK6	RANK
Compound_1806-P9	46.7299	-43.2352	0.98
Compound_1808-P9	68.8611	-46.9763	1.47
Compound_1809-P9	48.1966	-41.4197	0.96
Compound_1810-P9	54.6069	-45.2270	1.18
Compound_1814-P9	65.1453	-44.1495	1.32
Compound_1827-P9	57.8427	-44.4921	1.21
Compound_1828-P9	61.1266	-44.0879	1.25
Compound_1829-P9	53.5435	-44.9733	1.15
Compound_1963-P9	75.2702	-44.8408	1.52
Compound_1964-P9	64.6144	-44.9779	1.34
Compound_1965-P9	36.7678	-43.5817	0.83
Compound_1966-P9	60.1827	-43.9701	1.23
Compound_1980-P9	57.6712	-45.2954	1.23
Compound_1987-P9	57.4954	-42.8834	1.16
Compound_1988-P9	53.4074	-43.5373	1.11
Compound_2012-P9	57.0437	-46.0182	1.24
Compound_2013-P9	53.8472	-45.6514	1.18
Compound_2014-P9	58.3722	-47.6886	1.31
Compound_2062-P9	44.0666	-40.5500	0.86
Compound_2063-P9	58.6174	-40.7501	1.11
Compound_2064-P9	53.0274	-42.3817	1.07
Compound_2077-P9	46.4774	-44.0407	1.00
Compound_2084-P9	38.7815	-45.1497	0.91
Compound_2107-P9	57.3940	-42.9564	1.16
Compound_2108-P9	41.8756	-41.5723	0.85
Compound_2151-P9	45.6113	-42.8464	0.95
Compound_2152-P9	56.4150	-44.8409	1.20
Compound_2153-P9	64.8657	-44.1578	1.32
Compound_2166-P9	51.4718	-42.7985	1.05
Compound_2172-P9	46.9481	-47.1272	1.10
Compound_2195-P9	63.1438	-47.3715	1.38
Compound_2233-P9	45.7319	-41.2276	0.91
Compound_2234-P9	59.3901	-41.8725	1.16
Compound_2235-P9	39.6725	-44.4722	0.90
Compound_2236-P9	64.2093	-42.4152	1.26
Compound_2250-P9	60.1441	-42.7639	1.20
Compound_2256-P9	55.0731	-46.3385	1.22
Compound_2258-P9	57.1712	-44.3751	1.20
Compound_2259-P9	67.4395	-43.9396	1.36
Compound_2260-P9	51.6293	-46.5666	1.16
Compound_2283-P9	40.4029	-44.2979	0.91
Compound_2284-P9	55.8945	-44.6155	1.18
Compound_2285-P9	49.6169	-44.5675	1.07
Compound_2332-P9	50.4441	-46.0259	1.13
Compound_2354-P9	53.4648	-45.4808	1.16
Compound_2364-P9	42.9190	-46.2681	1.01

Compound	Docking energy, kJ mol^{-1}		
	GOLD	DOCK6	RANK
Compound_2368-P9	51.1516	-45.6172	1.13
Compound_2379-P9	51.8825	-45.4440	1.14
Compound_2380-P9	39.2950	-47.9497	0.99
Compound_2401-P9	49.7271	-41.8335	1.00
Compound_2402-P9	47.3024	-44.9053	1.04
Compound_2415-P9	48.4849	-47.3998	1.14
Compound_2428-P9	34.6541	-45.4594	0.84
Compound_2436-P9	60.6219	-45.0694	1.27
Compound_2450-P9	41.8648	-45.0780	0.96
Compound_2457-P9	37.3772	-44.6400	0.87
Compound_2477-P9	42.6218	-46.7665	1.02
Compound_2487-P9	54.2181	-46.5911	1.21
Compound_2517-P9	63.1955	-45.9437	1.34

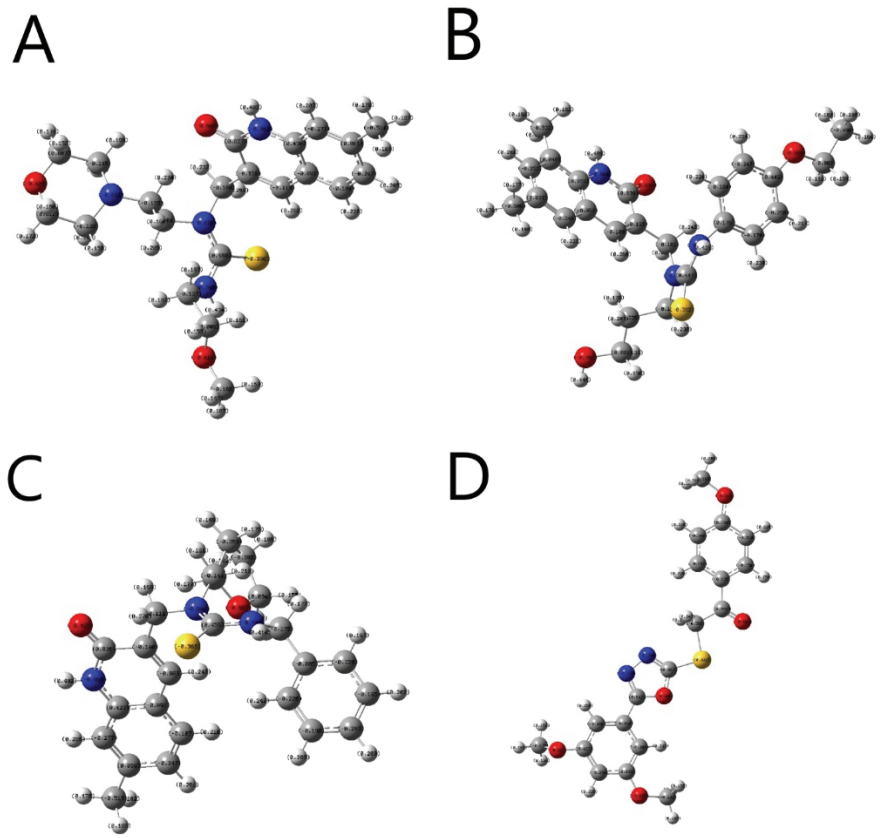

Fig. S-1. Atomic charges of the ligands were calculated using the restrained electrostatic potential (RESP) protocol at the HF/6-31G* level of theory using the Gaussian 09 software. A-3-P5; B-33-P5; C-1466-P6; D-2645-P15.

Journal of the Serbian Chemical Society
JSCS@tmf.bg.ac.rs • www.shd.org.rs/JSCS

J. Serb. Chem. Soc. 87 (6) 707–721 (2022)
JSCS–5552

Original scientific paper
Published 2 February 2022

Unveiling the regioselective synthesis of antiviral 5-isoxazol-5-yl-2'-deoxyuridines from the perspective of a molecular electron density theory

NIVEDITA ACHARJEE[1]*, HAYDAR A. MOHAMMAD-SALIM[2] and MRINMOY CHAKRABORTY[3]

[1]*Department of Chemistry, Durgapur Government College, Durgapur-713214, West Bengal, India,* [2]*Department of Chemistry, University of Zakho, Duhok 42001, Iraq and* [3]*Department of Electronics and Communication Engineering, Dr. B. C. Roy Engineering College, Durgapur-713206, West Bengal, India*

(Received 14 October, revised 3 December, accepted 7 December 2021)

Abstract: The regioselective synthesis of a potent antiviral sugar nucleoside isoxazole analogue in the [3+2] cycloaddition (32CA) reaction of acetonitrile-N-oxide (ANO) and acetyl-protected 5-ethynyl-2'-deoxyuridine (EDU) has been studied at the MPWB1K/6-311G(d,p) level within perspective of the molecular electron density theory (MEDT). From an electron localization function (ELF) analysis, ANO is classified as a zwitterionic species devoid of any pseudoradical or carbenoid centre. The *ortho* regioisomer is energetically preferred over the *meta* one by the activation enthalpy of 21.7–24.3 kJ mol^{-1}, suggesting complete regioselectivity in agreement with the experiment. The activation enthalpy increases from 53.9 kJ mol^{-1} in the gas phase to 71.5 kJ mol^{-1} in water, suggesting more facile reaction in low polar solvents. The minimal global electron density transfer (GEDT) at the TSs suggests non-polar character and the formation of new covalent bonds has not been started at the located TSs, showing non-covalent intermolecular interactions from an atoms-in-molecules (AIM) study and in the independent gradient model (IGM) isosurfaces. The AIM analysis shows more accumulation of electron density at the C–C interacting region relative to the C–O one, and earlier C–C bond formation is predicted from a bonding evolution theory (BET) study.

Keywords: isoxazole; MEDT; electron localization function; IGMH.

INTRODUCTION

The diverse biological properties of heterocyclic compounds[1,2] have attracted worldwide investigations on their synthetic aspects.[3] Isoxazoles[4] **1** (Scheme 1), an important class of five membered heterocycles serve as the key

* Corresponding author. E-mail: nivchem@gmail.com
https://doi.org/10.2298/JSC211014106A

pharmacophores in natural products and exhibit anti-inflammatory (**2**),[5] anticancer (**3**),[6] antimicrobial (**4**),[7] antidepressant (**5**),[8] anticonvulsant (**6**)[9] and several other medicinal properties[10] (Scheme 1).

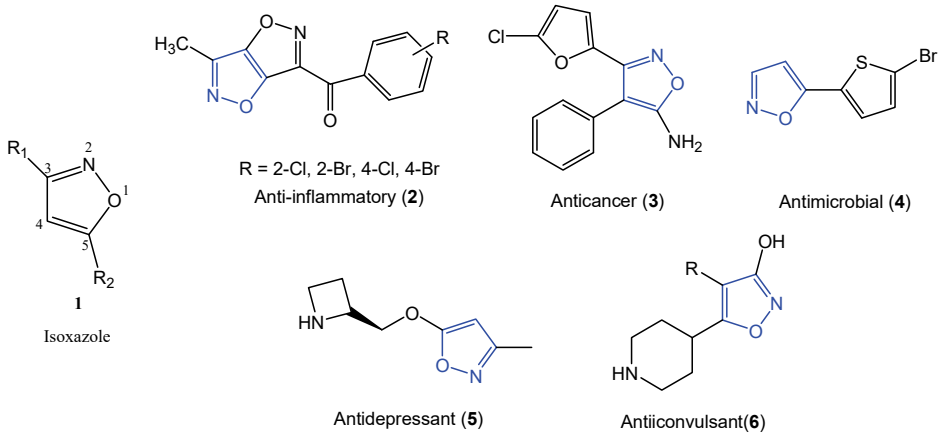

Scheme 1. Biologically active compounds containing the isoxazole ring.

The therapeutic potential of isoxazoles was reviewed in 2018 by Agarwal and Mishra,[10] while another review in the same year by Zhu *et al.*[11] focused on some of the significant applications of the isoxazoles in medicinal chemistry. Very recently, in 2021, Eid *et al.*[12] reported the anticancer and antioxidant properties of novel isoxazole-amide analogues.

The first synthesis of isoxazoles dates back to 1903 by Claisen[13] from the oximation of propargylaldehyde acetal. In 2005, Hansen *et al.*[14] reported the more convenient regioselective synthesis of 3,5-disubstituted isoxazoles **7** from the *in situ* generated nitrile oxide **9** (oximation of aldehyde **8**) and terminal alkynes **10** (Scheme 2). Recently, Carloni *et al.*[15] synthesized 3,5-disubstituted isoxazoles from the O-silylated hydroxamic acid generated nitrile oxides and alkynes.

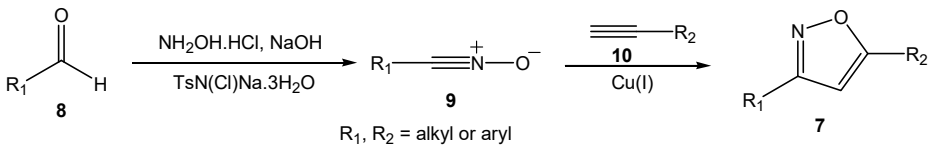

Scheme 2. 32CA reaction of nitrile oxide **9** and terminal alkyne **10**.

Nucleoside analogues[16,17] represent an important class of antiviral drugs and the synthesis of sugar modified nucleosides[18] has gained sincere attention owing to the search for non-toxic antiviral agents, especially against the HIV-1 and the herpes virus. Lee *et al.*[19] reported the synthesis of modified sugar nucleoside isoxazole (Scheme 3) possessing potent activity against the Herpes simplex virus

(HSVs) 1 and 2 in the [3+2] cycloaddition (32CA) reaction of acetonitrile-N--oxide ANO **11** and acetyl-protected 5-ethynyl-2'-deoxyuridine EDU **12**. The nitrile oxide ANO **11** was generated *in situ* from the corresponding oxime on treatment with a commercial bleach agent (4 % NaOCl in THF). The reaction was performed at room temperature and was found to be completely *ortho* regioselective, leading exclusively to the isoxazole **13** (Scheme 3).

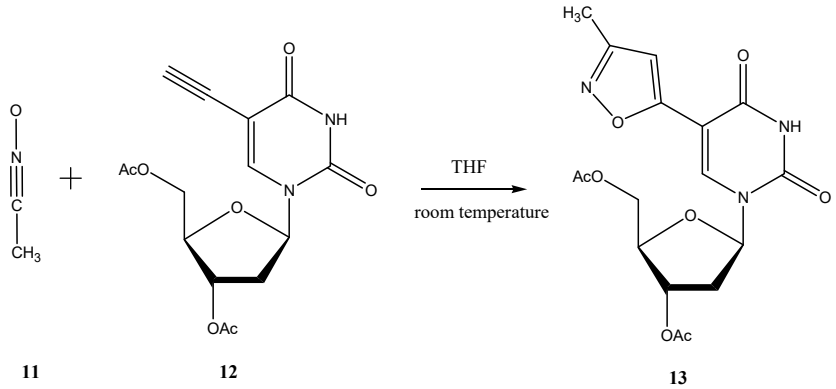

Scheme 3. 32CA reaction of ANO **11** and EDU **12**.

In 2016, Domingo proposed the molecular electron density theory (MEDT)[20,21] when considering the decisive role of electron density changes in the molecular reactivity of chemical reactions. A reasonably good correlation can be established within MEDT between the electronic structure and the reactivity of the three atom components (TACs) participating in 32CA reactions,[20,21] allowing the classification of the respective reactions into the pseudodiradical[20,21] type (pdr-type: when the TACs show the presence of two pseudoradical centres and are associated with very low energy barrier and earlier TSs), the pseudo(mono)radical[20] type,[21] (pmr-type: when the TACs show the presence of one pseudoradical centres and less reactivity than the pdr-type), the carbenoid[20,21] type (cb-type; when, the TACs show the presence of one carbenoid centres and almost similar reactivity as the pmr-type) and the zwitterionic[21] type (zw-type: when the TACs do not show the presence of any pseudoradical or carbenoid centres and demand highest energy barrier with adequate electrophilic-nucleophilic interactions). The predicted reactivity[21] trend, pdr-type > pmr-type ≈ cb-type > zw-type was observed in the experimental findings. MEDT has been successfully applied to study several aspects of cycloaddition reactions, namely the chemo,[21] regio[21] and stereoselectivity,[21] substituent effects,[21] copper catalyzed[21] and Grignard reagent[21] mediated 32CA reactions, strain promoted azide-alkyne cycloadditions (SPAAC),[22] unexpected reactivity of electrophilic diazo-

alkanes,[23] 32CA reactions of strained allenes,[21] competitiveness of Diels Alder and Alder ene reactions,[21] *etc.*

Herein, the MEDT report on the 32CA reaction of acetonitrile-N-oxide ANO **11** and acetyl-protected 5-ethynyl-2'-deoxyuridine EDU **12** experimentally performed by Lee *et al.*[19] are presented to generate the antiviral sugar nucleoside isoxazole. This MEDT study provides the selectivity and solvent effect predictions for the antiviral isoxazole synthesis that to the best of knowledge has not been reported. The MPWB1K/6-311G(d,p) level of theory has been reported as the appropriate computational model for 32CA reactions in several recent studies[21] and is therefore applied for this investigation.

This study is divided into five sections: 1) the electron localization function[24,25] (ELF) of the reagents ANO **11** and EDU **12** were studied to determine the electronic structures; 2) a conceptual density functional theory[26,27] (CDFT) analysis at the ground state of the reagents ANO **11** and EDU **12** was performed to initially comprehend the electronic flux between the reagents; 3) the potential energy surfaces[28] (PES) along the feasible regioisomeric pathways were followed to study the energy profile. Note that the energy profile was studied in the gas phase, toluene, THF, dichloroethane, acetonitrile, DMSO and water to assess the influence of solvent polarity on the energy profile. The global electron density transfer[29] (GEDT)[29] at the TSs was calculated to predict the polar character; 4) the intermolecular interactions at the TSs were studied from the topological analysis of the ELF and the quantum theory of atoms-in molecules (QTAIM),[30,31] with the characterization of the non-covalent interactions from the independent gradient model[32] (IGM) analysis considering the Hirshfield partition of electron density[33] (IGMH); 5) and finally, the mechanism of the energetically feasible reaction path was studied from the bonding evolution theory (BET) study.[34]

COMPUTATIONAL METHODS

Computation details are given in Supplementary material to this paper.

RESULTS AND DISCUSSION

*Analysis of the ELF topology of the reactants acetonitrile-N-oxide ANO **11** and acetyl-protected 5-ethynyl-2'-deoxyuridine EDU **12***

The ELF constructed by Becke and Edgecombe[24] gives a precise mathematical representation of the electronic structure in a chemical system and was subsequently extended by Silvi and Savin[25] to define three localization attractors, namely the core, bonding and non-bonding ones to characterize different electronic regions in a chemical system. The core basins C(x) are considered by the topological partitioning of the ELF gradient field surrounding the atomic nuclei; the monosynaptic valence basins V(X) are associated with the non-bonding electron density of the lone pair or the pseudoradical centre at atom X and the disynaptic basins V(X,Y) are associated with the bonding region between X and

Y. Depending on the topological analysis of the ELF, the standard classification of the three atom components (TACs) participating in 32CA reactions was proposed by Domingo[20], namely the pseudodiradical,[20,21] pseudo(mono)radical,[20,21] carbenoid[20,21] and the zwitterionic TACs.[20,21,] The ELF localization domains and the most significant valence basin populations of the MPWB1K/6--311G(d,p) optimized reagents acetonitrile-N-oxide ANO **11** and acetyl-protected 5-ethynyl-2'-deoxyuridine EDU **12** are given in Fig. 1.

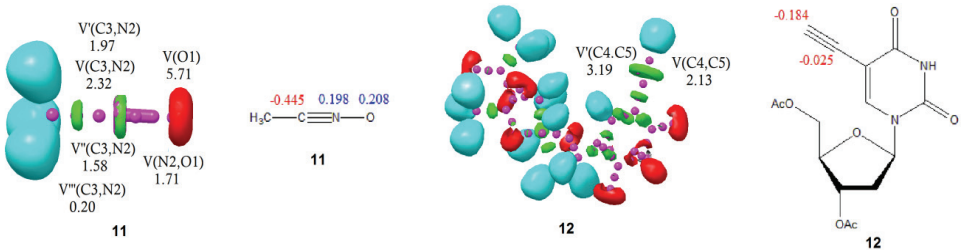

Fig 1. MPWB1K/6-311G(d,p) ELF localization domains and the basin attractor positions of the acetonitrile-N-oxide ANO **11** and acetyl-protected 5-ethynyl-2'-deoxyuridine EDU **12** and the proposed Lewis-like structures together with the natural atomic charges in average number of electrons e. Negative and positive charges are shown in red and blue colours, respectively. Protonated basins are shown in blue, monosynaptic basins in red, disynaptic basins in green and the attractor positions in magenta colour (Isovalue = 0.83).

The ELF of ANO **11** shows the presence of V(O1) monosynaptic basin integrating 5.71 e associated with the non-bonding electron density on O1 oxygen, the V(C3,N2), V′(C3,N2), V″(C3,N2) and V‴(C3,N2) disynaptic basins integrating a total population of 6.07 e associated with the C3–N2 triple bond and V(N2,O1) disynaptic basin integrating 1.71 e associated with the N2–O1 single bond. The absence of any pseudoradical or carbenoid centre in ANO **11** classifies it as a zwitterionic TAC. The ELF of EDU **12** shows the presence of disynaptic basins V(C4,C5) and V′(C4,C5) integrating a total population of 5.32 e associated with the C4–C5 triple bond. The Lewis like structures of the reagents ANO **11** and EDU **12** and the NBO derived charges are given in Fig. 1. O1 oxygen is positively charged by 0.21 e, while C3 carbon is negatively charged by –0.45 e, indicating the polarization of charge in the nitrile oxide framework. C_α carbon of EDU **12** shows a negligible charge of –0.03, while the C_β carbon is negatively charged by –0.18 e owing to the conjugated double bond with the C_α–C_β triple bond moiety.

Analysis of the CDFT indices

The analysis of CDFT[26,27]reactivity indices allows an initial comprehension of the direction of electronic flux between the reagents to be obtained. The standard reactivity[27,35,36] scales were defined at the B3LYP/6-31G(d) level of theory and

accordingly, the CDFT indices, namely the electronic chemical potential – μ,[26] chemical hardness – η,[37] electrophilicity – ω[38] and nucleophilicity[36] N indices in eV of the reagents ANO **11** and EDU **12** were computed at the B3LYP/6-31G(d) computational level. The electronic chemical potential μ of ANO **11** (μ = –2.90 eV) is higher than that of EDU **12** (μ = –3.90 eV), suggesting the electronic flux from ANO **11** to EDU **12** along the 32CA reaction. ANO **11** (ω= 0.55 eV) is classified as the marginal electrophile, while EDU **12** (ω= 1.58 eV) as the strong electrophile. Both ANO **11** (N = 2.39 eV) and EDU **12** (N = 2.80 eV) are classified as the moderate nucleophiles within the standard nucleophilcity scale.[36]

Analysis of the potential energy surface along the feasible regioisomeric pathways

The 32CA reaction of ANO **11** and EDU **12** can occur along two regioisomeric paths, namely *ortho* and *meta*, associated respectively with the attack of nitrone oxygen to the C_α and C_β carbon of EDU **12** (Scheme 4). The search for the stationary points along the PES of these two reaction paths allowed the location of the reagents ANO **11** and EDU **12**, the TSs (**TS1** and **TS2**) and the products **13** and **14**. Some appealing conclusions could be derived from the energy profile study:

i) The 32CA reaction of ANO **11** and EDU **12** shows negative reaction free energies from –262.5 to –306.4 kJ mol^{-1}, suggesting kinetic control and hence, irreversibility.

ii) The enthalpy of activation of **TS1** is lower than that of **TS2** by 24.3, 23.0, 22.1, 21.7, 22.1, 21.7 and 21.7 kJ mol^{-1} in gas phase, toluene, THF, dichloroethane, acetonitrile, DMSO and water, respectively, suggesting exclusive *ortho* selectivity in complete agreement with the experimental finding.[19]

iii) **TS1** shows an activation enthalpy of 53.9 kJ mol^{-1} in gas phase that is increased to 63.5 kJ mol^{-1} in toluene, 69.0 kJ mol^{-1} in THF, 71.1 kJ mol^{-1} in acetonitrile and 71.5 kJ mol^{-1} in dichloroethane, DMSO and water, suggesting an increase of 17.6 kJ mol^{-1} from gas phase to water, thus indicating the energetically feasible reaction in low polar solvents.

iv) The 32CA reaction shows negative entropies of activation owing to the bimolecular character. The unfavourable entropies result in the increase in the free energies of activation by 49.7–56.5 kJ mol^{-1} relative to the activation enthalpies, while the reaction free energies were decreased by 51.9–69.0 kJ mol^{-1} due to the entropy factor consideration.

Thermodynamic correction to the reaction energies results in increase in the activation enthalpies by 0–4.2 kJ mol^{-1}, while the reaction enthalpies are decreased by 15.5–19.6 kJ mol^{-1} relative to the activation energies. The GEDT at the TSs were calculated to assess the polar character and are listed in Table I. The located TSs show minimal GEDT from 0.001 to 0.055 e characteristic of null

electron density flux[39] (NEDF), indicating the non-polar character of the 32CA reaction.

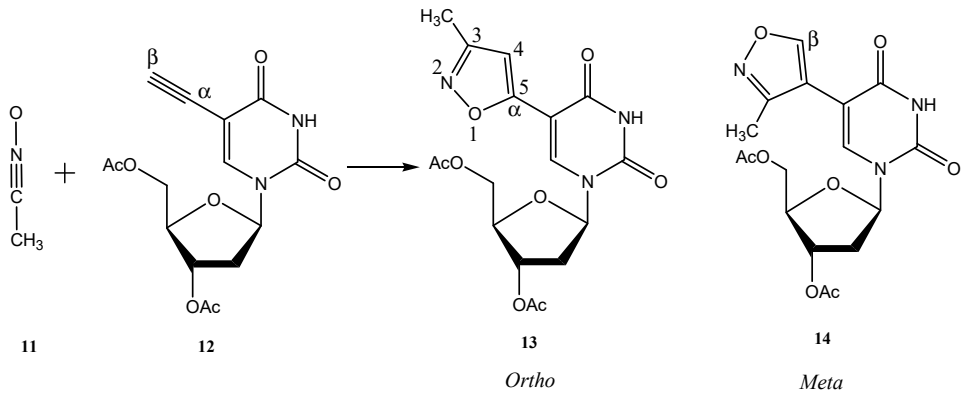

Scheme 4. Studied regioisomeric paths for the 32CA reactions of ANO **11** and EDU **12**.

TABLE I. MPWB1K/6-311G(d,p) relative changes in energies (ΔE), enthalpies (ΔH), free energies (ΔG), kJ mol^{-1}, entropies (ΔS), J mol^{-1} K^{-1}, and GEDT (in average number of electrons, calculated as the summation of the difference in the total electronic population of the two reacting counterparts in the transition state) of TSs and products for the 32CA reactions of ANO **11** and EDU **12**

Cmpd.	Solvent	ΔE	ΔH	ΔS	ΔG	GEDT	Product	ΔE	ΔH	ΔS	ΔG
TS1	Gas phase	53.5	53.9	–174.7	106.2	0.001	**13**	–380.8	–365.3	–198.6	–306.4
TS2	Gas phase	76.1	78.2	–188.5	134.2	0.055	**14**	–361.6	–345.7	–231.2	–276.7
TS1	Toluene	62.7	63.5	–180.2	117.0	0.005	**13**	–367.0	–351.1	–197.3	–292.6
TS2	Toluene	84.9	86.5	–188.9	143.0	0.043	**14**	–348.2	–332.3	–202.7	–271.7
TS1	THF	68.6	69.0	–184.8	124.1	0.005	**13**	–358.2	–342.3	–191.0	–285.1
TS2	THF	89.9	91.1	–184.8	146.3	0.033	**14**	–341.9	–325.6	–210.7	–262.5
TS1	Dichloroethane	67.7	71.5	–167.2	121.2	0.006	**13**	–357.4	–338.2	–173.5	–286.3
TS2	Dichloroethane	89.0	93.2	–166.4	143.0	0.031	**14**	–341.5	–321.9	–186.8	–266.3
TS1	Acetonitrile	71.1	71.1	–175.6	123.7	0.005	**13**	–354.5	–338.2	–188.1	–282.2
TS2	Acetonitrile	92.0	93.2	–181.0	147.1	0.027	**14**	–339.4	–323.1	–197.7	–264.2
TS1	DMSO	71.1	71.5	–175.6	123.7	0.006	**13**	–354.5	–337.7	–187.7	–281.7
TS2	DMSO	92.0	93.2	–180.6	147.1	0.027	**14**	–339.0	–322.7	–194.8	–264.6
TS1	Water	71.5	71.5	–175.6	124.1	0.005	**13**	–354.0	–337.3	–187.3	–281.7
TS2	Water	92.0	93.2	–180.2	147.1	0.026	**14**	–339.0	–322.7	–199.0	–263.3

The gas phase geometries of **TS1** and **TS2** are given in Fig 2. At **TS1**, the distance between the C5 and O1 interacting centres is greater than that between the C3 and C4 interacting centres by 0.235 Å, while at **TS2**, the distance between the C3 and C4 interacting centres is more than that between the C5 and O1 interacting centres by 0.142 Å, suggesting higher asynchronicity in **TS1** relative to **TS2**. Inclusion of solvent effects causes minimal changes in the distance between the C3 and C4 interacting centres, which are between 2.118–2.145 Å in **TS1** and between

2.125–2.250 Å in **TS2**, while the distance between the C5 and O1 interacting centres are between 2.340–2.380 Å in **TS1** and between 2.108–2.229 Å in **TS2**.

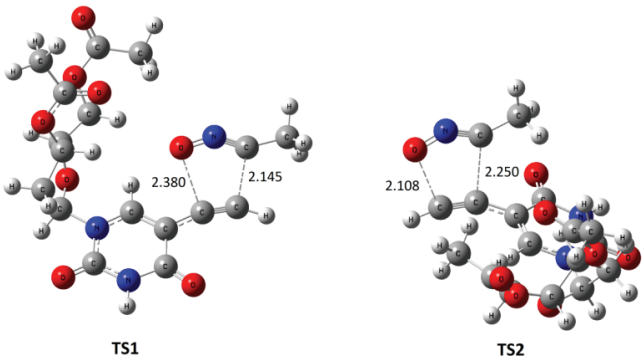

Fig. 2. MPWB1K/6-311G(d,p) optimized gas phase TSs.

Topological analysis of the ELF and AIM at the TSs

The topological analysis of the ELF at the TSs allows their electronic structure and the extent of the bond formation process to be assessed. The ELF localization domains and the basin attractor positions at the gas phase TSs associated with the 32CA reaction are shown in Fig 3. The ELF of **TS1** shows the presence of V(O1) and V′(O1) monosynaptic basins integrating a total population of 5.70 e while the ELF of **TS2** shows the presence of V(O1), V′(O1) and V″(O1) integrating 5.61 e associated with the non-bonding electron density on O1 oxygen. The ELF of **TS1** and **TS2** show the presence of V(C3,N2) and V′(C3,N2) disynaptic basins integrating a total population of 4.45 e associated with the C3–N2 bonding region and the V(N2) monosynaptic basin integrating 1.95 and 1.94 e at **TS1** and **TS2** associated with the non-bonding electron density at N2 nitrogen. Note that the C3–N2 bonding region is depopulated from 6.07 e at ANO **11** to 4.45 e at **TS1** and **TS2**, indicating the rupture of the C3–N2 triple bond at the TSs to create the non-bonding electron density at the N2 nitrogen. The V(N2,O1) disynaptic basin is depopulated from 1.71 e at ANO **1** to 1.48 e at **TS1** and **TS2**. Thus, the V(N2) monosynaptic basin mainly derives the electron density from the C3–N2 bonding region. The ELF of **TS2** shows the presence of V(C3) monosynaptic basin integrating 0.04 e associated with the formation of pseudoradical centre at C3, which is absent in **TS1**, suggesting that the less energetically feasible **TS2** is more advanced than **TS1** along the reaction path. The ELF of **TS1** and **TS2** show the presence of V(C4,C5) and V′(C4,C5) disynaptic basins integrating 5.00 and 4.92 e associated with the C4–C5 bonding region. Note that the C4–C5 bonding region experiences depopulation from 5.32 e in EDU **2** to 5.00 e and 4.92 e at the TSs to create a pseudoradical centre at C4

indicated by the presence of the monosynaptic basin V(C4) integrating 0.14 e and 0.33 e at **TS1** and **TS2**, respectively.

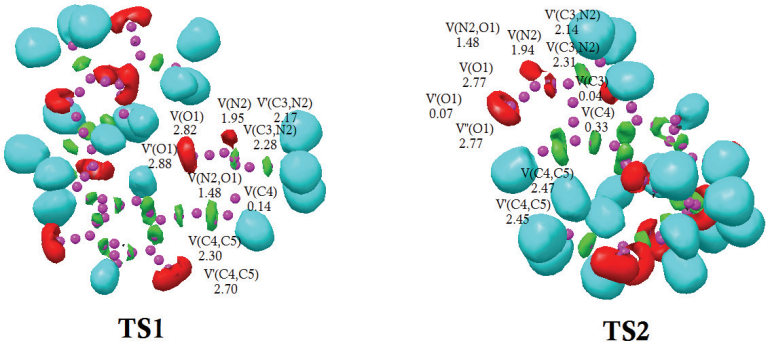

TS1 **TS2**

Fig. 3. MPWB1K/6-311G(d,p) ELF localization domains and the basin attractor positions of gas phase TSs **TS1** and **TS2**. Protonated basins are shown in blue, monosynaptic basins in red, disynaptic basins in green and the attractor positions in magenta colour (Isovalue = 0.83).

The intermolecular interactions at the TSs can be characterized from the topological analysis of the AIM proposed by Bader and coworkers.[30,31]

The contour line maps of the Laplacian of the electron density $\nabla^2\rho(r_c)$ at **TS1** and **TS2** on the molecular plane defined by atoms for C-O and C-C bond formation are shown in Fig. 4. The bond critical points **CP1** and **CP2** are associated with the C–O and C–C interacting regions of the TSs. The total electron density ρ at **CP1** are 0.034 and 0.056 e while those at **CP2** are 0.060 and 0.051 e for **TS1** and **TS2** respectively, suggesting higher accumulation of electron density at the C–C interacting region compared to that at the C–O interacting region of **TS1**, while the total electron density at the C–C and C–O interacting regions are comparable at **TS2**, in line with the higher asynchronicity in **TS1** (Fig. 2). **CP1** ($\nabla^2\rho(r_c)$ = 0.084 au) and **CP2** ($\nabla^2\rho(r_c)$ = 0.058 au) show the positive Laplacian of the electron densities at **TS1,** suggesting non-covalent interactions. Similarly, the positive Laplacian of the electron densities 0.136 and 0.061 au are calculated at **CP1** and **CP2** of **TS2**. These values suggest that the formation of covalent bonds has not commenced at the TSs in agreement with the ELF study.

The non-covalent interactions at the TSs can be characterized from the recently proposed IGM analysis based on Hirshfield partition of electron density. The IGMH isosurfaces of **TS1** and **TS2** are given in Fig 5. The C5–O1 interacting region of **TS1** shows strong attractive non-covalent interactions (blue portions), while the C3–C4 interacting region shows both strong repulsive (red portions) as well as strong attractive (blue portions) interactions. At **TS1**, hydrogen bonding (green portion) is also observed with the O1 oxygen and the nearby hydrogen atoms. The C5–O1 and C3–C4 interacting regions of **TS2** show both

strong attractive (blue portions) and strong repulsive (red portions) non-covalent interactions in the IGMH isosurface (Fig. 5).

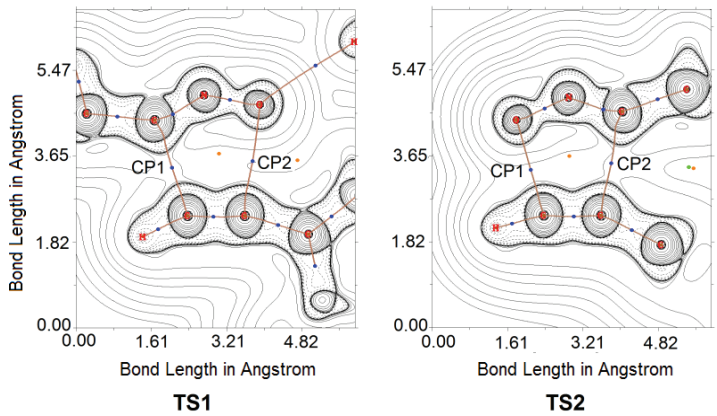

Fig. 4. Representations of the contour line maps of the Laplacian of the electron density at TS1 and TS2 on the molecular plane defined by atoms for C5–O1 (C–O) and C3–C4 (C–C) bond formation, **CP1** and **CP2** critical points respectively are marked on the representation.

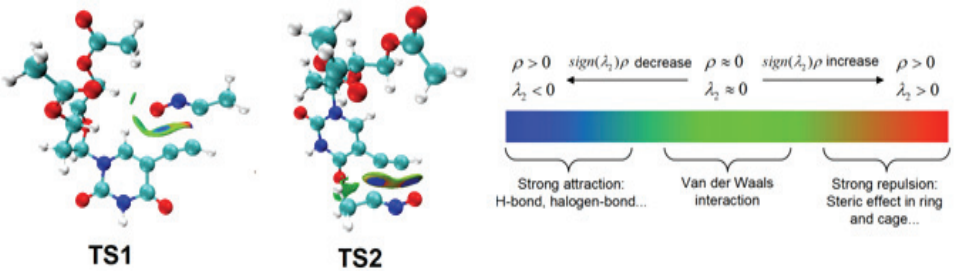

Fig. 5. IGMH isosurfaces (Isovalue = 0.01) at the **TS1** and **TS2**.

BET study along the favoured regiochemical pathway

The BET proposed by Krokoidis[34] applies the conjunction of the ELF[24,25] and the Thom's Catastrophe theory[40] to structure the plausible mechanism of a chemical reaction. Herein, the BET of the energetically feasible *ortho* pathway is studied at MPWB1K/6-311G(d,p) level of theory, which divides the reaction path into seven topological phases. The most significant ELF valence basin populations at the starting point of each phase (**S0**–**S6**) and the product **13** are given in Table II, with the simple representation of the predicted mechanism in Scheme 5. Phase I starts at **S0** (d(O–C5) = 2.75 Å and d(C3–C4) = 2.76 Å) and shows the presence of five V(O1) monosynaptic basins integrating a total population of 5.76 e associated with the non-bonding electron density of O1 oxygen. The V(N2,O1) and V(C3,N2) disynaptic basins integrate at 1.66 and 6.00 e associated with the N2–O1 single bond and the C3–N2 triple bond respectively. The ELF of

S0 also shows the presence of three V(C4,C5) disynaptic basins integrating 5.28 e associated with the C4–C5 triple bond. Thus, the ELF of **S0** is similar to that of the separated reagents ANO **11** and EDU **12** (Fig. 1) and shows minimal electron density flux with the GEDT of 0.03 e. Phase II starts at **S1** (*d*(O1–C5) = 2.55 Å and *d*(C3–C4) = 2.44 Å) and is characterized by the presence of V(N2) monosynaptic basin integrating 0.90 e associated with the non-bonding electron density at N2 nitrogen which mainly derives the electron density from the C3–N2 bonding region.

TABLE II. ELF valence basin populations, distances of the forming bonds, and relative electronic energies of the IRC structures **S0**–**S6** defining the seven phases characterizing the molecular mechanism of the 32CA reaction of **11** and **12**

Parameter	Phase							
	I	II	III	IV	V	VI	VII	
	Structure							
	S0	**S1**	**S2**	**S3**	**S4**	**S5**	**S6**	**13**
d(O1–C5) / Å	2.749	2.546	2.380	2.353	2.241	2.072	1.553	1.333
d(C3–C4) / Å	2.758	2.440	2.145	2.095	1.893	1.657	1.937	1.417
ΔE / kJ mol^{-1}	0.0	29.3	53.5	52.3	18.8	–74.4	–137.5	–380.8
GEDT	0.03	0.05	0.001	0.02	0.11	0.22	0.26	0.27
V(O1)	2.25	2.89	2.88	2.89	2.88	2.91	2.63	4.39
V'(O1)	2.48	2.58	2.82	2.81	2.80	2.75	2.62	
V''(O1)	0.65	0.26						
V'''(O1)	0.23							
V''''(O1)	0.15							
V(N2,O1)	1.66	1.60	1.48	1.46	1.40	1.33	1.36	1.16
V(C3,N2)	6.00	2.68	2.28	2.06	1.89	1.74	1.75	2.85
V'(C3,N2)		2.53	2.17	2.09	1.84	1.65	1.53	
V(C4,C5)	3.35	5.25	2.30	2.35	2.24	2.03	1.92	2.59
V'(C4.C5)	1.84		2.70	2.53	2.21	2.03	1.91	
V''(C4,C5)	0.09							
V(N2)		0.90	1.95	2.02	2.33	2.59	2.63	3.09
V(C4)			0.14	0.29				
V(C3)				0.27				
V(C5)						0.13		
V(C3,C4)					1.32	1.86	2.09	2.50
V(O1,C5)							0.68	1.70

Note that the V(C3,N2) disynaptic basin experiences depopulation from 6.00 e in **S0** to 5.21 e in **S1**. This electronic change requires 29.3 kJ mol^{-1} and the GEDT at **S1** is 0.05 e. Phase III starts at **S2** (*d*(O1–C5) = 2.38 Å and *d*(C3–C4) = = 2.15 Å) and is characterized by the presence of V(C4) monosynaptic basin integrating 0.14 e associated with the pseudoradical centre at C4, which derives electron density from the C4–C5 bonding region. Note that the C4–C5 bonding region is depopulated from 5.25 e in **S1** to 5.00 e in **S2**. **TS1** belongs to this phase

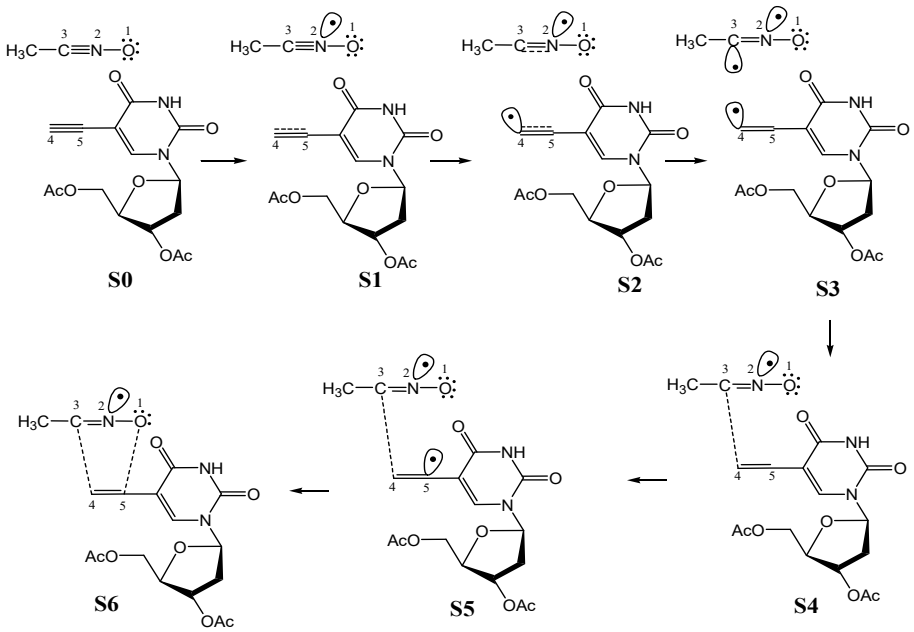

Scheme 5. Simplified representation of the mechanism along the *ortho* reaction path form the bonding evolution theory study.

with the GEDT of 0.001 suggesting non polar character of the 32CA reaction. Phase IV starts at **S3** (d(O1–C5) = 2.35 Å and d(C3–C4) = 2.10 Å) and is characterized by the presence of V(C3) monosynaptic basin integrating 0.27 e associated with the pseudoradical centre at C3, which is created by deriving electron density from the C3–N2 bonding region. Note that the C3–N2 bonding region is depopulated from 4.45 e in **S2** to 4.15 e in **S3**. Phase V starts at **S4** (d(O1–C5) = = 2.24 Å and d(C3–C4) = 1.89 Å) and is characterized by the formation of V(C3,C4) disynaptic basin integrating 1.32 e associated with the C3–C4 single bond. Note that the pseudoradical centres at C3 and C4 couple to form the C3–C4 bond at a distance of 1.89 Å and accordingly, the V(C3) and V(C4) monosynaptic basins are not observed in this phase. Phase VI starts at **S5** (d(O1–C5) = = 2.07 Å and d(C3–C4) = 1.66 Å) and is characterized by the by the presence of V(C5) monosynaptic basin integrating 0.13 e associated with the pseudoradical centre at C5, which derives electron density from the C4–C5 bonding region. Note that the C4–C5 bonding region is depopulated from 4.45 e in **S4** to 4.06 e in **S5**. Phase VII starts at **S6** (d(O1–C5) = 1.55 Å and d(C3–C4) = 1.94 Å) and is characterized by the formation of the V(O1,C5) disynaptic basin integrating 0.68 e associated with the C5–O1 single bond. Note that the pseudoradical centres at C5 couples with part of the non-bonding electron density at O1 oxygen to form the C3–C4 bond at a distance of 1.55 Å and accordingly, the V(C5) monosyn-

aptic basin is not observed in this phase. Note that the formation of the O1–C5 bond begins when the formation of C3–C4 bond has been 84 %, completed suggesting the high asynchronicity in the bond formation process. This is in agreement with the longer C5–O1 bond distance compared to C3–C4 at **TS1** and greater accumulation of electron density in the C3–C4 interacting region relative to that in the C5–O1 observed in the AIM study.

CONCLUSIONS

The 32CA reaction of acetonitrile-N-oxide ANO **11** and acetyl-protected 5-ethynyl-2'-deoxyuridine EDU **12** leading to the sugar nucleoside isoxazole has been studied within the MEDT framework at the MPWB1K/6-311G(d,p) level of theory. The ELF topological study classifies ANO **11** as a zwitterionic species and the CDFT reactivity indices predict electronic flux from ANO **11** to EDU **12** along the 32CA reaction. The reaction is kinetically controlled with complete *ortho* regioselectivity in agreement with the experimental findings. The activation parameters increase with increasing solvent polarity, suggesting facile reaction in low polar solvents. The minimal GEDT at the TSs from ANO **11** to EDU **12** predicts non-polar character. Early TSs were located in which the formation of covalent bonds has not commenced, while the strong repulsive and strong attractive non-covalent interactions were visualized in the IGMH isosurfaces of the TSs. The BET study predicts earlier C3–C4 bond formation with high asynchronicity in the bond formation process.

SUPPLEMENTARY MATERIAL

Additional data and information are available electronically at the pages of journal website: https://www.shd-pub.org.rs/index.php/JSCS/article/view/11277, or from the corresponding author on request.

ИЗВОД

СКИДАЊЕ КОПРЕНЕ СА РЕГИОСЕЛЕКТИВНЕ СИНТЕЗЕ АНТИВИРУСНОГ 5-ИЗОКСАЗОЛ-5-ИЛ-2'-ДЕЗОКСИУРИДИНА СА ПЕРСПЕКТИВЕ ТЕОРИЈЕ ЕЛЕКТРОНСКЕ ГУСТИНЕ МОЛЕКУЛА

NIVEDITA ACHARJEE[1], HAYDAR A MOHAMMAD-SALIM[2] и MRINMOY CHAKRABORTY[3]

[1]*Department of Chemistry, Durgapur Government College, Durgapur-713214, West Bengal, India,* [2]*Department of Chemistry, University of Zakho, Duhok 42001, Iraq и* [3]*Department of Electronics and Communication Engineering, Dr. B. C. Roy Engineering College, Durgapur-713206, West Bengal, India*

Проучавана је региоселективна синтеза изоксазолских аналога, моћних антивирусних шећерних нуклеозида, помоћу [3+2] циклоадиционе реакције (32CA) ацетонитрил-N-оксида (ANO) и ацетилом заштићеног 5-етинил-2'-дезоксиуридина (EDU), на MPWB1K/6-311G(d,p) нивоу теорије из перспективе теорије електронске густине у молекулу (MEDT). ANO је на основу анализе функције локализације електрона (ELF) класификован као zwitter-јонска врста без икаквог псеудорадикалског или карбеноидног центра. *ortho* Региоизомер је енергетски повољнији у односу на *meta* уз промену енталпије активације од 21,7 до 24,3 kJ mol^{-1}, што сугерише потпуну региоселективност у

складу са експериментом. Промена енталпија активације од 53,9 kJ mol^{-1} у гасној фази расте до 71,5 kJ mol^{-1} у води указујући да је реакција олакшана у неполарним растварачима. Минималан пренос глобалне електронске густине (GEDT) у прелазним стањима указује на неполаран карактер и да формирање нових ковалентних веза није почело у лоцираном прелазном стању и показује нековалентне међумолекулске интеракције на основу студије атома у молекулу (AIM и) из изо-површина модела независног градијента (IGM). AIM анализа показује повећану акумулацију електронске густине у области C–C везе у поређењу са C–O везом, а раније формирање C–C везе је предвиђено студијом теорије еволуције везивања (BET).

(Примљено 14. октобра, ревидирано 3. децембра, прихваћено 7. децембра 2021)

REFERENCES

1. J. Jampilek, *Molecules* **24** (2019) 3839 (https://doi.org/10.3390/molecules24213839)
2. A. P. Taylor, R. P. Robinson, Y. M. Fobian, D. C. Blakemore, L. H. Jones, O. Fadeyi, *Org. Biomol. Chem.* **14** (2016) 6611 (https://doi.org/10.1039/C6OB00936K)
3. A. Padwa, W. H. Pearson, *Synthetic Application of 1,3-Dipolar Cycloaddition Chemistry Toward Heterocycles and Natural Products*, Wiley, New York, 2002 (https://doi.org/10.1002/0471221902)
4. Y. Walunj, P. Mhaske, P. Kulkarni, *Mini-Rev. Org. Chem.* **18** (2021) 55 (https://doi.org/10.2174/1570193X17999200511131621)
5. E. Rajanarendar, S. Rama Krishna, D. Nagaraju, K. G. Reddy, B. Kishore, Y. N. Reddy, *Bioorg. Med. Chem. Lett.* **25** (2015) 1630 (https://doi.org/10.1016/j.bmcl.2015.01.041)
6. P. Vitale, MG Perrone, P. Malerba, A. Lavecchia, A. Scilimati, *Eur. J. Med. Chem.* **74** (2014) 606 (https://doi.org/10.1016/j.ejmech.2013.12.023)
7. R. J. Rama Rao, A. K. S. B. Rao, N. Sreenivas, B. S. Kumar, Y. L. N. Murthy, *J. Korean. Chem. Soc.* **55** (2011) 243 (https://doi.org/10.5012/jkcs.2011.55.2.243)
8. L-F. Yu, W. Tückmantel, J. B. Eaton, B. Caldarone, A. Fedolak, T. Hanania, D. Brunner, R. J. Lukas, A. P. Kozikowski, *J. Med. Chem.* **55** (2012) 812 (https://doi.org/10.1021/jm201301h)
9. B. Frølund, L. S. Jensen, S. I. Storustovu, T. B. Stensbøl, B. Ebert, J. Kehler, P. Krogsgaard-Larsen, T. Liljefors*, J. Med. Chem.* **50** (2007) 1988 (https://doi.org/10.1021/jm070038n)
10. N. Agarwal, P. Mishra, *Med. Chem. Res.* **27** (2018) 1309 (https://doi.org/10.1007/s00044-018-2152-6)
11. J. Zhu, J. Mo, H-z. Lin, Y. Chen, Hao-peng Sun, *Bio. Med. Chem.* **26** (2018) 3065 (https://doi.org/10.1016/j.bmc.2018.05.013)
12. A. M. Eid ,M. Hawash,J. Amer, A. Jarrar, S. Qadri, I. Alnimer,A. Sharaf, R. Zalmoot, O. Hammoudie,S. Hameedi, A. Mousa, *BioMed Res. Int.* (2021) 6633297(https://doi.org/10.1155/2021/6633297)
13. L. Claisen, *Ber der Dtsch Chem Ges*. **36** (1903) 3664 (https://doi.org/10.1002/cber.190303603168)
14. T. V. Hansen, P. Wu, V. V. Fokin, *J. Org. Chem.* **70** (2005) 7761 (https://doi.org/10.1021/jo050163b)
15. L.-E. Carloni, S. Mohnani,D. Bonifazi, *Eur. J. Org. Chem.* (2019) 7322(https://doi.org/10.1002/ejoc.201901045)
16. K. L. Seley-Radtke, M. K. Yates, *Antivir. Res.* **154** (2018) 66 (https://doi.org/10.1016/j.antiviral.2018.04.004)

17. L. P. Jordheim, D. Durantel, F. Zoulim, C. Dumontet, *Nat. Rev. Drug. Discov.* **12** (2013) 447 (https://doi.org/10.1038/nrd4010)
18. E. Ichikawa, K. Kato, *Curr. Med. Chem.* **8** (2001) 385 (https://doi.org/10.2174/0929867013373471)
19. Y-S. Lee, S. M. Park, B. H. Kim, *Bioorg. Med. Chem. Lett.* **19** (2009) 1126 (https://doi.org/10.1016/j.bmcl.2008.12.103)
20. L. R. Domingo, *Molecules* **21** (2016) 1319 (https://doi.org/10.3390/molecules21101319)
21. L. R. Domingo, N. Acharjee, *Molecular Electron Density Theory: A New Theoretical Outlook on Organic Chemistry*. in *Frontiers in Computational Chemistry*, Z. Ul-Haq, A. K. Wilson, Eds., Bentham and Science, Singapore, 2020, pp. 174–227 (https://doi.org/10.2174/9789811457791120050007)
22. L. R. Domingo, N. Acharjee, *New J. Chem.* **44** (2020) 13633 (https://doi.org/10.1039/D0NJ02711A)
23. L. R. Domingo, M. R. Gutiérrez, N. Acharjee, *Chemistry* **3** (2021) 74 (https://doi.org/10.3390/chemistry3010006)
24. A. D. Becke, K. E. Edgecombe, *J. Chem. Phys*. **92** (1990) 5397 (https://doi.org/10.1063/1.458517)
25. B. Silvi, A. Savin, *Nature* 371 (1994) 683 (https://www.nature.com/articles/371683a0)
26. R. G. Parr, W. Yang, *Density functional theory of atoms and molecules*, Oxford University Press, New York, 1989
27. L. R. Domingo, M. R. Gutiérrez, P. Pérez, *Molecules* **21** (2016) 748 (https://doi.org/10.3390/molecules21060748)
28. S. J. Moss, C. J. Coady, *J. Chem. Educ.* **60** (1983) 455 (https://doi.org/10.1021/ed060p455)
29. L. R. Domingo, *RSC Adv*. **4** (2014) 32415 (https://doi.org/10.1039/C4RA04280H)
30. R. F. W. Bader, In *Atoms in Molecules: A Quantum Theory*, Clarendon Press, New York, 1990
31. R. F. W. Bader, H. Essén, *J. Chem. Phys*. **80** (1984) 1943 (https://doi.org/10.1063/1.446956)
32. C. Lefebvre, H. Khartabil, J.-C. Boisson, J. Contreras-García, J.-P. Piquemal, E. Hénon, *ChemPhysChem* **19** (2018) 724 (https://doi.org/10.1002/cphc.201701325)
33. F. De Proft, R. V-Reyes, A. Peeters, C. Von Alsenoy, P. Geerlings, *J. Comput. Chem.* **24** (2003) 463 (https://doi.org/10.1002/jcc.10241)
34. X. Krokidis, S. Noury, B. Silvi, *J. Phys. Chem., A* **101** (1997) 7277. (https://doi.org/10.1021/jp9711508)
35. L. R. Domingo, M. J. Aurell, P. Pérez, R. Contreras, *Tetrahedron* **58** (2002) 4417 (https://doi.org/10.1016/S0040-4020(02)00410-6)
36. L. R. Domingo, P. Pérez, *Org. Biomol. Chem*. **9** (2011) 7168 (https://doi.org/10.1039/C1OB05856H)
37. R. G. Parr, R. G. Pearson, *J. Am. Chem. Soc*. **105** (1983) 7512 (https://doi.org/10.1021/ja00364a005)
38. R. G. Parr, L. von Szentpaly, S. Liu, *J. Am. Chem. Soc.* **121** (1999)1922 (https://doi.org/10.1021/ja983494x)
39. L. R. Domingo, M. R. Gutiérrez, P. Pérez, *RSC Adv*. **10** (2020) 15394 (https://doi.org/10.1039/D0RA01548B)
40. R. Thom, *Stabilité Structurelle et Morphogenèse*, Interéditions, Paris, 1972 (ISBN 2-7296-0081-7).

Journal of the Serbian Chemical Society
JSCS@tmf.bg.ac.rs • www.shd.org.rs/JSCS
J. Serb. Chem. Soc. 87 (6) S235–S236 (2022) *Supplementary material*

SUPPLEMENTARY MATERIAL TO

Unveiling the regioselective synthesis of antiviral 5-isoxazol-5-yl-2'-deoxyuridines from the perspective of a molecular electron density theory

NIVEDITA ACHARJEE[1]*, HAYDAR A. MOHAMMAD-SALIM[2] and MRINMOY CHAKRABORTY[3]

[1]*Department of Chemistry, Durgapur Government College, Durgapur-713214, West Bengal, India,* [2]*Department of Chemistry, University of Zakho, Duhok 42001, Iraq and* [3]*Department of Electronics and Communication Engineering, Dr. B. C. Roy Engineering College, Durgapur-713206, West Bengal, India*

J. Serb. Chem. Soc. 87 (6) (2022) 707–721

COMPUTATIONAL METHODS

Recent studies on polar and non-polar cycloaddition reactions have allowed selecting the MPWB1K[1] functions in conjunction with the 6-311G(d,p)[2] as the most adequate computational model to study 32CA reactions and has been consequently applied in the present MEDT study. The Berny analytical gradient optimization method[3] was used for the optimizations and the stationary points were characterized by frequency calculations verifying the absence of imaginary frequency for the minima and TSs with one imaginary frequency. The energy profile connecting the TS and the associated minima was verified from the Intrinsic Reaction Coordinate (IRC)[4] calculations using the second order González–Schlegel integration method.[5,6] Solvents effects in toluene, THF, dichloroethane, acetonitrile, DMSO and water were studied by optimizing the structures in the respective solvents using the polarizable continuum model (PCM)[7,8] within the self-consistent reaction field (SCRF)[9–11] framework at PCM/ /MPWB1K/6-311G(d,p) level of theory. The thermodynamic calculations were performed at 298 K and 101.325 kPa pressure. Natural population analysis (NPA)[12,13] was performed at the TSs to calculate the GEDT[11] from the sum of natural atomic charges (q) at each framework (f) using the formula GEDT:

$$(f) = \sum_{q \in f} q \tag{1}$$

* Corresponding author. E-mail: nivchem@gmail.com

where the positive GEDT denotes transfer of electron density from the considered framework. The CDFTindices[12,13] were calculated from the standard equations reviewed in Reference 14. All calculations were performed using the Gaussian 16 suite of programs.[14] The topological analysis of the ELF and the AIM and the IGMH calculations were realized using Multiwfn[15] software. The ELF isosurfaces were visualized using UCSF Chimera[16] software, and the IGMH isosurfaces were visualized by VMD software.[17]

REFERENCES

1. Y. Zhao, D. G. Truhlar, *J. Phys. Chem., A* **108** (2004) 6908 (https://doi.org/10.1021/jp048147q)
2. W. J. Hehre, L. Radom, PVR Schleyer, J. Pople, *Ab initio Molecular Orbital Theory*. Wiley, New York, 1986
3. H. B. Schlegel, *J. Comput. Chem.* **3** (1982) 214 (https://doi.org/10.1002/jcc.540030212)
4. K. Fukui, *J. Phys. Chem.* **74** (1970) 4161 (https://doi.org/10.1021/j100717a029)
5. C. González, H. B. Schlegel, *J. Phys. Chem.* **94** (1990) 5523 (https://doi.org/10.1021/j100377a021)
6. C. González, H. B. Schlegel *Chem. Phys.* **95** (1991) 5853 (https://doi.org/10.1063/1.461606)
7. J. Tomasi, M. Persico, *Chem. Rev.* **94** (1994) 2027 (https://doi.org/10.1021/cr00031a013)
8. B. Y. Simkin, I. Sheikhet, *Quantum Chemical and Statistical Theory of Solutions-A Computational Approach*, Ellis Horwood, London, 1995
9. E. Cances, B. Mennucci, J. Tomasi, *J. Chem. Phys.* **107** (1997) 3032 (https://doi.org/10.1063/1.474659)
10. M. Cossi, V. Barone, R. Cammi, J. Tomasi, *Chem. Phys. Lett.* **255** (1996) 327 (https://doi.org/10.1016/0009-2614(96)00349-1)
11. V. Barone, M. Cossi, J. Tomasi, *J. Comput. Chem.* **19** (1998) 404. (https://doi.org/10.1002/(SICI)1096-987X(199803)19:4<404::AID-JCC3>3.0.CO;2-W)
12. A. E. Reed, R. B. Weinstock, F. Weinhold, *J. Chem. Phys*. **83** (1985) 735 (https://doi.org/10.1063/1.449486)
13. A. E. Reed, L. A.Curtiss, F. Weinhold, *Chem. Rev*. **88** (1985) 899 (https://doi.org/10.1021/cr00088a005)
14. *Gaussian 16*, Gaussian, Inc., Wallingford, CT, 2016
15. T. Lu, F. Chen, *J. Comp. Chem*. **33** (2012) 580 (https://doi.org/10.1002/jcc.22885)
16. E. F. Pettersen, T. D. Goddard, C. C. Huang, G. S. Couch, D. M. Greenblatt, E. C. Meng, T. E. Ferrin, *J. Comput. Chem*. **25** (2004) 1605 (https://doi.org/10.1002/jcc.20084)
17. W. Humphrey, A. Dalke, K. Schulten, *J. Molec. Graphics* **14** (1996) 33 (https://doi.org/10.1016/0263-7855(96)00018-5).

Journal of the Serbian Chemical Society
JSCS-info@shd.org.rs • www.shd.org.rs/JSCS

J. Serb. Chem. Soc. *87* (6) 723–734 (2022)
JSCS–5553

Original scientific paper
Published 2 February 2022

Toxic elements in children's crayons and colored pencils: Bioaccessibility assessment

SVETLANA ĐOGO MRAČEVIĆ[1]*, SLAVICA RAŽIĆ[1#], JELENA TRIŠIĆ[2], NIKOLA MITROVIĆ[3] and DANIJELA ĐUKIĆ-ĆOSIĆ[4]

[1]*Department of Analytical Chemistry, University of Belgrade – Faculty of Pharmacy, Vojvode Stepe 450, 11221 Belgrade, Serbia,* [2]*Roche d.o.o., Milutina Milankovića 11a, 11000 Belgrade, Serbia,* [3]*University of Belgrade – Faculty of Pharmacy, Vojvode Stepe 450, 11221 Belgrade, Serbia and* [4]*Department of Toxicology "Akademik Danilo Soldatović", University of Belgrade – Faculty of Pharmacy, Vojvode Stepe 450, 11221 Belgrade, Serbia*

(Received 10 September, revised 23 September, accepted 5 October 2021)

Abstract: Crayons and colored pencils for children may contain toxic elements (TEs) exhibiting potential risk for children's health including cognitive development, after their ingestion, through mouthing and chewing and eventually, their accumulation. The aim of this study was to determine total content of As, Pb, Cr, Cd, Ni and Sb and estimate their bioaccessibility conducting artificial saliva extraction. Sixty samples of colored pencils and crayons from 10 manufacturers were analyzed. Microwave acid assisted digestion followed by inductively coupled plasma optical spectroscopy (ICP-OES) was performed for determination of total content of TEs. Simulation of extraction by artificial saliva was applied to get more reliable data when bioavailability is concerned. The total concentrations of TEs were higher in colored pencils than in crayons and their maximum levels were: 5.78, 9.36, 9.97, 0.615, and 6.63 mg kg^{-1} for As, Pb, Cr, Cd and Ni, respectively. Concentration of Sb was below the detection limit for all investigated samples. This study showed that concentration of As and Pb in several samples did not comply with European Union regulative. Bioaccessibility study showed the high degree of leaching of Cr and As from pencils, but regardless of extracted portions, concentrations of selected investigated TEs were below allowed levels.

Keywords: children toys; toxic elements; ICP-OES, bioaccessibility study; health risk.

* Corresponding author. E-mail: svetlana.djogo@pharmacy.bg.ac.rs
# Serbian Chemical Society member.
https://doi.org/10.2298/JSC20091078D

INTRODUCTION

Children are most susceptible to harmful effects of TEs, having in mind their insufficiently developed detoxication mechanisms, increased intake of food and drinks compared with adults (per unit of mass) as well as tendencies to put things from their environment, especially toys and crayons, in mouth causing the extraction of harmful substances via saliva and swallowing.[1,2] An increased exposition elevates hazardous effects with direct impact on TEs bioavailability, indirectly affecting to physiological parameters and behavioral patterns.[3,4] Drawing and painting in early childhood help children to express themselves and contribute to their physical and psychological development.[1–3] However, it must be taken into account that toys and crayons may have high levels of TEs, such as lead, arsenic, cadmium, chromium and nickel, which can provoke serious health problems.[5] Besides, there are various stabilizers, minerals and pigments, which naturally contain heavy metals and can additionally contribute to potential toxicity. For example, kaolinite, as a constituent in clay and chalk, which is used for children's crayons, contains Pb in concentration range 29–91 mg kg^{-1} of sample.[6] This is serious threat since even a multiple purification processes are frequently insufficient for their removal.

It is common knowledge that children are most vulnerable population when lead poisoning is concerned. For example, two-year old children have the highest concentration of Pb in their blood, partly because they put toys and various objects in their mouth, and recent studies showed that blood Pb concentration even less than 10 mg dm^{-3} can cause adverse health effects and/or decrease cognitive development.[7,8] Canfield *at al.*[8] have shown significant correlation between increased Pb concentration in blood and decrease of full-scale IQ in children. In order to address this problem, European Union adopted new annex[9] to the Toy Safety Directive 2009/48/EC, in late 2016 early 2017, with lower allowable limits for Pb concentrations in children's toys. For dry, brittle, powder-like and playable toys including wooden crayons this value is 2 mg kg^{-1} (instead of previous 13.5 mg kg^{-1}), and for liquid or sticker toys including water colors 0.5 mg kg^{-1} (instead of previous 3.4 mg kg^{-1}).

According to the Agency for Toxic Substances and Disease Registry (ATSDR) 2021[10] As is the first one at the Priority List of Hazardous Substances. Besides that inorganic arsenic is, according to the World Health Organisation (WHO),[11] the International Agency for Research on Cancer (IARC),[12] and the Environmental Protection Agency (EPA),[13] marked as human carcinogen. The arsenic exposure can also cause serious respiratory, gastroinestinal, hepatic, neurological, and immunological effects, as well as effects on the central nervous system and impact on cognitive development of children.[1,14,15] Different studies reported a decrease in Full Scale IQ, verbal comprehension, and working memory in children aged 6–15, associated with increased levels of As in water, urine or

blood.[1,4,16] Cadmium is commonly used in Ni–Cd battery manufacturing, but it is also used as a pigment in plastic, ceramic, and glass industry.[1] Some studies reported correlation of decrease of full-score and performance IQ, with four-years children, and higher frequency of attention and behavioral disorders in children aged 7–16 years with higher levels of Cd in blood and hair.[1,4,17–21] Similarly to the Pb, EU adopted recently new limits for cadmium content in children's toys: 1.3 mg kg^{-1} (instead of previous 1.9 mg kg^{-1}) for dry, brittle, powder-like and playable toys and 0.3 mg kg^{-1} (instead of previous 0.5 mg kg^{-1}) for liquid or sticker toys.[9]

Chromium is present in our environment as a result of both natural occurring element in Earth's crust and anthropogenic activities, such as mining and industrial activities. This element is 17th at the ATSDR list[10] as human carcinogenic and associated with neurological and developmental disorders.[22,23] The main source of children's exposure to cadmium, beside water and food consumption, is associated with chewing and ingestion of inedible materials.[22]

Antimony has a wide range of industrial applications including electronics, plastics and pants production.[24] This element has been used as a pigment for centuries, mainly as antimony sulphide and lead antimonite.[24] Exposure to Sb may result in eye, skin, and lung irritation, but on long-term and chronic exposure may result in the formation of antimoniosis, and causes heart, gastrointestinal, and lung diseases, including pneumoconiosis, and lung cancer.[25] According to EU legislation the permissible limits for Sb content in toys is 45 mg kg^{-1}. However, there is a significant knowledge gap in different areas (environmental chemistry, toxicology and bioavailability of antimony in the environment), and harmonization of required standards for Sb limits is needed.[24]

Human exposure to the nickel can cause various health effects, including immunologic, neurologic and reproductive disorder developments or even carcinogenic effects.[26] Beside, skin allergic reactions can occur after contact, oral intake or inhalation.[27] We are exposed to great number of nickel sources in everyday life, thus European Food Safety Authority (EFSA)[28] stated that more information should be collected based on its bioavailability in foodstuffs, all in order to facilitate the establishment of food quality standards for this metal.

Determination TEs total content is important but, having in mind that mouthing behavior plays an important role in children exposure to metal contamination in toys, pencils, and crayons, the predict of mobilization of heavy metals into saliva and their ingestion during mouthing requires additional attention. Several studies on *in vitro* bioaccessibility tests for prediction of bioavailability of metals to children are published.[4,5,29,30] Those tests were based on extraction with artificial saliva (to simulate mouthing), or/and dil. HCl (to simulate conditions in stomach).

This important topic defined our goals: to evaluate total content of As, Pb, Cr, Cd, Ni and Sb in samples of 30 coloring pencils and 30 crayons from differ-

ent vendors available on the Belgrade's markets and to predict bioavailability of metals based on artificial saliva extraction.

EXPERIMENTAL

Instrumentation and operating conditions

Acid digestion of the samples was performed using microwave digestion system (CEM Mars 5, USA) equipped with polytetrafluoroethylene (PTFE) tubes.

For elements determination inductively coupled plasma optical emission spectrometer (ICP-OES) with axial view (Thermo scientific iCAP 6000 series ICP-spectrometer, USA) coupled with auto sampler Cetac ASX-510 was used. The wavelength used to determine elements were: As (189.042 nm), Cd (214.400 nm), Pb (220.353 nm), Cr (267.716 nm), Ni (231.604 nm) and Sb (206.833 nm). During the analysis, the following instrumental operation conditions were used: RF frequency 27.12 MHz; operating power, 1150 W; peristaltic pump rate: 50 rpm; plasma argon flow rate 0.5 dm^3 min^{-1}; argon carrier flow rate 0.5 dm^3 min^{-1}; sample flow rate 0.02 cm^3 min^{-1}.

For pH control of artificial saliva pH meter Hanna Instruments 901 was used and extraction was performed using IKA® KS 260 Basic shaker.

Materials, reagents and solutions

For the evaluation of heavy metals content, 5 packages of colored pencils and 5 packages of crayons from different manufactures / country of origin (A / China, B / Italy, C / China, D / Czech Republic, E / Germany, F / China and G / China) and different cost range were provided from Belgrade's bookstores. Six samples of different colors from each package were analyzed: three major (yellow, red, and blue) and three derived colors obtained by mixing major ones (green, orange and purple). In that way, the pool of 60 samples was created (30 samples of colored pencils, and 30 of crayons).

All solutions were prepared using analytical grade reagents and deionized water with resistivity of 18.2 MΩ cm, obtained by a Milli-Q system (Millipore, Bedford, USA). Nitric acid (65 %) suprapure quality (HNO_3, G.R., Lach-ner s.r.o., Czech Republic) and H_2O_2 30 % solution (Macron Fine Chemicals, Avantor Performance Materials, Poland) were used for sample digestion. All containers used in the experiments were previously soaked in nitric acid solution (10 %) for 24 h and rinsed with deionized water afterwards.

For ICP OES analysis, external calibration was conducted using 5 working standards obtained by dilution of multi-elementary stock solution (Titrisol, Merck, Darmstadt, Germany) containing 1000 mg dm^{-3} of As, Pb, Cd, Cr, Ni and Sb. The correlation coefficients were higher than 0.99 in all cases.

The values obtained for limits of detection (*LOD*) and quantification (*LOQ*) were calculated based on $3SD/m$ and $10SD/m$, respectively, where m is the slope of the calibration curves and *SD* is standard deviation of 10 consecutive measurements of the blank, multiplied by the dilution factor used for sample preparation. For method validation, specificity, linearity, working range, accuracy, precision, *LOD* and *LOQ* were estimated and presented in Table I.

The accuracy of ICP-OES method was tested in analysis of certified reference materials (CRM), fish protein (DORM-4, National Research Council, Canada) and cooking chocolate (Standard Reference Material® 2384, National Institute of Standards & Technology, USA). The obtained recovery values were in the range 82–116 %. The precision was expressed as relative standard deviation (*RSD*) and was less than 10 % in all cases (n = 3, Table I).

TABLE I. Parameters of method validation for As, Cd, Pb, Cr, Ni, and Sb in ICP-OES analysis

Element	R^2	*LOD* / mg kg^{-1}	*LOQ* / mg kg^{-1}	*RSD* / %
As	0.9997	0.05	0.15	0.92
Cd	0.9996	0.01	0.03	0.94
Pb	0.9968	0.01	0.02	0.97
Cr	0.9992	0.01	0.03	0.93
Sb	0.9986	0.07	0.20	0.92
Ni	0.9998	0.07	0.20	0.94

Microwave-assisted sample preparation

The crayons and the solid pigment cores of pencils were manually crushed with a porcelain mortar and pestle to obtain smaller particles and better homogenization. Portions of 0.5 g homogenized samples were transferred to PTFE tubes and 4 cm^3 HNO_3 (65 %) and 1 cm^3 H_2O_2 (30 %) were added. The tubes were submitted to a temperature of at 200 °C for 20 min under a microwave irradiation power of 800 W. After digestion, samples were filtrated through 0.45 µm PTFE membrane filter and diluted with deionized water to the total volume of 50 cm^3. The sample preparation procedure was carried out in triplicate, including the blank solutions and certified reference materials.

Bioaccessibility study

For bioaccessibility study all pencils and crayons were subjected to leaching procedure with artificial saliva in order to simulate chemical environment in a mouth. Artificial saliva was prepared according to unified BARGE method.[31] Bioavailability tests were conducted under the controlled conditions of temperature and pH. Each sample (0.5 g) was mixed with 25 cm^3 artificial saliva and shaken for 30 min (200 rpm, 37±2 °C), filtered through 0.45 µm PTEF filter. Bioavailability tests were made in triplicate including the blank solutions.

RESULTS AND DISCUSSION

Concentration of total and oral bioaccessible toxic elements (As, Pb, Cr, Cd, Ni and Sb) in the samples of 30 colored pencils and 30 crayons from different vendors provided at Belgrade's markets were analyzed.

Prior to measurements of As, Pb, Cr, Cd, Ni and Sb concentrations, the samples were subjected to microwave acid assisted digestion. To assess the bioavailability of TEs in the samples, extraction was performed using artificial saliva, according to the procedure presented elsewhere.[31] The TEs concentrations in all aliquots were measured by ICP-OES. The obtained concentrations for the TEs, expressed as average, are presented in (Tables II and III).

Generally, the total TEs content in the majority of tested samples is higher in pencils than in crayons. Besides, the concentrations of TEs in artificial saliva extracts were much higher from colored pencils, as expected, because of the coloration of filtrate due to dissolution of solid pigment core during the extraction process. That is probably related to different material composition of crayons and pencils.

According to the recently updated European Union Directive[9], allowed concentrations of heavy metals in children's toys are as follows: As 3.8 mg kg^{-1}, Pb 2 mg kg^{-1}, Cd 1,3 mg kg^{-1}, Cr 37,5 mg kg^{-1}, Ni 75 mg kg^{-1} and Sb 45 mg kg^{-1}.

TABLE II. Concentration (mg kg^{-1}, mean value, n = 3 determinations) of As, Cd, Pb, Cr and Ni in crayons samples (C) of different manufacturers (A, B, C, D, and E) after microwave assisted acid digestion and artificial saliva extraction with summary statistics; the concentrations of Sb (total content), Cd, Ni and Sb (artificial saliva extracts) were below the method detection limits and from that reason not presented

Label	Color/ manufacturer	Method							
		Microwave assisted acid digestion					Artificial saliva extraction		
		As	Cd	Pb	Cr	Ni	As	Pb	Cr
CA1	Yellow/A	0.382	ND	0.312	0.163	ND	0.170	0.055	0.058
CA2	Red/A	0.247	ND	1.30	1.87	0.311	0.074	0.169	0.623
CA3	Blue/A	0.274	ND	0.148	0.917	ND	0.129	ND	0.362
CA4	Green/A	0.258	ND	0.949	0.889	0.241	0.084	0.165	0.286
CA5	Orange/A	0.258	ND	0.994	0.761	ND	0.099	0.154	0.264
CA6	Purple/A	0.495	ND	2.78	0.850	ND	0.141	0.167	0.208
CB1	Yellow/B	0.668	0.102	3.25	1.93	0.965	0.250	ND	0.468
CB2	Red/B	0.688	0.095	3.13	2.27	0.886	0.219	ND	0.532
CB3	Blue/B	0.783	0.118	3.44	2.37	0.997	0.298	ND	0.845
CB4	Green/B	0.962	0.122	3.07	1.54	4.20	0.305	ND	0.572
CB5	Orange/B	0.556	0.137	3.84	1.75	0.937	0.284	ND	0.403
CB6	Purple/B	0.933	0.147	6.87	1.27	4.347	0.327	ND	0.366
CC1	Yellow/C	0.402	ND	0.687	0.906	0.234	0.185	ND	0.287
CC2	Red/C	0.305	0.042	1.29	2.48	0.344	0.088	ND	0.674
CC3	Blue/C	0.390	0.032	0.032	0.974	0.253	0.149	ND	0.289
CC4	Green/C	0.397	ND	0.630	2.55	0.861	0.183	ND	0.888
CC5	Orange/C	0.386	ND	0.846	2.12	0.695	0.142	ND	0.711
CC6	Purple/C	0.276	ND	2.63	2.59	0.637	0.091	0.146	0.692
CD1	Yellow/D	0.367	ND	1.17	1.91	0.695	0.127	ND	0.484
CD2	Red/D	0.358	0.032	2.59	4.76	1.32	0.043	ND	0.596
CD3	Blue/D	0.583	ND	3.03	2.84	1.17	0.236	ND	0.750
CD4	Green/D	0.337	ND	0	2.30	0.913	0.263	ND	0.573
CD5	Orange/D	0.377	ND	0	1.33	0.613	0.164	ND	0.451
CD6	Purple/D	0.655	ND	4.94	2.17	1.17	0.315	ND	0.751
CE1	Yellow/E	0.745	ND	0	0.659	0.235	0.238	ND	0.237
CE2	Red/E	0.702	ND	0	1.20	0.975	0.302	ND	0.357
CE3	Blue/E	0.622	ND	0	1.49	3.85	0.237	ND	0.430
CE4	Green/E	0.353	ND	0	0.928	2.22	0.144	ND	0.263
CE5	Orange/E	0.392	ND	0	1.10	0.344	0.112	ND	0.269
CE6	Purple/E	0.517	ND	0	2.23	0.953	0.227	ND	0.362
Average		0.489	0.027	1.59	1.70	1.17	0.19	0.143	0.468
SD		0.202	0.049	1.76	0.906	1.18	0.082	0.044	0.208
Maximum		0.962	0.147	6.87	4.76	4.35	0.327	0.169	0.888

Arsenic content in the investigated samples was in the ranges of 1.67–5.78 and 0.246–0.9619 mg kg^{-1}, for pencils and crayons, respectively. With exception of two samples of pencils of different manufacturers (F and D), both of purple color, CPF6 (5.78 mg kg^{-1}) and CPD6 (4.15 mg kg^{-1}), arsenic concentration was below the allowable limit of 3.8 mg kg^{-1} in all others.[9]

TABLE III. Toxic elements concentrations (mean value n = 3 determinations; mg kg^{-1}) in colored pencils samples of different manufacturers (B, D, E, F, and G) after microwave assisted acid digestion and artificial saliva extraction with summary statistics; the concentrations of Sb (total content), Cd, Ni and Sb (artificial saliva extracts) were below the method detection limits and from that reason not presented

Label	Color/ manufacturer	Method							
		Microwave assisted acid digestion					Artificial saliva extraction		
		As	Cd	Pb	Cr	Ni	As	Pb	Cr
CPF1	Yellow/F	0.505	0.111	1.481	3.58	0.375	0.233	0.18	0.945
CPF2	Red/F	0.538	0.087	0.957	1.24	0.419	0.245	ND	0.259
CPF3	Blue/F	1.34	0.071	8.415	2.26	2.06	0.623	0.220	0.731
CPF4	Green/F	0.405	0.076	0.678	1.77	1.61	0.139	ND	0.637
CPF5	Orange/F	0.445	0.082	1.021	3.99	0.846	0.176	0.186	0.974
CPF6	Purple/F	5.78	0.615	8.613	1.82	3.61	2.509	0.779	0.532
CPB1	Yellow/B	0.599	0.113	1.165	1.27	0.532	0.163	ND	0.348
CPB2	Red/B	0.423	0.085	0.524	1.15	0.466	0.125	ND	0.467
CPB3	Blue/B	0.492	0.089	0.75	0.915	0.402	0.170	ND	0.246
CPB4	Green/B	0.589	0.103	0.951	0.637	0.423	0.24	ND	0.179
CPB5	Orange/B	0.442	0.107	0.942	2.62	0.532	0.184	ND	0.490
CPB6	Purple/B	1.04	0.1	0.914	5.02	0.745	0.471	0.208	0.692
CPD1	Yellow/D	0.652	0.079	1.760	4.84	2.92	0.227	ND	0.558
CPD2	Red/D	0.213	0.078	0.543	2.01	1.01	0.081	ND	0.671
CPD3	Blue/D	0.602	0.080	0.705	1.54	1.81	0.247	ND	0.597
CPD4	Green/D	0.691	0.070	2.561	2.72	2.40	0.292	0.699	0.586
CPD5	Orange/D	0.439	ND	1.517	4.59	2.48	0.168	ND	0.736
CPD6	Purple/D	4.15	0.075	4.623	1.60	0.695	1.814	ND	0.620
CPE1	Yellow/E	1.64	ND	ND	0.818	0.222	0.433	ND	0.285
CPE2	Red/E	1.14	0.127	3.311	3.85	3.28	0.413	0.525	0.793
CPE3	Blue/E	1.04	ND	ND	1.94	0.795	0.246	ND	0.257
CPE4	Green/E	1.22	0.081	1.878	0.988	0.036	0.476	ND	0.248
CPE5	Orange/E	1.12	ND	ND	1.10	0.351	0.461	ND	0.236
CPE6	Purple/E	1.68	ND	0.055	1.36	0.485	0.467	ND	0.326
CPG1	Yellow/G	0.412	0.033	0.393	11.17	6.63	0.136	0.107	1.94
CPG2	Red/G	0.286	0.039	0.185	9.44	5.62	0.097	0.042	1.99
CPG3	Blue/G	0.415	0.071	7.946	9.98	2.26	0.164	0.198	2.24
CPG4	Green/G	0.370	ND	ND	5.59	3.68	0.103	0.208	0.804
CPG5	Orange/G	0.339	ND	5.24	6.07	4.29	0.117	0.149	0.789
CPG6	Purple/G	1.06	ND	9.36	6.12	4.78	0.315	0.151	1.47
Aver.		1.002	0.079	2.22	3.40	1.86	0.385	0.281	0.722
SD		1.16	0.109	2.84	2.84	1.77	0.511	0.231	0.532
Max		5.78	0.615	9.36	11.17	6.63	2.509	0.779	2.24

Arsenic is naturally present in a yellow pigment (orpiment), as arsenic sulfide but its highest concentration was measured in purple color. In artificial saliva extracts of crayon samples, manufacturers A and C, the concentrations of As were below the detection limit, while 28.5 to 51.2 % of extracted As was found in the rest of samples. In majority of extracts obtained from pencils As was extracted up

to 46.7 %. It is noteworthy that two samples with total As contents exceeded the allowed concentration (CPF6 and CPD6). In those samples the extracted portions were 43.4 and 43.7 %. These concentrations were below the allowable limit.

According to the reported data, kaolinite (contains Pb) is usually used as a component of children's crayons[8], but besides that, Pb compounds are commonly used as pigments, for example: lead (II) chromates (yellow, orange, red, and green), lead oxides (red), lead (II) carbonates (white lead) and lead molybdates (red orange).[8,32] Following the obtained results for the Pb content in crayon samples, it can be observed that the concentration of this metal varies widely among manufacturers (Tables II and III). For example, Pb concentration in all samples of crayons by manufacturer E is below the detection limits, and for all samples of crayons manufacturer B, Pb content is above the EU safety limit. Lead was detected in all colored pencils, with exception of four samples (CPE1, CPE3, CPE5 and CPG4) where it was below the detection limit. Some of the samples (manufacturers F, D, and G) had several times higher concentrations than permitted by EU regulative (CPF3 8.41 mg kg^{-1}, CPF6 8.61 mg kg^{-1}, CPD6 4.62 mg kg^{-1}, CPG3 7.95 mg kg^{-1}, CPG5 5.24 mg kg^{-1} and CPG6 9.36 mg kg^{-1}). Moreover, higher concentrations of this metal were founded in blue and purple colors. According to an earlier legislation[6], the lead content was below the allowable concentration (13.5 mg kg^{-1}) for all manufacturers. However, when updated and stricter regulations are applied, only manufacturer E met the requirement for wooden pencils and wax crayons. These results can suggest that price and, in some cases, country of origin (directives that some country follow during the manufacturing and distribution) of investigated samples are the most significant factors in potential health risk for children.

In general, lead exposure causes health problems but, more significant with children mostly because of mouthing habits, and also due to facilitated gastrointestinal lead absorption.[32] It is important to know that lead has a half-life of 35 days in erythrocytes, two years in the brain cells and decades in the bones, with evidence of greater absorption in children compared with adults.[33] According to the reported data[5] safe concentration of Pb in the blood, without effect on the children's intelligence quotient (*IQ*), is 10 mg dl^{-1}. In another study,[8] the analysis was done with 172 children aged 0.5–5 years. It was found that increase of Pb concentration from 1 to 10 mg dl^{-1}, reduces *IQ* for 7.4 units. It can be concluded that there is no safe limit for lead, so control of its content in crayons, as well as in other toys should be mandatory. The extracted portion of Pb in the artificial saliva varies up to 47 %, independently on color or the manufacturer, but none of the samples exceeded the allowable value.

Chromium concentrations were all bellow the allowable limits (0.6368–0.974 and 0.1632–4.76 mg kg^{-1} for pencils and crayons, respectively). Also, it has been observed that Cr in all samples is extracted in similar portions (20–30 %), but these

concentrations are far below the permitted values. According to the literature, higher content of this metal was expected in the yellow and orange colors, because of lead (II)-chromate, which is used as a basic pigment.[5,34,35] However, the obtained results showed no correlation between Cr concentration and sample color. Guney and Zagury[36] reported that no one of 30 investigated metallic toys and jewelry exceeds the EU limit for Cr. On the other hand, Cui *et al.*[5] tested 45 children's toys and jewelry for total and bioaccessible metal concentrations and found that those items were significant source of Ni and Cr. They also emphasized the importance and need for more strict regulation of Cr concentration in toys and jewelry.

After a total digestion, Cd was detected in crayon samples of two different manufacturers: B (all colors) and C (only red and blue crayons) in the concentration range 0.032–0.147 mg kg^{-1}. In pencils, Cd was detected in range of 0.033–0.615 mg kg^{-1} in the samples of all manufacturers except the manufacturer E. It is found that concentration of Cd in all samples was below the EU limit (1.3 mg kg^{-1}) and no significant correlation was noticed between color and cadmium content. In artificial saliva extracts, concentration of cadmium was below the detection limit for all investigated samples. With exception of four wax crayons (CA1, CA3, CA5 and CA6), nickel was founded in all samples, in the range from 0.235 to 6.63 mg kg^{-1} and below the EU safety limits. Concentrations of Ni in artificial saliva extracts were all below the detection limits. Finally, concentration of Sb was below the detection limits, as well as below the EU safety limits, for all investigated samples.

CONCLUSION

The results presented in this study are important for many reasons, mostly as potential health risk for children as well as environmental issues. In general, total TEs contents, and their concentrations in artificial saliva extracts, were higher in colored pencils than in crayons, due to better dissolution of solid pigment core. Total concentrations of TEs in pencils and crayons vary widely among manufacturers, and for some samples of colored pencils concentration of As and Pb excided the levels permitted by EU legislative. Chromium and arsenic showed the very high leaching potential in bioaccessibility study (around 30 %, on average), but regardless of the portion of extracted elements by artificial saliva, all values were below the allowable limits. The differences between these two types of coloring pencils are probably related to their material composition, type of used pigments, and manufacturing process, but it was not possible to make some valid correlation without specific information and knowledge of these parameters, indicating that more research, in this field, is needed. To our best knowledge, this is the first comprehensive study, of this type, in Serbia and tends to contribute to the database of similar published reports in Europe.

Acknowledgement. This work was supported by the Ministry of Education, Science and Technological Development of Republic of Serbia. Contract number: 451-03-68/2020-14/ /200161.

ИЗВОД

ТОКСИЧНИ ЕЛЕМЕНТИ У ВОШТАНИМ И ДРВЕНИМ БОЈИЦАМА ЗА ДЕЦУ: ПРОЦЕНА БИОДОСТУПНОСТИ

СВЕТЛАНА ЂОГО МРАЧЕВИЋ[1], СЛАВИЦА РАЖИЋ[1], ЈЕЛЕНА ТРИШИЋ[2], НИКОЛА МИТРОВИЋ[3] и ДАНИЈЕЛА ЂУКИЋ-ЋОСИЋ[4]

[1]*Катедра за аналитичку хемију, Универзитет у Београду, Фармацеутски факултет, Војводе Степе 450, 11221 Београд,* [2]*Roche d.o.o., Милутина Миланковића 11а, 11000 Београд,* [3]*Универзитет у Београду, Фармацеутски факултет, Војводе Степе 450, 11221 Београд и* [4]*Катедра за токсикологију „Академик Данило Солдатовић", Универзитет у Београду, Фармацеутски факултет, Војводе Степе 450, 11221 Београд*

Уобичајена навика деце да оловке жваћу или држе устима може довести до ослобађања евентуално присутних токсичних елемената и њиховог уношења у организам. Већина таквих елемената, захваљујући великом кумулативном потенцијалу, представљају потенцијални ризик по здравље деце ометајући, пре свега, њихов когнитивни развој. Циљ овог рада био је одређивање укупног садржаја As, Pb, Cr, Cd, Ni и Sb у узорцима дрвених и воштаних бојица, те процена њихове биодоступности. Испитивано је укупно 60 узорака бојица, различитих боја, 10 различитих произвођача. Узорци су припремани методом микроталасне дигестије, а за процену биодоступности примењена је екстракција вештачком саливом. Садржај испитиваних елемената је одређиван методом индуктивно спрегнуте плазме оптичке емисионе спектрометрије (ICP-OES). Укупан садржај свих испитиваних елемената је био већи у дрвеним него у воштаним бојицама и максималне измерене концентрације (mg kg^{-1}) износе: 5,78 (As); 9,36 (Pb); 9,97 (Cr); 0,615 (Cd); 6,63 (Ni). Садржај Sb је за све испитиване узорке нижи од границе детекције. Добијени резултати су показали да концентрација As и Pb у неколико узорака бојица није у сагласности са важећом регулативом Европске Уније. Испитивање биодоступности токсичних елемената је показало да су As и Cr лако екстрактабилни, али независно од процента екстракције садржај свих испитиваних елемената у екстрактима вештачке саливе је нижи од дозвољених вредности.

(Примљено 10. септембра, ревидирано 23. септембра, прихваћено 5. октобра 2021)

REFERENCES

1. M. Rodríguez-Barranco, M. Lacasaña, C. Aguilar-Garduño, J. Alguacil, F. Gil, B. González-Alzaga, A. Rojas-García, *Sci. Total Environ*. **454–455** (2013) 562 (https://doi.org/10.1016/j.scitotenv.2013.03.047)
2. W. W. Au, *Int. J. Hyg. Environ. Health* **205** (2002) 501 (https://doi.org/10.1078/1438-4639-00179)
3. A. Rebelo, E. Pinto, M. V. Silva, A. A. Almeida, *Microchem. J.* **118** (2015) 203 (https://doi.org/10.1016/j.microc.2014.09.008)
4. M. Guney, G. J. Zagury, *J. Hazard. Mater.* **271** (2014) 321 (https://doi.org/10.1016/ j.jhazmat. 2014.02.018)
5. X-Y. Cui, S-W. Li, S-J. Zhang, Y-Y. Fan, L. Q. Ma, *Environ. Pollut.* **200** (2015) 77 (https://doi.org/10.1016/j.envpol.2015.01.035)

6. EU Commossion, *Directive 2009/48/EC of the European Parliament and of the Council of 18 June 2009 on the safety of toys*, https://www.legislation.gov.uk/eudr/2009/48/article/20/data.pdf (accessed 6 September, 2021)
7. M. Hanna-Attisha, J. LaChance, R. C. Sadler, A. C. Schnepp, *AJPH* **106** (2016) 283 (https://dx.doi.org/10.2105%2FAJPH.2015.303003)
8. R. L. Canfield, C. R. Henderson, D. A. Cory-Slechta, C. Cox, T. A. Jusko, B. P. Lanphear, *N Engl J Med.* **348** (2003) 1517 (https://doi.org/10.1056/NEJMoa022848)
9. EU Commossion, *Executive summary of the impact assessment*, https://eur-lex.europa.eu/LexUriServ/LexUriServ.do?uri=SWD:2016:0289:FIN:EN:PDF (accessed 6 September, 2021)
10. Agency for Toxic Substances and Disease Registry, *ATSDR's Substance Priority List*, https://www.atsdr.cdc.gov/spl/index.html (accessed 6 September, 2021)
11. Worl Health Organisation, *Exposure to arsenic: A major public health concern*, https://www.who.int/ipcs/features/arsenic.pdf (accessed 6 September, 2021)
12. Worl Health Organisation, *Agents Classified by the IARC Monographs*, https://monographs.iarc.who.int/agents-classified-by-the-iarc/(accessed 6 September, 2021)
13. US Environmental Protection Agency, *Arsenic Compounds*, https://www.epa.gov/sites/default/files/2016-09/documents/arsenic-compounds.pdf (accessed 6 September, 2021)
14. M. Argos, T. Kalra, P. J. Rathouz, Y. Chen, B. Pierce, F. Parvez F, T. Islam, A. Ahmed, M. Rakibuz-Zaman, R. Hasan, G. Sarwar, V. Slavkovich, A. van Geen, J. Graziano, H. Ahsan, *Lancet* **376** (2010) 252 (https://doi.org/10.1016/S0140-6736(10)60481-3)
15. J. L. Rosado, D. Ronquillo, K. Kordas, O. Rojas, J. Alatorre, P. Lopez, G. Garcia-Vargas, M. del Carmen Caamaño, M. E. Cebrián, R. J. Stoltzfus, *Environ. Health Perspect*. **115** (2007) 1371 (https://doi.org/10.1289/ehp.9961)
16. S. Abbas, E. M. A. Qureshi, F. Ahmad, S. Vehra, A. U. Khan, *Pak. J. Nutr*. **11** (2012) 150 (DOI:10.3923/pjn.2012.150.153)
17. M. Guney, S. Kismelyeva, Z. Akimzhanova, K. Beisova, *Environ. Pollut*. **264** (2020) 114627 (https://doi.org/10.1016/j.envpol.2020.114627)
18. L. Xu, X. Huo, Y. Liu, Y. Zhang, Q. Qin, X. Xu, *Chemosphere* **246** (2020) 125829
19. (https://doi.org/10.1016/j.chemosphere.2020.125829)
20. A. A. Dahab, D. E. A. Elhag, A. B. Ahmed, H. A. Al-Obaid, *Environ. Sci. Pollut. Res.* **23** (2016) 3406 (DOI 10.1007/s11356-015-5594-0)
21. S. I. Korfali, R. Sabra, M. Jurdi, R. I. Taleb, *Arch. Environ. Contam. Toxicol.* **65** (2013) 368 (DOI 10.1007/s00244-013-9925-1)
22. M. Guney, G. J. Zagury, *Environ. Sci. Technol.* **46** (2012) 4265 (https://doi.org/10.1021/es203470x)
23. R. A. Caparros-Gonzalez, M. J. Gimenez-Asensio, B. González-Alzaga, C. Aguilar-Garduño, J. A. Lorca-Marín, J. Alguacil, I. Gómez-Becerra, J. L. Gómez-Ariza, T. García--Barrera, A. F. Hernandez, I. López-Flores, D. S. Rohlman, D. Romero-Molina, I. Ruiz--Pérez, M. Lacasaña, *Environ. Pollut., B* **252** (2019) 1550 (https://doi.org/10.1016/j.envpol.2019.06.084)
24. A. Chen, K. N. Dietrich, X. Huo, S. Ho, *Environ. Health Perspect.* **119** (2011) 431 (https://doi.org/10.1289/ehp.1002452)
25. A. Turner, M. Filella, *Sci. Total Environ*. **713** (2020) 136588 (https://doi.org/10.1016/j.scitotenv.2020.136588)

26. S. Bagherifam, T. C. Brown, C. M. Fellows, R. Naidu, *Pedosphere* **29** (2019) 681 (https://doi.org/10.1016/S1002-0160(19)60843-X)
27. J. K. Nduka, H. I. Kelle, J. O. Amuka, *Toxicol. Rep.* **6** (2019) 449 (https://doi.org/10.1016/j.toxrep.2019.05.007)
28. M. Babaahmadifooladi, L. Jacxsens, T. Van de Wiele, E. C. da Silva Júnior, G. Du Laing, *Food Chem.* **342** (2021) 128210 (https://doi.org/10.1016/j.foodchem.2020.128210)
29. EFSA (European Food Safety Authority), *EFSA J.* **13** (2015) 4002 (https://doi.org/10.2903/j.efsa.2015.4002)
30. Z. N. Igweze, O. C. Ekhator, O. E. Orisakwe, *Heliyon* **6** (2020) e03732 (https://doi.org/10.1016/j.heliyon.2020.e03732)
31. A. O. Oyeyiola, M. I. Akinyemi, I. E. Chiedu, O. T. Fatunsin, K. O. Olayinka, *J. Taibah Univ. Sci.* **11** (2017) 842 (http://dx.doi.org/10.1016/j.jtusci.2017.02.005)
32. J. Wragg, M. Cave, N. Basta, E. Brandon, S. Casteel, S. Denys, C. Gron, A. Oomen, K. Reimer, K. Tack, T. Van de Wiele, *Sci. Total Environ.* **409** (2011) 4016 (https://doi.org/10.1016/j.scitotenv.2011.05.019)
33. S. Y. Njati, M. M. Maguta, *Environ. Pollut.* **249** (2019) 1091 (https://doi.org/10.1016/j.envpol.2019.03.062)
34. M. M. Hillyer, L. E. Finch, A. S. Cerel, J. D. Dattelbaum, M. C. Leopold, *Chemosphere* **108** (2014) 205 (https://doi.org/10.1016/j.chemosphere.2014.01.041)
35. L. Monico, K. Janssens, C. Miliani, B. G. Brunetti, M. Vagnini, F. Vanmeert, G. Falkenberg, A. Abakumov, Y. Lu, H. Tian, J. Verbeeck, M. Radepont, M. Cotte, E. Hendriks, M. Geldof, L. van der Loeff, J. Salvant, M. Menu, *Anal. Chem.* **85** (2012) 851 (https://doi.org/10.1021/ac302158b)
36. J. A. Greenway, S. Gerstenberger, *Bull. Environ. Contam. Toxicol.* **85** (2010) 363 (https://doi.org/10.1007/s00128-010-0100-3)
37. M. Guney, G. J. Zagury, *Environ. Sci. Technol.* **47** (2013) 5921 (https://doi.org/10.1021/es304969n).

Journal of the Serbian Chemical Society
JSCS@tmf.bg.ac.rs • www.shd.org.rs/JSCS

J. Serb. Chem. Soc. *87* (6) 735–747 (2022)
JSCS–5554

Original scientific paper
Published 18 February 2022

Correlation of the solubility of solid hydrocarbons in supercritical CO_2 using different equations of state and mixing rules

NARJES SETOODEH and ABOLHASAN AMERI*

Department of Chemical Engineering, Shiraz Branch, Islamic Azad University, Shiraz, Iran

(Received 17 August 2021, revised 3 December 2021, accepted 15 January 2022)

Abstract: The supercritical extraction process is a technique that has increasingly been applied in various industries in recent years. Solubility determination in the supercritical region is the key feature for this process. However, high expenses and time consuming experiments for this task obligates the need for process modeling. In this study, a thermodynamic model is proposed to correlate the solubility of solid hydrocarbons, namely, 1-hexadecanol, 1-octadecanol, anthracene, benzoin, fluorene, hexamethylbenzene, mandelic acid, naphthalene, palmitic acid, phenanthrene, propyl 4-hydroxybenzoate, pyrene and stearic acid in supercritical conditions, using Peng–Robinson (PR) and Soave–Redlich–Kwong (SRK) equations of state with one-parameter van der Waals (vdW1) and two-parameters (vdW2) and covolume dependent (CVD) mixing rules. For the above combination of equations of state and mixing rules, binary interaction parameters were determined, utilizing the differential evolution optimization strategy. The validity of the model was assessed by comparing the experimental solubility data with the results obtained from thermodynamic model based on average absolute relative deviation (*AARD*). An empirical correlation was proposed for the correlation of the solid solubilities in supercritical CO_2. For each compound, the constants of this equation were obtained in such a manner to correlate the solubility at different temperatures and pressures.

Keywords: supercritical extraction; solid compounds; thermodynamic modelling; PR; SRK.

INTRODUCTION

Application of new technologies in different industrial processes has led to increase in the yield of processes. The supercritical fluid extraction (SFE) process is a technology of growing interest in recent years covering various industries, such as food, pharmaceutical, chemical, perfume and essence.

* Corresponding author. E-mail: ameri@iaushiraz.ac.ir
https://doi.org/10.2298/JSC210817002S

Application of SFE in separation processes results in reducing energy consumption, extraction at ambient temperature, improving product quality and being healthy, full extraction of solute from solvent by the change of pressure or temperature and reducing environmental pollution.[1]

The relatively high density of supercritical fluids leads to high solubility of heavy hydrocarbons in supercritical fluid (SCF), while their solubility in fluids in the gaseous state is low. Despite this, the solubility of compounds in SCF depends on the solute and solvent properties. A supercritical fluid such as CO_2 plays the role of solvent and dissolves a solid compound in itself. The solubility of these solid compounds in CO_2 depends on temperature and pressure. This solubility can be calculated using phase equilibrium relations by equations of state and mixing rules for a mixture of solid and SCF.

One of the most important applications of the SFE process is the extraction of heavy hydrocarbons from the solid phase using supercritical CO_2. In order to correlate the solubility of heavy components in supercritical CO_2, the use of an appropriate equation of state (EoS) and mixing rule are required. As a result, it is important to verify which EoS and mixing rule could better correlate the solubility and are in better agreement with the experimental data.

Chafer *et al.* proposed a thermodynamic model for the solubility of quercetin in supercritical CO_2 using the group contribution equation of state (GC-EoS), and the Soave–Redlich–Kwong (SRK) EoS. They used ethanol as a co-solvent.[2] Yang and Zhong used the statistical associating fluid theory (SAFT) equation of state with a one-parameter mixing rule.[3] They modeled the solubility of aromatic compounds in supercritical fluids. Schultz *et al.* predicted the solubility of hexane in supercritical carbon dioxide with the virial equation of state (V EoS) and calculated its coefficients up to fourth-order using Mayer-sampling Monte Carlo.[4] Two sparse Bayesian methods were applied by Tarasova *et al.* to derive predictive models of the solubility of organic dyes and polycyclic aromatic compounds in supercritical carbon dioxide.[5] Zeinolabedini *et al.* correlated the solubility of mefenamic acid in supercritical carbon dioxide with four empirical correlations, namely Chrastil, Mendez–Santiago–Teja (MST), Bartle and Kumar and Johnston (K-J).[6] A model was proposed for the solubility of fifteen pharmaceutical compounds in supercritical carbon dioxide with the regular solution model and the Flory–Huggins equation by Huang *et al.*[7] Chie-Shaan Su fitted the experimental data for the solubility of some fatty acids in supercritical carbon dioxide by using a two-parameter solution model developed from the regular solution model coupled with the Flory–Huggins equation.[8] Shojaee *et al.* correlated the solubility data of carvedilol in supercritical carbon dioxide. Their model was fitted using density-based semi-empirical models, namely Bartle *et al.*, Mendez–Santiago–Teja, Chrastil and Kumar and Johnston.[9] Cheng *et al.* correlated the solubility data of ergosterol in supercritical carbon dioxide at high pressures

by the Schmitt–Reid and Giddings models.[10] A model was developed for drug solubility in supercritical carbon dioxide using equation of state based on the the hole theory with molecular surface charge density by Sakabe *et al.*[11] Asgarpour Khansary *et al.* developed a new model for the empirical prediction of solute solubility in supercritical carbon dioxide.[12] Li *et al.* investigated the solubilities of organic compounds in supercritical CO_2 using a modified solution model and expanded liquid model.[13]

Due to the time-consuming and high expense of experimental measurements, modeling of the solubility behavior of solid compounds is needed. In this study, a thermodynamic modeling was performed to correlate the solubility of thirteen solid compounds, namely, 1-hexadecanol, 1-octadecanol, anthracene, benzoin, fluorene, hexamethylbenzene, mandelic acid, naphthalene, palmitic acid, phenanthrene, propyl 4-hydroxybenzoate, pyrene and stearic acid under supercritical conditions, in the range of 303.1–343.1 K and 52.1–574.8 bar for various solid compounds,[10,14–21] using the PR and SRK equations of state with vdW1, vdW2 and CVD mixing rules. For the above combinations of equations of state and mixing rules, binary interaction parameters were determined, utilizing the differential evolution optimization strategy. As a result, which EoS and mixing rule could better correlate the solubility behavior of compounds in supercritical CO_2 could be chosen. In addition, an empirical correlation is proposed for the correlation of the solid solubilities in supercritical CO_2. For each compound, the constants of this equation were determined in such a manner to correlate the solubility at different temperatures and pressures.

THERMODYNAMIC MODEL

One of the important issues in order to correlate the solubility of heavy hydrocarbons from the solid or liquid phase in SCF is the proper selection of the EoS and mixing rule. Authors have used different equations of state, such as Peng-Robinson (PR), Redlich–Kwong (RK), perturbed-hard-chain, Carnahan–Starling–van der Waals (CS-vdW); and different mixing rules such as van der Waals 1 (vdW1), van der Waals 2 (vdW2), Huron–Vidal, modified Huron and Viddal of order 1 (MHV1), modified Huron and Viddal of order 1 (MHV2), group contribution of the Vidal and Michelsen (GCVM), linear combination of the Vidal and Michelsen (LCVM), Wong–Sandler (WS), Orbey–Sandler (OS) and covolume dependent (CVD). In this study, the PR and SRK equation of states along with vdW1, vdW2 and CVD mixing rules were used and a comparison was made with experimental data for thirteen heavy compounds, namely, 1-hexadecanol, 1-octadecanol, anthracene, benzoin, fluorene, hexamethylbenzene, mandelic acid, naphthalene, palmitic acid, phenanthrene, propyl 4-hydroxybenzoate, pyrene and stearic acid.[22,23]

Using phase equilibrium relations for a mixture of a solid and a supercritical fluid, Eq. (1) was obtained:

$$f_2^{s} = f_2^{scf} \tag{1}$$

Subscript 2 represents the heavy component and f^{s} and f^{scf} are fugacities of the solid compound and supercritical fluid, respectively. The solid phase is pure and nonideal behavior

is for the supercritical fluid. Thus, the fugacity of the pure solid component, f_2^s, at a specific pressure P and temperature T is calculated by Eq. (2):

$$f_2^s = P_2^{sat}\,\phi_2^{sat,s}\exp\left[\frac{v_2^s\left(P-P_2^{sat}\right)}{RT}\right] \tag{2}$$

where, P_2^{sat} and $\phi_2^{sat,s}$ are representative of the saturation vapor pressure and saturation fugacity coefficient of solid compound, v_2^s is molar volume of solid solute and P, T and R are pressure, temperature and universal gas constant, respectively. Due to low vapor pressure of a solid compound, $\phi_2^{sat,s}$ is assumed to equal 1. On the other hand, the fugacity of a solid compound in SCF, f_2^{scf} is obtained by Eq. (3):

$$f_2^{scf} = y_2\varphi_2^{scf}P \tag{3}$$

where, y_2 and φ_2^{scf} represent solubility and fugacity coefficient of solid compound in SCF. Now, with assumption of equilibrium between the two phases, by equating Eqs. (2) and (3), the solubility relation for solid compound in the SCF is given by Eq. (4):

$$y_2 = \left(\frac{P_2^{sat}}{P}\right)\left(\frac{1}{\phi_2^{scf}}\right)\exp\left[\frac{v_2^s\left(P-P_2^{sat}\right)}{RT}\right] \tag{4}$$

P_2^{sat}, the vapor pressure of the heavy component, is calculated from the Antoine Equation.

The accuracy of the solubility calculation depends on the proper selection of the equation of state and mixing rule for the calculation of ϕ_2^{scf}. The two parameters PR and SRK equations of state can be written as in Eq. (5):

$$P = \frac{RT}{v-b} - \frac{a}{(v+c_1b)(v+c_2b)} \tag{5}$$

where, a and b are constants of the equation of state and v represents the molar volume. The constants of Eq. (5) for the PR and SRK equations of state and vdW1, vdW2 and CVD mixing rules are given in the Supplementary material to this paper.

The optimal values of these model adjustable parameters were obtained using the robust population-based differential evolution (DE) method for experimental data points. The most accurate combination of equations of states with the mixing rules, which leads to the least "absolute average relative deviation" (*AARD*, Eq. (6)) of the results from experimental values are reported.

$$AARD = \sum_i^N\left(\left|\frac{y_{exp}^i - y_{calc}^i}{y_{exp}^i}\right|\frac{1}{n}\right)100 \tag{6}$$

where y^i_{exp} and y^i_{calc} are experimental and calculated solubilities, respectively and n is the number of data points. The value of ϕ_2^{scf} is identified with ϕ_i in Eq. (7).[24] Considering a mixture of solid compound and SCF for PR and SRK equations of states we have:

$$\ln\hat{\phi}_i = -\ln(Z-B) + \frac{\hat{b}_i}{b}(Z-1) + \frac{a}{bRT(c_1-c_2)}\left[-\frac{\hat{a}_i}{a}+\frac{\hat{b}_i}{b}\right]\ln\frac{Z+c_1B}{Z+c_2B} \tag{7}$$

$\hat{a}_i$ and $\hat{b}_i$ in Eq. (7) are derivatives related to the attractive and repulsive parameters of EoS and can be calculated according to equations in the Supplementary material to this paper.

The compressibility factor value, Z, needed for calculation of ϕ_i is obtained from the EoS using Eqs. (8) or (9):

For PR EoS:

$$Z^3 - (1 - B)Z^2 + (A - 3B^2 - 2B)Z - (AB - B^2 - B^3) = 0 \tag{8}$$

For SRK EoS:

$$Z^3 - Z^2 + (AB - B^2)Z - AB = 0 \tag{9}$$

Parameters A and B are defined by Eqs. (10) and (11):

$$A = \frac{aP}{R^2T^2} \tag{10}$$

$$B = \frac{bP}{RT} \tag{11}$$

The adjustable parameters in the mixing rules (k_{ij}, l_{ij} and M_{ij}, see Supplementary material) were fitted to the experimental data by the following objective function:

$$OF = \sum_i^N \left(\frac{y_{\text{exp}}^i - y_{\text{calc}}^i}{y_{\text{exp}}^i} \right)^2 \tag{12}$$

The physical properties of 1-hexadecanol, 1-octadecanol, anthracene, benzoin, fluorene, hexamethylbenzene, mandelic acid, naphthalene, palmitic acid, phenanthrene, propyl 4-hydroxybenzoate, pyrene and stearic acid are given in Table I. Joback group contribution methods were applied for the calculation of the critical temperature and pressure.[25] The values of the acentric factor were estimated using the Ambrose–Walton corresponding-state method.[25] The Molbase chemical E-commerce platform site was referenced for the introduction of the molar volume of the solid compounds.

TABLE I. Physical properties of the studied compounds

Component	T_c / K	P_c / bar	ω	v^s_2 / m^3 kmol^{-1}
Carbon dioxide (solvent)	304.2	73.7	0.225	–
1-Hexadecanol	761	14.9	0.748	0.2965
1-Octadecanol	777	13.4	0.863	0.3330
Anthracene	869.15	30.8	0.353	0.1426
Benzoin	853.52	26.6	0.599	0.1620
Fluorene	826.4	29.5	0.406	0.1393
Hexamethylbenzene	758	24.4	0.515	0.1527
Mandelic acid	903.79	34.73	34.73	0.1170
Naphthalene	748.4	40.51	0.302	0.111
Palmitic acid	776	14.9	1.083	0.2857
Phenanthrene	882.65	31.715	0.437	0.182
Propyl 4-hydroxybenzoate	815.92	31.30	0.722	0.1316
Pyrene	936	25.7	0.509	0.1585
Stearic acid	779	13.4	1.084	0.3024

RESULTS AND DISCUSSION

The fitted binary parameters for modeling results and *AARD* for the combination of PR or SRK EoS and three mixing rules are given for 1-hexadecanol, 1-octadecanol, anthracene, benzoin, fluorene, hexamethylbenzene, mandelic acid, naphthalene, palmitic acid, phenanthrene, propyl 4-hydroxybenzoate, pyrene and stearic acid at different pressures and temperatures in Table S-I (Supplementary material) for the calculation of the solubility of heavy compounds in supercritical CO_2.

At higher temperatures and pressures for some compounds, the *AARD* becomes greater. 1-Hexadecanol shows high errors at 318.1 and 338.15 K for vdW1 and all temperatures of the CVD mixing rule. 1-Octadecanol does not match well with the experimental data at 328.1 and 338.1 K for vdW1 and CVD mixing rules. Antheracene shows acceptable *AARD* values at almost all temperatures and mixing rules. Benzoin compound depicts *AARD* less than 10 % at all its data points. CVD mixing rule at 343.1 K for fluorene does not show tolerable *AARD*. Although, other conditions are in an appropriate circumstances. Hexamethylbenzene is another solid compound with low values of *AARD* for all temperature and pressure ranges and mixing rules. Only the vdW2 mixing rule resulted in low *AARD* for mandelic acid, and vdW1 and CVD mixing rules did not respond well for this substance. All temperatures of the vdW2 mixing rule illustrate a low *AARD* for naphthalene.

However, the vdW1 and CVD mixing rules show good results only for temperatures of 308.1 and 328.1 K. This model did not responded well for palmitic acid and high AARD values were obtained at all temperatures and for all mixing rules. On the other hand, the results of phenanthrene were in good agreement with the experimental data and all *AARD* values were acceptable enough over wide temperature and pressure ranges. Propyl 4-hydroxybenzoate was also a compound with low *AARD* values, except at 328.1 K, which showed a little higher *AARD*. Pyrene and stearic acid did not show low *AARD* values for any mixing rules at 343.15 and 338.1 K, respectively. Moreover, some compounds, such as 1-hexadecanol, 1-octadecanol, mandelic acid and palmitic acid, showed greater deviation from the experimental data due to their chemical structure and intermolecular forces and bonds and irregular trend of experimental data according to pressure. As they are alcohols and carboxylic acids and their –OH and –COOH functional groups caused inappropriate *AARD* values. For instance, at higher pressures, the cubic EoS could not well predict the solubilities of solids in SCF and this causes higher error values at high pressures. As the values of T_c, P_c and ω are not from experimental data and have been calculated from correlations, this also could be considered as another source of uncertainty of data correlated by the proposed model. The results show that the PR EoS has more accuracy than the SRK EoS at most data points. In addition, the vdW2 mixing rule is more accurate than vdW1, as was to be expected. Finally, the CVD mixing rule revealed less accuracy compared with the other mixing rules. Comparison of the *AARD* values for different compounds revealed that the applied thermodynamic model was not satisfactory for four compounds, namely, 1-hexadecanol, 1-octadecanol, mandelic acid and palmitic acid and the calculated and experimental solubilities deviate greatly. This could be due to their linear structure unlike the other compounds that contain an aromatic ring in their chemical structure. This shows that the proposed model could not well correlate the solubilities of hydrocarbons

containing only a linear chain no aromatic ring. In almost most compounds, the modeling results indicated less accuracy at higher temperatures. This fact could be related to the non-ideality of the system due to the effect of factors such as molecular weight and molecular interaction of solid compound and Brownian motion at higher temperatures. The intermolecular forces are more dominant at higher pressures and lower temperatures due to the reduced kinetic energy. As a result, the non-ideality of the gas becomes more prominent. As the gas molecules would be close to each other at low temperatures and reach conditions for converting into the liquid phase. As a result, the physical and thermodynamic properties of the compounds could alter the accuracy of the proposed model the base of which is theoretical.

A comparison of the calculated solubility results with the experimental data[10,17,18,26] for some solid compounds in supercritical carbon dioxide is shown in Fig. 1 for the PR EoS and vdW2 mixing rule at 308.15 K, for example. The solubility of a solid compound in SCF increases with increasing pressure due to a reduction of the intermolecular distance. This leads to increasing density of the supercritical CO_2. As a result, the solubility of a solid compound in SCF increases due to the higher solvating strength at higher pressures.

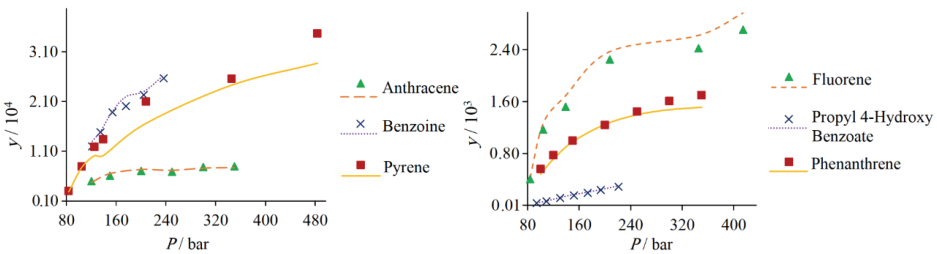

Fig. 1. Comparison of solubility of solid components in supercritical CO_2 using the PR EoS and vdW2 mixing rule at $T = 308.15$ K with experimental data[10,17,18,26] (symbols: experimental data, lines: calculated data).

Temperature has the same effect on the solubility of hydrocarbons in SCF as pressure. The solubility increases with temperature at a constant pressure. Unfortunately, the solvating strength decreased as the temperature increases due to increasing density. On the other hand, increasing the temperature favors the solubility of a solid in SCF due to enhanced solid vapor pressure. The net effect of these two factors is in favor of solubility improvement.

For compounds shown in Fig. 1, anthracene, benzoine, pyrene, fluorene, propyl 4-hydroxy benzoate and phenanthrene, it could be seen that the correlated model results are in close agreement with the experimental data at most points.

A comparison of the results for different mixing rules with PR and SRK EoS with the experimental data for phenanthrene at 308.15 K is shown in Fig. 2. It

could be observed that the vdW2 mixing rule is better than the vdW1 rule and then the CVD, and PR results are more exact than the SRK EoS results. This trend holds for most of the data obtained from modeling.

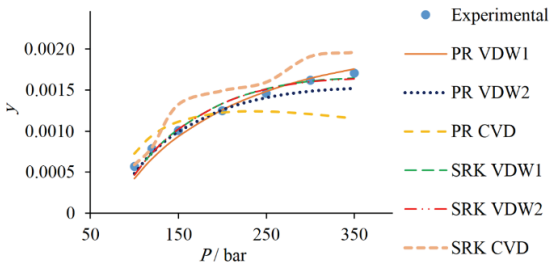

Fig. 2. Comparison of solubility of phenanthrene in supercritical CO_2 at 308.15 K for PR and SRK EoS and three different mixing rules with the experimental data.[18]

In this study, an empirical correlation was evaluated by Eq. (13), by fitting experimental data for thirteen solid compounds at various temperature and pressure conditions:

$$y = a + \frac{b}{T} + c\ln P + \frac{d}{T^2} + e(\ln P)^2 + f\frac{\ln P}{T} + \frac{g}{T^3} + h(\ln P)^3 + i\frac{(\ln P)^2}{T} + j\frac{\ln P}{T^2} \quad (13)$$

where, a, b, c, d, e, f, g, h, i and j are the constants of the equation and T is in K and P is in bar. This kind of equation with ten constants was chosen in order to contain all compounds investigated in this study. The constants of the proposed equation are given in Table II along with *AARD* and the *R*-squared values (r^2) for

TABLE II. Constants of the correlated Eq. (13) from solubility data of different solid components in supercritical CO_2

Component	*a*	*b*	*c*	*d*
1-Hexadecanol	11.54705	–1106.09888	–6.11915	–1684300.000
1-Octadecanol	58.09549	–47365.50854	–6.04540	12968094.14
Anthracene	–0.08523	70.96200	0.00544	–17060.97261
Fluorene	0.02995	20.50137	–0.05487	25370.86890
Hexamethylbenzene	–0.20310	383.07771	–0.14506	–98450.62687
Mandelic acid	0.43494	222.04041	–0.40145	–115354.7488
Naphthalene	–778.75029	716040.4887	23.55648	–217758344.2
Palmitic acid	29.98129	–19851.83296	–5.71884	5389525.856
Phenanthrene	–1.04090	938.09129	–0.00131	–286301.88
Propyl 4-hydroxybenzoate	0.17340	–1.833323	–0.10634	–30732.90725
Pyrene	0.18200	–117.85981	–0.03993	28506.07751
Stearic acid	26.55206	–18856.81082	–4.39775	4924193.745
Component	*e*	*f*	*g*	*h*
1-Hexadecanol	0.44706	2474.25705	295954000	–0.00422
1-Octadecanol	0.24566	3162.35737	–1212649300	0.00127

TABLE II. Continued

Component	*e*	*f*	*g*	*h*
Fluorene	0.02569	–36.37337	–9020275.86	–0.00059
Hexamethylbenzene	0.04026	–24.61846	5557533.278	–0.00171
Mandelic acid	0.06161	57.53582	–1639495.818	0.00109
Naphthalene	0.64636	–16838.10238	21924540172	–0.01076
Palmitic acid	0.67430	1397.120595	–716773367.1	0.00626
Phenanthrene	0.00416	–2.44702	30967674	–0.00044
Propyl 4-hydroxybenzoate	0.00868	40.690182	3269272.063	0.00037
Pyrene	0.00426	13.02016	–2736351.611	0.000070
Stearic acid	0.38118	1573.72658	295954000	–0.00422

Component	*i*	*j*	No. of points	*AARD* / %	r^2
1-Hexadecanol	–120.32106	–204469.418	43	4.95	0.999
1-Octadecanol	–85.97946	–378429.2624	41	3.71	0.999
Anthracene	–0.17868	1288.87653	140	9.78	0.997
Fluorene	–5.31945	12796.2177	157	8.73	0.998
Hexamethylbenzene	–4.64411	9827.18519	23	9.70	0.997
Mandelic acid	–23.67834	27243.98579	21	8.84	0.998
Naphthalene	–153.59875	2889216.912	66	9.41	0.997
Palmitic acid	–251.28354	205916.2349	19	9.50	0.997
Phenanthrene	0.72572	–2029.6518	151	7.50	0.999
Propyl 4-hydroxybenzoate	–4.34060	101.23586	21	7.35	0.999
Pyrene	–1.01282	–632.60526	142	5.38	0.999

each equation obtained from comparing experimental data and results of this equation for several sets of data. As could be seen, the results are in good agreement with the experimental data and the *AARD* is given for each set of data for each component. Hence, in the absence of experimental data at different temperatures and pressures and due to high expense and time-consuming experiments, the proposed equation could be used to obtain the solubility of the herein studied solid compounds in supercritical CO_2 at different temperatures and pressures with good accuracy and reliability.

As an example, the solubility data obtained from Eq. (13) for some of these solid compounds namely, pyrene, anthracene, Mandelic acid and propyl 4-hydroxybenzoate, are compared with experimental data in Fig. 3, which shows that the correlated results with proposed equation match well with experimental data.

CONCLUSIONS

In this work, a thermodynamic approach was applied for the calculation of the solubility of heavy hydrocarbons in supercritical CO_2 using PR and SRK EoS's and three vdW1, vdW2 and CVD mixing rules. The results were in good agreement with the experimental data reported for the specified temperature and pressure ranges. The results showed that the points correlated using the PR EoS were more precise than those using the SRK EoS for most points. Additionally, the vdW2 mixing rule revealed the maximum accuracy followed by the vdW1 and

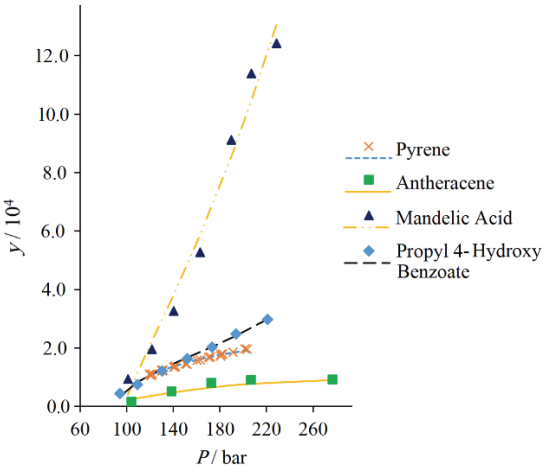

Fig. 3. Comparison of solubility of some compounds in supercritical CO_2 from Eq. (13) with experimental data[10,17,20,26] (symbols: experimental data, lines: calculated data).

CVD mixing rules. Furthermore, the solubility values increased with increasing temperature and pressure. For each combination of equation of state and mixing rule, the optimized binary interaction parameters were reported for different cases by fitting. In order to correlate the solubility of heavy compounds in supercritical CO_2, an empirical equation with 10 constants was evaluated and proposed by fitting several experimental sets of data according to temperature and pressure. The constants of this equation were given for the compounds investigated in this study in order to predict the solubilities of these thirteen solid compounds in SCF at other temperatures and pressures without need to perform experiments. In the same manner, a separate empirical equation could be obtained for other solid compounds for the prediction of their solubility in SCF.

NOMENCLATURE

AARD	Absolute average relative deviations
k_{ij}	Binary interaction parameter
OF	Objective function
l_{ij}	Binary interaction parameter
P_c	Critical pressure
n	Number of points
P^{sat}	Saturation vapor pressure
vdW1	One-parameter van der Waals
PR	Peng-Robinson
vdW2	Two-parameter van der Waals
SCFs	Supercritical fluids
y	Solubility of solid solute
SRK	Soave–Redlich–Kwong
y^i_{calc}	Calculated mole fraction of component i
T_c	Critical temperature
y^i_{exp}	Experimental mole fraction of component i
T_r	Reduced temperature

ϕ^{scf}	Fugacity coefficient of supercritical fluid
Z	Compressibility factor
φ^{sat}	Saturation fugacity coefficient
a	Indicative of intermolecular attractive energy
ϕ_i	Fugacity coefficient
b	Indicative of size of the molecule
v	Molar volume
f^s	Fugacity of solid
v^s	Molar volume of the solid solute
f^{scf}	Fugacity of supercritical fluid
ω	Acentric factor

SUPPLEMENTARY MATERIAL

Additional data and information are available electronically at the pages of journal website: https://www.shd-pub.org.rs/index.php/JSCS/article/view/11074, or from the corresponding author on request.

ИЗВОД

КОРЕЛИСАЊЕ РАСТВОРЉИВОСТИ ЧВРСТИХ УГЉОВОДОНИКА У НАДРКРИТИЧНОМ CO_2 КОРИШЋЕЊЕМ РАЗЛИЧИТИХ ЈЕДНАЧИНА СТАЊА И ПРАВИЛА МЕШАЊА

NARJES SETOODEH и ABOLHASAN AMERI

Department of Chemical Engineering, Shiraz Branch, Islamic Azad University, Shiraz, Iran

Надкритична екстракција се последњих година све више примењује у разним индустријским процесима. Један од најважнијих параметара који је потребно одредити за ове процесе је растворљивост једињења у надкритичној области. Међутим, услед високих трошкова и дуготрајних експеримената јавља се потреба за одређивањем растворљивости моделовањем. У овом раду предложен је термодинамички модел за корелисање растворљивости чврстих угљоводоника (1-хексадеканола, 1-октадеканола, антрацена, бензоина, флуорена, хексаметилбензена, бадемове киселине, нафталена, палмитинске киселине, фенантрена, пропил 4-хидробензобензола, пирена и стеаринске киселине) у надкритичним условима, коришћењем Peng–Robinson (PR) и Soave–Redlich–Kwong (SRK) једначине стања, и њиховим комбиновањем са једнопараметарским (vdW1), двопараметарским (vdW2) van der Waals и (CVD) правилима мешања. За наведене комбинације једначина стања и правила мешања, бинарни интеракциони параметри су одређени оптимизацијом, применом алгоритма диференцијалне еволуције. Валидност модела је утврђена на основу апсолутне вредности средњег процентуалног релативног одступања (*AARD*), односно, поређењем експерименталних података растворљивости са резултатима добијеним применом термодинамичког модела. Такође, на основу резутата, предложена је емпиријска корелација растворљивости чврстих угљоводоника у надкритичном CO_2. Добијене константе предложене корелације се могу користити за одређивање растворљивост на различитим температурама и притисцима.

(Примљено 17. августа 2021, ревидирано 3 децембра 2021, прихваћено 15. јануара 2022)

REFERENCES

1. R. D. Smith, J. P. Blitz, J. L. Fulton, in *Supercritical Fluid Science, Technology*, Vol. 406, K. P. Johnston, J. M. L. Penninger, Eds., ACS Publications, Washington DC, 1989, pp. 165

2. A. Chafer, T. Fornari, A. Berna, R. P. Stateva, *J. Supercrit. Fluids* **32** (2004) 89 (https://doi.org/10.1016/j.supflu.2004.02.005)
3. H. Yang, C. Zhong, *J. Supercrit. Fluids* **33** (2005) 99 (https://doi.org/10.1016/j.supflu.2004.05.008)
4. A. J. Schultz, K. R. S. Shaul, S. Yang, D. A. Kofke, *J. Supercrit. Fluids* **55** (2010) 479 (https://doi.org/10.1016/j.supflu.2010.10.042)
5. A. Tarasova, F. Burden, J. Gasteiger, D. A. Winkler, *J. Mol. Graphics Modell.* **28** (2010) 593 (https://doi.org/10.1016/j.jmgm.2009.12.004)
6. A. Z. Hezave, M. H. Khademi, F. Esmaeilzadeh, *Fluid Phase Equilib.* **313** (2012) 140 (https://doi.org/10.1016/j.fluid.2011.09.031)
7. C.-Y. Huang, L.-S. Lee, C.-S. Su, *J. Taiwan Inst. Chem. Eng.* **44** (2013) 349 (https://doi.org/10.1016/j.jtice.2012.12.004)
8. C.-S. Su, *J. Supercrit. Fluids* **81** (2013) 79 (https://doi.org/10.1016/j.supflu.2013.05.001)
9. S. A. Shojaee, H. Rajaei, A. Z. Hezave, M. Lashkarbolooki, F. Esmaeilzadeh, *J. Supercrit. Fluids* **81** (2013) 42 (https://doi.org/10.1016/j.supflu.2013.04.013)
10. S.-H. Cheng, F.-C. Yang, Y.-H. Yang, C.-C. Hu, W.-T. Chang, *J. Taiwan Inst. Chem. Eng.* **44** (2013) 19 (https://doi.org/10.1016/j.jtice.2012.09.001)
11. J. Sakabe, H. Uchida, Y. Shimoyama, *Chem. Eng. Res. Des.* **92** (2014) 2970 (https://doi.org/10.1016/j.cherd.2014.08.003)
12. M. A. Khansary, F. Amiri, A. Hosseini, A. H. Sani, H. Shahbeig, *Chem. Eng. Res. Des.* **93** (2015) 355 (https://doi.org/10.1016/j.cherd.2014.05.004)
13. H. Li, D. Jia, R. Liu, B. Shen, *Fluid Phase Equilib.* **385** (2015) 10 (https://doi.org/10.1016/j.fluid.2014.10.036)
14. K. P. Johnston, C. A. Eckert, *AlChE J.* **27** (1981) 773 (https://doi.org/10.1002/aic.690270511)
15. A. Kramer, G. Thodos, *J. Chem. Eng. Data* **33** (1988) 230 (https://doi.org/10.1021/je00053a002)
16. A. Kramer, G. Thodos, *J. Chem. Eng. Data* **34** (1989) 184 (https://doi.org/10.1021/je00056a011)
17. E. Kosal, G. D. Holder, *J. Chem. Eng. Data* **32** (1987) 148 (https://doi.org/10.1021/je00048a005)
18. J. M. Dobbs, K. P. Johnston, *Ind. Eng. Chem. Res.* **26** (1987) 1476 (https://doi.org/10.1021/ie00067a035)
19. J. Kwiatkowski, Z. Lisicki, W. Majewski, *Ber. Bunsen. Phys. Chem.* **88** (1984) 865 (https://doi.org/10.1002/bbpc.19840880919)
20. K. D. Bartle, A. A. Clifford, S. A. Jafar, *J. Chem. Eng. Data* **35** (1990) 355 (https://doi.org/10.1021/je00061a037)
21. M. McHugh, M. E. Paulaitis, *J. Chem. Eng. Data* **25** (1980) 326 (https://doi.org/10.1021/je60087a018)
22. M. Mukhopadhyay, *Natural extracts using supercritical carbon dioxide*, CRC press, Cleveland, OH, 2000
23. G. M. Kontogeorgis, G. K. Folas, *Thermodynamic models for industrial applications: from classical, advanced mixing rules to association theories*, John Wiley & Sons, Hoboken, NJ, 2009
24. I. Polishuk, I. Kapry, M. Madar, *Chem. Eng. Commun.* **196** (2008) 448 (https://doi.org/10.1080/00986440802483970)

25. R. C. Reid, J. M. Prausnitz, B. E. Poling, *The properties of gases, liquids*, McGraw Hill Book Co., New York, 1987
26. K. P. Johnston, D. H. Ziger, C. A. Eckert, *Ind. Eng. Chem. Fundam.* **21** (1982) 191 (https://doi.org/10.1021/i100007a001).

Journal of the Serbian Chemical Society
JSCS@tmf.bg.ac.rs • www.shd.org.rs/JSCS
J. Serb. Chem. Soc. 87 (6) S237–S246 (2022)
Supplementary material

SUPPLEMENTARY MATERIAL TO

Correlation of the solubility of solid hydrocarbons in supercritical CO_2 using different equations of state and mixing rules

NARJES SETOODEH and ABOLHASAN AMERI*

Department of Chemical Engineering, Shiraz Branch, Islamic Azad University, Shiraz, Iran

J. Serb. Chem. Soc. 87 (6) (2022) 735–747

The constants of PR and SRK equations of state are as below:

For SRK equation of state, c_1=0 and c_2=1.

$$a = a_c\left[1 + m\left(1 - \sqrt{T_r}\right)\right]^2 \tag{S-1}$$

$$a_c = 0.42748\frac{R^2T_c^2}{P_c} \tag{S-2}$$

$$m = 0.48 + 1.574\omega - 0.176\omega^2 \tag{S-3}$$

$$b = 0.08664\frac{RT_c}{P_c} \tag{S-4}$$

where, T_c, P_c and ω are indicative of critical temperature, critical pressure and acentric factor. T_r and R are the reduced temperature and universal gas constant. Similarly, for the PR equation of state, c_1=1-2$^{1/2}$ and c_2=1+2$^{1/2}$.

$$a = a_c\left[1 + m\left(1 - \sqrt{T_r}\right)\right]^2 \tag{S-5}$$

$$a_c = 0.45724\frac{R^2T_c^2}{P_c} \tag{S-6}$$

$$m = 0.37464 + 1.54226\omega - 0.26992\omega^2 \tag{S-7}$$

$$b = 0.007780\frac{RT_c}{P_c} \tag{S-8}$$

For a mixture of heavy component and SCF, the EOS parameters a and b are calculated by the following mixing rules:[1]

vdW1 mixing rule:

* Corresponding author. E-mail: ameri@iaushiraz.ac.ir

$$a = \sum_{\mathrm{i}} \sum_{\mathrm{j}} y_{\mathrm{i}} y_{\mathrm{j}} a_{\mathrm{ij}} \tag{S-9}$$

$$b = \sum_{\mathrm{j}} y_{\mathrm{j}} b_{\mathrm{j}} \tag{S-10}$$

$$a_{\mathrm{ij}} = \sqrt{a_{\mathrm{i}} a_{\mathrm{j}}} \left(1 - k_{ij}\right) \tag{S-11}$$

vdW2 mixing rule:

$$a = \sum_{\mathrm{i}} \sum_{\mathrm{j}} y_{\mathrm{i}} y_{\mathrm{j}} a_{\mathrm{ij}} \tag{S-12}$$

$$b = \sum_{\mathrm{i}} \sum_{\mathrm{j}} y_{\mathrm{i}} y_{\mathrm{j}} b_{\mathrm{ij}} \tag{S-13}$$

$$a_{\mathrm{ij}} = \sqrt{a_{\mathrm{i}} a_{\mathrm{j}}} \left(1 - k_{\mathrm{ij}}\right) \tag{S-14}$$

$$b_{ij} = \frac{b_i + b_j}{2} \left(1 - l_{ij}\right) \tag{S-15}$$

CVD mixing rule:

$$a = \sum_{\mathrm{i}} \sum_{\mathrm{j}} y_{\mathrm{i}} y_{\mathrm{j}} a_{\mathrm{ij}} \left(\frac{b}{b_{ij}}\right)^{M_{ij}} \tag{S-16}$$

$$b = \sum_{\mathrm{j}} y_{\mathrm{j}} b_{\mathrm{j}} \tag{S-17}$$

$$a_{ij} = \sqrt{a_{\mathrm{i}} a_{\mathrm{j}}} \tag{S-18}$$

$$b_{\mathrm{ij}} = \sqrt{b_{\mathrm{i}} b_{\mathrm{j}}} \tag{S 19}$$

Where, y_{i} and y_{j} are the mole fractions of the components i and j, and k_{ij} and l_{ij} are the binary interaction parameters, and i and j refer to ith and jth compound in the mixture. M_{ij} indicates the adjustable parameter in the CVD mixing rule. $\hat{a}_{\mathrm{i}}$ and $\hat{b}_{\mathrm{i}}$ in equation (7) of the manuscript are derivatives related to the attractive and repulsive parameters of EOS, which are calculated from the following equations:

vdW1 mixing rule:

$$\hat{a}_{\mathrm{i}} = \left[\frac{\partial(na)}{\partial n_{\mathrm{i}}}\right]_{T,P,n_{j\neq i}} = 2\sum_{\mathrm{j=1}}^{\mathrm{N}} y_{\mathrm{j}} a_{\mathrm{ij}} \tag{S-20}$$

$$\hat{b}_{\mathrm{i}} = \left[\frac{\partial(nb)}{\partial n_{\mathrm{i}}}\right]_{T,P,n_{\mathrm{j}\neq\mathrm{i}}} = b_i \tag{S-21}$$

vdW2 mixing rule:

$$\hat{a}_{\mathrm{i}} = \left[\frac{\partial(na)}{\partial n_{\mathrm{i}}}\right]_{T,P,n_{\mathrm{j\neq i}}} = 2\sum_{\mathrm{j=1}}^{\mathrm{N}} y_{\mathrm{j}} a_{\mathrm{ij}} \tag{S-22}$$

$$\hat{b}_{\mathrm{i}} = \left[\frac{\partial(nb)}{\partial n_{\mathrm{i}}}\right]_{T,P,n_{\mathrm{j\neq i}}} = 2\sum_{\mathrm{j=1}}^{\mathrm{N}} y_{\mathrm{j}} b_{\mathrm{ij}} \tag{S-23}$$

CVD mixing rule:

$$\hat{a}_{\mathrm{i}} = \left[\frac{\partial(na)}{\partial n_{\mathrm{i}}}\right]_{T,P,n_{\mathrm{j\neq i}}} = 2\sum_{\mathrm{j=1}}^{\mathrm{N}}\left(y_{\mathrm{j}} a_{\mathrm{ji}}\left(\frac{b}{b_{\mathrm{ij}}}\right)^{M_{\mathrm{ij}}}\right) + \left(\frac{b_{\mathrm{i}}}{b} - 1\right)\left[\sum_{\mathrm{i}}\sum_{\mathrm{j}} y_{\mathrm{i}} y_{\mathrm{j}} a_{\mathrm{ij}} M_{\mathrm{ij}}\left(\frac{b}{b_{\mathrm{ij}}}\right)^{M_{\mathrm{ij}}}\right] \tag{S-24}$$

$$\hat{b}_{\mathrm{i}} = \left[\frac{\partial(nb)}{\partial n_{\mathrm{i}}}\right]_{T,P,n_{\mathrm{j\neq i}}} = b_{\mathrm{i}} \tag{S-25}$$

The fitted binary parameters for modeling results and AARD for the combination of PR or SRK EoS and three mixing rules are given for 1-hexadecanol, 1-octadecanol, anthracene, benzoin, fluorene, hexamethylbenzene, mandelic acid, naphthalene, palmitic acid, phenanthrene, propyl 4-hydroxybenzoate, pyrene and stearic acid at different pressures and temperatures in Table S-I for calculation of solubility of heavy compounds in supercritical CO_2.

TABLE S-I. AARD for the solubility of pure component in supercritical CO_2 with the combination of three mixing rules and the PR and SRK EoS and optimized values of the binary interaction parameters (k_{ij}, l_{ij} and M_{ij}) for these EoS's

Component: 1-Hexadecanol						
T / K	Pressure range, bar	Number of points	Ref.	EoS	Mixing rule: vdW1	
					k_{ij}	AARD
318.1	52.1-415.1	7	15	PR	0.01587	48.906
				SRK	0.20536	51.786
328.15	141.8-415.9	5	15	PR	0.04241	14.342
				SRK	0.05924	15.202
338.15	147.1-373	6	15	PR	0.08148	82.776
				SRK	0.09667	86.544

Component: 1-Hexadecanol						
T / K	Pressure range, bar	Mixing rule: vdW2			Mixing rule: CVD	
		k_{ij}	l_{ij}	AARD	M_{ij}	AARD
318.1	52.1-415.1	0.01572	0.09993	12.271	0.84757	55.306
		0.15127	0.25232	15.270	0.89164	55.306
328.15	141.8-415.9	0.04209	0.06995	13.290	0.85462	50.206
		0.06198	0.09457	13.416	0.87767	52.505
338.1	147.1-373	0.08308	0.15000	10.780	0.98826	100.204
		0.14340	0.17999	11.032	0.91475	105.040

Component: 1-Octadecanol						
T / K	Pressure range, bar	Number of points	Ref.	EoS	Mixing rule: vdW1	
					k_{ij}	AARD
318.1	152.437.9	4	16	PR	0.15736	8.756
				SRK	0.18064	10.970

328.1	139.9-447.7	7	16	PR	0.19985	69.686
				SRK	0.22394	72.450
338.1	145.8-452.8	6	16	PR	0.13451	70.238
				SRK	0.14392	74.256

Component: 1-Octadecanol

T / K	Pressure range, bar	Mixing rule: vdW2			Mixing rule: CVD	
		k_{ij}	l_{ij}	AARD	M_{ij}	AARD
318.1	152.437.9	0.01604	0.05836	2.756	0.89275	10.044
		0.10013	0.13714	4.128	0.91746	14.206
328.1	139.9-447.7	0.13672	0.22387	7.128	0.93276	84.947
		0.14236	0.23713	11.239	0.97265	85.283
338.1	145.8-452.8	0.15219	0.21613	8.237	0.98735	88.385
		0.16513	0.21624	9.023	0.98725	80.039

Component: Anthracene

T / K	Pressure range, bar	Number of points	Ref.	EoS	Mixing rule: vdW1	
					k_{ij}	AARD
303.1	104.3-414.5	4	24	PR	0.06689	14.106
				SRK	0.07081	22.321
308.0	104.3-276.7	5	17	PR	0.06627	27.724
				SRK	0.07145	31.244
308.1	120-350	6	18	PR	0.23268	6.294
				SRK	0.15031	8.859
313.1	100-200	7	19	PR	0.25591	7.764
				SRK	0.17976	10.071
318.1	104.3-276.7	6	17	PR	0.07212	14.413
				SRK	0.07588	13.584
323.1	90.6-414.5	10	24	PR	0.07064	23.709
				SRK	0.07116	30.354
343.1	118.1-414.5	9	24	PR	0.07226	12.258
				SRK	0.06983	13.430

Component: Anthracene

T / K	Pressure range, bar	Mixing rule: vdW2			Mixing rule: CVD	
		k_{ij}	l_{ij}	AARD	M_{ij}	AARD
303.1	104.3-414.5	0.05597	89.99946	7.358	0.79824	16.310
		5.83E-02	84.99995	12.202	0.89274	15.320
308.0	104.3-276.7	0.05411	0.13341	26.105	0.76264	30.029
		0.05136	0.14497	27.607	0.79284	31.394
308.1	120-350	0.03878	0.07999	4.373	0.84463	7.020
		0.07346	1.99830	6.685	1.04595	11.800
313.1	100-200	0.04999	0.10454	4.401	0.86808	17.117
		0.09315	0.12673	9.229	1.12968	20.102
318.1	104.3-276.7	0.07639	0.09930	12.988	0.84728	15.094
		0.08054	0.11931	12.429	0.87163	14.292
323.1	90.6-414.5	0.05834	0.14067	20.872	0.91273	23.695
		0.05316	0.16772	25.762	0.88264	29.290
343.1	118.1-414.5	0.06244	0.14487	10.054	0.78216	13.395
		0.05683	0.16436	10.844	0.81738	15.204

Component: Benzoin

T / K	Pressure range, bar	Number of points	Ref.	EoS	Mixing rule: vdW1	
					k_{ij}	AARD
308.1	121.6-236.1	6	25	PR	0.10237	5.317
				SRK	0.11717	5.915
318.15	111.3-241.9	7	25	PR	0.11718	6.383
				SRK	0.09175	6.014
328.1	114.8-244.3	6	25	PR	0.12747	8.264
				SRK	0.13473	7.276

Component: Benzoin

T / K	Pressure range, bar	Mixing rule: vdW2			Mixing rule: CVD	
		k_{ij}	l_{ij}	AARD	M_{ij}	AARD
308.1	121.6-236.1	0.09372	0.16382	4.183	0.81265	6.024
		0.12175	0.15172	5.128	0.71636	6.847
318.1	111.3-241.9	0.10983	0.13286	5.185	0.87264	8.305
		0.08617	0.17648	3.836	0.83764	7.430
328.1	114.8-244.3	0.11364	0.16353	7.763	0.80373	10.295
		0.14524	0.15473	6.263	0.81646	9.205

Component: Fluorene

T / K	Pressure range, bar	Number of points	Ref.	EoS	Mixing rule: vdW1	
					k_{ij}	AARD
303.1	83.6-483.5	7	24	PR	0.12918	12.481
				SRK	0.19448	18.104
308.1	83.7-414.5	6	24	PR	0.15221	15.929
				SRK	0.15728	24.671
308.2	78.3-203.5	47	21	PR	0.12756	10.473
				SRK	0.13139	10.986
308.2	83.6-483.4	7	24	PR	0.13105	12.054
				SRK	0.13889	14.129
313.1	100-200	5	19	PR	0.16936	6.369
				SRK	0.17854	7.827
318.2	85-254	21	21	PR	0.28537	10.477
				SRK	0.26448	12.685
323.15	69.9-414.5	9	24	PR	0.13858	25.059
				SRK	0.16692	29.287
343.1	104.3-483.4	7	24	PR	0.14536	27.494
				SRK	0.15939	30.209

Component: Fluorene						
T / K	Pressure range, bar	Mixing rule: vdW2			Mixing rule: CVD	
		k_{ij}	l_{ij}	AARD	M_{ij}	AARD
303.15	83.6-483.5	0.18373	0.20947	9.937	1.03837	15.303
		0.21045	0.28728	11.193	1.73734	20.294
308.15	83.7-414.5	0.15226	0.22999	7.394	0.99837	16.394
		0.15463	0.69999	20.439	1.02928	27.447
308.2	78.3-203.5	0.13819	0.19628	5.202	1.01038	11.233
		0.13574	0.20483	6.037	0.99783	19.304
308.2	83.6-483.4	0.15838	0.23950	8.938	1.03928	14.293
		0.14211	0.27985	10.392	1.01384	16.320
313.1	100-200	0.17837	0.21947	5.937	1.01923	7.029
		0.18476	0.22857	6.174	1.03284	8.393
318.2	85-254	0.15839	0.19583	9.094	1.07363	12.119
		0.16837	0.17483	11.449	1.04627	14.203
323.1	69.9-414.5	0.12958	0.14979	12.546	1.09237	35.303
		0.16097	0.20883	13.711	1.10498	37.202
343.1	104.3-483.4	0.13765	0.23834	12.093	1.09283	39.303
		0.14849	0.25829	13.059	0.99082	45.303

Component: Hexamethylbenzene						
T / K	Pressure range, bar	Number of points	Ref.	EoS	Mixing rule: vdW1	
					k_{ij}	AARD
303.1	69.9-345.6	7	24	PR	0.16938	9.984
				SRK	0.17839	10.203
308.15	150-350	4	19	PR	0.11849	10.048
				SRK	0.15927	14.593
323.1	69.9-345.6	10	24	PR	0.17470	12.049
				SRK	0.17462	13.208
343.1	83.7-483.5	10	24	PR	0.19284	10.446
				SRK	0.14828	13.588

Component: Hexamethylbenzene						
T / K	Pressure range, bar	Mixing Rule : vdW2			Mixing rule: CVD	
		k_{ij}	l_{ij}	AARD	M_{ij}	AARD
303.1	69.9-345.6	0.18746	0.18363	6.303	0.92736	10.084
		0.19283	0.21348	7.303	0.98165	11.918
308.1	150-350	0.20483	0.17366	5.483	1.01838	13.202
		0.26403	0.16362	7.302	0.99937	15.324
323.1	69.9-345.6	0.28472	0.19826	7.044	1.07374	14.203
		0.26173	0.20193	9.939	0.98326	16.125
343.1	83.7-483.5	0.21383	0.14726	11.434	0.98827	12.404
		0.23887	0.17646	11.381	1.0038	14.092

Component: Mandelic acid						
T / K	Pressure range, bar	Number of points	Ref.	EoS	Mixing rule: vdW1	
					k_{ij}	AARD
308.1	101-228.5	7	25	PR	0.07103	43.710
				SRK	0.07914	46.699
318.1	102.3-225.7	7	25	PR	0.07722	35.007
				SRK	0.08461	38.077
328.1	104.4-230.6	9	25	PR	0.07679	26.111
				SRK	0.08321	27.563

Component: Mandelic acid

T / K	Pressure range, bar	Mixing Rule : vdW2			Mixing rule: CVD	
		k_{ij}	l_{ij}	AARD	M_{ij}	AARD
308.1	101-228.5	0.18347	0.41843	12.304	0.69294	57.303
		0.08035	0.37998	12.999	0.65123	60.202
318.1	102.3-225.7	0.17476	0.37592	14.437	0.68871	35.203
		0.08656	0.39999	13.059	0.69012	40.227
328.1	104.4-230.6	0.16832	0.41847	12.448	0.59283	33.203
		0.16482	0.43284	10.403	0.61385	32.403

Component: Naphthalene

T / K	Pressure range, bar	Number of points	Ref.	EoS	Mixing rule: vdW1	
					k_{ij}	AARD
308.15	86.8-255.3	9	22	PR	0.09665	8.843
				SRK	0.09987	5.357
328.1	82.2-287.8	16	22	PR	0.09852	23.707
				SRK	0.09921	21.278
333.5	82.2-291.4	19	22	PR	0.10633	38.764
				SRK	0.10529	30.104
338.0	165-252.4	7	22	PR	0.11224	22.926
				SRK	0.11127	31.287

Component: Naphthalene

T / K	Pressure range, bar	Mixing rule: vdW2			Mixing rule: CVD	
		k_{ij}	l_{ij}	AARD	M_{ij}	AARD
308.1	86.8-255.3	0.10868	0.49998	3.237	0.99272	9.101
		0.10679	0.25133	4.244	0.82826	7.494
328.1	82.2-287.8	0.00309	0.24324	11.385	0.82716	25.209
		0.02585	0.20343	7.491	0.84374	26.303
333.5	82.2-291.4	0.15622	0.18057	5.390	0.60929	41.304
		0.08823	0.25722	7.044	0.62847	45.339
338.0	165-252.4	0.07404	0.22484	2.786	0.78284	24.203
		0.082027	0.25373	3.539	0.7182	35.294

Component: Palmitic acid

T / K	Pressure range, bar	Number of points	Ref.	EoS	Mixing rule: vdW1	
					k_{ij}	AARD
318.1	142.1-360.6	5	15	PR	0.04015	46.881
				SRK	0.06423	55.141
328.1	144.1-573.5	7	15	PR	0.03676	104.982
				SRK	0.06380	101.197
338.1	142.5-574.8	7	15	PR	0.04938	111.431
				SRK	0.07862	94.291

Component: Palmitic acid

T / K	Pressure range, bar	Mixing rule: vdW2			Mixing rule: CVD	
		k_{ij}	l_{ij}	AARD	M_{ij}	AARD
318.15	142.1-360.6	0.01054	0.19484	34.311	0.76725	51.045
		0.04610	0.24637	36.403	0.79135	52.037
328.1	144.1-573.5	0.07827	0.15737	45.302	0.79274	110.04
		0.00793	0.16810	47.148	0.71546	113.504
338.1	142.5-574.8	0.05169	0.17383	35.492	0.82725	150.023
		0.09273	0.18393	37.428	0.87146	155.303

Component: Phenanthrene						
T / K	Pressure range, bar	Number of points	Ref.	EoS	Mixing rule: vdW1	
					k_{ij}	AARD
303.1	80.9-414.5	8	24	PR	0.11939	6.303
				SRK	0.13847	7.493
308.1	100-350	7	18	PR	0.12802	7.910
				SRK	0.13311	5.969
308.2	78.3-203.5	47	21	PR	0.13029	12.493
				SRK	0.12948	11.874
313.1	100-200	5	19	PR	0.11282	15.303
				SRK	0.10943	20.202
318.1	101-201	5	26	PR	0.12060	12.817
				SRK	0.12734	13.727
318.2	95-254	20	21	PR	0.09237	16.193
				SRK	0.13857	16.094
323.1	104.3-414.5	6	24	PR	0.13193	14.978
				SRK	0.13346	10.992
328.2	90-245	23	21	PR	0.09937	12.048
				SRK	0.12847	13.857
343.15	104.3-414.5	7	24	PR	0.13757	15.303
				SRK	0.14828	14.049

Component: Phenanthrene						
T / K	Pressure range, bar	Mixing rule: vdW2			Mixing rule: CVD	
		k_{ij}	l_{ij}	AARD	M_{ij}	AARD
303.1	80.9-414.5	0.13734	0.02857	6.304	1.01838	7.409
		0.16657	0.03827	7.000	1.12743	13.102
308.1	100-350	0.10240	0.07309	6.692	1.10348	18.912
		0.13357	0.16339	6.046	1.14257	14.385
308.2	78.3-203.5	0.19245	0.00002	10.019	0.93473	15.202
		0.20103	0.01833	11.303	0.94637	17.101
313.1	100-200	0.02938	0.38287	8.028	0.91636	20.202
		0.19373	0.01736	9.038	0.93727	22.371
318.15	101-201	0.14274	0.06999	6.992	1.10338	14.234
		0.12682	0.05727	13.724	1.21212	47.381
318.2	95-254	0.07173	0.02748	12.203	0.81636	18.202
		0.08273	0.01384	10.039	0.87463	17.209
323.1	104.3-414.5	0.10240	0.07309	6.692	1.10297	25.202
		0.12682	0.11938	9.652	1.39386	26.302
328.2	90-245	0.05663	-0.09983	8.0384	0.93874	18.503
		0.02348	0.18373	12.393	0.91837	17.493
343.1	104.3-414.5	0.07263	0.08726	12.394	0.82737	22.224
		0.07282	0.09826	13.928	0.82747	23.290

Component: Propyl 4-hydroxybenzoate						
T / K	Pressure range, bar	Number of points	Ref.	EoS	Mixing rule: vdW1	
					k_{ij}	AARD
308.15	94.1-220.9	7	25	PR	0.12737	10.2937
				SRK	0.14829	16.293
318.1	96.8-214.7	7	25	PR	0.15828	14.203
				SRK	0.12848	15.238
328.1	105.1-220.2	7	25	PR	0.15838	19.230
				SRK	0.17683	21.103

Component: Propyl 4-hydroxybenzoate						
T / K	Pressure range, bar	Mixing rule: vdW2			Mixing rule: CVD	
		k_{ij}	l_{ij}	AARD	M_{ij}	AARD
308.1	94.1-220.9	0.20193	0.19383	6.403	0.86253	15.204
		0.27467	0.17472	7.302	0.81543	14.204
318.1	96.8-214.7	0.21737	0.18237	9.129	0.79384	13.204
		0.21384	0.19438	10.39	0.81264	16.204
328.1	105.1-220.2	0.28577	0.20194	18.303	0.83727	22.405
		0.21747	0.17436	20.203	0.87464	26.304

Component: Pyrene						
T / K	Pressure range, bar	Number of points	Ref.	EoS	Mixing rule: vdW1	
					k_{ij}	AARD
308.2	80.4-203.5	45	21	PR	0.17473	15.393
				SRK	0.15177	14.203
308.2	83.6-483.4	7	24	PR	0.14900	14.126
				SRK	0.16027	16.301
318.2	95-254	20	21	PR	0.11393	10.934
				SRK	0.12859	11.304
323.15	104.3-483.4	7	24	PR	0.142989	23.531
				SRK	0.14786	28.384
328.2	105-245	20	21	PR	0.12848	8.282
				SRK	0.15626	7.827
343.1	104.3-483.4	8	24	PR	0.17827	34.283
				SRK	0.19383	37.292

Component: Pyrene						
T / K	Pressure range, bar	Mixing rule: vdW2			Mixing rule: CVD	
		k_{ij}	l_{ij}	AARD	M_{ij}	AARD
308.2	80.4-203.5	0.19193	0.17736	13.102	0.93736	18.403
		0.18436	0.16382	13.872	0.89273	16.302
308.2	83.6-483.4	0.13469	0.16226	12.638	0.91920	18.102
		0.14892	0.29847	15.392	0.93747	20.102
318.2	95-254	0.18943	0.09848	9.029	0.96282	11.103
		0.15839	0.11483	10.903	0.92726	13.203
323.1	104.3-483.4	0.12978	0.15030	12.550	0.90283	28.039
		0.13718	0.49999	18.922	0.89293	36.304
328.2	105-245	0.17837	0.13727	7.928	0.96635	11.048
		0.18173	0.17165	6.239	0.92374	9.093
343.15	104.3-483.4	0.26473	0.20198	26.303	0.89276	35.34
		0.21283	0.26438	30.202	0.80837	40.303

Component: Stearic acid						
T / K	Pressure range, bar	Number of points	Ref.	EoS	Mixing rule: vdW1	
					k_{ij}	AARD
318.1	145.4-361.5	6	16	PR	0.05372	17.309
				SRK	0.06838	16.093
328.1	154.8-467.5	6	16	PR	0.078283	25.320
				SRK	0.04829	32.292
338.1	161.5-463.8	5	16	PR	0.00017	41.039
				SRK	0.01736	40.293

Component: Stearic acid						
T / K	Pressure range, bar	Mixing rule: vdW2			Mixing rule: CVD	
		k_{ij}	l_{ij}	AARD	M_{ij}	AARD
318.1	145.4-361.5	0.01837	0.01288	10.010	0.89264	20.293
		0.02913	0.00182	11.202	0.82615	21.303
328.1	154.8-467.5	0.09837	0.16373	16.028	0.79374	34.204
		0.11433	0.26736	17.439	0.79832	40.203
338.1	161.5-463.8	0.11284	0.21938	20.202	0.81763	50.393
		0.02737	0.32278	21.239	0.89274	49.202

Journal of the Serbian Chemical Society
JSCS-info@shd.org.rs • www.shd.org.rs/JSCS

J. Serb. Chem. Soc. 87 (6) 749–760 (2022)
JSCS–5555

Original scientific paper
Published 18 February 2022

Influence of boron doping on characteristics of glucose-based hydrothermal carbons

ANA M. KALIJADIS[1], MARINA M. MALETIĆ[2*#], ANĐELIKA Z. BJELAJAC[2,3], BILJANA M. BABIĆ[4], TAMARA Z. MINOVIĆ ARSIĆ[1] and MARIJA M. VUKČEVIĆ[5#]

[1]*Department of Materials „Vinča" Institute of Nuclear Sciences – National Institute of the Republic of Serbia, University of Belgrade, Mike Petrovića Alasa 12–14, 11000 Belgrade, Serbia,* [2]*Innovation Center of the Faculty of Technology and Metallurgy, Karnegijeva 4, 11000 Belgrade, Serbia,* [3]*C2N – Centre for Nanoscience and NanoTechnology, University Paris-Saclay, 10 boulevard Thomas Gobert, 91120 Palaiseau, France,* [4]*Institute of Physics – National Institute of the Republic of Serbia, University of Belgrade, Pregrevica 118, 11080 Belgrade, Serbia and* [5]*Faculty of Technology and Metallurgy, University of Belgrade, Karnegijeva 4, 11000 Belgrade, Serbia*

(Received 11 October 2021, revised 30 December 2021, accepted 3 January 2022)

Abstract: In this study, the influence of boron doping on structural and surface properties of carbon material synthesized by a hydrothermal method was investigated, and the obtained results were compared with the previously published influence that boron has on characteristics of carbonized boron-doped hydrothermal carbons (CHTCB). Hydrothermal carbons doped with boron (HTCB) were obtained by the hydrothermal synthesis of glucose solutions with different nominal concentrations of boric acid. It was found that glucose based hydrothermal carbon does not have developed porosity, and the presence of boron in their structure has insignificant influence on it. On the contrary, additional carbonization increases the specific surface area of the undoped sample, while an increase in boron content drastically decreases the specific surface area. Boron doping leads to a decrease in the amount of surface oxygen groups, for both, hydrothermally synthesized and additionally carbonized materials. Raman analysis showed that the boron content does not affect a structural arrangement of the HTCB samples, and Raman structural parameters show a higher degree of disorder, compared to the CHTCB samples. Comparison of structural and surface characteristics of hydrothermal carbons and carbonized materials contributes to the study of the so far, insufficiently clarified influence that boron incorporation has on the material characteristics.

Keywords: hydrothermal synthesis; boric acid; Raman analysis; specific surface area; surface oxygen groups.

* Corresponding author. E-mail: mvukasinovic@tmf.bg.ac.rs
# Serbian Chemical Society member.
https://doi.org/10.2298/JSC211011001K

INTRODUCTION

Carbon can be found in a wide variety of allotropes from crystalline (diamond, graphite) to amorphous (carbon black, activated carbon, glassy carbon, *etc.*). In the past decades, nanostructured forms of crystalline carbon have received increasing attention due to their remarkable properties based on their unusual physicochemical properties.[1,2] The main disadvantage of using such crystalline nanocarbons for energy and environmental-related application is their high production costs. This is related to the rather expensive precursors and catalysts utilized, as well as to the complicated apparatus needed for their production normally involving high temperatures.

Conversely, hydrothermal carbonization has gained increasing attention in the field of material science, since it can successfully exploit cheap and renewable biomass as the carbon precursor.[3–6] In addition, hydrothermal carbonization demonstrates the capability of producing highly functionalized carbon material under a mild temperature (≈200 °C) and self-generated pressure.[7,8] The resultant materials were solid hydrophilic carbon microspheres with abundant functional groups on the surface. The characteristics of these microspheres, such as size, microstructure, and crystallinity, are controllable by the synthesis process and its respective experimental parameters.[9] It was reported that the sizes of the carbon spheres from styrene as a precursor can be controlled quite well by adjusting the pyrolysis parameters.[10] The carbon spheres obtained after pyrolysis showed a higher carbonization degree than those obtained by hydrothermal carbonization because the pyrolysis occurs at much higher temperatures.

However, just because of its low process temperature, the materials obtained by hydrothermal carbonization have some limiting factors, such as low ash content, low porosity, low aromatic structure, and low recalcitrance,[8] and the possibility to modify some of these properties is crucial for the expansion of its application. One of the most important prerequisites for the successful performance of hydrothermal carbonization-based materials in various applications is material functionality. Typical materials produced by hydrothermal carbonization contain polar surface oxygen groups, such as –COOH, −OH and –C=O.[11] The flexibility of hydrothermal carbonized materials is that groups present on the surface can be further functionalized. Two of the most commonly used methods of functionalization are: *in situ* functionalization and post-modification strategies. Heteroatom doping represents one of the possibilities for obtaining functionalized material *in situ* in one-step (bulk/surface) functionalization.[12,13] Among many heteroatoms, boron has been proved to induce interesting electronic properties to carbon materials.[14–17] Boron with its electrical structure shows a tendency for substitution incorporation in carbon structure up to its solid solubility limit. Above this limit, boron atoms have been shown to occupy interstitial positions in the lattice and have a disturbing effect on the structural properties.[18] The

presence of substitutionally bonded boron atoms in a carbon structure inhibit the C–O_2 reaction because boron acts as an electron acceptor, which could decrease the electron density at the carbon crystallite edges and this consequently leads to a reduction of both the number of active sites and the reactivity of these sites.[19] Nevertheless, a previous study showed that the number and nature of active sites and, consequently, the formation of surface oxides are dependent on the distribution of boron in the precursors.[20,21]

High-temperature treatment (HTT) of hydrothermally derived spheres represents one of the post-modification strategies that could lead to the removal of most of the oxygenated groups and convert the structure into a turbostratic-like disordered carbon structure with aromatic character and hydrophobic properties.[12] A previous study was focused on the characterization of boron-doped hydrothermal carbon with post high temperature treatment.[22] It was shown that the synergy of boron doping and thermal treatment to 1000 °C facilitated the preparation of a material with specific structural and surface chemistry characteristics, which are crucial for the application of the obtained material as a carbon paste electrode.

Many previous studies were focused on both applications and fundamental aspects motivated by the interest in producing carbonaceous powders with tunable sizes and surface properties.[23–26] To the best of our knowledge, there is no publication regarding the characterization of boron-doped hydrothermal carbons. Moreover, the influence that boron atoms have on the characteristics of carbon materials have not yet been fully clarified and, based on previous work,[20–22] it could be quite different, depending on boron concentration and distribution in the carbon material, the type of the carbon material and the stage of its modification. Considering these facts, the present study was aimed at the clarification of the influence of boron doping on the structural and surface properties of carbons synthesized by hydrothermal carbonization and the comparison of the obtained results with previously published results that are related to carbonized glucose based hydrothermal carbons. This comparison could provide a better insight into the influence of B doping on the structural and surface characteristics of carbon materials in the different stages of synthesis.

EXPERIMENTAL

To produce boron doped hydrothermal carbon (HTCB) samples, a 2 M aqueous solution of D(+)-glucose was prepared. Boric acid was used as the source of boron and it was added to the starting solution to obtain nominal boron concentrations of 0.0 (undoped sample), 0.2, 0.6 and 1.0 wt. %. After sealing, the autoclave was heated in a programmable oven for 24 h at 180 °C. The obtained samples were filtered, washed with distilled water and ethanol, and marked as hydrothermally carbonized samples: $HTCB_0$, $HTCB_{0.2}$, $HTCB_{0.6}$ and $HTCB_1$.

In order to reveal the influence of boron doping on the surface and structural characteristics of the hydrothermally synthesized carbons, the HTCB samples were characterized and the obtained results compared with the previously published[22] characteristics of boron-doped

hydrothermal carbons, synthesized in the same way, subsequently carbonized in nitrogen to 1237 K, and marked as $CHTCB_0$, $CHTCB_{0.2}$, $CHTCB_{0.6}$ and $CHTCB_1$.

Final boron concentrations were determined using inductively coupled plasma mass spectrometry (ICP-MS, Agilent 7500ce) with a detection limit for B of 0.1 g dm^{-3}. The samples were prepared according to the preparation method described in the literature: the samples were digested by fusing with sodium carbonate and dissolving the resulting melt in water with a small amount of hydrochloric acid.[14]

Raman spectra were taken with an Advantage 532 Raman spectrometer (DeltaNu Inc.) by a frequency doubled diode pumped YAG type laser operating at 532 nm.

Surface structure and morphology were studied by scanning electron microscopy (Mira Tescan X3).

Qualitative analyses of surface oxygen groups of samples were performed by Fourier transform infrared spectroscopy (FT-IR, Bomem MB-Series, Hartmann & Braun). The FT-IR measurements were performed at wavelengths in the range 4000 to 400 cm^{-1}.

The specific surface area of the HTCB samples was analyzed using the Surfer (Thermo Fisher Scientific, USA), and the mesopore surface and micropore volume were estimated using the *t*-plot method.[27] The tested samples were degassed at 100 °C for 4 h, and N_2 adsorption and desorption isotherms were obtained at the temperature of liquid nitrogen.

The Boehm method[28] was used for the determination of acidic and basic oxygen groups, present on the surface of the HTCB and CHTCB samples. For determination of the acidic sites, small quantities (0.1 g) of HTCB and CHTCB samples were mixed with 10 cm^3 of base solutions (0.1 M NaOH, 0.1 M $NaHCO_3$ or 0.05 M Na_2CO_3) in 25 cm^3 beakers. The beakers were sealed and shaken for 24 h. The solutions were then filtered and titrated with 0.05 M H_2SO_4. Similarly, the basic sites were determined by mixing 0.1 g of the examined materials with 10 cm^3 of 0.1 M HCl. The obtained solutions were titrated with 0.1 M NaOH.

RESULTS AND DISCUSSION

The presence of B in the structure of the examined samples was confirmed by ICP-MS, and the results are given in Table I. Considering that for the B-doped samples the initial concentrations of boron in the starting glucose solution were 0.2, 0.6 and 1.0 wt. %, it could be concluded that a considerable portion (60–72 %) of the boron atoms was incorporated into the HTCB samples. In contrast to that, the boron content in carbonized samples was significantly reduced and ranged from 0.09 to 0.19 wt.%,[22] indicating that a significant amount of boron is lost during thermal treatment. The results show that the content of dopant in the carbon materials obtained by the subsequent carbonization is not proportional to the concentration of dopant in the precursor. Furthermore, these results indicate that the chemical bonds between the boron and carbon atoms within the HTCB samples are quite weak, especially for the samples with the high nominal concentration of boron (0.6 and 1.0 wt. %), since most of the boron atoms leave the material during HTT, and only a small portion of the boron atoms manage to create chemical bonds and incorporate into the the structure of the carbonized material.

The SEM photographs of HTCB samples are shown in Fig. 1. In general, the morphologies of all samples consist of carbon spheres with a smooth surface.

The presence of 1.0 % of boron in the precursor solution induced a significant increase in the particle size, as well as an increase in the inhomogeneity of the size of the spheres.

TABLE I. Measured boron concentration and incorporation efficiency, and calculated Raman spectra parameters for the HTCB samples

Sample	c_B wt. %	B incorporation efficiency, %	Peak	Peak position cm^{-1}	Bandwidth cm^{-1}	I_D/I_G
$HTCB_0$	–	–	D	1390	221	1.7
			G	1608	136	
$HTCB_{0.2}$	0.12	60	D	1389	218	1.7
			G	1605	130	
$HTCB_{0.6}$	0.38	63	D	1382	220	1.6
			G	1597	133	
$HTCB_1$	0.72	72	D	1389	221	1.6
			G	1607	138	

As was previously shown,[29] more acidic conditions of starting glucose solutions induced by the addition of the boric acid could cause am enhancement of the hydrothermal reactions, which could induce particle condensation. The same trend of increasing particle size with the nominal concentration of boron is maintained after high temperature treatment.[22]

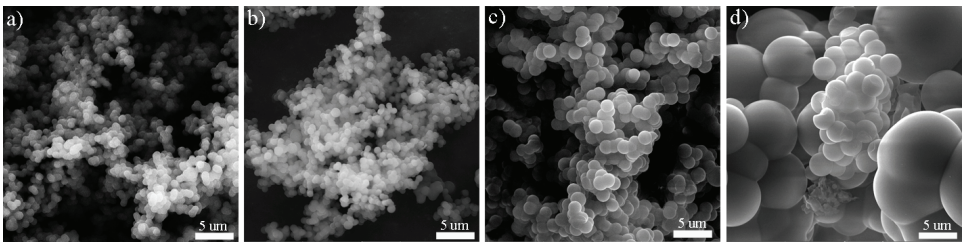

Fig. 1. SEM photographs of a) $HTCB_0$, b) $HTCB_{0.2}$, c) $HTCB_{0.6}$ and d) $HTCB_1$.

The structural characteristics of the HTCB samples were analyzed by Raman spectroscopy. From the Raman spectra of the HTCB samples (Fig. 2), it could be noticed that the D and G peaks, which are characteristic of the disordered carbon structure, are very well defined.[20,30,31] As previously shown,[22] incorporation of boron into the structure of CHTCB samples to a nominal concentration of 0.6 wt. % induced some kind of structural ordering, but for the sample with a nominal boron concentration of 1.0 wt. %, deterioration of structural parameters was observed as a result of the greater lattice point occupation by boron atoms. Nevertheless, the peaks of the HTCB Raman spectra are similar to each other and significantly wide, which indicates a more disordered structure of the HTCB samples compared to the CHTCB samples. In order to analyze changes in the bonding

structure, Raman spectra parameters (peaks position, bandwidth and intensity, I_D and I_G) were obtained by deconvolution of the spectra (not shown here), using Gaussian fitting. Values of I_D/I_G (Table I) also confirm the higher degree of disorder for the HTCB samples compared to CHTCB. Namely, for CHTCB samples, the values of I_D/I_G were in the range from 0.9 to 1.2, while for HTCB samples the values were 1.6 or 1.7 and this difference is a direct consequence of the thermal treatment up to 1000 °C, which involves the formation of a more carbonic structure with a higher degree of structural arrangement.[32–34] According to the Raman spectra parameters, B incorporation does not affect the structural characteristics of the HTCB samples.

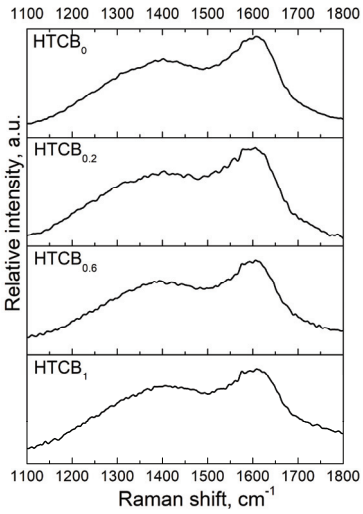

Fig. 2. Raman spectra of the HTCB samples.

Nitrogen adsorption-desorption isotherms for the HTCB samples, as the amount of N_2 adsorbed as function of relative pressure at –196 °C, are shown in Fig. 3.

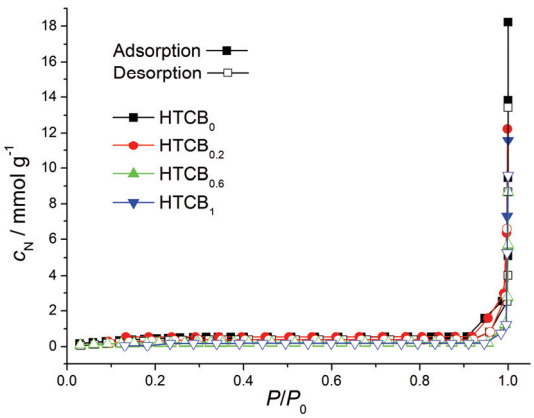

Fig 3. Nitrogen adsorption–desorption isotherms obtained for the HTCB samples.

According to the IUPAC classification,[35] the isotherms of the samples are of type II. Reversible type II isotherms are correlated with nonporous or macroporous adsorbents. The shape of isotherms is a consequence of the multilayer adsorption where thickness of the adsorbed multilayer sharply increases without limit at relative pressures close to 1. Specific surface areas calculated by the BET equation, S_{BET}, volume of micropores, V_{micro}, and mesoporous surface area, S_{meso}, are listed in Table II.

TABLE II. Textural characteristics of HTCB samples

Sample	S_{BET} / m^2 g^{-1}	S_{meso} / m^2 g^{-1}	V_{micro} / 10^{-3} cm^3 g^{-1}
$HTCB_0$	9.87	6.24	0.54
$HTCB_{0.2}$	8.12	4.98	0.47
$HTCB_{0.6}$	4.03	2.19	0.35
$HTCB_1$	4.98	2.93	0.39

The obtained S_{BET} values lie within 4–10 m^2 g^{-1} for all the tested samples and, along with other presented textural characteristics, confirm that the HTCB samples are nonporous. The reason for this lay in the chemical processes that follow hydrothermal carbonization, and involve carbonization and solubilization of the organics. Through these processes, tarry substances are formed, leading to plugging of the pores and cause the formation of carbon materials with closed porosity and very small values of the BET surface area.[36–38]

The ΔS_{BET} values, which represent the magnitude of the change in the S_{BET} values after thermal treatment of HTCB samples, are shown in Fig. 4 (ΔS_{BET} = = $S_{BET}(CHTCB_x) - S_{BET}(HTCB_x)$). A significant difference in the S_{BET} values before and after HTT, of almost 40 times, can be noticed for the undoped sample (0.0 wt.% B). However, for B-doped samples, the differences in the S_{BET} values decrease drastically, without showing a strictly doping-level dependence, even having a negative value for the sample with the highest nominal boron concen-

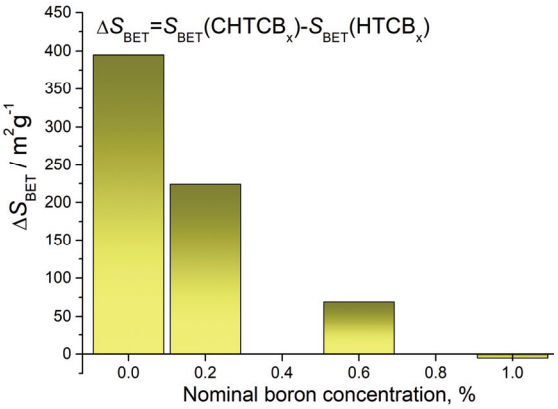

Fig. 4. The differences in S_{BET} values induced by subsequent carbonization of the HTCB samples.

tration (1.0 wt.% B). Based on this comparative analysis, it seems that the thermal treatment of undoped sample, $HTCB_0$, has an improvement effect on the surface area and porosity. On the contrary, the presence of B in the HTCB samples induced an inhibition of the development of the surface area for the final CHTCB samples. This may be a consequence of the alterations in the chemical reactions and processes, which follow the arranging carbon structure during carbonization, along with boron atom diffusion and its packing into the pores.[22,39]

Hydrothermally derived carbons are generally characterized with abundant functional groups on their surface.[40] To analyze the type of surface oxygen groups, FT-IR analysis of HTCB samples was performed, and FT-IR spectra are shown in Fig. 5. The broard band between 3000 and 3700 cm^{-1} is assigned to the stretching vibrations of O–H (hydroxyl or carboxyl), and the bands around 2815 to 3000 cm^{-1} are the characteristic stretching vibrations of aliphatic C–H. The bands near 1706 cm^{-1} and at 1622 cm^{-1} are attributed to C=O and C–C vibrations, suggesting aromatization of the samples during the hydrothermal treatment.[41,42] The peak at 1384 cm^{-1} is related to the deformation vibration of the C–O bond in the carboxyl group,[22] while the peaks in the range of 1300–1000 cm^{-1} may originate from the stretching vibrations of the C–OH bond, or bending vibrations of the O–H bond, indicating the presence of hydroxyl groups.[22] The peak at 797 cm^{-1} originates from the out-of-plane bending vibration of the aromatic C–H bond, while the peak at 1510 cm^{-1} originates from stretching vibrations of the aromatic ring.[43] It could be noted that the intensity of FT-IR spectra bands decreases for samples with higher boron content. A similar phenomenon was previously observed for carbonized HTCB samples.[22] The reduction of the content of surface oxygen groups related to the presence of B atoms in carbon structure is a well-known phenomenon. One of the explanations for this phenomenon is the redistribution of charge in a carbon material, which occurs when boron is substituted into its structure in a way to block the otherwise accessible active sites, and protect them from interaction with oxygen.[20,44]

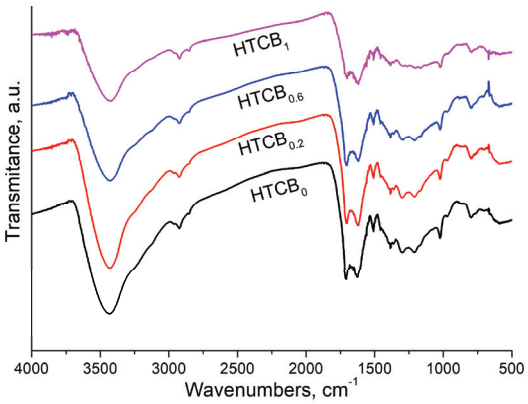

Fig. 5. FT-IR spectra of the HTCB samples.

The Boehm method was used to determine the acid/basic character of the HTCB samples, through the amounts of acidic surface oxygen groups (carboxyl, lactone, phenol), and basic functionalities (chromene, ketone, and pyrone groups, along with the delocalized π-electrons of graphene layers). The results obtained by Boehm titrations (Table III) confirmed the influence that the incorporated boron has on the content of surface oxygen groups, through the trend of decreasing the number of surface oxygen groups with increasing boron content. The obtained results showed that basic groups are dominant on the surface of both HTCB and CHTCB types of samples. The total amount of functional groups present on the surfaces of CHTCB samples was drastically lower, compared with HTCB samples, which is the consequence of the applied thermal treatment, which leads to the conversion of the more disorder (hydrothermal) carbon structure into a carbon structure with more prominent aromatic character and hydrophobic properties, characteristic for carbon materials obtained by carbonization.[12]

TABLE III. Amount of acidic and basic surface oxygen groups for the HTCB and carbonized HTCB samples

Sample	Amount of acidic groups, mmol g^{-1}	Amount of basic groups, mmol g^{-1}
$HTCB_0$	1.142	4.695
$HTCB_{0.2}$	1.153	4.502
$HTCB_{0.6}$	0.925	1.892
$HTCB_1$	0.896	1.388
$CHTCB_0$	0.162	0.187
$CHTCB_{0.2}$	0.038	0.066
$CHTCB_{0.6}$	0.031	0.056
$CHTCB_1$	0.030	0.058

CONCLUSIONS

Hydrothermal carbonization of glucose in the presence of boric acid led to a significant incorporation of boron atoms into the structure of hydrothermal carbon samples. However, under the high-temperature treatment, most of the boron atoms leave the material structure, due to the weak bonding established between boron atoms and hydrothermal carbon structure. Boron addition of 1.0 % in precursor solution induced significant enhancement of particles size, although high-temperature treatment led to a decrease of the particle size as a consequence of mass loss and shrinkage processes, which occur during the treatment. The number of surface oxygen groups was reduced by incorporation of boron, and further, even more reduced by additional high-temperature treatment. Raman analysis showed that the boron-doped hydrothermal carbon samples are characterized by a lower carbonic structure with a lower degree of structural arrangement without a clear dependence between parameters values and boron content in the structure. Due to the structural transition that occurs during high-temperature treatment, carbon-

ized boron-doped samples show much higher values of the specific surface area compared to the boron-doped hydrothermal carbon samples, but inversely proportional to the content of boron, the presence of which has a strong inhibitory effect on the development of porosity. Nevertheless, comparison of the results obtained for hydrothermal carbons in different stages of synthesis suggest that the presence of boron brings significant changes in the characteristics of the material, hence boron doping represent an effective method for tailoring the structure, morphology, and surface properties of hydrothermally synthesized carbons.

Acknowledgement. The research was funded by the Ministry of Education, Science and Technological Development of the Republic of Serbia (Contracts No. 451-03-9/2021-14/ /200135, 451-03-9/2021-14/200287 and 451-03-9/2021-14/200017).

ИЗВОД

УТИЦАЈ ДОПИРАЊА БОРОМ НА КАРАКТЕРИСТИКЕ ХИДРОТЕРМАЛНИХ КАРБОНА НА БАЗИ ГЛУКОЗЕ

АНА М. КАЛИЈАДИС[1], МАРИНА М. МАЛЕТИЋ[2], АНЂЕЛИКА З. БЈЕЛАЈАЦ[2,3], БИЉАНА М. БАБИЋ[4], ТАМАРА З. МИНОВИЋ АРСИЋ[1] и МАРИЈА М. ВУКЧЕВИЋ[5]

[1]*Лабораторија за материјале, Институт за нуклеарне науке Винча-Институт од националног значаја, Универзитет у Београду, Мике Петровића Аласа 12–14, 11000 Београд,* [2]*Иновациони центар Технолошко–металуршког факултета, Карнегијева 4, 11000 Београд,* [3]*C2N – Centre for Nanoscience and Nanotechnology Universite Paris-Saclay, 10 boulevard Thomas Gobert, 91120 Palaiseau, France,* [4]*Институт за физику-Институт од националног значаја, Универзитет у Београду, Прегревица 118, 11080 Београд и* [4]*Технолошко–металуршки факултет, Универзитет у Београду, Карнегијева 4, 11000 Београд*

У овом раду испитан је утицај инкорпорације бора на структурне и површинске карактеристике хидротермалних карбона (HTCB), добијених хидротермалном карбонизацијом глукозе у присуству различитих концентрација борне киселине, као прекурсора бора. Извршена је површинска и структурна карактеризација материјала, а добијени резултати су упоређени са карактеристикама накнадно карбонизованих HTCB. Резултати су показали да хидротермални карбон на бази глукозе нема развијену порозност, а присуство бора у структури ових материјала нема значајнијег утицаја на специфичну површину. С друге стране, додатна карбонизација повећава специфичну површину недопираног узорка, а повећање садржаја бора доводи до драстичног смањења специфичне површине. Допирање бором доводи до смањења количине површинских кисеоникових група, како код хидротермално синтетисаних, тако и код додатно карбонизованих материјала. Анализом Раманских спектара утврђено је да садржај бора не утиче на структурно уређење узорака HTCB, као и да накнадна карбонизација доводи до повећања уређености структуре. Поређење структурних и површинских карактеристика хидротермалних карбона допираних бором и накнадно карбонизованих материјала допринеће разјашњењу утицаја инкорпорације бора на карактеристике ових материјала.

(Примљено 11. октобра 2021, ревидирано 30. децембра 2021, прихваћено 3. јануара 2022)

REFERENCES

1. M. W. Moon, H. Y. Kim, A. Wang, A. Vaziri, *J. Nanomater.* **2015** (2015) 916834 (http://dx.doi.org/10.1155/2015/916834)

2. A. Hirsch, The era of carbon allotropes, *Nat. Mater.* **9** (2010) 868 (https://doi.org/10.1038/nmat2885)
3. M. M. Titirici, M. Antonietti, *Chem. Soc. Rev.* **39** (2010) 103 (https://doi.org/10.1039/b819318p)
4. Y. Wang, L. Qiu, M. Zhu, G. Sun, T. Zhang, K Kang, *Sci. Rep.* **9** (2019) 5535 (https://doi.org/10.1038/s41598-019-38849-4)
5. P. Zhu, J. Liu, J. Ma, L. Li, X. Zhang, *J. Biobased. Mater. Bio.* **15** (2021) 97 (https://doi.org/10.1166/jbmb.2021.2030)
6. C. Falco, F. Perez Caballero, F. Babonneau, C. Gervais, G. Laurent, M. M. Titirici, N. Baccile, *Langmuir* **27** (2011) 14460 (https://doi.org/10.1021/la202361p)
7. M. M. Titirici, A. Thomas, M. Antonietti, *New J. Chem.* **31** (2007) 787 (https://doi.org/10.1039/b616045j)
8. X. Zhu, Y. Liu, F. Qian, S. Zhang, J. Chen, *Energy Fuels* **29** (2015) 5222 (https://doi.org/10.1021/acs.energyfuels.5b00512)
9. X. Sun, Y. Li, *Angew. Chem. Int. Ed.* **43** (2004) 597 (https://doi.org/10.1002/anie.200352386)
10. Y. Z. Jin, C. Gao, W. Kuang Hsu, Y. Zhu, A. Huczko, M. Bystrzejewski, M. Roe, C. Y. Lee, S. Acquah, H. Kroto, D. R. M. Walton, *Carbon* **43** (2005) 1944 (https://doi.org/10.1016/j.carbon.2005.03.002)
11. S. A. Nicolae, H. Au, P. Modugno, H. Luo, A. E. Szego, M. Qiao, L. Li, W. Yin, H. J. Heeres, N. Berge, M. M. Titirici, *Green Chem.* **22** (2020) 4747 (https://doi.org/10.1039/d0gc00998a)
12. A. Kalijadis, N. Gavrilov, B. Jokić, M. Gilić, A. Krstić, I. Pašti, B. Babić, *Mater. Chem. Phys.* **239** (2020) 122120 (https://doi.org/10.1016/j.matchemphys.2019.122120)
13. M. M. Titirici, R. J. White, C. Falcoa, M. Sevilla, *Energy Environ. Sci.* **5** (2012) 6796 (https://doi.org/10.1039/c2ee21166a)
14. Y. J. Lee, Y. Uchiyama, Lj. R. Radovic, *Carbon* **42** (2004) 2233 (https://doi.org/10.1016/j.carbon.2004.04.030)
15. X. Wu, Lj. R. Radovic, *Carbon* **43** (2005) 1768 (https://doi.org/10.1016/j.carbon.2005.02.029)
16. Y. J. Leea, H. J. Joo, Lj. R. Radovic, *Carbon* **41** (2003) 2591 (https://doi.org/10.1016/S0008-6223(03)00372-5)
17. J. S. Đorđević, A. M. Kalijadis, K. R. Kumrić, Z. M. Jovanović, Z. V. Laušević, T. M. Trtić--Petrović, *Cent. Eur. J. Chem.* **10** (2012) 1271 (https://doi.org/10.2478/s11532-012-0042-1)
18. S. Marinkovic, in *Chemistry and physics of carbon*, P. A. Thrower, Ed., Marcel Dekker Inc., New York, 1984., p. 1
19. Z. Huang, X. Liu, K. Li, D. Li, Y. Luo, H. Li, W. Song, L. Q. Chen, Q. Meng, *Electrochem. Commun.* **9** (2007) 596 (https://doi.org/10.1016/j.elecom.2006.10.028)
20. A. Kalijadis, Z. Jovanović, M. Laušević, Z. Laušević, *Carbon* **49** (2011) 2671 (https://doi.org/10.1016/j.carbon.2011.02.054)
21. A. Kalijadis, Z. Jovanović, I. Cvijović-Alagić, Z. Laušević, *Nucl. Instrum. Methods, B* **316** (2013) 17 (http://dx.doi.org/10.1016/j.nimb.2013.08.030)
22. A. Kalijadis, J. Đorđević, T. Trtić-Petrović, M. Vukčević, M. Popović, V. Maksimović, Z. Rakočević, Z. Laušević, *Carbon* **95** (2015) 42 (http://dx.doi.org/10.1016/j.carbon.2015.08.016)
23. C. Falco, N. Baccile, M. M. Titirici, *Green Chem.* **13** (2011) 3273 (http://dx.doi.org/10.1039/c1gc15742f)

24. J. A. Libra, K. S. Ro, C. Kammann, A. Funke, N. D. Berge, Y. Neubauer, M. M. Titirici, C. Fühner, O. Bens, J. Kern, K. H. Emmerich, *Biofuels* **2** (2011) 89 (http://dx.doi.org/10.4155/bfs.10.81)
25. A. D. Roberts, X. Li, H. Zhang, *Chem. Soc. Rev.* **43** (2014) 4341 (http://dx.doi.org/10.1039/c4cs00071d
26. P. Zhang, Z. A. Qiaoa, S. Dai, *Chem. Commun.* **51** (2015) 9246 (http://dx.doi.org/10.1039/c5cc01759a)
27. B. C. Lippens, B. G. Linsen, J. H. de Boer, *J. Catal.* **3** (1964) 32 (https://doi.org/10.1016/0021-9517(64)90089-2)
28. A. M. Kalijadis, M. M. Vukčević, Z. M. Jovanović, Z. V. Laušević, M. D. Laušević, *J. Serb. Chem. Soc.* **76** (2011) 757 (http://dx.doi.org/10.2298/JSC091224056K)
29. M. M. Titirici, in *Novel Carbon Adsorbents*, J. M. D. Tascón, Ed., Elsevier, Oxford, 2012, p. 351 (http://dx.doi.org/10.1016/B978-0-08-097744-7.00012-0)
30. A. C. Ferrari, J. Robertson, *Phys. Rev., B* **61** (2000) 14095 (https://doi.org/10.1103/PhysRevB.61.14095)
31. S. Urbonaite, L. Halldahl, G. Svensson, *Carbon* **46** (2008) 1942 (https://doi.org/10.1016/j.carbon.2008.08.004)
32. Z. Wang, H. Ogata, G. J. Hong Melvin, M. Obata, S. Morimoto, J. Ortiz-Medina, R. Cruz-Silva, M. Fujishige, K. Takeuchi, H. Muramatsu, T. Y. Kim, Y. A. Kim, T. Hayashi, M. Terrones, Y. Hashimoto, M. Endo, *Carbon* **121** (2017) 423 (http://dx.doi.org/10.1016/j.carbon.2017.06.003)
33. H. Fujimoto, *Carbon* **41** (2003) 1585 (http://dx.doi.org/10.1016/S0008-6223(03)00116-7)
34. Z. Q. Li, C. J. Lu, Z. P. Xia, Y. Zhou, Z. Luo, *Carbon* **45** (2007) 1686 (http://dx.doi.org/10.1016/j.carbon.2007.03.038)
35. K. S. W. Sing, D. H. Everett, R. A. W. Haul, L. Moscou, R. A. Pierotti, J. Rouquerol, T. Siemieniewska, *Pure Appl. Chem.* **57** (1985) 603 (https://doi.org/10.1351/pac198557040603)
36. S. E. Elaigwu, G. M. Greenway, *Int. J. Ind. Chem.* **7** (2016) 449 (http://dx.doi.org/10.1007/s40090-016-0081-0)
37. M. M. Titirici, M. Antonietti, N. Baccile, *Green Chem.* **10** (2008) 1204 (http://dx.doi.org/10.1039/b807009a)
38. M. Sevilla, A. B. Fuertes, *Chem. Eur. J.* **15** (2009) 4195 (http://dx.doi.org/10.1002/chem.200802097)
39. S. Karthikeyan, K. Viswanathan, R. Boopathy, P. Maharaja, G. Sekaran, *J. Ind. Eng. Chem.* **21** (2015) 942 (https://doi.org/10.1016/j.jiec.2014.04.036)
40. S. Kubo, I. Tan, R. J. White, M. Antonietti, M. M. Titirici, *Chem. Mater.* **22** (2010) 6590 (http://dx.doi.org/10.1021/cm102556h)
41. Y. Gao, X. Wang, J. Wang, X. Li, J. Cheng, H. Yang, H. Chen, *Energy* **58** (2013) 376 (http://dx.doi.org/10.1016/j.energy.2013.06.023)
42. Z. Zhang, K. Wang, J. D. Atkinson, X. Yan, X. Li, M. J. Rood, Z. Yan, *J. Hazard. Mater.* **229–230** (2012) 183 (http://dx.doi.org/10.1016/j.jhazmat.2012.05.094)
43. M. Zbair, M. Bottlinger, K. Ainassaari, S. Ojala, O. Stein, R. L. Keiski, M. Bensitel, R. Brahmi, *Waste Biomass Valor.* **11** (2020) 1565 (https://doi.org/10.1007/s12649-018-00554-0)
44. Lj. R. Radovic, M. Karra, K. Skokova, P. A. Thrower, *Carbon* **36** (1998) 1841 (https://doi.org/10.1016/S0008-6223(98)00156-0).

Journal of the Serbian Chemical Society
JSCS-info@shd.org.rs • www.shd.org.rs/JSCS

J. Serb. Chem. Soc. 87 (6) 761–773 (2022)
JSCS–5556

Original scientific paper
Published 23 March 2022

Self-aggregation of soil humic acids with respect to their structural characteristics

UROŠ D. JOVANOVIĆ[1], MIRJANA M. MARKOVIĆ[1]*, ĐURO M. ČOKEŠA[1], NIKOLA V. ŽIVKOVIĆ[1] and SVJETLANA B. RADMANOVIĆ[2]

[1]*University of Belgrade – Vinča Institute of Nuclear Sciences, P.O. Box 522, 11001 Belgrade, Serbia and* [2]*University of Belgrade – Faculty of Agriculture, Nemanjina 6, 11080 Belgrade, Serbia*

(Received 25 November 2021, revised 16 February, accepted 21 February 2022)

Abstract: The main goal of this work was to estimate the influence of carboxyl and phenolic groups, as well as aromatic, aliphatic and polysaccharide components, on the soil humic acids (HA) self-aggregation process. Soil HAs (leptosol and regosol) were separated using base resin getting fractions with different functional group contents. Blocking of carboxyl groups was performed using the esterification procedure to estimate the participation of each functional group in the HA aggregation. The presence of HA structural components was evaluated by potentiometric titration and ATR-FTIR. The aggregation was monitored at pH 3 using dynamic light scattering. Results indicated that the higher group content, the HA aggregation is less pronounced. A significant positive correlation of aliphatic C and aggregate size revealed their dominant influence in the HA self-aggregation. A lower abundance of aliphatic C in HA fractions could be considered as not sufficient to start the process. An increase of aromatic C in esters likely pointed out to its participation in hydrophobic bonding and, consequently, more pronounced aggregation. The relation of HA self-aggregate size with carboxyl and phenolic group, as well as aliphatic C, at low pH, could be considered universal regardless of the structural characteristics of the original or modified HA forms.

Keywords: fractionation; esterification; carboxyl group; phenolic group; aliphatic C; aromatic C.

INTRODUCTION

Humic substances (HS), having significant environmental functions, are the most important organic components present in water, soil, and sediments.[1] HS affect the soil and water properties through their participation in the dynamic processes where their constituent molecules interact with other molecules or ions

* Corresponding author. E-mail: mmmark@vinca.rs
https://doi.org/10.2298/JSC211125010J

(complexation/decomplexation), solid surfaces (adsorption/desorption) and among themselves (aggregation/deaggregation).[2]

The concept of HS molecular organization is based on the main principles of supramolecular chemistry, namely HS represents ensembles of relatively small organic molecules.[3] Humic acids (HA), as one of the HS fractions, behave as molecular aggregates or supramolecular structures, formed from small individual moieties.[4] The HA aggregation process depends on various environmental conditions such as suspension pH, ionic strength, HA concentration, residence time, type and concentration of organic and inorganic ions and presence of solid particles, *etc*., as well as on the HA structural properties (size, shape, conformation, functional groups).[4–6]

Humic acids have a large number of reactive functional groups influencing their environmental behavior. That is why the HA functional groups recently became the subject of great research interest. Most of the studies are related to their interaction with various organic and inorganic compounds in soil and water, predominantly pollutants. Some articles are dealing with the role of reactive functional groups in the HA aggregation process in the presence of ionic or molecular species.[7–9] Mecozzi and Pietrantonio[10] which suggested that, besides functional groups, other HA structural components such as carbohydrates, proteins and lipids also participate in the HA self-aggregation process. Chilom *et al.*[11] and Hoffman *et al.*[12] emphasized that lipid HA components play a facilitative role in the forming of HA aggregates. Hakima and Kobayash[13] concluded that a higher aromatic content induces more pronounced HA self-aggregation.

As the complex nature of HA makes it difficult to get precise information on their chemical structure and properties, their heterogeneity can be reduced by separating them into various fractions.[14] Different types of HA fractionations were performed in order to obtain fractions with various structural properties. Size-exclusion chromatography and electrophoresis, as well as their combination, are widely used for HA fractionation.[15] In addition to the above, other fractionation methods were used such as such as reversed-phase high-performance liquid chromatography, aqueous alkaline and organic solvent extractions, subsequent dissolution in buffers adjusted to different pH and sequential dissolution in buffers with increasing pH values, separation by secondary amine weak base resin *etc*.[11,14,16,17]

To the best of our knowledge, the relation between HA self-aggregation and their functional group content, although very important, was not comprehensively studied. Additionally, despite the participation of other structural components in HA self-aggregation has been previously studied, no unambiguous conclusions were drawn. Hence, the main goal of this work is to estimate the influence of carboxyl and phenolic groups as well as aromatic, aliphatic and polysaccharide components on the soil HA self-aggregation process. In order to achi-

eve this, two soil humic acids of different origin were separated using base resin thus getting fractions which have different functional group contents. To estimate the participation of each particular functional group in HA aggregation, blocking of carboxyl groups was performed using the esterification procedure. The presence of structural components in the original and modified HAs was evaluated by potentiometric titration and/or ATR-FTIR spectroscopy. The aggregation process was monitored using dynamic light scattering (DLS) measurements.

EXPERIMENTAL

Humic acid extraction

Rendzic Calcaric Leptosol humic acid (RCLHA) was isolated from soil classified as Rendzic Calcaric Leptosol (Loamic),[18] originating from Negotin, Serbia. The soil has developed on indurated limestone, at 199 m above sea level (MASL), area under forest. The soil sample taken from the A horizon (0–25 cm depth) had the following characteristics: light clay texture, 4.2 % $CaCO_3$, pH 7.71, 6.25 % total organic C. Leptic Calcaric Regosol humic acid (LCRHA) was isolated from soil classified as Leptic Calcaric Regosol (Loamic, Aric),[18] originating from Stari Slankamen, Serbia, developed on sandy marl, at 187 MASL, area under grassland. The soil sample taken from the A horizon (0–20 cm depth) had the characteristics as follows: sandy loam texture, 14.78 % $CaCO_3$, pH 7.69, 4.31 % total organic C. Soil texture, pH (soil/water = 1/2.5), carbonate and total organic C content were determined by common methods.[19]

Humic acid (HA) samples were isolated using a modified International Humic Substance Society (IHSS) method (HA gel was dried at 35 °C, powdered, and sieved using a 0.05 mm sieve).[20]

HA elemental composition was determined to be as follows: C 51.82 %, H 4.80 %, O 39.98 %, N 3.40 %, for RCLHA and C 52.04 %, H 5.18 %, O 37.96 %, N 4.82 % for LCRHA. Elemental composition was determined by using the elemental analyzer (CHNS 628, LECO Corporation, St. Joseph, MI, USA) after drying the samples over P_2O_5 under vacuum. Their percentage was calculated on an ash-free basis.

The IHSS standard humic acid (ESHA) was isolated from Elliott Soil.[20] Elliott Soil is silt loam, silty clay loam or loam, moderately acid to neutral. In this study, ESHA was used only in its unmodified form.

Humic acid fractionation

HA fractionation was performed according to Lin *et al.*[16] The secondary amine weak base resin (Amberlyst® A21 free base, Aldrich Chemistry, Germany) was soaked with 10 % NaCl (Kemika, Croatia) solution, left for two hours and used as a column (1.95 cm diameter, 27 cm height) package (approx. resin volume 80 cm^3). The resin was washed using deionized water.

HA water suspension (0.1 %) was initially adjusted to pH 7, stirred overnight at 25±2 °C and pumped through a column at a rate of 4 mL min^{-1}. The effluent collected is termed as fraction 1 (F1). After rinsing with deionized water, the resin was eluted with 1 M NaOH solution until the discoloration and fraction 2 (F2) were obtained. The resin was washed again with deionized water and as HA was not completely eluted, 10 % NaCl solution was pumped through the column eluting fraction 3 (F3). To precipitate all the HA fractions obtained, pH was adjusted to <1, centrifuged (4000 rpm) washing it with 0.1 M HCl until Na^+ concentration in filtrates was less than 0.1 ppm (determined by atomic atomic absorption spectrometry

(AAS), AAnalyst 700, Perkin Elmer, USA). Precipitates were dried at 38 °C and used for further analyses.

Humic acid esterification

To block HA functional groups, the esterification procedure proposed by Andjelkovic *et al.*[21] was modified as follows: 5 ml of thionyl chloride (Merck, Germany) was added dropwise using a dropping funnel to a stirred HA solution (300 mg of HA in 12 ml of methanol (Merck) at approximately 5 °C (ice-cooling) and the mixture was stirred for 3 hours at the same temperature. Afterwards, the reaction mixture was left overnight at 25±2 °C to decompose excess thionyl chloride. The HA suspension was centrifuged at 4000 rpm for 10 min and the precipitated ester was washed using distilled water and 0.1 M HCl until the test for sulphates was negative. The esterification procedure was repeated twice, and the final esterified products (HA E) were dried at 38 °C overnight.

Elemental analysis (C, H, N and S)

The C content of HA samples was determined by the elemental analyzer (CHNS 628, LECO Corporation) after drying the samples over P_2O_5 under vacuum, carboxyl and phenolic group contents were calculated.

Attenuated total reflection Fourier-transform infrared spectroscopy (ATR-FTIR)

ATR-FTIR spectra of HAs in the 4000–400 cm^{-1} range were recorded by an Alpha spectrometer (Bruker, Germany, 4 cm^{-1} resolution, 64 scans). The air spectrum was used as background. Peak intensities were determined relative to the baseline dependent on the spectral region. Baselines in the 3700–1800 and 3000–2800 cm^{-1} range were used for 3283 and 2920 cm^{-1} bands, respectively. Intensities of 1705, 1620, 1520, 1080 and 1030 cm^{-1} bands were determined using the baseline between 1830 and 400 cm^{-1}. Relative peak intensities of 3283, 2920, 1705, 1620, 1080 and 1030 cm^{-1} bands were calculated by dividing peak intensity values by that for the 1520 cm^{-1} band.[22] Each peak height was calculated as an average of two replicates.

Acid–base titrations

The modified procedure of Ritchie and Perdue[23] was used for acid–base titrations of HA functional groups. HA suspensions (0.36 g L^{-1}) were prepared in 10 mL of 0.1 M NaCl, after which 0.2 mL of 0.1 M NaOH were added and left overnight to be completely dissolved. To neutralize the added NaOH, 0.2 mL of 0.1 M HCl was added, and titrations performed using the automatic titrator (Radiometer TTT85, Denmark). The previously calibrated (pH 4, 7 and 10 standard buffers) combined pH electrode (Radiometer PHC2601-8, France) was used to monitor pH. Temperature was maintained at 25.00±0.02 °C and the sample continually stirred under a nitrogen atmosphere. The initial pH suspension was recorded. The NaOH titrant was added in 7 μL increments (titration rate 12.5 μL min^{-1}) and the next titration step was not initiated until a pH value stable for 7 s (with drift of no more than 0.001 pH unit) was obtained. Each sample was titrated from its initial pH (3.0 to 3.3) to maximum 10.5-10.7 pH within 25 to 35 min. Three replicate titrations were performed for each HA sample, fourth titration done only if unusual pH behavior or equipment malfunction were noticed.

Dynamic light scattering

To perform dynamic light scattering (DLS) measurements, the HA suspensions (0.02 g dm^{-3}) were prepared in 0.1 M NaCl to maintain the ionic strength constant. Their pH value was adjusted to pH 10 using 0.1 and 1.0 M NaOH solutions and suspensions were equilibrated for 72 h at 25±2 °C and their pH values checked prior to the measurement. Due to pronounced

HA aggregation at low pH values, alkaline suspensions were acidified to pH 3 by HCl (0.1 and 1.0 M) for further size measurements.

Size measurements were performed using a Zeta-sizer Nano ZS with 633 nm He–Ne laser (Malvern Panalytical, Malvern, UK), and data analyzed by the Zetasizer Software version 6.20 (Malvern Panalytical, Malvern, UK). Measurement details are presented in Jovanović *et al.*[4] Absorbances of alkaline and acid suspensions at 633 nm, needed for size measurements, were recorded by UV–Vis spectroscopy (Evolution 60s, Thermo Fisher Scientific, Waltham, MA, USA).

The aggregate size for both HAs, esters and fractions was correlated to carboxyl and phenolic group content (obtained by the titration method) using Origin 8.5.1 software.

RESULTS AND DISCUSSION

HA carboxyl and phenolic functional groups content

Carboxyl and phenolic group content, obtained by titration method, as well as the most intensive peak in the PSD (d), are summarized in Table I. With a goal to separate carboxyl and phenolic functional groups, HAs studied were fractionated using the secondary amine weak base resin. According to Lin *et al.*,[16] HA solution, after passing through the resin column, should contain a higher content of carboxyl group (F1), while the phenolic group should be retained at the resin and eluted with 1 M NaOH solution (F2). But, as in this study, HA was not completely eluted (the resin remained dark colored), 10 % NaCl solution was pumped through the column obtaining fraction F3. It is evident from functional group contents obtained by the titration method that the separation procedure used did not completely fractionate humic acids into phenolic and carboxyl groups, as already concluded by Lin *et al.*[16]

TABLE I. Functional groups content and the most intensive peak in particle size distribution (d) of Rendzic Calcaric Leptosol (RCLHA), Leptic Calcaric Regosol (LCRHA) humic acids, their fractions (F1-F3) and esterified forms (E), and IHSS standard Elliott Soil humic acid (EHA)

HA sample	Functional group content, mqe gC^{-1}		d / nm	log (d / nm)
	Carboxyl	Phenolic		
RCLHA	10.8±0.2	2.8±0.7	515.0	2.712
RCLHA E	9.7±0.3	2.1±0.2	3265	3.514
RCLHA F1	10.4±0.4	2.71±0.04	873.7	2.941
RCLHA F2	14.8±4.3	4.8±1.2	31.71	1.501
RCLHA F3	15.5±0.7	4.6±0.7	9.290	0.968
LCRHA	8.2±1.2	3.0±1.1	32.66	1.514
LCRHA E	4.0±0.5	4.0±1.3	506.3	2.704
LCRHA F1	8.3±1.0	3.3±1.1	997.4	2.999
LCRHA F2	13.9[a]	5.4[a]	39.44	1.596
LCRHA F3	11.9±0.2	3.02±0.06	9.483	0.977
EHA	7.5±0.5	2.7±0.1	5180	3.714

[a]One measurement due to small F2 quantity

By comparing carboxyl and phenolic groups content in fractions and unfractionated RCLHA, a difference was noticed within measurement uncertainty for F1, while increase was obvious for F2 and F3. Both functional group contents for LCRHA and F1, within measurement uncertainty, remained unchanged. LCRHA F2 and F3 revealed carboxyl group content increase in comparison to unfractionated HA and F1, while the phenolic group content was higher in F2 only. The differences noticed between unfractionated RCLHA and LCRHA and their fractions, as well as among fractions themselves, were even less significantly pronounced in comparison to Lin *et al.*[16]

RCLHA E and LCRHA E were obtained using the esterification procedure. According to Andjelkovic *et al.*[21] the esterification resulted in carboxyl group blocking. It is obvious that carboxyl group content was slightly lower in RCLHA E, but remarkably lower in LCRHA E in comparison with non-esterified forms.

HA ATR-FTIR spectra

ATR-FTIR spectra are illustrated in Fig. 1, while some relative band intensities (*I*) and aromaticity index values obtained by ATR-FTIR are depicted in Table II. ATR-FTIR spectra of RCLHA, LCRHA, their fractions and esters as well as EHA, with absorption bands typical of humic acids,[24] had most of the peaks in the same position but with different intensities. Spectra of RCLHA, LCRHA and EHA were quite alike suggesting their similar structure.

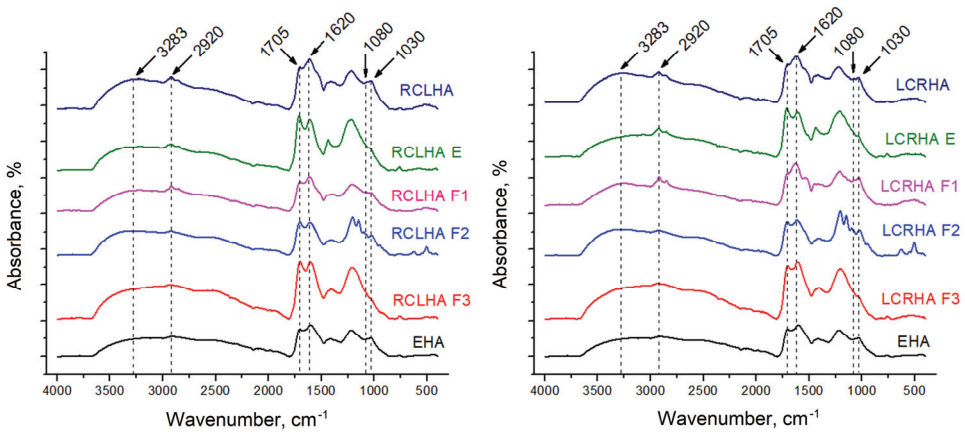

Fig. 1. ATR-FTIR spectra of Rendzic Calcaric Leptosol (RCLHA) and Leptic Calcaric Regosol (LCRHA) humic acids, their fractions (F1–F3) and esterified forms (E), and IHSS standard Elliott Soil humic acid (EHA).

The applied fractionation and esterification procedures obviously led to structure changes and resulted in different band intensities of fraction and ester spectra. A mutual comparison of the recorded spectra was done using relative band intensities. Both F1 fractions did not undergo any changes in the relative

abundances of either phenolic (I_{3273}) or carboxyl C (I_{1705}). In F2 fractions there was an obvious increase of both functional group relative abundances, while in both F3 fractions the carboxyl C relative abundance was higher. Both esters underwent an evident increase in I_{1705} relative intensity due to the stretching vibration of ester groups formed. For both HAs the aromatic C (I_{1620}) relative abundance increased in fractions and especially in esters. Regarding the aliphatic C (I_{2923}), it was noticed that relative abundance values are higher in esters and F1, while a decrease was obvious in F2, and particularly in the F3 fraction. Regarding polysaccharide C (I_{1080} and I_{1030}), the relative abundance increased in order F2 > E > F1 and decreased in F3 fraction.

TABLE II. Some relative band intensities (I) (to intensity of C=C aromatic band at 1520 cm^{-1}) and aromaticity index values of Rendzic Calcaric Leptosol (RCLHA), Leptic Calcaric Regosol (LCRHA) humic acids, their fractions (F1–F3) and esterified forms (E), and IHSS standard Elliott Soil humic acid (EHA), obtained by ATR-FTIR (measurement uncertainty < 5 %)

HA sample	I_{3273}	I_{2923}	I_{1705}	I_{1620}	I_{1080}	I_{1030}
RCLHA	0.877	0.181	1.262	1.518	0.828	0.880
RCLHA E	1.029	0.205	2.481	2.321	1.190	1.055
RCLHA F1	1.092	0.300	1.550	1.810	1.006	0.986
RCLHA F2	1.378	0.139	1.953	1.924	1.287	1.187
RCLHA F3	0.986	0.083	1.975	1.957	0.871	0.657
LCRHA	0.928	0.204	1.258	1.531	0.797	0.840
LCRHA E	0.862	0.310	2.303	2.078	1.192	1.036
LCRHA F1	0.864	0.380	1.249	1.590	0.914	1.008
LCRHA F2	1.256	0.126	1.669	1.748	1.337	1.322
LCRHA F3	0.948	0.089	1.628	1.734	0.800	0.664
EHA	0.897	0.110	1.352	1.523	0.864	0.907

HA self-aggregation

The volume-based particle size distribution (PSD) of unfractionated HAs, fractions and esters is depicted in Fig. 2, while the most intensive peak in their PSD (d) is summarized in Table I. PSD was obviously different for RCLHA, LCRHA and EHA. Also, RCLHA E and LCRHA E differed in their PSD significantly, while their fractions revealed quite similar PSD. It is clear that, after the fractionation procedure had been performed, both HAs aggregated in a similar way. Opposite to other authors,[25–28] who detected three particle size populations, PSDs obtained in this study did not show defined particle size regions.

It is obvious from Table I that the decreased content of both carboxyl and phenolic groups in RCLHA F1 and E, in comparison to RCLHA, resulted in a pronounced aggregate size (d = 873.7, 3265 and 515.0 nm, respectively). Vice versa, for a higher functional groups content in both RCLHA F2 and F3, a lower aggregate particle size was noticed (d = 31.71 and 9.290 nm, respectively). Although both functional group contents were changed within measurement

uncertainty, F1 and E aggregate sizes were remarkably higher compared to LCRHA (d = 997.4, 506.3 and 32.66 nm, respectively). Both F2 and F3, having higher carboxyl, and F2 with higher phenolic concentration, showed a less pronounced aggregation (d = 39.44 and 9.483 nm, respectively) than LCRHA and F1. Although the LCRHA aggregate size was lower than for RCLHA, the particle size of its fractions retained the same order as for RCLHA (F1 > F2 > F3).

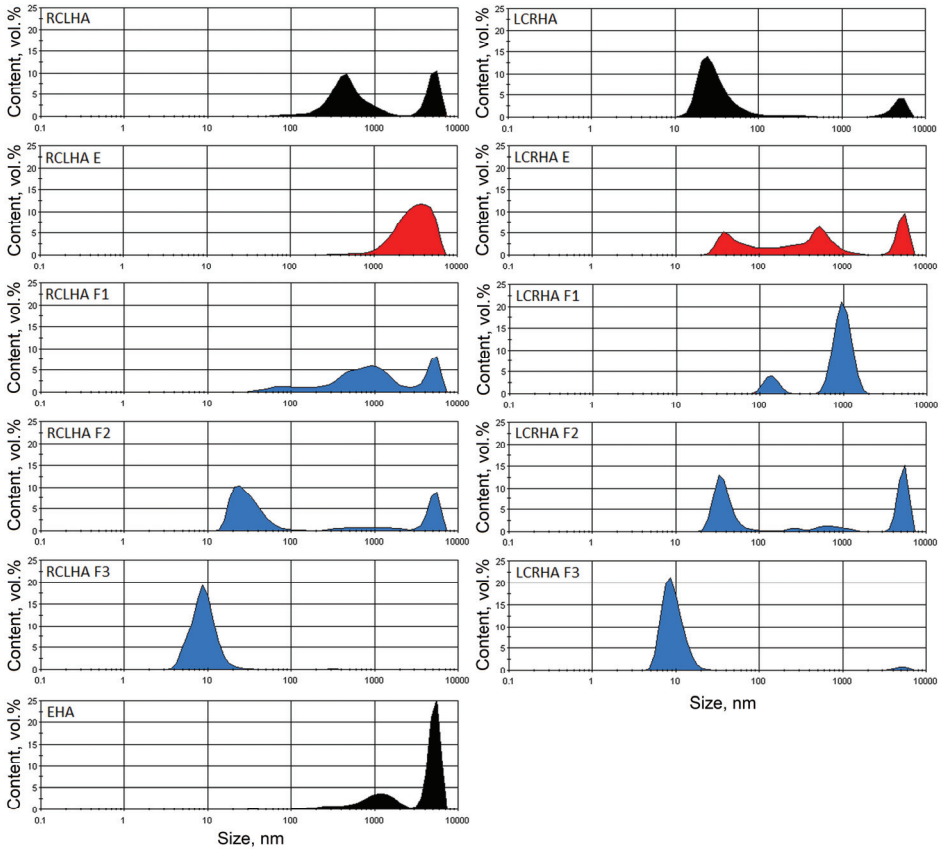

Fig. 2. Particle size distribution by volume (particle size content, vol.%) of Rendzic Calcaric Leptosol humic acid (RCLHA) and Leptic Calcaric Regosol humic acid (LCRHA), their fractions (F1-F3) and esterified forms (E), and IHSS standard Elliott Soil humic acid (EHA) at pH 3 after 3 days.

To confirm dependence observed, the aggregate size for both HAs, esters and fractions was correlated to carboxyl and phenolic group contents obtained by the titration method and correlation presented in Fig. 3. Although the correlations obtained were not strong (R = 0.588, p = 0.073 and R = 0.574, p = 0.083 for

carboxylic and phenolic groups, respectively), it is apparent that, at low pH, the higher groups content bring about the less pronounced HA aggregation.

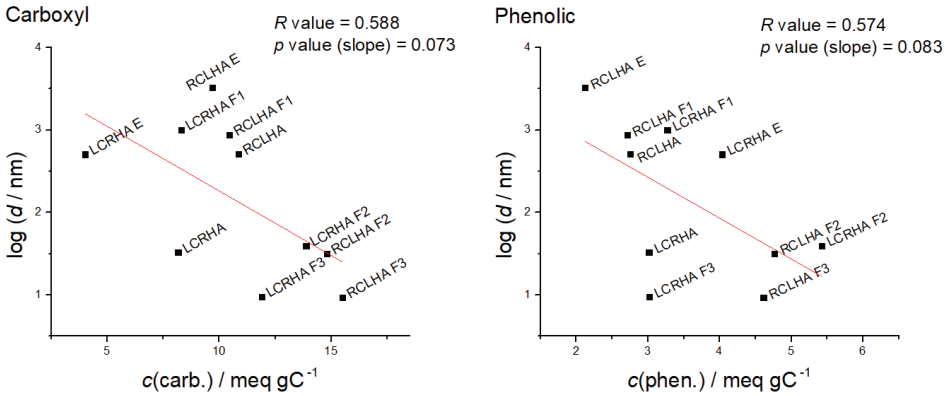

Fig. 3. The most intensive peak in particle size distribution (particle size log *d*) *versus* carboxyl and phenolic group content (RCLHA - Rendzic Calcaric Leptosol humic acid, LCRHA – Leptic Calcaric Regosol humic acid, F1–F3 – fractions; E – esterified form).

As the applied HA fractionation and esterification procedures led to structure changes resulted in different ATR-FTIR band intensities, the aggregate size for both HAs, esters and fractions was correlated to relative band intensities from FTIR spectra. A significant positive correlation ($R = 0.76$), depicted in Fig. 4, was obtained for the 2923 cm^{-1} band only, indicating that the higher aliphatic C components content influences the more pronounced HA aggregation.

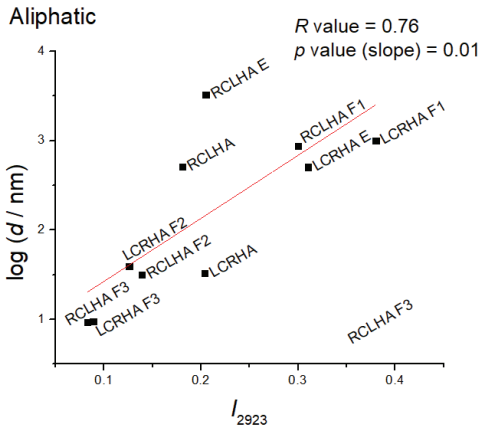

Fig. 4. The most intensive peak in particle size distribution (particle size log *d*) versus 2923 cm^{-1} relative FTIR band intensity (RCLHA – Rendzic Calcaric Leptosol humic acid, LCRHA – Leptic Calcaric Regosol humic acid, F1–F3 – fractions; E – esterified form).

As already emphasized, fractionation and esterification procedures performed led to structure changes, consequently influencing HA self-aggregation process. Functional group contents indicated that the separation procedure used

did not completely fractionate humic acids into phenolic and carboxyl groups. Nevertheless, change of functional groups content in fractions was achieved. Additionally, esterification led to change of functional groups content, both resulting in different HA aggregate sizes. The correlation analysis indicated that with the higher group content the HA aggregation is less pronounced, and one can assume that both carboxyl and phenolic group are not predominant in the HA self-aggregation process at low pH. According to the literature data,[4,9] the hydrogen from functional groups, forming hydrogen bonds at low pH, is likely responsible for HA self-aggregation. Besides functional groups, from this study arises that other HA components also participate in various phases of HA self-aggregation process, as already suggested by Mecozzi and Pietrantonio.[10]

As previously mentioned, correlation coefficient between aggregate size and aliphatic, in comparison to other components, was obviously the highest. Since the correlation for aliphatic components is stronger than for carboxylic and phenolic groups, it can be concluded that they strongly influence the self-aggregation process in comparison to functional groups. Thus, F2 and particularly F3 fractions revealed the less intense self-aggregation. It can be seen that aromatic C was slightly higher and aliphatic C relative abundance profoundly lower in F2, and especially F3. Some literature data[10–12] have suggested that carbohydrates and proteins, as well as lipids, play a facilitative role in formation of HS aggregates. Hence, the lower abundance of aliphatic C in F2 and F3 could be considered as insufficient to start the self-aggregation process. Regarding polysaccharide relative abundance, no obvious regularity and influence to HA self-aggregation was observed.

The largest aggregates were measured for esterified forms with blocked carboxyl groups. Although the particle size vs. aromatic C correlation was not high, the increased relative abundance of aromatic C in esters is obvious, assuming their participation in hydrophobic bonding and consequent influence to more pronounced aggregation. Hakima and Kobayash[13] already emphasized that higher hydrophobicity, *i.e.*, aromaticity induces stronger hydrophobic interactions and more pronounced HA self-aggregation.

The relation of HA self-aggregate size with carboxyl and phenolic group content, as well as aliphatic C relative abundance, at low pH, could be considered universal regardless of the structural characteristics of original or modified HA forms.

CONCLUSION

To investigate the influence of structural components on the HA self-aggregation process, soil humic acids were fractionated, using the secondary amine weak base resin, and esterified to selectively block carboxyl groups. Both the fractionation and esterification processes, herein applied, contribute to the HA

structural changes which resulted in the content of functional groups determined by titration, as well as from the ATR-FTIR spectra intensities. The performed modifications influence the HA self-aggregation process by giving different particle size distributions.

According to the not strong negative correlations, between the carboxylic and phenolic group content and aggregate size at low pH, the higher the groups content is, the less pronounced is the HAs aggregation. It can be assumed that functional group content, both carboxyl and phenolic, is not predominant in the HA self-aggregation process.

Based on the ATR-FTIR data, the significant positive correlation of aliphatic C components and aggregate size could indicate a dominant influence of these components in the HA self-aggregation process. A lower abundance of aliphatic C components in HA fractions could be considered as not sufficient to start the self-aggregation process. Obviously, the increased relative abundance of aromatic C in esters likely points to its participation in hydrophobic bonding and, consequently, more pronounced aggregation. The influence of polysaccharide C relative abundance to HA self-aggregation was not observed.

The relation of HA self-aggregate size with carboxyl and phenolic group content, as well as aliphatic C relative abundance at low pH, could be considered universal regardless of the structural characteristics of original or modified HA forms.

Acknowledgments. This work was partially supported by the Ministry of Education, Science and Technological Development of the Republic of Serbia (Grants no. 451-03-9/2021--14/200017 and 451-03-9/2021-14/200116).

ИЗВОД

САМОАГРЕГАЦИЈА ЗЕМЉИШНИХ ХУМИНСКИХ КИСЕЛИНА У ЗАВИСНОСТИ ОД ЊИХОВИХ СТРУКТУРНИХ КАРАКТЕРИСТИКА

УРОШ Д. ЈОВАНОВИЋ[1], МИРЈАНА М. МАРКОВИЋ[1], ЂУРО М. ЧОКЕША[1], НИКОЛА В. ЖИВКОВИЋ[1] и СВЈЕТЛАНА Б. РАДМАНОВИЋ[2]

[1]*Универзитет у Београду – Институт за нуклеарне науке Винча, п.пр. 522, 11001 Београд и*
[1]*Универзитет у Београду – Пољопривредни факултет, Немањина 6, 11080 Београд*

Основни циљ овог рада је испитивање утицаја карбоксилних и фенолних група, као и ароматичних, алифатичних и полисахаридних компоненти, на самоагрегацију земљишних хуминских киселина (HA). Да би се добиле фракције са различитим садржајем функционалних група, земљишне HA (Leptosol и Regosol) су фракционисане коришћењем јоноизмењивачке смоле. Да би се проценио утицај сваке функционалне групе на самоагрегацију, естерификацијом су блокиране карбоксилне групе. Присуство структурних компоненти у HA је одређено потенциометријском титрацијом и ATR-FTIR спектроскопијом. Процес агрегације на pH 3 је праћен техником динамичког расејања светлости. Резултати указују да је агрегација HA слабије изражена што је већи садржај функционалних група. Значајна позитивна корелација алифатичног C и величине агрегата указује на њихов доминантан утицај на самоагрегацију HA. Постоји могућност да је,

због ниске заступљености алифатичног C, започињање процеса агрегације отежано. Повећање присуства ароматичног C у естрима вероватно указује на њихово учешће у хидрофобним везама, услед чега је израженија агрегација. Однос величине агрегата и карбоксилне и фенолне групе, као и алифатичног C, на ниском pH, може се сматрати универзалним без обзира да ли се ради о структурним особинама изворне или модификоване форме HA.

(Примљено 25. новембра 2021, ревидирано 16. фебруара, прихваћено 21. фебруара 2022)

REFERENCES

1. A. Piccolo, *Adv. Agron.* **75** (2002) 57 (https://doi.org/10.1016/S0065-2113(02)75003-7)
2. K. Wilkinson, M. Avena, *Environ. Sci. Technol.* **36** (2002) 5100 (https://doi.org/10.1021/es025582u)
3. S. A. Dolenko, M. Y. Trifonova, Y. I. Tarasevich, *J. Water Chem. Technol.* **39** (2017) 360 (https://doi.org/10.3103/S1063455X17060091)
4. U. Jovanović, M. Marković, S. Cupać, Z. Tomić, *J. Plant Nutr. Soil Sci.* **176** (2013) 674 (https://doi.org/10.1002/jpln.201200346)
5. E. Galicia-Andrés, Y. Escalona, C. Oostenbrink, D. Tunega, M. Gerzabek, *Geoderma* **401** (2021) 115237 (https://doi.org/10.1016/j.geoderma.2021.115237)
6. E. Tombácz, *Soil Sci.* **164** (1999) 814 (https://doi.org/10.1097/00010694-199911000-00005)
7. R. Angelico, A. Ceglie, J. Z. He, Y. R. Liu, G. Palumbo, C. Colombo, *Chemosphere* **99** (2014) 239 (https://doi.org/10.1016/j.chemosphere.2013.10.092)
8. P. Boguta, V. D'Orazio, N. Senesi, Z. Sokołowska, K. Szewczuk-Karpisz, *J. Environ. Manage.* **245** (2019) 367 (https://doi.org/10.1016/j.jenvman.2019.05.098)
9. L. F. Zara, A. H. Rosa, I. A. S. Toscanoc, J. C. Rocha, *J. Braz. Chem. Soc.* **17** (2006) 1014 (https://doi.org/10.1590/S0103-50532006000500028)
10. M. Mecozzi, E. Pietrantonio, *Marine Chem.* **101** (2006) 27 (https://doi.org/10.1016/j.marchem.2006.01.001)
11. G. Chilom, A. Bruns, J. Rice, *Org. Geochem.* **40** (2009) 455 (https://doi.org/10.1016/j.orggeochem.2009.01.010)
12. L. W. Hoffman, G. Chilom, S. Venkatesan, J. A. Ri, *Microsc. Microanal.* **20** (2014) 521 (https://doi.org/10.1017/S1431927614000038)
13. A. Hakima, M. Kobayash, *Colloids Surfaces, A* **540** (2018) 1 (https://doi.org/10.1016/j.colsurfa.2017.12.065)
14. M. Klučáková, M. Kalina, *J. Soils Sediments* **1** (2015) 1900 (https://doi.org/10.1007/s11368-015-1142-2)
15. S. Karim, M. Aoyama, *Soil Sci. Plant Nutr.* **59** (2013) 827 (https://doi.org/10.1080/00380768.2013.844078)
16. C. F. Lin, S. H. Liu, O. Hao, *Wat. Res.* **35** (2001) 2395 (https://doi.org/10.1016/S0043-1354(00)00525-X)
17. O. Trubetskaya, O. Trubetskoj, C. Richard, *J. Soils Sediments* **14** (2014) 292 (https://doi.org/10.1007/s11368-013-0667-5)
18. S. Radmanović, Lj. Životić, N. Nikolić, A. Đorđević, in *Proceedings of 2nd International and 14th National Congress of Soil Science Society of Serbia*, 2017, Novi Sad, Serbia, *Solutions and Projections for Sustainable Soil Management*, Soil Science Society of Serbia, Novi Sad, 2018, p. 1 (ISBN 978-86-7520-410-7)

19. M. Carter, *Soil sampling and methods of analysis.* Lewis Publishers, Boca Raton, CA, 1993 (ISBN 0-87371-861-5)
20. International Humic Substances Society, *Source Materials for IHSS Samples, Standard samples*, http://humic-substances.org/source-materials-for-ihss-samples (15 May 2017)
21. T. Anđelković, J. Perović, M. Purenović, S. Blagojević, R. Nikolić, D. Anđelković, A. Bojić, *Eclec. Quim.* **31** (2006) 39 (https://doi.org/10.1590/S0100-46702006000300005)
22. D. P. Dick, H. Knicker, L. G. Ávila, A. V. Inda, E. Giasson, C. A. Bissani, *Org. Geochem.* **37** (2006) 1537 (https://doi.org/10.1016/j.orggeochem.2006.06.017)
23. J. Ritchie, M. Perdue, *Geochim. Cosmochim. Acta* **67** (2003) 85 (https://doi.org/10.1016/S0016-7037(02)01044-X)
24. J. Wu, R. Jiang, Q. Liu, G. Ouyang, *Chemosphere* **263** (2021) 127967 (https://doi.org/10.1016/j.chemosphere.2020.127967)
25. M. R. Esfahani, H. A. Stretz, M. J. M. Wells, *Sci. Total Environ.* **537** (2015) 81 (https://doi.org/10.1016/j.scitotenv.2015.08.001)
26. M. Klučáková, *Front. Chem.* **6** (2018) 235 (https://doi.org/10.3389/fchem.2018.00235)
27. M. Klučáková, K. Věžníková, *J. Mol. Structure* **1144** (2017) 33 (https://doi.org/10.1016/j.molstruc.2017.05.012)
28. Y. I. Tarasevich, M. Y. Tryfonova, S. A. Dolenko, E. V. Aksenenko, *Adsorpt. Sci. Technol.* **34** (2016) 125 (https://doi.org/10.1177/0263617415623421).

Journal of the Serbian Chemical Society
JSCS@tmf.bg.ac.rs • www.shd.org.rs/JSCS

J. Serb. Chem. Soc. 87 (6) 775–784 (2022)
JSCS–5557

Original scientific paper
Published 8 March 2022

Application of microbial fuel cell for simultaneous treatment of metallurgical and municipal wastewater – A laboratory study

STEFAN ĐORĐIEVSKI[1]*, HYUSEIN YEMENDZHIEV[2], RALITZA KOLEVA[2], VALENTIN NENOV[2], DRAGANA MEDIĆ[3#], VANJA TRIFUNOVIĆ[1] and ANA MAKSIMOVIĆ[4]

[1]*Mining and Metallurgy Institute Bor, Zeleni Bulevar 35, Bor 19210, Serbia,* [2]*"Prof. D-r Assen Zlatarov" University, Y.Yakimov blvd. 1, Burgas 8010, Bulgaria,* [3]*Technical Faculty in Bor, Vojske Jugoslavije 12, Bor 19210, Serbia and* [4]*Independent consultant, Belgrade 11000, Serbia*

(Received 8 October 2021, revised 16 February, accepted 17 February 2022)

Abstract: Microbial fuel cell (MFC) is a hybrid technology that produces electricity and recovers resources from wastewater through biocatalytic and electrochemical reactions. Metallurgical facilities in Bor, Serbia, are a source of copper-rich metallurgical wastewater, and the Town of Bor is a source of municipal wastewater rich in organic matter. The aim of this paper is to investigate the possibility of application of MFC for the treatment of metallurgical and municipal wastewater that are released into the Bor River in Serbia. A prototype of MFC was constructed for this study, and 3 sets of experiments were performed using model solutions and real wastewater. Copper was successfully removed from the treated model solution with 99.42 % efficiency. Solid copper particles were obtained with a particle size of about 1 µm. Maximum chemical oxygen demand (COD) removal rate of 191.7 mg L^{-1} h^{-1} was observed in the anodic compartment. The impact of this study is significant because MFC was implemented for the simultaneous treatment of two types of wastewaters, one containing metals and the other containing organic matter, and both types of wastewater are released into the same river.

Keywords: Bor River; copper; organic matter; bacteria; electrochemical; prototype.

INTRODUCTION

Copper mine and metallurgical facilities in Bor, Serbia, are a large source of pollution. A very high concentration of contaminants poses a serious concern to scientists, experts, and citizens due to the effect on living organisms and environ-

* Corresponding author. E-mail: stefan.djordjievski@irmbor.co.rs
# Serbian Chemical Society member.
https://doi.org/10.2298/JSC211008009D

mental health.[1] Metal-rich metallurgical wastewater and acid mine drainage are released into the Bor River without treatment. Municipal wastewater from the Town of Bor is also released into the Bor River without treatment. This unique phenomenon, where the river water is formed solely by mixing of untreated wastewater containing a high concentration of metals and untreated wastewater containing a high concentration of organic matter, is shown in Fig. S-1 of the Supplementary material to this paper.[2] The concentration of copper in Bor River ranges from 5 to 30 mg L^{-1}, and about 500 t of copper per year is released into the Bor River through the metallurgical wastewater.[2–4] About 910 t of copper per year is transported by Bor River and Timok River to the Danube River in dissolved and particulate form, which creates transboundary pollution, affecting the Danube River in Romania and Bulgaria.[5] Various treatment methods could be used for the purification of metallurgical and municipal wastewater from Bor, however, by applying MFC, it could be possible to treat both types of wastewaters simultaneously.[6–8]

MFCs are hybrid bio-electrochemical reactors able to use concentrated organic waste streams, produce electricity, and recover resources from wastewater through biocatalytic and electrochemical reactions.[9] MFC consists of an anode and a cathode chamber which are generally separated by a proton exchange membrane (PEM) to avoid the migration of electrolytes from one chamber to the other (Fig. 1a).[10,11] There are few types of MFC systems, and this separate system is applied only to the two-chamber MFC system. In the anode compartment, bacteria are used as catalysts to break down organic matter to carbon dioxide, protons, and electrons through respiration mechanisms, but in the absence of oxygen. The resulting electrons are transferred to the anode surface which plays the role of electron acceptor. Then, they are transferred to the cathode via an external circuit, while the protons diffuse through the PEM.[12–15] The final reduction reaction is performed in the cathode compartment where protons, electrons, and usually oxygen are recombined to complete the reactor's electrochemistry. As an alternative, various metal ions can be electrochemically reduced in this reaction and eventually recovered from the solution by their conversion to elemental form. In addition to metals, free radicals can also be used as electron acceptors in the cathodic compartment.[16]

The maximum current that can be produced by an MFC depends on the actual rate of substrate biodegradation, whereas maximum theoretical cell voltage (also called electromotive force or emf) depends on Gibbs energy change of the overall reaction and can be calculated as the difference between the standard reduction potentials of the cathodic oxidant (oxygen) and the chosen anodic substrate.[17] Power output of MFC could be enhanced by modification of electrodes and PEM using polymeric nanocomposites.[18] However, the main advantages of the MFC type reactors are beyond energy production and they could be a power-

ful tool for wastewater treatment, as an alternative to the conventional biological processes.

There are several reports on the successful application of MFC to remove copper from model solutions with efficiency up to 99.88 % and yield of electrical energy reaching 3.2 A m^{-2}.[19,20] The most promising characteristic of the process is that simultaneously in the anodic chamber domestic or other high organic content wastewater could be treated, as well. The existing studies reported chemical oxygen demand (COD) removal efficiency as high as 83 % in such a setup.[21] The optimal conditions for MFC operation were obtained using the microbial cultures isolated from freshwater sediments, such as the sediment from Danube River in Serbia and the sediment from Lake Uzungeren in Bulgaria.[22,23]

Based on the recent development in the field and taking into account the situation in the region of Bor, Serbia, this paper aimed to investigate the eventual application of MFC as an approach to manage the wastewater streams generated by the local metallurgical industry and community. The performance of a lab-scale reactor towards Cu ions and COD removal was tested using a model and real wastewater samples.

EXPERIMENTAL

The details of the sampling of the wastewaters are given in Supplementary material.

Materials and MFC operation

The MFC used in this study was assembled as a cylindrical plastic reactor consisting of two chambers separated by Nafion® 424 perfluorinated proton exchange membrane (Fig. 1). The cell segments were equipped with the respective sampling and gas/liquid transport ports. The electrodes were 30 mm in diameter and they were made of carbon cloth with stainless steel current collectors. They were connected with an external electric circuit loaded with a 1000-Ohm resistor. The volumes of cathode and anode chambers were 40 cm^3.

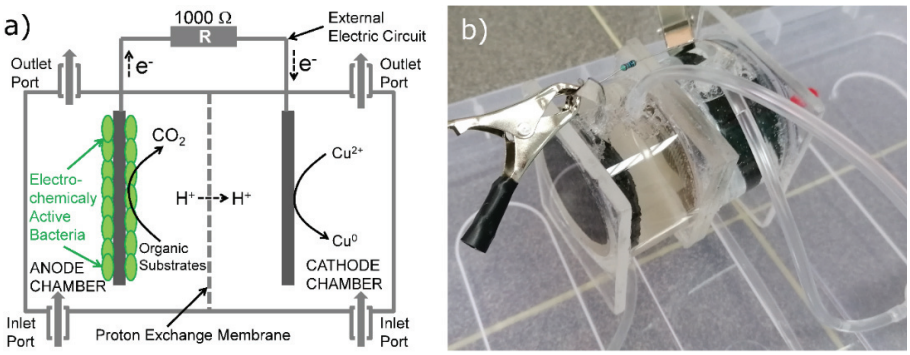

Fig. 1. Microbial fuel cell; a) schematic diagram and b) the prototype constructed for this study.

The electrochemically active microorganisms (electrogenes) were isolated from the bottom sediments of "Poda" protected site located on the outfall of Lake Uzungeren, south of

Burgas. The water of Lake Uzungeren is characterized by relatively high electrical conductivity and pH value (5230 μS/cm and 8.2, respectively), and a very low dissolved oxygen content (1.4–2.2 mg/l O_2).[23] The lake sediment had relatively high contents of organic matter (22.5 %), iron (3.05 % Fe), and manganese (935 mg/kg Mn).[23] Mersinkova and Yemendzhiev demonstrated that the mixed culture of anaerobic bacteria isolated from this lake sediment was capable of powering MFC.[23]

The enrichment of the mixed culture was performed in anaerobic conditions by inoculation of sediment samples in 20 g L^{-1} Luria–Bertani (LB) nutrient medium (10 g L^{-1} tryptone, 5 g L^{-1} yeast extract, and 5 g L^{-1} NaCl, pH 7) containing 15 g L^{-1} glucose. After 96 h of cell growth at 18 °C, the enriched culture was suspended in a fresh nutrient medium with a lower concentration of organics (5 g L^{-1} LB) and 1 g L^{-1} acetate, as a carbon source, in order to avoid fermentative metabolism. The initial microbial concentration in the anodic chamber was set to be 10^7 CFU L^{-1}. The process was conducted at 18 °C. In order to represent the biological condition specific for the municipal wastewater, glucose solution inoculated with municipal wastewater and sewage sludge from the Town of Bor were used in the Experiment 2 (Table I).

TABLE I. Compositions of solutions in anodic and cathodic compartments that were used in 3 different experiments.

Experiment	Composition of solution in the anode chamber	Composition of solution in the cathode chamber
1	Bacteria isolated from the lake sediment and LB nutrient medium	Model solution containing 200 mg L^{-1} Cu^{2+}
2	Bacteria from municipal wastewater and glucose	Model solution containing 450 mg L^{-1} Cu^{2+}
3	Bacteria isolated from the lake sediment and LB nutrient medium	Metallurgical wastewater

2 % Potassium hexacyanoferrate solution or 1 M potassium permanganate solution was used as catholyte for preconditioning of MFC, and the model solution containing copper sulfate pentahydrate in deionized water, or real wastewater stream such as metallurgical wastewater (collected at the outlets near mining and metallurgical facilities in Bor, Serbia) were used as catholyte depending on the purpose of the experimental sets performed. Three sets of experiments that were performed using the described solutions are summarised in Table I.

Analytical methods

The pH values of underground mine wastewater, Robule Lake wastewater, and metallurgical wastewater were measured in the field using the pH meter model IM-23P.

The concentrations of elements in the wastewaters were measured using PerkinElmer ICP-MS NexION 1000. Rh was used as an internal standard for the determination of Cd, Co, Cu, Mn, Ni, Zn, As and Cr. Re was used as an internal standard for the determination of Pb. All elements were determined in Ar mode, except As which was determined in He mode. The appropriate dilutions of original samples were made to match the concentration range of the calibration curve. Certified standard solutions containing the applied elements were used for calibration and quality control. The dynamics of Cu concentration during the experiments were monitored both by ICP–MS and spectrophotometrically by HACH DR 3900 spectrophotometer with Lange LCK 329 cuvette test. COD was determined spectrophotometrically

by HACH DR 3900 spectrophotometer and Lange LCK 514 cuvette test. Change of voltage was measured using a multimeter. Particle size analysis was carried out using a Microtract Nanowave II particle size analyzer.

All measurements were performed in triplicate and the results presented here are mean values.

RESULTS AND DISCUSSION

The results of the chemical characterization of the underground mine wastewater, the Robule Lake wastewater, and the metallurgical wastewater are presented in Table II. The metallurgical wastewater had higher concentrations of toxic elements such as Cd, Cu, Ni, Pb, Zn, As and Cr, when compared to the other two wastewaters. The concentration of arsenic (As) was exceptionally high in the metallurgical wastewater, reaching 28.8 ppm, which is about 3000 times higher than the limit value for drinking water (0.010 ppm). On the other hand, the concentrations of Co and Mn were the highest in the wastewater of Robule Lake (1.19 and 84.8 ppm, respectively). The metallurgical wastewater had the highest concentration of copper (215.5 ppm of Cu), so this wastewater was used as an object to test.

TABLE II. Chemical characteristics of wastewaters around Bor

Parameter	Underground mine wastewater	Robule Lake wastewater	Metallurgical wastewater	Municipal wastewater
pH	2.74	2.62	1.89	7.82
c_{Cd} / ppm	0.13	<0.10	4.38	<0.00010
c_{Co} / ppm	0.52	1.19	0.6	0.00081
c_{Cu} / ppm	130.1	41.8	215.5	<0.010
c_{Mn} / ppm	17.3	84.8	16.9	0.111
c_{Ni} / ppm	2.19	0.68	18.35	0.0033
c_{Pb} / ppm	<0.10	<0.10	3.15	0.00057
c_{Zn} / ppm	9.2	25.3	51.5	0.0140
c_{As} / ppm	0.28	<0.10	28.8	0.0037
c_{Cr} / ppm	<0.10	<0.10	0.11	<0.00050

The change of voltage during the Experiment 1 (Table I) showed that the reactor reached its optimal condition (in terms of electricity production) after 144 h of operation, which is probably a result of the growth and development of the functional anodic biofilm that accelerated the activity of the electrogenic microorganisms (Fig. 2a). On the other hand, the voltage decreased gradually during the experiment with the bacteria from municipal wastewater (the Experiment 2, Fig. 2b). Copper concentration decreased along the time in both experiments with model solution (the Experiments 1 and 2, Fig. 2d and e). However, the decrease in the concentration of copper during the Experiment 1 was more drastic compared to that in the Experiment 2. During the Experiment 1, the copper concentration decreased from 200 to 1.15 mg L^{-1} for 188 h, but the highest drop in Cu

concentration occurred during the first 24 h of the experiment, from 200 to 22.6 mg L^{-1}. During the Experiment 2, the copper concentration decreased from 434 to 194 mg L^{-1} for 170 h. The efficiency of copper removal was better during the Experiment 1 (99.42 %) compared to the Experiment 2 (55.40 %).

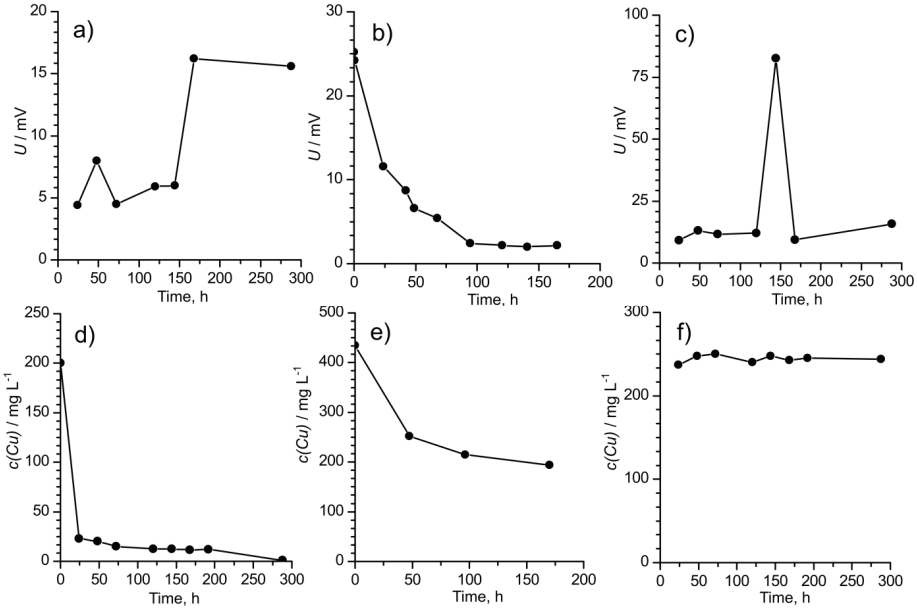

Fig. 2. Change of voltage during Experiments: a) 1, b) 2 and c) 3; change of copper concentration during Experiments: d) 1, e) 2 and f) 3.

The voltage during the Experiment 3 (Fig. 2c) increased drastically after 140 h from the beginning of the experiment. The reason for this change is unknown, and there is also a possibility of measurement error. The copper concentration did not change during the experiment with metallurgical wastewater (Fig. 2f) because of the low pH value of this water (pH 1.89), and probably the presence of other metal ions which are preferred as electron acceptors (Table II).

The effect of the cathodic reduction of the dissolved metal ions and their transformation into an elemental (unsoluble) form is also demonstrated by the data obtained from the particle size and distribution tests (Fig. 3). In the metallurgical wastewater before the start of Experiment 2, the particle size ranged from 1 to 2 nm, which is typical for smaller colloidal particles. However, larger particles were obtained in metallurgical wastewater after the treatment with a mode of about 0.9 μm, which suggests that some chemical species changed their form from dissolved or colloidal to solid during the treatment. Since the copper concentration did not change during the treatment of metallurgical wastewater (Fig. 2f), there is a possibility that chemical species other than copper were pre-

cipitated. After the treatment of model solution containing Cu ions in Experiment 1, two particle size distributions were obtained with modes around 1 µm and 2.5 µm, which suggests that two processes of solid particles formation took place. These solid particles were sedimented on the cathode chamber bottom or collected on the cathode surface.

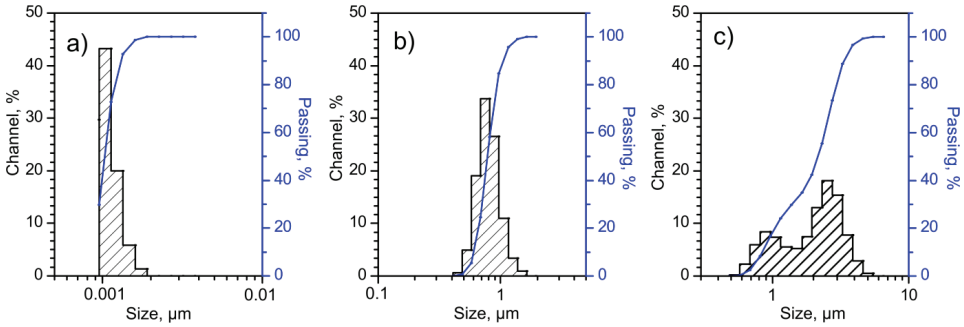

Fig. 3. Particle size distribution diagrams: a) metallurgical wastewater before the start of Experiment 3; b) metallurgical wastewater after 144 h of Experiment 3; c) model solution with copper ions after 144 h of Experiment 1.

The COD removal rate was measured in the anode chamber to estimate the organic matter degradation rate. When bacteria isolated from the lake sediment and the model solution containing copper were used (Experiment 1), the maximum COD removal rate was 191.7 mg L^{-1} h^{-1}. When the metallurgical wastewater was used as a catholyte, the maximum COD removal rate was 179.2 mg L^{-1} h^{-1} (Experiment 3).

The removal of copper from the model solution using MFC was relatively efficient in all experiments and reached 99.42 %. The removal of copper from real metallurgical wastewater using MFC did not show this positive result mostly due to the bad physicochemical conditions of the wastewater, namely low pH. Besides this, the presence of other metal ions with higher standard electrode potential could explain the low effect on copper in this set of experiments. Pretreatment (neutralization) of wastewater such as metallurgical wastewater could significantly improve the process.[6,19,24] Even after neutralization, the copper reduction and removal will start after depletion of the high potential ions available in the catholyte. The evidence that other chemical species from the metallurgical wastewater were reduced in the cathodic compartment instead of copper is the fact that a relatively high COD removal rate (179.2 mg L^{-1} h^{-1}) was observed, and larger particles were present in the anodic compartment after the Experiment 3 (Fig. 3b).

CONCLUSION

The prototype of MFC constructed for this study was efficient for the removal of copper from the model solution. Bacteria isolated from the lake sediment had a higher ability to produce electrons and reduce copper ions from the model solution than the bacteria from the municipal wastewater. Acidic pH value and the presence of reducible chemical compounds with higher redox potential than copper constrained the removal of copper from metallurgical wastewater. Additional experiments should be carried out in order to improve the efficiency of MFC for the treatment of metallurgical and municipal wastewater. The impact of this study is significant because MFC was implemented for the simultaneous treatment of two types of wastewaters, one containing metals and the other containing organic matter, and both types of wastewater are released into the same river. This is also an initial attempt to apply this technology for the purification of locally present metallurgical and municipal wastewater in the region of Bor, Serbia (Fig. S-1).

SUPPLEMENTARY MATERIAL

Additional data and information are available electronically at the pages of journal website: https://www.shd-pub.org.rs/index.php/JSCS/article/view/11261, or from the corresponding author on request.

Acknowledgments. This paper is a result of the 6-week placement of the first author at the "Prof. D-r. Assen Zlatarov" University in Burgas in the scope of Pioneers into Practice program and Alumni Micro Award, both financed by the EIT Climate-KIC, which is supported by the European Institute of Innovation and Technology, a body of the European Union. The authors would also like to acknowledge the support of the Ministry of Education, Science and Technological Development of the Republic of Serbia, Grants No. 451-03-9/ /2021-14/200052 and 451-03-9/2021-14/200131, and Project BG05M2OP001-1.002-0019: Clean technologies for sustainable environment – water, waste, energy for circular economy (Clean&Circle), Centre of Competence.

ИЗВОД

ПРИМЕНА МИКРОБНЕ ГОРИВЕ ЋЕЛИЈЕ ЗА ИСТОВРЕМЕНИ ТРЕТМАН МЕТАЛУРШКЕ И КОМУНАЛНЕ ОТПАДНЕ ВОДЕ – ЛАБОРАТОРИЈСКА СТУДИЈА

СТЕФАН ЂОРЂИЕВСКИ[1], HYUSEIN YEMENDZHIEV[2], RALITZA KOLEVA[2], VALENTIN NENOV[2], ДРАГАНА МЕДИЋ[3], ВАЊА ТРИФУНОВИЋ[1] и АНА МАКСИМОВИЋ[4]

[1]*Институт за рударство и металургију Бор, Зелени Булевар 35, 19210 Бор,* [2]*"Prof. Dr Assen Zlatarov" University, Y.Yakimov blvd. 1, Burgas 8010, Bulgaria и* [3]*Технички факултет у Бору, Војске Југославије 12, 19210 Бор и* [4]*Независни консултант, 11000 Београд*

Микробна горивна ћелија (MFC) представља хибридну технологију помоћу које је могуће добити електричну енергију и метале из отпадних вода путем биокаталитичких и електрохемијских реакција. Металуршки објекти у Бору извор су металуршких отпадних вода богатих бакром, а град Бор је извор комуналних отпадних вода богатих органским материјама. Циљ овог рада је да се испита могућност примене MFC за пречишћавање металуршких и комуналних отпадних вода које се испуштају у Борску реку. За ову студију конструисан је прототип MFC и изведене су 3 серије експеримената корис-

теђи припремљене растворе и стварне отпадне воде. Бакар је успешно уклоњен из припремљеног растовра са ефикасношћу од 99,42 %. Добијене су чврсте честице бакра величине од око 1 μm. Максимална брзина смањења хемијске потрошње кисеоника (COD) од 191,7 mg O_2/L на сат је измерена у анодном одељку. Значај ове студије огледа се у томе што је MFC имплементирана за истовремени третман две врсте отпадних вода, од којих једна садржи метале, а друга која садржи органске материје, а обе врсте отпадних вода испуштају се у исту реку.

(Примљено 8. октобра 2021, ревидирано 16. фебруара, прихваћено 17. фебруара 2022)

REFERENCES

1. A. Sumisha, A. Jiben, A. Aswathy, S. Karthick, K. Haribabu, *Sep. Sci. Technol.* **55** (2019) 2391 (https://doi.org/10.1080/01496395.2019.1625919)
2. S. Đorđievski, D. Ishiyama, Y. Ogawa, Z. Stevanović, *Environ. Sci. Pollut. Res.* **25** (2018) 25005 (https://doi.org/10.1007/s11356-018-2541-x)
3. D. Ishiyama, H. Kawaraya, H. Sato, L. Obradović, B. Blagojević, J. Petrović, V. Gardić, Z. Stevanović, A. Shibayama, N. Masuda, Y. Takasaki, *Sci. Tech. Rep. Grad. School Eng. Res. Sci. Akita Univ.* **33** (2012) 41 (https://air.repo.nii.ac.jp/?action=repository_uri&item_id=1988&file_id=48&file_no=1)
4. V. Gardić, J. Petrović, L. Đurđevac-Ignjatović, S. Kolaković, S. Vujović, *Chem. Ind.* **69** (2015) 165 (https://doi.org/10.2298/HEMIND140128031G)
5. D. Adamovic, D. Ishiyama, S. Dordievski, Y. Ogawa, Z. Stevanovic, H. Kawaraya, H. Sato, Lj. Obradovic, V. Marinkovic, J. Petrovic, V. Gardic, *Resour. Geol.* **71** (2021) 123 (https://doi.org/10.1111/rge.12254)
6. V. Nenov, H. Yemendzhiev, R. Koleva, J. Dimitrova, G. Peeva, B. Midjurova, F. Zerrouq, *J. Mater. Environ. Sci.* **8** (2017) 2327 (http://www.jmaterenvironsci.com/Document/vol8/vol8_N7/251-JMES-Nenov.pdf)
7. W. Liu, X. Yin, *Int. J. Miner. Metall. Mater.* **24** (2017) 621(https://doi.org/10.1007/s12613-017-1444-z)
8. S. Rikame, A. Mungray, A. Mungray, *Electrochim. Acta* **275** (2018) 8 (https://doi.org/10.1016/j.electacta.2018.04.141)
9. Y. Wu, X. Zhao, M. Jin, Y. Li, S. Li, F. Kong, J. Nan, A. Wang, *Bioresour. Technol.* **253** (2018) 372 (https://doi.org/10.1016/j.biortech.2018.01.046)
10. H. Song, Y. Zhu, J. Li, *Arabian J. Chem.* **12** (2019) 2236 (https://doi.org/10.1016/j.arabjc.2015.01.008)
11. S. Dharmadhikari, P. Ghosh, M. Ramachandran, *J. Serb. Chem. Soc.* **83** (2018) 611 (https://doi.org/10.2298/JSC170902016D)
12. G. Peeva, H. Yemendzhiev, B. Bonev, F. Zerrouq, V. Nenov, *J. Mater. Environ. Sci.* **5** (2014) 2350 (http://www.jmaterenvironsci.com/Document/vol5/vol5_NS1/47-JMES-S1-PEEVA.pdf)
13. M. Rahimnejad, G. Najafpour, A. Ghoreyshi, *Intech* **5** (2011) 233 (http://doi.org/10.5772/19675)
14. M. Rahimnejad, A. Adhami, S. Darvari, A. Zirepour, S.E. Oh, *Alexandria Eng. J.* **54** (2015) 745 (https://doi.org/10.1016/j.aej.2015.03.031)
15. Y. Sharma, B. Li, *Bioresour. Technol.* **101** (2010) 1844 (https://doi.org/10.1016/j.biortech. 2009.10.040)
16. R. Koleva, H. Yemendzhiev, V. Nenov, *Biotechnol. Biotechnol. Equip.* **31** (2017) 511 (https://doi.org/10.1080/13102818.2017.1304183)

17. A.G. Capodaglio, D. Molognoni, E. Dallago, A. Liberale, R. Cella, P. Longoni, L. Pantaleoni, *Sci. World J.* **17** (2013) 634738 (https://doi.org/10.1155/2013/634738)
18. S. A. A. Olayiwola, M. S. M. Annuar, *J. Serb. Chem. Soc*. **86** (2021) 1 (https://doi.org/10.2298/JSC200402054S)
19. A. T. Heijne, F. Liu, R. V. D. Weijden, J. Weijma, C. J. N. Buisman, H. V. M. Hamelers, *Environ. Sci. Technol.* **44** (2010) 4376 (https://doi.org/10.1021/es100526g)
20. Y. J. Zhang, M. Zhang, X. Yao, Y. F. Li, *Adv. Mater. Res.* **156–157** (2011) 500 (https://doi.org/10.4028/www.scientific.net/AMR.156-157.500)
21. S. A. Cheng, B. S. Wang, Y. H. Wang, *Bioresour. Technol.* **147** (2013) 332 (https://doi.org/10.1016/j.biortech.2013.08.040)
22. K. Joksimović, A. Žerađanin, D. Randjelović, J. Avdalović, S. Miletić, G. Gojgić-Cvijović, V. P. Beškoski, *J. Power Sources* **476** (2020) 228739 (https://doi.org/10.1016/j.jpowsour.2020.228739)
23. Y. Mersinkova, H. Yemendzhiev, *J. adv. biol. biotechnol.* **23** (2020) 19 (https://journaljabb.com/index.php/JABB/article/view/30135)
24. Z. Wang, B. Lim, H. Lu, J. Fan, C. Choi, *Bull. Korean Chem. Soc.* **31** (2010) 2025 (https://doi.org/10.5012/bkcs.2010.31.7.2025).

Journal of the Serbian Chemical Society
JSCS@tmf.bg.ac.rs • www.shd.org.rs/JSCS
J. Serb. Chem. Soc. 87 (6) S247–S248 (2022)
Supplementary material

SUPPLEMENTARY MATERIAL TO

Application of microbial fuel cell for simultaneous treatment of metallurgical and municipal wastewater – A laboratory study

STEFAN ĐORĐIEVSKI[1]*, HYUSEIN YEMENDZHIEV[2], RALITZA KOLEVA[2], VALENTIN NENOV[2], DRAGANA MEDIĆ[3], VANJA TRIFUNOVIĆ[1] and ANA MAKSIMOVIĆ[4]

[1]*Mining and Metallurgy Institute Bor, Zeleni Bulevar 35, Bor 19210, Serbia,* [2]*"Prof. Dr Assen Zlatarov" University, Y.Yakimov blvd. 1, Burgas 8010, Bulgaria,* [3]*Technical Faculty in Bor, Vojske Jugoslavije 12, Bor 19210, Serbia and* [4]*Independent consultant, Belgrade 11000, Serbia*

J. Serb. Chem. Soc. 87 (6) (2022) 775–784

Fig. S-1. Mixing of municipal wastewater (brown) and metallurgical wastewater (green) in the canal of Bor River in Serbia.[1]

Sampling of the wastewaters

The wastewater samples are collected in plastic bottles at the outlets around mining and metallurgical facilities in Bor in September 2020. The coordinates of sampling points of

* Corresponding author. E-mail: stefan.djordjievski@irmbor.co.rs

underground mine wastewater, Robule Lake wastewater, and metallurgical wastewater were 44.093551, 22.095781; 44.063313, 22.136585; and 44.061819, 22.131387, respectively.

REFERENCES

1. S. Đorđievski, D. Ishiyama, Y. Ogawa, Z. Stevanović, *Environ. Sci. Pollut. Res.* **25** (2018) 25005 (https://doi.org/10.1007/s11356-018-2541-x).